Directed wet-chemical synthesis of metallic nanoparticles of different sizes and shapes: control mechanisms

Síntesis química de nanopartículas metálicas de diferentes tamaños y formas: mecanismos de control

Yasser Attia Attia

University of Santiago de Compostela

Faculty of Chemistry

Department of physical chemistry

Directed wet-chemical synthesis of metallic nanoparticles of different sizes and shapes: control mechanisms

Síntesis química de nanopartículas metálicas de diferentes tamaños y formas: mecanismos de control

**A thesis submitted to the University of Santiago de Compostela
In partial fulfillment of the requirements for
the degree of doctor in chemistry in the
department of physical chemistry,
Faculty of Chemistry**

By

Yasser Attia Attia

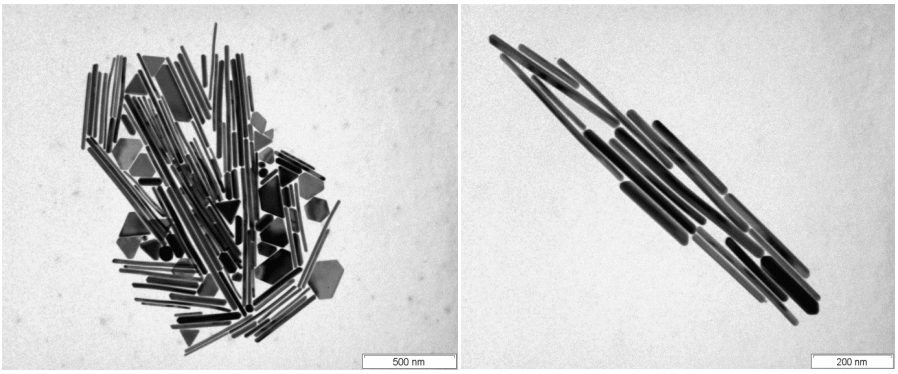

Santiago de Compostela University
Faculty of Chemistry

Approval Sheet

Title of thesis:

Directed wet-chemical synthesis of metallic nanoparticles of different sizes and shapes: control mechanisms

Name of student:

Yasser Attia Attia Awad Khalifa

Approved by:

Prof. Dr. M. Arturo López-Quintela

Dpt. Physical Chemistry, Fac. Chemistry

University of Santiago de Compostela

Santiago de Compostela, 2011

MANUEL ARTURO LÓPEZ QUINTELA,

CATEDRÁTICO DE QUÍMICA DEL DEPARTAMENTO DE QUÍMICA FÍSICA DE LA UNIVERSIDAD DE SANTIAGO DE COMPOSTELA

CERTIFICA:

La presente tesis titulada¨ **Síntesis química de nanopartículas metálicas de diferentes tamaños y formas: mecanismos de control¨** que presenta **Yasser Attia Attia** para optar al grado de doctor en Química, ha sido realizada bajo mi dirección, en el Departamento de Química Física de la facultad de Químicas de la Universidad de Santiago de Compostela, y hallándose concluida, autorizo su presentación para que sea evaluada por el tribunal correspondiente:

Y para que así conste, firmo en la presente en Santiago de Compostela, Diciembre, 2011.

Dedication

This work is dedicated to my parents, my wife, my kids and my country Egypt.

ACKNOWLEDGEMENTS

First and foremost, I wish to thank my supervisor Professor **M. Arturo López-Quintela** for giving me the opportunity to conduct my research in his research group. My gratitude to him for his invaluable support, encouragement and guidance during my study years can never be fully expressed.

I wish to thank to my research group in Spain and Egypt for great discussions and enjoyable moments.

Special thanks for my master advisors Professor **El-Sayed El-Sherbini** and Dr. **Mona Bakr Mohamed** for giving me the chance to work under their supervision in my master and for their continuous support and enormous encouragement.

I would like to thank those whom helped me to finish my work.

Special thanks for my friends and my colleagues in NANOMAG-España, NANOTECH-Egypt and NILES for all of their support, love and prayer.

I would also like to dedicate this work to the martyrs of the revolution of Egypt.

Last but not least, my deepest appreciation goes to my parents, my father whom lost him recently, my wife (**HALA**), my kids (**SAMA**, **JANA** and **REEM)** and all my family members for their support, love, prayer and caring attitude which kept me going until the end of my work. I could not have done this work without them.

Table of Contents

List of Figures:

List of Tables

List of Schemes

Publications

1- UV-light induced shape changes of gold nanoparticles, S.A.M.Al-Sherbini, Y.Attia*, M.M.Baker; Vol. 2, Issue 1, 2008, Nano Science&Nano Technology: An Indian Journal.

2- Formation and dissolution of gold nanorods by means of photoelectrical catalytic Ag-clusters, Yasser A. Attia*, Kallol Mohanta, M. C. Blanco and M. Arturo Lopez-Quintela.(Under submission)

3- Metal clusters: a key missing point in the synthesis of high yield and high aspect ratios gold nanorods, Yasser A. Attia*, Carlos Vázquez-Vázquez, M.C. Blanco and M. Arturo Lopez-Quintela. (Under submission)

4- The effect of gold nanoparticles shape on their Thermal and Photostability: nanorods vs nanoprisms, Yasser A. Attia*, Mona B. Mohamed, and M. Arturo Lopez-Quintela. **(**Under submission **)**

Summary

The successful applications of nanoparticles require the ability to tune their properties by controlling size and shape at the nanoscale. Therefore, it is very important to prepare nanoparticles of well-defined sizes and shapes in order to control their physicochemical characteristics.

In this work we described an improved seed mediated synthesis to prepare gold nanoparticles of different shapes (Spheres, Rods, Prisms,…..). New absorption features different from that of the classical surface plasmon absorption bands of rods and spheres are found to be associated with the appearance of nanoprisms, and snapped prism shaped gold nanoparticles. The effect of [Ag-ions], [seed], [ascorbic acid], [Cl^-] and the aging of the seed solution were studied in order to get a deeper understanding of the growth mechanism. Our results indicate that the ratio of [Ag^+] to [seed] is one of the key parameters for controlling the shape of the particles, e.g. rods, prisms or snapped prisms. We proposed a mechanism for the formation of the different gold shapes that takes in account the reduction of Ag ions by ascorbic acid forming intermediate small Ag clusters, which can then act as catalysts for the formation of gold nanoparticles. The mechanism has been proved using externally prepared Ag clusters instead of adding Ag ions. The results also indicate that, to get such different shapes, the used CTAB concentration should be above the CMC and is independent of the CTAB supplier. It seems therefore that, the catalytic activity of clusters needs the presence of micelles, whose micellar surface can be viewed as a kind of catalyst *nanosupport.* These results open a new way of thinking in the interpretation of the mechanisms involved in the anisotropic growth of nanoparticles.

In order to confirm that mechanism, we developed a simple method to synthesize gold nanorods with high aspect ratios using gold clusters (Au_2-

Au_6) stabilized by CTAB. These clusters were added to gold ions in the growth solution without adding any surfactant or polymer. The mechanism proposed for the formation of gold nanorods with high aspect ratios in the absence / presence of the seeds is based on the deposition of these catalytic clusters on active sites of the gold surface. The deposition and the corresponding reduction reaction mainly occur at the end (tips) of the nanorods. The concentration of these clusters was calculated from the UV-vis absorption of the solutions at different reaction times. The effects of the dilution of CTAB in the clusters solution and the dilution of the seed solution on the growth of gold nanorods were also studied. The results showed that gold nanorods can be formed without addition of the seeds indicating that the seed particles do not directly affect the growth of gold nanorods.

The effect of the gold nanoparticle shape on the stability (thermal heating and photo stability by UV-light and laser) was also studied. It was found that the mechanism of the particle dissociation in the case of nanoprisms is different from than that of nanorods under thermal heating. Great enhancement of the thermal stability has been achieved by adding specific amounts of polyvinyl pyrrolidone (PVP) to the gold nanoparticles of different shapes capped with cetyltrimethylammonium bromide (CTAB). It is worth to mention that gold nanorods stabilized by PVP are totally stable up to 220 ^{0}C. The effect of irradiation with UV-light on gold nanoparticles also showed different mechanisms depending on the shape of the NPs. Under long irradiation times (up to approx. 30 h), gold nanorods totally decomposed and another band started to appear at 398nm , corresponding to the formation of the Au(III)-CTAB complex, indicating that the gold(0) NRs are dissolved and transformed to gold-ions. The photocorrosion of the Au nanoparticles was explained assuming that semiconducting Ag-clusters are attached to the tips of the NRs as we assumed in the growth

mechanism. This photocatalytic activity of Ag clusters was confirmed adding ethanol to the irradiated rods, which acts as hole scavenger and avoids in this way the dissolution of the rods. The inhibition of the Au photocorrosion can also be done by pre-heating the irradiated rods to 130^0C which corresponds to the fusion temperature. Further experiments were used to analyze the Au ions produced during the photocorrosion and to confirm the high stability of the photocatalytic Ag clusters, which can be reused to direct again the formation of Au NRs after its photodissolution.

Finally, the effect of different types of nanosecond lasers (CW and pulsed) on different aspect ratio gold nanorods was studied and the corresponding mechanisms (fragmentation and melting) were proposed to explain the different observed nanosecond pulsed laser effects.

Resumen

En la actualidad, la nanotecnología ocupa un lugar preferente tanto en lo que se refiere a los importantes retos científicos que tiene planteados, como a las enormes potencialidades de aplicación que ofrece esta disciplina científica. Dentro de esta nueva gran área de investigación, la preparación de los nanomateriales (nanoparticulas, NPs) es uno de sus puntos clave, requiriéndose un perfecto control de su tamaño y forma a escala nanométrica para que puedan ser aplicadas con éxito. Por ello, es de gran importancia desarrollar métodos adecuados que permitan obtener nanopartículas de tamaño y forma controladas.

Aunque se han desarrollado un gran número de métodos para la fabricación de nanoestructuras anisotrópicas, el proceso de crecimiento anisotrópico utilizando semillas es uno de los más ampliamente utilizados debido a la posibilidad que ofrece de producir nanoestructuras muy diferentes, tales como nanobarras, nanoalambres, nanofibras, nanotriángulos, nanoprismas, nanoestrellas, nanoflores, etc., mediante el control de un número determinado de sus variables experimentales. Este popular procedimiento de siembra ha venido utilizándose -con sus diversas variaciones- para la producción de diferentes tipos de nanomateriales, entre los que destacan las partículas metálicas. Aunque durante los últimos años se han hecho importantes avances en esta técnica, respecto al aumento del rendimiento de la reacción, sin embargo, la preparación de distribuciones muy monodispersas de tamaño y forma es todavía un reto científico, sin cuya resolución resultan inviables la mayoría de sus potenciales aplicaciones.

El método de siembra implica un proceso de, al menos, dos pasos. El primer paso es la síntesis de nanopartículas que han de servir como semillas para el posterior crecimiento anisotrópico de las mismas. En el

caso de los metales este proceso consiste en una simple reducción de la correspondiente sal del metal mediante reductores adecuados en presencia de agentes estabilizantes o complejantes. El segundo paso consiste en el crecimiento de las semillas para la obtención de las nanopartículas con las formas y tamaños deseados. La disolución de crecimiento contiene generalmente un agente tensioactivo (para orientar el crecimiento), y/o un agente que limita el crecimiento (como por ej. un polímero), así como un reductor suave que ayuda a controlar cinéticamente la formación de estructuras poco favorables desde el punto de vista termodinámico. En este proceso, las sales de los metales se reducen preferentemente en la superficie de las nanopartículas utilizadas como semillas, en un proceso favorecido por la menor energía implicada en la nucleación heterogénea. Agentes externos, tales como varios tipos de moléculas o iones, e incluso el propio disolvente o la temperatura de reacción, pueden también alterar la dirección del crecimiento de las nanopartículas ayudando o, más bien, complicando en muchos casos, el control del crecimiento anisotrópico de las mismas. Conocer, pues, con detalle, los complejos mecanismos implicados en el crecimiento de las nanopartículas es una condición *sine qua non* para poder obtener procedimientos con altos rendimientos de nanopartículas monodispersas en cuanto a su tamaño y forma, que puedan ser fácilmente escalables con vistas a su aplicación industrial.

En el presente trabajo se ha realizado una investigación sistemática del método de siembra para la síntesis de nanopartículas anisotrópicas (preferentemente en forma de nanobarras) lo que ha permitido descubrir aspectos muy importantes del complejo mecanismo implicado no reconocidos hasta la fecha. Ello ha permitido no sólo la preparación de diferentes tipos de nanopartículas con variada morfología (nanoesferas, nanobarras, nanoprismas, ..) con mayores rendimientos y relaciones de

aspecto (relaciones entre los ejes menores/mayores de las NPs) mucho mayores que las conocidas hasta la fecha, sino también simplificar enormemente los protocolos de síntesis lo que permite un más fácil escalado de los mismos.

Como comentamos, a pesar de la gran cantidad de bibliografía existente acerca de la síntesis química de estructuras anisótropas, los mecanismos que determinan el tipo de estructura cristalina final del nanomaterial y la morfología no son bien conocidos, e incluso cambios sutiles en las condiciones experimentales, como por ejemplo, la empresa proveedora de algunos productos químicos utilizados en la síntesis (disolvente, surfactantes, etc.) parece tener una gran influencia en la forma, tamaño y rendimiento final de las nanopartículas. De forma concreta, en el método de siembra para la preparación de nanopartículas anisotrópicas de oro, mediante semillas obtenidas con $AgNO_3$, no se conoce actualmente todavía la naturaleza de las especies de plata formadas durante la síntesis, a pesar de ser un tema crítico en dicho método y haberse debatido ampliamente por muchos grupos de investigación pioneros en el desarrollo de estos métodos. Varios grupos han propuesto diferentes razones del por qué las especies de plata pueden ayudar al crecimiento anisotrópico de nanobarras de oro, siendo una de las posibilidades más aceptadas que los complejos de bromuro de plata juegan un papel fundamental en este mecanismo. A pesar de carecerse de una comprensión completa de este método de síntesis, se aceptan actualmente dos mecanismos principales como los más relevantes. El primer mecanismo considera que la estructura rígida de los monómeros del surfactante CTAB (bromuro de cetiltrimetilamonio) adsorbidos sobre algunas de las caras del nanocristal de oro que está creciendo, ayuda no sólo a mantener un crecimiento unidimensional, sino que también sirve para controlar la velocidad de la reducción de oro, de una manera similar al

mecanismo que se propone para la formación de nanovarillas muy largas en ausencia de iones de plata. Se supone en este mecanismo, tal como se comentó, que los iones de plata no se reducen por el ácido ascórbico presente en el medio de reacción, sino que se forma bromuro de plata durante la síntesis. Murphy y colaboradores propusieron que la adsorción de bromuro de plata sobre algunas de las caras de los nanocristales de oro, frenan la reducción del mismo sobre esas caras contribuyendo de esa forma al crecimiento cristalino en forma de nanobarras. La presencia de especies de bromuro de plata se basa en los datos de XPS que sugieren la presencia de Ag en forma de Ag(I). A favor de esta hipótesis se han utilizado resultados de NMR ^{1}H realizados con nanobarras de oro obtenidas por este procedimiento observándose que sus espectros eran idénticos a los de mezclas de AgBr-CTAB. Sin embargo, la presencia de bromuro de plata libre (ya que las condiciones de la reacción se producen por encima del producto de solubilidad del AgBr) pone en duda estos resultados. Otros autores encontraron pruebas, por espectrometría de masas, de la existencia de $AgBr_2^-$, así como $AuBr_2$, en la superficie de nanobarras de oro obtenidas por síntesis fotoquímica. Hafner y colaboradores obtuvieron por espectroscopía Raman pruebas de la formación del enlace Au-Br a 180 cm^{-1}, que desaparece cuando se añaden tioles para reemplazar los bromuros adsorbidos en la superficie de las nanobarras de oro. Otros grupos, sin embargo, proponen un segundo modelo en el que el bromuro de plata no juega ningún papel en el crecimiento anisotrópico argumentando en su lugar que la deposición a sub-potenciales (UPD) de una sola capa o una sub-monocapa de plata elemental en la superficie de las nanobarras de oro es de gran importancia. Así, Guyot-Sionnest y colaboradores propusieron que la deposición de la plata a subpotenciales tiene lugar preferentemente sobre las caras de oro {110} frente a las {111} y {100}, en las que la deposición es menor. En este modelo, una monocapa de plata

protege fuertemente la cara {110} y, aunque la plata se acaba oxidando y se sustituye por el oro, esta oxidación-sustitución es más lenta que la propia reacción de crecimiento de las NPs, por lo que dicha reacción procede preferentemente sobre las otras caras del nanocristal no recubiertas por la plata. Mediante espectroscopia de emisión atómica se ha observado que hasta cuatro monocapas de plata están presentes en las barras, aunque estos datos no son concluyentes ya que esta técnica no hace diferencias entre Ag (0) y Ag (I). Finalmente conviene indicar que estudios de espectroscopía de absorción de Rayos X (EXAFS) han permitido deducir que la plata se encuentra en forma de Ag (0) en nanobarras de plata obtenidas mediante métodos fotoquímicos, por lo que se ha concluido que la presencia de plata elemental es de vital importancia no sólo para la técnica estándar de siembra, sino también para otros tipos de métodos de síntesis disponibles para producir nanobarras de oro.

Para tratar de dilucidar los complejos mecanismos implicados en la formación de estas nanopartículas de Au, se procedió al estudio del efecto de la concentración de Ag^+, semillas, ácido ascórbico, Cl^-, así como el tiempo de envejecimiento de la disolución de semillas. Los resultados indicaron que la relación de la concentración de Ag^+ frente a la de las semillas utilizadas es uno de los parámetros clave para el control de la forma de las NPs (nanobarras, nanoprismas, nanoprismas truncados, etc). A partir de los resultados obtenidos se propuso un mecanismo que permite explicar la formación de las nanopartículas con diferentes estructuras basado en la formación de pequeños clústeres de Ag que actúan como catalizadores en la síntesis de dichas partículas. Este mecanismo, propuesto al inicio de la tesis, se pudo comprobar que explicaba adecuadamente muchos otros resultados obtenidos a lo largo de la misma, por lo que

constituyó finalmente el hilo conductor que da sentido y unificación a la misma.

En primer lugar, el mecanismo se comprobó utilizando clústeres de Ag preparados *ex situ*. Estos clústeres de Ag, suministrados por la empresa Nanogap (Santiago de Compostela) y preparados mediante síntesis electroquímica, fueron adicionados a la mezcla de reacción en lugar de la sal de plata, consiguiéndose obtener nanobarras de Au de gran relación de aspecto con rendimientos mayores del 90%. Los resultados indicaron también que, para conseguir la formación de nanoestructuras anisotrópicas, la concentración de CTAB utilizada ha de estar por encima de la concentración micelar crítica (CMC), siendo independiente de la empresa proveedora utilizada, en contra de los resultados publicados anteriomente por el grupo de Korgel el al. Por lo tanto, parece que la actividad catalítica de los clústeres necesita, para que sea eficaz, la presencia de micelas en el medio de reacción, por lo que la superficie micelar puede ser vista como una especie nanosoporte del catalizador. Aunque no se han podido obtener pruebas directas de la presencia de clústeres en las micelas de CTAB, esta asociación clústeres-CTAB podría estar relacionada con el hecho de que los pequeños clústeres de plata con estructura plana (como los que se proponen y se utilizan aquí para dirigir el crecimiento controlado en las distintas morfologías) se sabe que se forman y se estabilizan preferentemente en las interfaces, como las películas de surfactante en las microemulsiones.

Como segunda prueba de que los clústeres metálicos (independientemente de su naturaleza) representan un paso muy importante en el mecanismo de la formación de estructuras anisotrópicas y con el fin de confirmar el mecanismo propuesto se desarrolló un método simple para la síntesis de nanobarras de oro con altas relaciones de aspecto en ausencia de plata. Este

método se basó en el uso de clústeres de oro (Au_2-Au_6), estabilizados por bromuro de cetiltrimetilamonio, los cuales se añadían a los iones de oro en la disolución de crecimiento en ausencia de agentes tensioactivos o polímeros. El mecanismo propuesto para la formación de las nanobarras de oro con altas relaciones de aspecto en la ausencia/presencia de la disolución de semillas se basa en el depósito de los clústeres catalíticos en los lugares activos de la superficie de los nanocristales de oro durante su crecimiento, preferentemente localizados en los extremos de las nanobarras. Los clústeres depositados catalizan la reacción de reducción en esos extremos lográndose de esta forma aumentar considerablemente la relación de aspecto de las nanobarras y el rendimiento de la reacción.

También se estudiaron los efectos de la concentración de CTAB en la disolución de clústeres y la concentración de la disolución de semillas en el crecimiento de las nanobarras de oro. Los resultados mostraron que dichas nanobarras se pueden formar incluso sin la adición de la disolución de semillas, lo que parece indicar que no es la siembra con semillas sino la presencia de los clústeres la que ejerce un papel importante en el crecimiento de las nanobarras de oro.

Se estudió finalmente la influencia de la forma de las nanopartículas de oro en su estabilidad térmica y fototérmica (mediante luz ultravioleta y láser) observándose, en primer lugar, que el mecanismo de la disociación térmica de las nanopartículas prismáticas es diferente al de las nanobarras. Se observó una gran mejoría de la estabilidad térmica de las nanopartículas protegidas con CTAB mediante la adición de determinadas cantidades de polivinilpirrolidona (PVP). Es importante destacar en este aspecto que las nanobarras de oro estabilizadas por PVP se mantienen estables hasta temperaturas de aproximadamente 220 ^{0}C.

La irradiación con luz ultravioleta mostró también que el comportamiento de las nanopartículas depende de su forma. Así, contrariamente a lo que sucedía cuando se irradiaba nanoesferas de Au, cuando se sometía a las nanobarras de Au a una iluminación prolongada (aproximadamente 30h), se observó que se disolvían completamente transformándose de nuevo en iones Au(III), que en presencia de CTAB, forman el complejo Au(III)-CTAB con una banda de absorción característica a 398nm. Este totalmente inesperado y novedoso efecto de "fotocorrosión" de las nanopartículas de Au, se explicó suponiendo la presencia de clústeres semiconductores de Ag depositados en los extremos de las nanobarras, tal como se proponía en el mecanismo de formación de las nanopartículas. Aunque, en los mecanismos deducidos en los estudios anteriores de la presente tesis doctoral, se suponía que tales clústeres estaban presentes en los extremos de las nanobarras de Au durante su formación, no se pensaba que su estabilidad fuera tal que permanecieran como tales después de finalizar la reacción. Sin embargo, estos resultados de su clara actividad fotocatalítica demostraban lo contrario. La actividad fototocatalítica de los clústeres se confirmó realizando la irradiación en presencia de etanol que, al actuar como captor de huecos, evita la oxidación/disolución de las nanobarras. La inhibición de la fotocorrosión se puede también realizar sometiendo la disolución de las nanobarras de Au a un tratamiento térmico a 130^0C, que es la temperatura a la que se funden los clústeres de plata. En tales casos, se observó que la fotocorrosión resulta muy inhibida. El efecto de la fotocorrosión se amplió con la introducción de captores de huecos y electrones originado, dependiendo de las condiciones, la producción de hidrógeno u oxígeno, como se pudo comprobar por los experimentos electroquímicos que se llevaron a cabo, que permitieron confirmar la oxidación del oro y la formación de iones de oro (en ausencia de captores de huecos), así como también la generación de hidrógeno (en

presencia de captores de huecos). Estos resultados resultan de gran importancia no solo en la demostración definitiva de la existencia de clústeres en la formación de las nanopartículas –algo que hasta la fecha había pasado totalmente desapercibido- sino también (y, quizás, de mucho mayor importancia) por las importantes aplicaciones que pueden tener estos resultados en aplicaciones de fotocatálisis y células fotovoltaicas.

Por último, se estudió el efecto de diferentes tipos de láser de nanosegundos (CW y pulsado) sobre las nanobarras de oro de diferentes relaciones de aspecto, proponiéndose la existencia de diversos mecanismos (fragmentación y fusión) para explicar los diferentes resultados obtenidos dependiendo de las condiciones experimentales.

Una visión general del trabajo de tesis

En este trabajo de tesis, hemos re-examinado cuidadosamente el proceso de síntesis de nanopartículas de oro de diferentes formas (esferas, barras, etc) preparadas mediante método basado en el empleo de semillas para tener una mejor comprensión y conocimiento de los mecanismos.

En este trabajo hemos modificado este método para producir nanopartículas de oro de morfología predefinida con un alto rendimiento. Se determinó el importante papel de grupos subnanométricos (Ag y Au) sobre el crecimiento anisotrópico de las nanopartículas de oro. Las propiedades ópticas y térmicas, así como la fotoestabilidad de estas partículas de diferentes formas y composiciones fue estudiada en detalle. Estas muestran que las clústeres jugaron un papel importante en la " fotocorrosión " de oro, observada por primera vez en este trabajo. Se encontró que este comportamiento inesperado de oro está relacionado con la actividad fotocatalítica de los grupos subnanométricos, que siguen permaneciendo principalmente unidos a algunos planos particulares de las nanopartículas de oro después de su síntesis.

El presente trabajo de tesis se divide en los siguientes capítulos. Después del capítulo de introducción, los métodos experimentales relacionados con la preparación de muestras, caracterización y mediciones ópticas son discutidas en detalle en el capítulo 2.

El capítulo 3 describe la modificación de la metodología de síntesis de las nanobarras de oro y nanoprismas basada en el método empleando semillas desarrollado en este trabajo de tesis. Se han estudiado diferentes condiciones experimentales basadas en variaciones en la composición de sistema para controlar la forma (y por lo tanto las propiedades ópticas) de las nanopartículas. Un nuevo mecanismo de la formación de estas partículas se propone mostrar la importancia de la presencia de Ag-

clústeres en el crecimiento anisotrópico de las nanopartículas. Las nuevas características en las bandas de absorción que aparecen en estas partículas, se asignan a la absorción de resonancia cuadripolar a lo largo del eje perpendicular corto de los prismas y los prismas truncados.

En el capítulo 4, se presentan los experimentos que se llevaron a cabo para explicar y probar el papel de los clústeres en el mecanismo de crecimiento de las nanobarras de oro. Estos experimentos se basaron en el uso de clústeres de oro (Au_2-Au_6), estabilizados por bromuro de cetiltrimetilamonio, los cuales se añadían a los iones de oro en la disolución de crecimiento en ausencia de agentes tensioactivos o polímeros. El mecanismo propuesto para la formación de las nanobarras de oro con altas relaciones de aspecto en la ausencia / presencia de la disolución de las semillas se basa en el depósito de los clústeres catalíticos en los lugares activos de la superficie de oro.

El capítulo 5 se dedicó al estudio de la estabilidad de nanopartículas de Au frente al calentamiento térmico, radiación UV y tratamiento con láser. Este nuevo método propone estabilizar las nanopartículas de oro hasta 220 ^{0}C en presencia de PVP como agente protector. El resultado más importante obtenido en esta parte es la de descubrir que nanobarras de oro mostraron un efecto de fotocorrosión con tiempo largo de irradiación con luz UV. Se realizaron varios experimentos para estudiar este efecto, lo que muestra claramente la importancia de la presencia de los clústeres en los fenómenos observados. Por último, se ha estudiado el efecto de la radiación con láser de las diferentes dispersiones de nanobarras variando la longitud de onda y la energía. Mecanismos de fragmentación y la fusión de las nanopartículas de oro se han propuesto para explicar la remodelación de la nanopartículas sometidas a esta irradiación láser.

ملخص

التطبيقات الناجحة للجسيمات النانوية تتطلب القدرة على ضبط خصائصها من حيث السيطرة على الحجم والشكل فى مقياس النانو. أصبح من المهم أن تحضير جسيمات محددة جيدا من الشكل والحجم بشكل صحيح لوصف الخصائص البصرية. وقد قمنا بوصف طريقة بوساطة حبيبات الذهب النانوية المحسنة لتحضير جسيمات الذهب من الأشكال المختلفة (الكروية ، العصوية، المنشورية ،.....). لقد وجد أن هناك أطياف أمتصاص جديدة لهذه الجسيمات تختلف عن التى لوحظت بالنسبة للأمتصاص الضوئى لكل من جسيمات الذهب ذات الشكل العصوى والشكل الكروى. ولقد تم توضيحها على أن أشكالها بلورية ذات شكل منشورى وذلك بدراستها باستخدام الميكروسكوب الألكترونى النافذ.تم الحصول على كميات كبيرة من جسيمات الذهب ذات الشكل العصوى لنتيجة لهذا التعديل فى الطريقة المستخدم بها الجسيمات المتناهيه الصغر.تم دراسة تأثيرتركيزات [ايونات الفضة] ، [حبيبات الذهب النانوية] ، [فيتامين أ] ، [حبيبات الذهب النانوية المحضرة باستخدام السيترات] ، [الكلور] ، و دراسة زيادة عمر الجسيمات المناهية الصغر من أجل فهم أكثر في آلية النمو. نتائجنا تشير الى ان نسبة [ايونات الفضة] و [حبيبات الذهب النانوية] هى واحدة من المعايير الأساسية للتحكم فى شكل هذه الجسيمات النانوية، على سبيل المثال الشكل العصوى ، المنشورى أو المنشورى الغير مكتمل.وقد اقترحنا آلية لنموالأشكال المختلفة من جسيمات الذهب والتى تأخذ في الاعتبار أختزال أيونات الفضة بواسطة فيتامين أ (حمض الاسوربك) لتكوين مجموعات وسيطة من جسيمات الفضه المتناهية جدا فى الصغر، والتي يمكن أن تعمل كمحفز لتكوين جسيمات الذهب النانوية. وقد أثبتت الآلية باستخدام مجموعات من جسيمات الفضة المتناهية الصغرالمحضرة خارجيا بدلا من إضافة أيونات الفضة. وتشير النتائج أيضا ، للحصول على أشكال مختلفة من هذا القبيل، وتركيز المادة المغلفة بالغرويات العضوية سيتيل تراى ميثيل أمونيوم بروميد المستخدمة ينبغي أن تكون فوق الحد المسموح به بصرف النظر عن مصدره. ولذلك يبدو أنه ، من أجل أن تكون جسيمات الفضة المتناهية الصغر فعالة في السلوك المحفز ، فإنها تحتاج إلى أن تستقر بوجود ماده مغلفة، والتي يمكن النظر اليها على انها نوع من المساند النانوى الحفاز. هذه النتائج تفتح طريقا جديدا للتفكير في تفسير الآليات التي تشارك في نمو متباين من النانوية.

وقد طورنا من أجل تأكيد هذه الآلية ، وهو أستخدام طريقة بسيطة لتحضير جسيمات الذهب العصوية مع نتاج عالى باستخدام حبيبات نانوية من الذهب المحضرة و المحمية بالمادة المغلفة

بالغرويات العضوية سيتيل تراى ميثيل أمونيوم بروميد ووصفها بأن عدد الذرات بها يترواح بين اثنين الى ستة ذرات وأضيفت إلى أيونات الذهب في محلول النمو الذى لا يحتوي على أي مادة مغلفة بالغرويات العضوية سيتيل تراى ميثيل أمونيوم بروميد .واقترحنا آلية جديدة لتشكيل جسيمات الذهب العصوية مع ناتج مرتفع في غياب / ووجود حبيبات الذهب وذلك اعتمادا على أمتزاز هذه المجموعات الحفازة على المواقع النشطة من سطح الذهب .الامتزاز والاختزال يحدث بشكل رئيسي في النهايات من الشكل العصوى. تم حساب تركيز هذه الكتل وتركيبها بواسطة محاكاة مونتي كارلو .وتمت دراسة الآثار المترتبة على التخفيف من المادة المغلفه بالغرويات العضوية سيتيل تراى ميثيل أمونيوم بروميد في تحضير هذه التجمات من الجسيمات المتناهية الصغر من الذهب والتخفيف من الحبيبات النانوية للذهب على نمو جسيمات الذهب العصوية . وأظهرت النتائج أيضا أن جسيمات الذهب العصوية يمكن تشكيلها من دون إضافة حبيبات الذهب النانوية و أيضا وجود هذه الحبيبات النانوية قد لا تؤثر مباشرة على نمو جسيمات الذهب النانوية العصوية.

تم دراسة تأثير الشكل لجسيمات الذهب على خواص الثبات (الثبات الحراري والثبات الضوئى للأشعة الفوق البنفسجية والليزر) .آلية تفكك هذه الجسيمات في حالة الشكل المنشورى يختلف عن ذلك من الشكل العصوى تحت تأثير الثبات الحراري وقد وجد أن هناك تحسن كبير فى درجة الثبات الحرارى لهذه الأشكال فى وجود مغلفات من البوليمرات مثل البولى فينيل بيريليدون وذلك بالنسبة لتلك المغلفة بالغرويات العضوية مثل سيتيل تراى ميثيل أمونيوم بروميد ومن الجدير بالذكر أن هناك درجة ثبات حرارى لجسيمات الذهب العصوية المغلفة بالبولى فينيل بيريليدون تصل حتى 220م° . بصريا ، وهذه الجسيمات النانوية للذهب التي ثبتت بشكل ملحوظ فى وجود مغلفات من البوليمرات مثل البولى فينيل بيريليدون فى درجة الثبات الحراري والثبات تحت الأشعة فوق البنفسجية .تأثير الأشعة فوق البنفسجية على جسيمات الذهب أظهرت آلية مختلفة من شكل إلى آخر . في إطار التعريض للاشعاع لوقت طويل يصل إلى 30 ساعة ، فالجسيمات العصوية للذهب تتفكك تماما و يبدأ ظهورامتصاص ضوئى عند الطول الموجى 398 و هو تقريبا نفس الطول الموجى لامتصاص الضوء لمركب ايونات الذهب مع الغرويات العضوية سيتيل ميثيل امونيوم بروميد وهو ما يعني أن الذهب (0) تحولت إلى أيونات الذهب وهذا يدل على حدوث تأكل ضوئى لهذه الجسيمات نتيجة تواجد تجمعات الفضة كما افترضنا وجودها ودورها فى الية النمو .وقد تأكد هذا التأكل بأضافة محلول الايثانول إلى الجسيمات العصوية وعن طريق اشعاع هذه الجسيمات بعد تسخينها لدرجة حرارة 130 م° وهى نفس درجه ذوبان هذه الحبيبات وعدم ظهور نفس درجة

امتصاص الضوء عند الطول الموجى السابق وهذا يدل على أهمية وجود هذه التجمعات فى الية النمو .وقد درسنا تأثيرالتأكل الضوئى لهذه الجسيمات من خلال استخدام تجارب الكهروكيميائية التي تؤكد حدوث الأكسدة لهذه الجسيمات وتحولها الى الأيونات ثانية ، و التي سببتها وجود هذه التجمعات. وتعد هذه النتيجة من أهم ما توصلنا له من نتائج خلال هذه الدراسة وهى حدوث الاكسدة لجزيئات الذهب المتناهية الصغر ذات الشكل العصوى عن طريق التاكل الضوئى بوجود مجموعات (كلسترز) الفضة.

أخيرا ، تم دراسة تأثير أنواع مختلفة من الليزر النانوسيكند(المستمر والوامض) على جسيمات الذهب العصوية ذات نسب طول وعرض مختلفيين و تم اقتراح آليات مختلفة (التفتت والذوبان) لتأثير الليزر النانوسيكند الوامض وباطوال موجية مختلفة.

Chapter one
Introduction

An Overview of the Dissertation Work

In this dissertation work, we have carefully re-examined the process of synthesis of gold nanoparticles of different shapes (e.g. spheres, rods, etc) by the seed's mediated method[64,142], to have a better understanding and insight into the mechanisms.

We modified this method in order to produce gold nanoparticles with selected shapes in high yields. We determined the very important role of subnanometric clusters (Ag and Au) on the anisotropic growth of Au nanoparticles. The optical and thermal properties, as well as the photostability of these particles of different shapes and compositions were studied in detail showing that clusters again play an important role in the "photocorrosion" of gold observed for the first time in this work. It was found that this unexpected behavior of gold is related with the photocatalytic activity of the subnanometric clusters, which remain mainly attached to some particular planes of the gold nanoparticles after their synthesis.

The thesis is divided in the following chapters.

After the first introduction chapter, the experimental methods regarding the sample preparation, characterization, and optical measurements are discussed in details in Chapter 2.

Chapter 3 describes the modified seed-mediated synthesis of gold nanorods and nanoprisms developed in the thesis using a rational choice of the experimental conditions and additives to select the shape (and consequently the optical properties) of the NPs. A novel mechanism of the formation of

these particles is proposed showing the important role of the presence of Ag-clusters in the anisotropic growth of nanoparticles. New absorption features appear for these particles, which are assigned to the quadruple resonance absorption along the short axis perpendicular of the prisms and snapped nanoparticles.

In chapter 4, other experiments were carried out to explain and confirm the role of clusters in the growth mechanism of gold nanorods.

Chapter 5 was devoted to the study of the stability of Au NPs against thermal heating, UV-irradiation and Laser treatment. A new method is proposed to stabilize gold nanoparticles up to 220 ^{0}C using PVP solution as protecting agent. The most important result obtained in this part is the discovering that gold nanorods showed a photocorrosion effect under long irradiation time of UV-light. Several experiments were performed to study this effect, which clearly shows the importance of the clusters in the observed phenomena. Finally, the effect of nanosecond laser at different wavelengths and power on the prepared gold nanorods with different aspect ratios was studied. Fragmentation and melting mechanisms for the gold nanoparticles were proposed for explaining the reshaping of the NPs with the laser irradiation.

.

Chapter I

1-1: General Introduction:

Metallic nanoparticle´s (especially gold and silver nanoparticles) research is currently an area of great intense scientific research, because of their unusual chemical and physical properties that make them suitable for many potential and promising applications such as catalysis, electronics, optics, imaging and biotechnology. Nanoparticles contain a small number of atoms or molecules that they differ from the properties inherent to their bulk counterparts. However, they contain sufficiently large number of atoms or molecules so that their properties differ from isolated groups of atoms or molecules (clusters). Nanoparticles can exhibit physicochemical properties that are different from both the bulk and the constituent atoms or molecules. For example, the striking colors of metallic nanoparticle solutions (such as gold and silver) are due to the red shift of the plasmon band to visible frequencies, unlike that for bulk metals where the plasmon absorption is in the UV region (a plasmon is a quantum of collective oscillation of free electrons in the metals). Although nanoparticles are generally considered an invention of modern science, they actually have a very long history. Egyptians, Greeks and Romans used many colored pigments for the decoration of their buildings, ceramics and glass-ware. The use of gold and silver particles in glassblowing can be seen in the famous Lycurgus Cup exposed in the British Museum[(1)]. Gold Juice, Kim Yeh, alkimiya, alchemy, and nanogold are names called for colloidal gold, which was known since ancient times. The synthesis of colloidal gold was originally used as a method of staining glass. Modern scientific studies of colloidal gold did not begin until Michael Faraday's work in the middle of the XIX century[(2)]. It is known that colloidal gold was used in roman times to color glass with intense shades of yellow, red, or mauve, depending on

the concentration of gold, and in the Hindu Chemistry, where they used various potions with the same purpose. In the 16th century, the alchemist Paracelsus claimed to have created a potion called *Aurum Potabile* (Latin: potable gold). In 1842, John Herschel invented a photographic process called Chrysotype (from the Greek word for gold) that used colloidal gold to record images on paper. Paracelsus' work is known to have inspired Michael Faraday to prepare the first pure sample of colloidal gold, which he called 'activated gold', in 1857. He used phosphorus to reduce a solution of gold chloride. Several chemists suspected it to be a gold tin compound, due to its preparation[3,4]. Faraday was the first to recognize that the color was due to the minute size of the gold particles[2]. In 1898, Richard Adolf Zsigmondy prepared the first colloidal gold in a diluted solution[5]. Apart from Zsigmondy, Svedberg (who invented the ultracentrifugation) and Mie (who provided the theory for scattering and absorption by spherical particles) were also interested in understanding the synthesis and properties of colloidal gold[6].

From the technological point of view, the capability of tuning their optical and electronic properties by controlling the particle size and shape make them unique systems. Metallic nanoparticles exhibit a strong UV-Vis absorption band that is not present in the spectrum of the bulk metal. This absorption band is due to the collective oscillation of the conduction electrons when the size of the particles is less than the mean free path of the electron in the metal. This is known as the localized surface plasmon resonance (LSPR)[7]. The position of the surface plasmon absorption band depends mainly on the shape of the particles, on their size, and also on the dielectric constant of the environment. For spherical gold nanoparticles, the surface plasmon absorption band has a maximum at around 520 nm. For gold nanorods, the surface plasmon resonance splits into a transverse and a longitudinal mode. Whereas the transversal plasmon band depends on the

diameter of the nanorod, the longitudinal plasmon band depends linearly on the aspect ratio of the gold nanorods[8]. This means that the absorption spectrum of gold nanoparticles is tunable from 520 nm to the mid IR region depending on the size and the shape of the nanoparticles.

The general vision of nanoscience depends strongly on the ability of creating and manipulating matter at the nanoscale[9]. Figure (1-1) shows the nanoscale illustrating the relation of sizes between different known objects, ranging from the macroscopic size of a football to a subnanometric carbon 60 molecule.

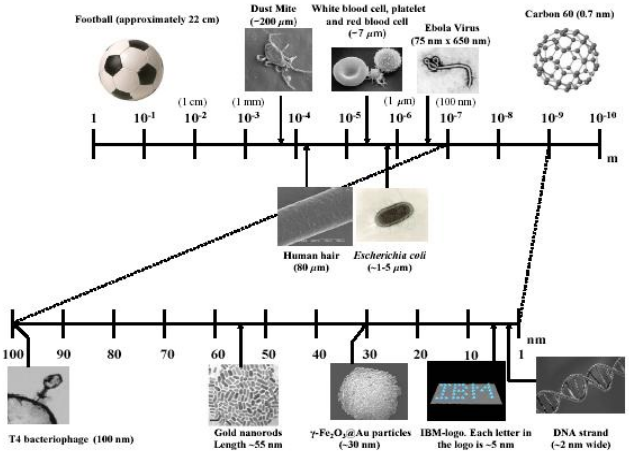

Figure 1-1: A picture showing the nanoscale in context. The length scale at the top ranges from 1 m to 10^{-10} m. The section from 10^{-7} m (100 nm) to 10^{-9} m (1nm) is expanded on the length scale below. The typical length scale of interest for nanoscience is from ≈ 100 nm down to the atomic scale.

Nanoscaled materials are usually categorized as materials having structured components with at least one dimension less than 100 nm[10]. The research in nanoscaled matter began to grow exponentially when it was recognized that the bulk properties of materials change as their sizes decrease from the bulk material to small clusters of atoms[11]. Suitable control of the properties of nanometer-scale structures can lead to new science as well as new products, devices and technologies[12]. Two principal factors are

responsible for causing the properties of nanoscaled materials to differ significantly from their behavior in bulk. Firstly, the increased relative surface area in nanomaterials and secondly, the size dependent properties which begin to dominate when matter is reduced to the nanoscale. These effects cannot only change the chemical reactivity and strength of the material, but also the electrical, optical and thermal characteristics. For example, when a metal particle decreases in size to become a nanoparticle or a nanocrystal, a great proportion of atoms is found at the surface. As catalytic chemical reactions occur at surfaces, this leads to much more reactivity when a given mass is used in nanoparticulate form. Metallic nanoparticles are built up by hexagonal (hcp) or cubic (ccp) close-packed atoms (nuclearities). This is the case in most bulk metals where a central atom is surrounded by 1, 2, 3, . .etc closed-packed shells. Table (1-1) shows a schematic illustration of metal nanocrystals of different sizes in geometrical closed-shell configurations and contains information of the percentage of surface atoms.

Full-shell Clusters	Total Number of Atoms	Surface Atoms %
1 Shell	13	92
2 Shells	55	76
3 Shells	147	63
4 Shells	309	52
5 Shells	561	45
7 Shells	1415	35

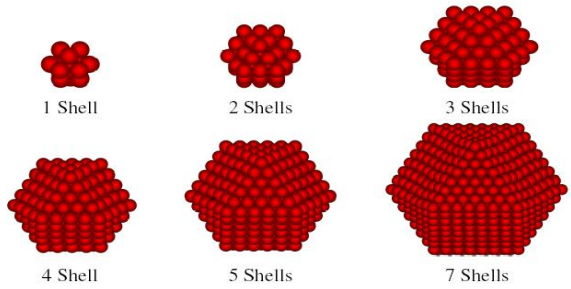

Table1-1: Schematic illustration of metal nanocrystals in geometrical closed-shell configurations with their magic numbers of atoms and the relation between the total number of atoms and the percentage of surface atoms[13].

The number of atoms per shell is $N_s = 10\ n^2 + 2$, where n is the number of the shell, and the total number of atoms (N) of the n shell is $N = (10n^3 + 15n^2 + 11n + 3) / 3$. Thus, the surface / volume ratio is Ns/N. The smallest closed-shell configuration consists of 1 + 12 = 13 atoms, the next of 13 + 42 = 55 and so on. The numbers 13, 55, 147, 309, 561 and 1451 stand for geometrical magic nuclearities corresponding to the closure of 1, 2, 3, 4, 5 and 7 shells respectively[14]. It is clear from table (1-1) that the percentage of surface atoms decreases as the closed-packed shells surrounding the central atom increases. For example, when the smallest full-shell cluster consists of 13 atoms, the surface atom ratio is 12/13= 92.3%. However, a spherical particle of 50 nm in diameter has only 6% of surface atoms left. Furthermore, it is obvious that for millimeter and micrometer-sized particles the surface atoms can be neglected. This has important practical consequences. Gold, for example, is a potentially valuable catalyst as it is inert in bulk, but it becomes highly reactive at the nanoscale range.

1-2: Synthesis of Metallic Nanoparticles.

A wide variety of different techniques are used to produce nanoparticles: wet chemical or solution method, mechanical size reduction, gas phase synthesis, etc. All of these are being used commercially and each has its own merits and drawbacks. The chemical synthesis of metal nanoparticles is the most widely and oldest method used to prepare metallic nanoparticles. This method of preparation generally involves the reduction of metal salts by reducing agents such as sodium citrate, sodium borohydride, hydrogen, carbon monoxide, acetylene, or phosphorus. The reaction proceeds then followed by nucleation and growth in the presence of stabilizing agents[15]. As it was mentioned, in the 17th century, Faraday was the first to recognize the metallic character of gold nanoparticles in solution[2]. Subsequently, a number of methods have been reported for the

synthesis of metal nanoparticles in aqueous solution involving stabilizing agents such as citrates[15,16], polymers[17,18], organic solvents such as THF[19] or THF/MeOH[20], long chain alcohols[21], surfactants[22,23], and organometallics[24]. The additions of stabilizing agents as protective capping materials are necessary to prevent aggregation and further growth of the particles. The pioneer work of Turkavich and co-workers [15, 25-27] showed that the size and the shape of the particles depend on the method of preparation and the capping material. They developed a method to prepare gold nanoparticles of different sizes and shapes depending on the reducing agent. The reduction by hot sodium citrate yields spherical particles of about 20 nm and of very narrow size distribution, while boiling with citrate acid produces large numbers of flat triangles and hexagonal plates[15], spheres and bipyramidal shapes. On the other hand, reduction with carbon monoxide gives elongated cylinders, whereas acetylene produces irregular flat plates[15].

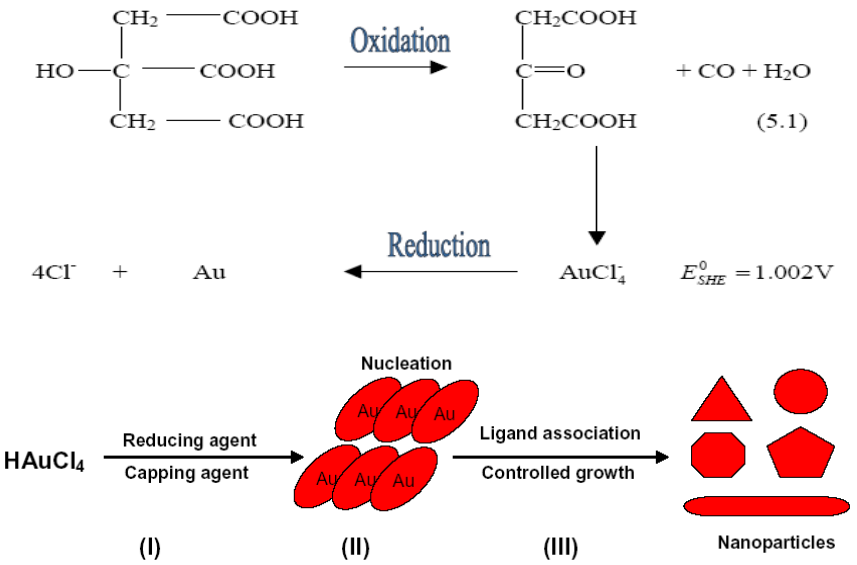

Figure 1-2: A sketch diagram of the gold nanoparticle growth.

Puntes et al.[28-31] achieved various particle shapes using the idea first described by Lohmer[22] that in sol processes monodisperse nanostructures require a single, short nucleation event followed by the slower growth on the existing nuclei[31]. This may be achieved by rapid addition of reagents into a reaction vessel containing a hot coordinating solvent. Sol-gel processes, which are used as one of the main preparation methods for the synthesis of nanoparticles, are based on inorganic polymerization reactions. This method includes four steps: hydrolysis, polycondensation, drying, and thermal decomposition[32]. Henglein[33,34]developed the radiolysis technique to prepare different shaped nanoparticles of cadmium, thallium, silver, lead, and gold. The reducing agents in this method are the free electrons or the radicals generated in solution by irradiation with a γ-ray source. Metallic nanoparticles can also be prepared by pyrolysis[35]**.** In this method, chemical precursors decompose under suitable thermal treatment into one solid compound and unwanted waste evaporates away. For example, Alivisatos and his group[31] were able to control the shape and the size of cobalt nanoparticles by the injection of an organometallic precursor into a hot surfactant mixture under an inert Ar atmosphere.

Photolysis[36], in which the chemical decomposition of organometallic precursors is induced by light or other radiant energy is another chemical method of preparation, which has been used to prepare Pd, Pt, Co and Au[37] nanoparticles. Laser irradiation has also been used to prepare gold nanoparticles by laser ablation of a metal gold plate in an aqueous micellar solution[38].

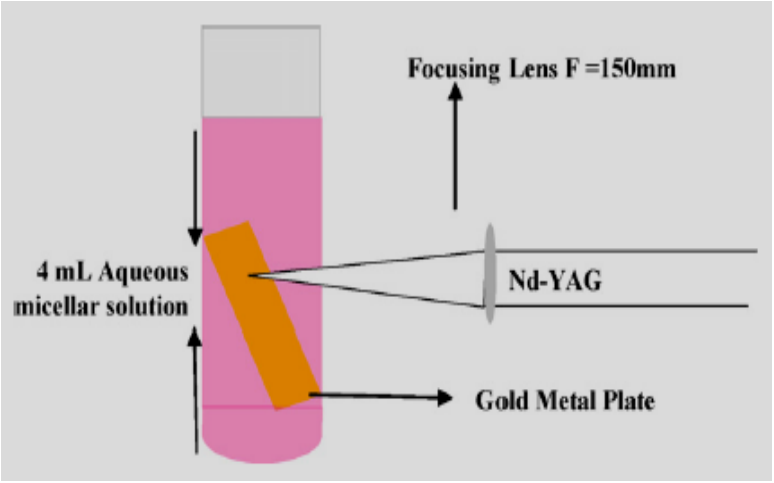

Figure 1-3: A diagram of the experimental set up for laser ablation to form gold nanoparticles.

Electrolysis[39, 40] has also been used successfully to prepare noble and transition metallic nanoparticles of different shapes. Metal nanoparticles can be also prepared by reducing metal salts in reversed micelles (water-in-oil microemulsions). Strong reducing agents such as $NaBH_4$, N_2H_4, and sometimes hydrogen gas were used for such purposes. Pt, Rh, Pd, Ir, Cu[41], Ag[16, 42-44], Au, Co[45], Ni, FeNi[46], Cu_3Au[47], CoNi[48], etc., have been synthesized using this method in which the size of the droplet containing the reactants is controlled by the ratio of the surfactant to the water concentration. Oil-in-water microemulsions have been also used for the synthesis of nanomaterials. For example, CdS and Cu nanoparticles were successfully produced using these types of microemulsions[49, 50].

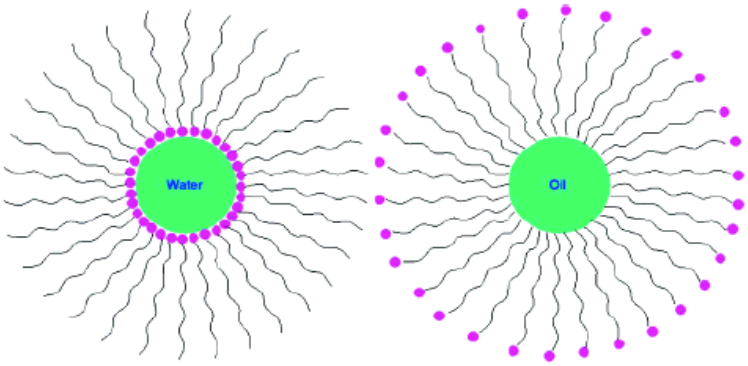

Figure 1-4: Water-in-oil and oil-in-water microemulsions.

In biological systems, shape controlled synthesis of nanomaterials has been achieved either by growth in constrained environments such as membrane vesicles or through functional molecules such as polypeptides that bind specifically to different crystallographic planes of inorganic surfaces. For example, triangular gold nanoprisms (Figure 1-5A) can be synthesized biologically[51] in high yield at room-temperature by the reduction of aqueous chloroaurate ions ($AuCl_4^-$) by the extract of the plant lemongrass (Cymbopogon flexuosus). During the reaction, a visible color change occurred from pale yellow to a ruby red, indicating the formation of gold nanoparticles. The reducing sugars (aldoses) present inside the lemongrass extract were found to be responsible for the reduction of Au^{3+}. By simple variation in the concentration of the lemongrass extract in the reaction medium, it is possible to vary the size of the nanoprisms[52], thereby the longitudinal SPR band in the nIR region can be easily tuned (Figure 1-5B). It was reported that tamarind leaf extract can also be used as the reducing agent for making gold nanotriangles[53].

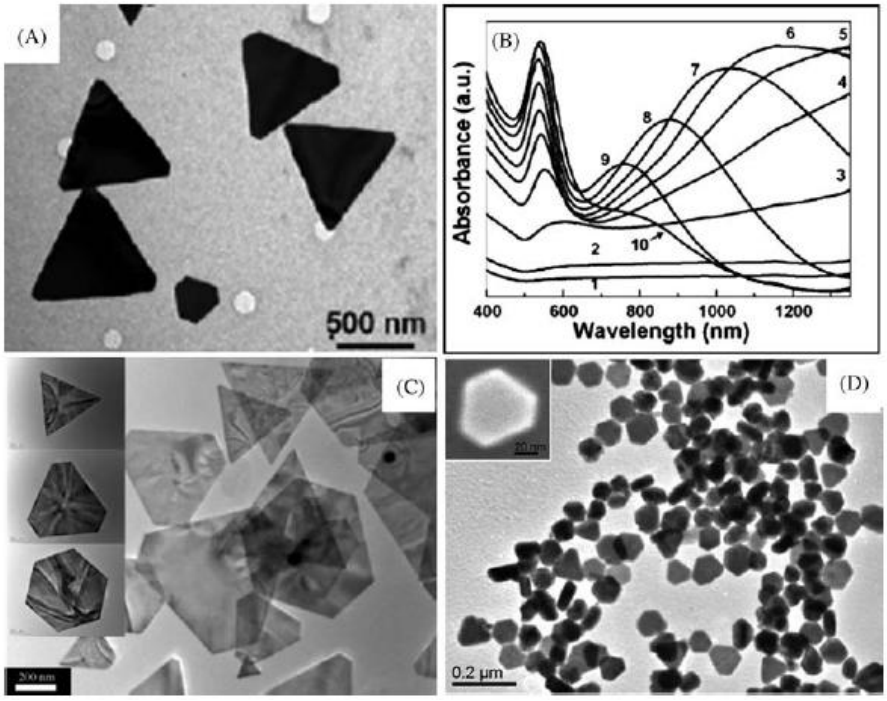

Figure 1-5: (A) TEM image of gold nanotriangles synthesized by the reduction of aqueous $HAuCl_4$ solution with lemon grass extract. B) UV-Vis-nIR spectra of gold nanoparticles synthesized by adding different amounts of lemongrass leaf extract to a $HAuCl_4$ solution. (C) TEM images of gold nanoplates synthesized by the reduction of aqueous $AuCl_4^-$ by seaweed extract. D) Single-crystalline Ag nanoplates synthesized in aqueous medium at room temperature using an extract of the unicellular green alga Chlorella vulgaris. Inset shows the SEM image of a single Ag nanoplate.

Light has been found to play an important role in shaping the nanoparticles[40]. For example, Ag triangles have been prepared photochemically by irradiation of very small Ag clusters at different wavelengths. Lasers have been also used to melt and reshape the nanocrystals formed in solution[54-56]. Spherical silver nanoparticles were converted into silver nanoprisms by exposure to UV and visible light[55,56]. It is possible to control the photochemical growth of metal nanoparticles by choosing the color of the light used to drive the reaction. The size and shape of the resulting nanoparticles can be controlled by selectively exciting the plasmon resonance of a given class of particles[56].

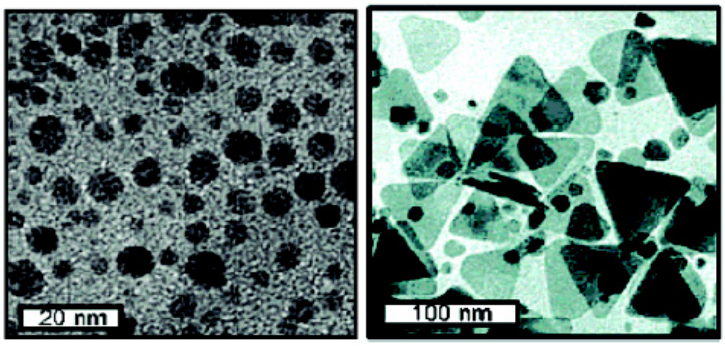

Figure 1-6: Silver nanoparticles and silver nanotriangles after illumination with a fluorescent lamp.

1-3: General methods to the synthesis gold nanorods.

One of the current major challenges in material´s research is to develop experimental recipes for the systematic control of the size and shape of metallic nanoparticles (gold nanoparticles). The size and shape of nanorods (NRs) are determined by the various experimental parameters that affect the growth mechanisms. However, the specific mechanisms governing the morphology and geometry control of the particle growth are not yet explicitly understood.

Here we will summarize the four major methods for the synthesis of gold nanorods.

1-3-1: Electrochemical method.

Gold nanorods were first prepared by the electrochemical method by Wang and co-workers[57]. This method provides a synthetic route for preparing high yields of gold nanorods. The synthesis is conducted within a simple two-electrode-type electrochemical cell, as shown in the figure (1-7). A gold metal plate is used as an anode while the cathode is a platinum plate with similar dimensions. Both electrodes are immersed in an electrolytic solution containing a cationic surfactant above its critical micelle concentration (CMC), hexadecyltrimethylammonium bromide (CTAB),

and a small amount of a much more hydrophobic cationic surfactant, tetradodecylammonium bromide (TCAB), which acts as a rod-inducing co-surfactant. The CTAB serves not only as the supporting electrolyte but also as the stabilizer for the nanoparticles, to prevent their aggregation. This method is simple, and NRs can be prepared in a short time.

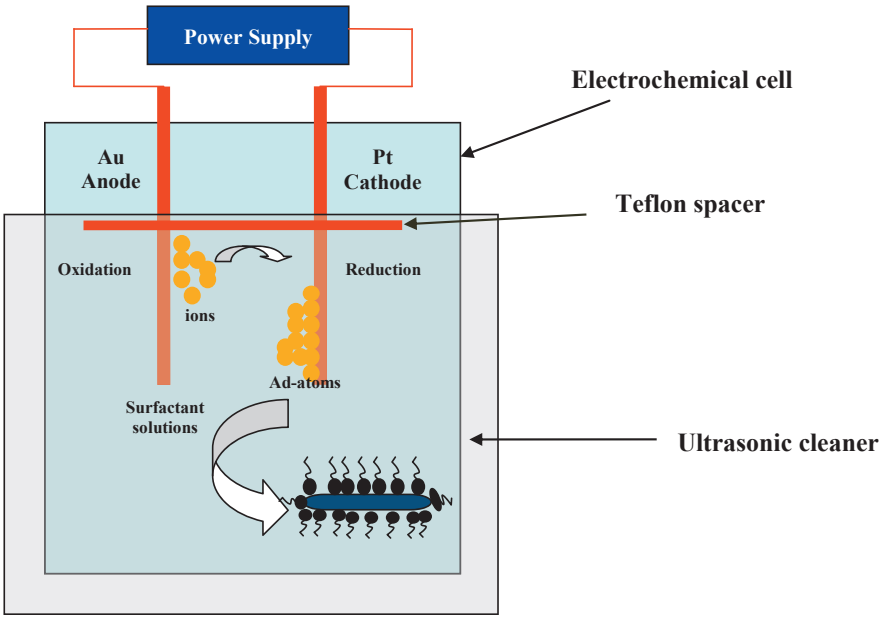

Figure 1-7: A diagram of the set-up for preparation of gold nanorods via the electrochemical method.

The electrolytic cell containing the mixed solution is then placed inside an ultrasonic bath at 36^0C. Before the electrolysis, appropriate amounts of acetone and cyclohexane are added into the electrolytic solution. Acetone is used for loosening the micellar framework facilitating the incorporation of the cylindrical-shape-inducing co-surfactant into the CTAB micelles, and cyclohexane is necessary for enhancing the formation of elongated rod-like CTAB micelles. Controlled-current electrolysis is used throughout the process with a typical current of 3mA and a typical electrolysis time of 30min. During the synthesis, the bulk gold metal anode is initially

consumed forming $AuBr_4^-$. These anions are complexed to the cationic surfactants and migrate to the cathode where reduction occurs. It is unclear at present whether nucleation occurs on the cathode surface or within the micelles. Sonication is needed to shear the resultant rods as they form away from the surface or possibly to separate the rod from the cathode surface. Another important factor controlling the aspect ratio of the Au nanorods is the presence of a silver plate inside the electrolytic solution, which is gradually immersed behind the Pt electrode. The redox reaction between gold ions generated from the anode and silver metal leads to the formation of silver ions. Wang and co-workers found that the concentration of silver ions and their release rate determined the length of the nanorods. The complete mechanism, as well as the role of silver ions, is still unknown.

1-3-2: Template method.

Gold nanorods were first synthesized by Martin and co-workers[58-60] using the template method. This method is based on the electrochemical deposition of Au within the pores of nanoporous polycarbonate or alumina template membranes. These authors showed that the Au/alumina composites can be optically transparent in the visible and also that, by changing the aspect ratio of the prepared nanocylinders, the color of composite membrane can be varied. Initially, the template method was employed to prepare microscopic electrodes by depositing Au on a polycarbonate membrane using electrochemical plating methods. Subsequently, the method has been applied not only to the synthesis of nanocomposites but also to the redispersion of the template-synthesized gold nanorods into water. Alternatively, the rods could be dispersed into organic solvents through the dissolution of the appropriate membrane followed by polymer stabilization. Schematically, the method can be explained as follows:

Initially a small amount of Ag or Cu is sputtered onto the alumina template membrane to provide a conductive film for electrode position. This is then used as a substrate onto which the Au nanoparticles can be electrochemically grown (stage I). Subsequently, Au is electrodeposited within the nanopores of alumina (stage II). The next stage involves the selective dissolution of both, the alumina membrane and the copper or silver film, in the presence of a polymeric stabilizer such as polyvinyl pyrrolidone (PVP) (stages III and IV). In the last stage, the rods are dispersed either in water or in organic solvents by means of sonication or agitation. The diameter of the gold nanoparticles synthesized coincides with the pore diameter of alumina membrane. This means that Au nanorods (GNR) with different diameters can be prepared by controlling the pore diameter of the template.

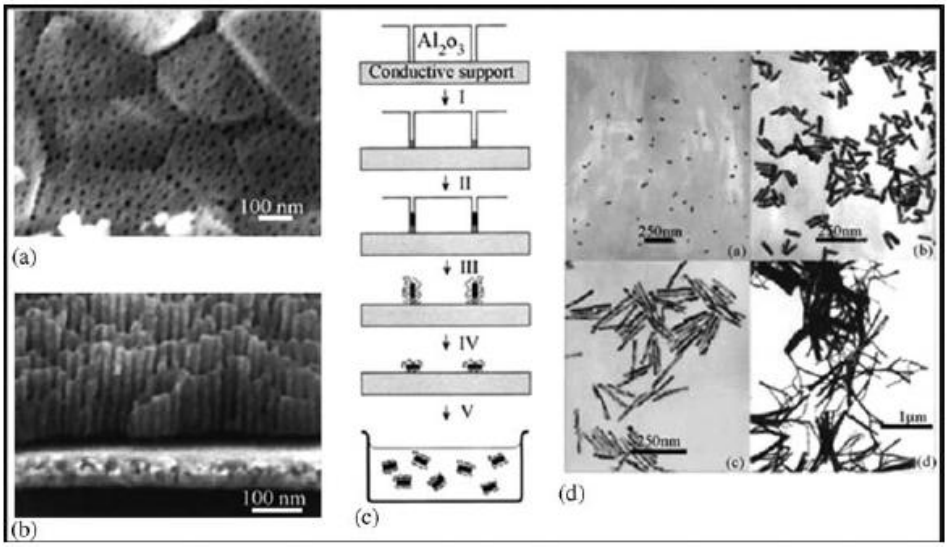

Figure 1-8: (A and B) FESEM images of an alumina membrane. (C) Schematic representation of the successive stages during formation of GNRs via the template method. (D) TEM micrographs of GNRs obtained by the template method.

The length of the nanorods can be controlled through the amount of gold deposited within the pores of the membrane.

Similar techniques have been successfully applied to the synthesis of gold nanotubes, and nanostructured composites, including tubular composites, which comprise coaxial nanotubes made of different materials. The growth mechanism is straightforward and the size and shape of the NRs are predetermined by the size and shape of the template. This method has advantages for obtaining monodisperse particles. But, the fundamental limitation of the template method is the yield. Since only monolayers of rods are prepared, even milligram amounts of rods are hard to prepare.

1-3-3: Photochemical method.

In the first observation of rod-like gold particles, UV-irradiation was used as a reducting agent and alkyltrimethylammonium chloride as a stabilizer. Synthesis conditions such as, the type and concentration of surfactant and the duration of UV-irradiation were modified to prepare NRs in great yield. Kim et al.[61] also used UV-irradiation to produce NRs. They changed the type of stabilizer to hexadecyltrimethylammonium bromide (CTAB) and tetradodecylammonium bromide. They were able to prepare NRs as the major component with the aspect ratio up to 5. The aspect ratio of the rods was controlled by the amount of silver ions (in the form of $AgNO_3$) added to the system. This process itself is highly promising for producing uniform nanorods and, more importantly, it will be useful in resolving the growth mechanism of anisotropic metal nanoparticles due to its simplicity and the relatively slow growth rate of the nanorods. In this method, a growth solution containing $AgNO_3$ and a small amount of cyclohexane (added to loosen the micellar structure) is putted in a quartz cell under UV-light for certain time. The irradiation time is the key factor to control the aspect ratio of the nanorods because with long times of irradiation, short gold nanorods are formed, which is possibly due to the transformation of the rods into the thermodynamically more stable spherical form.

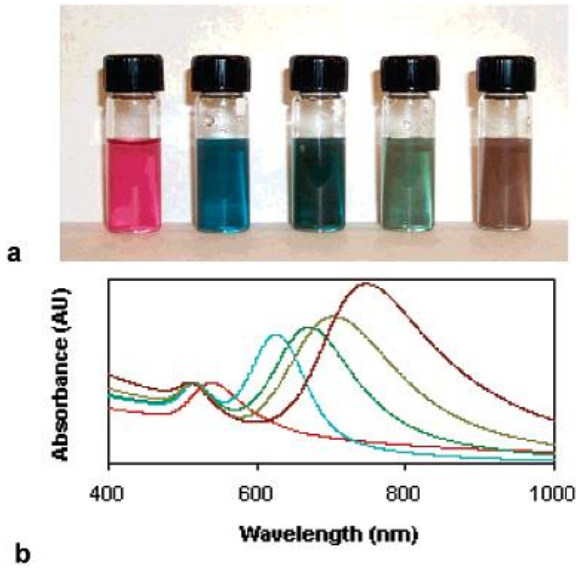

Figure 1-9: (a) Image of photochemically prepared gold nanorods solution using different concentrations of $AgNO_3$, and (b) corresponding UV-Vis spectrum.

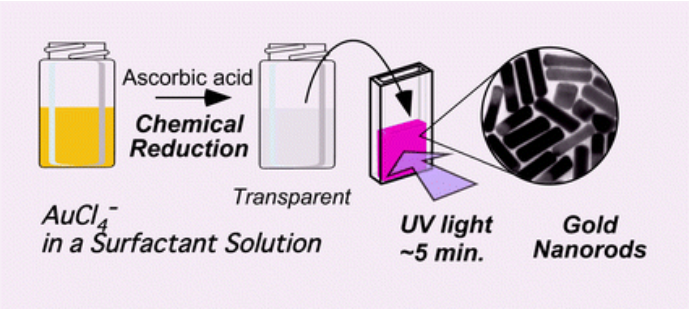

Scheme 1-1: Scheme showing the preparation of gold nanorods using UV-light irradiation.

Ahmed and Narain[62] were using a photoinitiator I-2959 as a source of ketyl radicals in addition to the growth solution and irradiated the solution with UV-light.

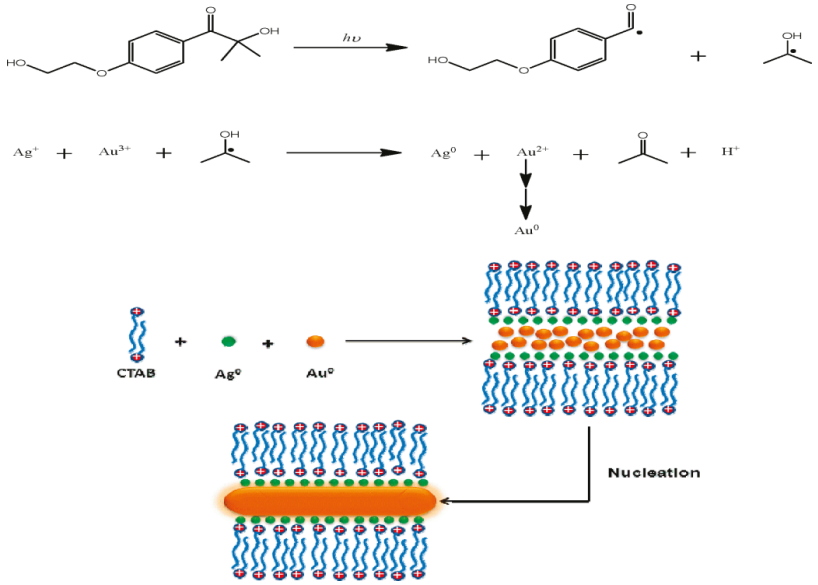

Scheme 1-2: Scheme showing the photochemical method for the generation of gold nanorods using photoinitiator.

By this UV-irradiation method, gold NRs having aspect ratio less than 5 were obtained. However, this method has a limitation to produce large quantities of NRs since the reactor size is limited.

1-3-4: Seed-growth method.

Even though a large number of methods have been used for making anisotropic nanostructures, the seed-mediated growth process is a widely used method that can yield various nanostructures such as rods, wires, triangles, stars, flowers, and so on. The seeding-growth procedure is the most popular technique that has been used for a number of years. This method is a modified form of Zsigmondy's ¨nuclear¨ method, which involved a two-step process for making nanoparticles[(63)]. In 2001, Jana et al. produced NRs in good yield by the seed-mediated method[(64)]. This method involves two steps. The first step is the synthesis of ¨seed nanoparticles¨ by a simple reduction process in which the metal salt is reduced by reducing agents in the presence of stabilizers. Sodium borohydride is the commonly used

reducing agent. Growth of seed nanoparticles into the desired shapes is the second step of this process. The growth solution contains a surfactant or a shaping agent and a mild reducing agent. In this process, metal salts are reduced on the surface of the seed nanoparticles. The surfactant molecules form suitable templates that facilitate the growth process to yield nanoparticles of desired morphology. The size of the nanoparticles can be tuned by changing the amount of seed nanoparticles added. In the case of GNRs, the size can be reduced by increasing the amount of seed particles. External agents, such as various molecules or ions can alter the growth direction of the nanoparticles and can result in the formation of various shaped nanoparticles.

Natan and co-workers proposed a seed-mediated approach to grow preformed, spherical gold nanoparticles in solution, based on the fact that gold colloid surfaces catalyze reduction of Au^{3+} by hydroxylamine (a weak reducing agent that favors the reduction of Au ions at metallic surfaces). Alternatively, seeds could be grown using sodium citrate as a reducing agent[(65)], producing Au nanoparticles with diameters between 20 and 100nm of improved monodispersity relative to the original Frens method[(65)]. Jana et al. studied the growth of citrate stabilized gold nanoparticles (12nm) by the seed-mediated method using a wide range of reducing agents and conditions[(66)]. They showed that even in the presence of seeds additional nucleation takes place[(67)]. Additional nucleation can be avoided by controlling critical parameters such as the rate of addition of reducing agent to the metal seed and metal salt solution, and the chemical reduction potential of the reducing agent.

The step-by-step particle enlargement is more effective than a one step seeding method to avoid secondary nucleation. In a typical seeded growth reaction, a previously synthesized "seed" nanoparticle is introduced to a growth solution containing a Au(III) salt, a weak reducing agent, and a

directing agent (most commonly a surfactant). Initially, the seed particles grow through the slow-diffusion of gold atoms onto their surfaces. After an initial period, the seeds grow into isometric crystals with well-defined Au {111} and Au {100} crystal faces. These enlarged seeds aggregate along these well-defined faces to form pentatwinned species that serve as the starting material for rod growth. Simultaneously with the twinning events, the surfactant begins to associate and assemble on the Au {100} faces acting as a directing agent and preventing further growth on this face. As a result, further growth occurs on the Au {111} faces and along the {110} axis, leading to an elongation of the crystal to form nanorods[68].

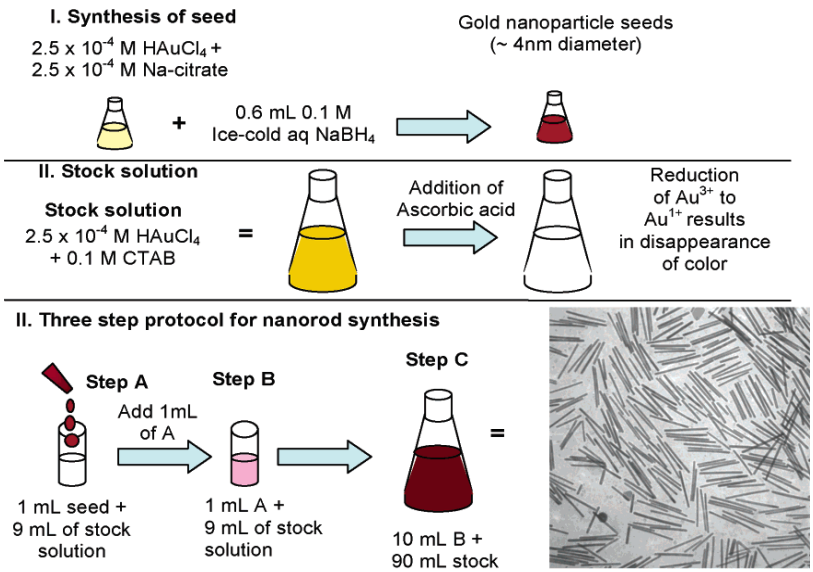

Scheme 1-3: Scheme showing the general methodology for the generation of gold nanorods.

By controlling the growth conditions in aqueous surfactant media it was possible to synthesize gold nanorods with tunable aspect ratios. It was found that addition of $AgNO_3$ influences not only the yield and aspect ratios of the gold nanorods, but also the mechanism and, correspondingly, its crystal structure. At this point, it is convenient to differentiate seed-

mediated approaches performed in the absence or in the presence of silver nitrate. As it will be discussed in the next chapters, it seems now that silver nitrate affects not just the yield of gold rods, but also plays a role in determining their crystal structure, morphology and their optical properties.
Besides the methods mentioned above, various other approaches have been attempted to produce gold NRs, such as bio-reduction[(69)] and growth of gold NRs directly on mica surface[(70)].

1-4: Optical properties of metallic nanoparticles.

The physical and chemical properties of materials are mostly determined by the motion of electrons. When the motion of electrons is confined in nanometer length scales (1-100 nm), which happens in nanomaterials, unusual effects are observed. The optical properties of metal nanoparticles are dominated by the collective oscillation of conduction electrons resulting from their interaction with electromagnetic radiation. These properties are mainly observed in Au, Ag, and Cu, in which plenty of free conduction electrons are available. The electric field of the incoming radiation induces the formation of a dipole in the nanoparticle. A restoring force in the nanoparticle tries to compensate for this, resulting in a unique resonance wavelength[(71)], which depends on a number of factors, among which particle size and shape, as well as the nature of the surrounding medium, are the most important[(72)].
Bulk Au looks yellowish in reflected light, but thin Au films look blue in transmitted light. This characteristic blue color steadily changes to orange, purple and red, as the particle size is reduced down to ~3 nm.
An understanding of the optical properties of noble metal nanoparticles holds both fundamental and practical significance. Fundamentally, it is important to systematically explore the nanostructure characteristics that cause the optical properties. Practically, the tunable optical properties of

nanostructures can be applied as materials for surface-enhanced spectroscopy [73-75], optical filters[76], plasmonic device [77,78], and sensors[79-81].

Metals absorb light primarily through electronic transitions. In metal particles, three types of transitions are possible, namely:

i. Interband transitions (excitation of electrons from the filled valence band to empty levels in the conduction band),
ii. Intraband transitions (transitions within the conduction band), and
iii. The plasmon band (a collective oscillation of the conduction electrons).

As the size of the metal particle decreases to length scales smaller than the electron mean free path (the distance in which the electron travels between scattering collisions with the lattice centers), surface plasmon band resonance develops[82]. Colloidal solutions of metallic nanoparticles such as gold or silver exhibit strong absorption in the visible region. This strong color originates from the excitation of the electrons in the conduction band and is called *surface plasmon resonance*. The surface plasmon resonance is the coherent excitation of the free surface electrons leading to a coherent oscillation[82-86].

A sketch explaining the surface plasmon absorption is shown in figure (1-10).

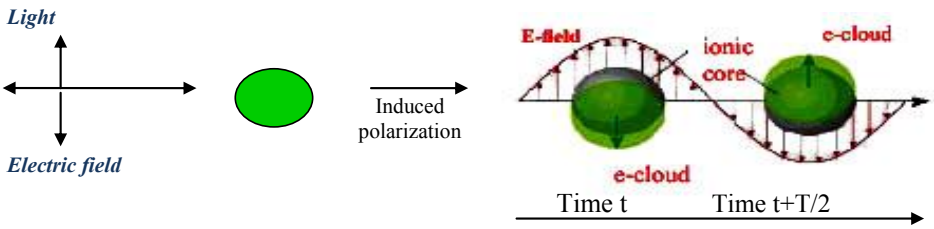

Figure 1-10: A sketch explaining the surface plasmon absorption. The electric field E of the incident light induces the polarization of the free surface electrons with respect to the heavier ionic core.

A plasmon is considered as a collective excitation for quantized oscillations of the electrons in a metal. A collective excitation is a quantized mode in many-body systems, occurring because of the cooperative motion of the whole system as a result of interaction between particles. Plasmons, as well as phonons in solids, are examples of collective excitations. The electric field of the incoming electromagnetic wave induces a polarization of the free surface electrons with respect to the heavier ionic core of the particles. A net charge difference is created at the nanoparticle surface, which acts as a restoring force. Thus a dipolar oscillation of the electrons is created with period T. This is known as surface plasmon absorption.

The oscillation frequency is determined by four factors: the density of electrons, the effective electron mass, the shape of the charge distribution, and the size of the charge distribution. The frequency and width of the surface plasmon absorption depend on the size and shape of the metal nanoparticles as well as on the dielectric constant of the metal itself and the surrounding medium[83-85,87]. Noble metals such as copper, silver, and gold have a strong visible-light plasmon resonance, whereas most other transition metals show only a broad and poorly resolved absorption band in the ultraviolet region[86,87]. This difference is attributed to the strong coupling between the plasmon transition and the interband excitation. In addition, the electrons of the conduction band of noble metals can move freely, independently from the ionic background, which acts only as scattering centers[88, 89]. This gives the electrons in noble metals a higher polarizability, which shifts the plasmon resonance to lower frequencies with a sharp bandwidth. As it was said before, the plasmon absorption in spherical gold nanoparticles occurs at about 520 nm. This absorption is absent for clusters (particles smaller than 2nm), as well as bulk gold (large particle sizes). The plasmon of gold nanoparticles originates from the oscillation of the free 6S-electrons of the conduction band (gold has the

electronic structure [Xe] $4f^{14}$ $5d^{10}$ $6s^{1}$). The rod-shaped gold nanoparticles have two absorption bands. The first one, which appears at ~ 520nm, corresponds to the oscillation of the electrons perpendicular to the long rod axis and is called transverse plasmon absorption. This band is insensitive to the nanorod length, and coincides with the surface plasmon absorption band of the gold nanospheres.

The second absorption band appears at a lower energy and is caused by the oscillation of the free electrons along the long rod axis and is known as the longitudinal surface plasmon absorption. This longitudinal plasmon band is very sensitive to the aspect ratio (length / width) of the rods where a shift to lower energy (red shift) occurs as the aspect ratio increases[(9)]. Furthermore, the relative intensity ratio of the longitudinal to the transverse mode increases with increasing aspect ratio.

The simplest theoretical approach available for modeling the optical properties of nanoparticles is the Mie theory[(82)]. In 1908, Mie solved the Maxwell's equations for the absorption and scattering of the electromagnetic radiation by spherical particles, which have sizes less than the wavelength of the incident light. One of the reasons why Mie's theory has remained important for so long is that it is the only simple, exact solution to Maxwell's equations that is relevant to particles. In addition, most of the standard colloidal preparations yield particles that are approximately spherical, and most of the optical methods for characterizing nanoparticle spectra probe a large ensemble of these particles. This leads to results that can be modeled reasonably well using the Mie theory. Recently, there has been growing interest in characterizing the optical properties of metal nanoparticles that are made using lithographic methods such as nanosphere lithography[(90)], e-beam lithography [(91)], and other methods [(92,93)], which produce well-defined sizes and nonspherical shapes without aggregation. In addition, as it was stated before, classical wet chemistry

techniques have been developed that give high yields of nonspherical particles, especially rods[94] and triangles[56]. The shapes and sizes of these particles are better characterized than in the past using electron and scanning probe microscopies allowing in some cases, the determination of the optical properties of individual nanoparticles[95].

Mie's theory and experimental spectra agree well in the size regime >20 nm until the normal incidence absorption no longer shows a plasmon resonance for bulk metals. The spectrum is composed of the sum of size-dependent absorption and scattering modes. Higher order modes become more dominant with increasing the particle size, causing the plasmon absorption band to red shift and resulting in increased bandwidth, because for larger particles, the light cannot polarize homogeneously the nanoparticles and retardation effects lead to the excitation of higher order modes[83]. The optical absorption spectra depend directly on the size of the nanoparticles, which is called the extrinsic size effect[83]. Figure (1-11) shows the absorption spectra of Au spherical nanoparticles with different sizes. As the size increases, the plasmon band shifts to the red.

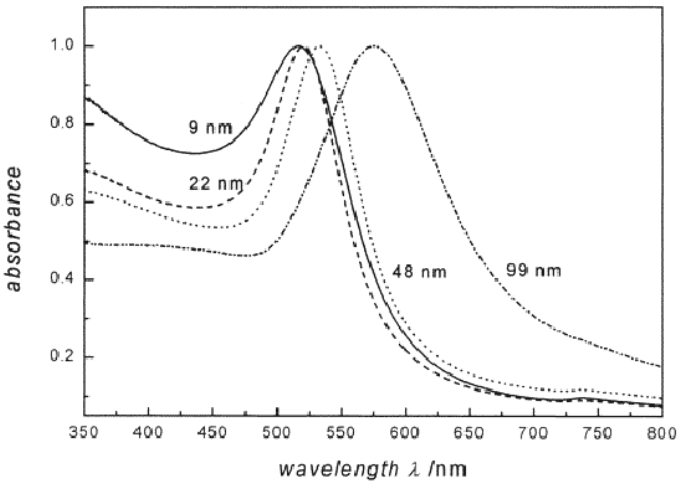

Figure 1-11: Size dependence of the plasmon absorption of spherical gold nanoparticles of different sizes.

When the size of nanoparticles is much smaller than the wavelength (<20 nm) of the interacting light, only the dipole oscillation contributes significantly to the extinction cross section. In this case the Mie's theory can be approximately expressed by the following equation (6):

$$\gamma = \frac{2 \cdot \pi \cdot N \cdot V \cdot \varepsilon_m^{3/2}}{3 \cdot \lambda} \cdot \frac{\varepsilon_2}{[\varepsilon_1 + 2 \cdot \varepsilon_m]^2 + \varepsilon_2^2} \qquad (6)$$

where, γ = extinction coefficient, V =particle volume, N = number of particles, λ = wavelength of the light, ε_m = medium dielectric constant, ε_1 and ε_2 represent the real and imaginary parts of the material dielectric function, respectively ($\varepsilon(\omega) = \varepsilon_1(\omega) + i\,\varepsilon_2(\omega)$, where ω is the angular frequency of the light). Even in this most primitive model, it is perfectly clear that the localized surface plasmon resonance spectrum of an isolated metallic nanosphere embedded in an external dielectric medium will depend on the nanoparticle material (ε_2 and ε_1), and the nanoenvironment's dielectric constant (ε_m).The resonance condition for the plasmon absorption is roughly fulfilled when $\varepsilon_1(\omega) = -2\varepsilon_m$ if ε_2 is small or weakly[83] dependent on ω. The plasmon bandwidth mainly depends on $\varepsilon_2(\omega)$.

Within this dipole approximation (eq 6), the surface plasmon resonance is independent of the particle size. This is contrary to the experimental results for metallic nanoparticles much smaller than 10 nm, where the plasmon band shows size dependence for small particles and even disappears completely for nanoparticles of ≤ 2 nm (clusters). Thus, the assumption of a free electron gas is no longer valid in the size range below 2 nm. It is in fact well established that the bandwidth is inversely proportional to the radius *r* of the particle for sizes smaller than about 20 nm[83, 96-98].Since Mie's theory has found wide applicability and has generally been successful in explaining optical absorption spectra of metallic nanoparticles

[99, 83-85], a size dependence for the quasi-static regime is introduced in eq 6 by assuming a size dependent material dielectric function $\varepsilon(\omega, R)$[100]. The dielectric function can be written as a combination of an interband term $\varepsilon_{IB}(\omega)$, accounting for the response of the d electrons, and a Drude term $\varepsilon_D(\omega)$ considering only the free conduction electrons ($\varepsilon(\omega) = \varepsilon_{IB}(\omega) + \varepsilon_D(\omega)$)[88,101]. The Drude term is given, within the free electron model, by the following expression[88].

$$\varepsilon_D(\omega) = 1 - (\omega_p^2 / \omega^2 + i\,\kappa\,\omega) \qquad (7)$$

where $\omega_p^2 = [ne^2/(\varepsilon_0 m_{eff})]$ is the bulk plasmon frequency expressed in terms of the free electron density n, the electron charge e, the vacuum permittivity ε_0, the electron effective mass m_{eff}, and κ, which is a phenomenological damping constant equals to the plasmon bandwidth. The constant κ is related to the lifetimes of all the electron scattering processes in occurring in the bulk material that are mainly due to electron-electron, electron-phonon, and electron-defect scattering. For a small particle, electron-surface scattering also becomes important, since the mean free path of the conduction electrons, typically in the range of tens of nanometers in noble metals, is limited because of the particle's boundaries. κ therefore becomes a function of the particle radius r [96,97],

$$\kappa(r) = \kappa_0 + A\,\upsilon_f/r \qquad (8)$$

where κ_0 is the bulk damping constant, υ_f is the velocity of the electrons at the Fermi energy, and A is a theory-dependent parameter that includes details of the scattering process (e.g., isotropic or diffuse scattering)[83, 96-98]. Kreibig was the first in introducing this classical picture of the limitation of the electron mean free path and found good agreement with experimental results[96]. An early quantum mechanical model developed by Kawabata and Kubo[102] also predicts a $1/r$ dependence of the plasmon bandwidth. However, their model does not treat the surface as a scatterer for the

electrons; rather the surface determines the energy of the system. Another more recent quantum mechanical model considers the adsorbed molecules on the nanoparticle surface[103]. It is suggested that the surface plasmon energy is transferred into excitation modes of the surface metal-adsorbate complex (chemical interface damping). Many more theories exist[83, 98,104-107], but all of them find a $1/r$ dependence, reflecting the importance of the ratio between the surface area and the volume. However, the slope parameter A (on the order of 1) depends on the theory[98]. Since the size dependence of the plasmon absorption in the quasi-static regime is introduced assuming a size dependent material dielectric function $\varepsilon(\omega, R)$, the related changes in the optical absorption spectra are referred to as intrinsic size effects[83].

For larger nanoparticles (>25 nm for gold particles), the extinction coefficient explicitly depends on the nanoparticle size as higher order terms contribute, which are functions of r [84, 85, 108]. For these large particles the plasmon bandwidth increases with increasing size as the wavelength λ of the interacting light becomes comparable to the dimension of the nanoparticle. This leads to an inhomogeneous polarization of the nanoparticle by the electromagnetic field. The broadening of the plasmon band is then usually ascribed to retardation effects[83]. The increased line width is also caused by the excitation of different multipole modes, which peak at different energies. This behavior is referred to as an extrinsic size effect because the size dependence enters through the full expression of Mie's theory[83].

Furthermore, when the nanoparticles are not spherical, as is always the case in real samples, the extinction spectrum will depend on the nanoparticle's in-plane diameter, out-of-plane height, and shape. The absorption spectrum of gold nanoparticles not only depends on the size and the dielectric constant of the surrounding medium but also the shape of the particles has a

very pronounced effect[9]. The rod shape dependence of the surface plasmon absorption has been studied by Gans[9]. It has been shown that the longitudinal plasmon band of the rod shaped particle is very sensitive to the aspect ratio of the rods as shown by the following equation (9)[84]:

$$\gamma = \frac{2 \cdot \pi \cdot N \cdot V \cdot \varepsilon_m^{3/2}}{3 \cdot \lambda} \cdot \sum_j \frac{(1/P_j^2) \cdot \varepsilon_2}{(\varepsilon_1 + \frac{1-P_j}{P_j} \cdot \varepsilon_m)^2 + \varepsilon_2^2} \qquad (9)$$

$$P_A = \frac{1-e^2}{e^2} \cdot \left[\frac{1}{2 \cdot e} \cdot \ln\left(\frac{1+e}{1-e}\right) - 1 \right]; \qquad P_B = P_C = \frac{1-P_A}{2}$$

where P_j are the depolarization factors for the three axes A, B, C of the rod with A > B = C. These factors are defined as:

$$e = (1- (B/A)^2)^{1/2} = (1-1/R^2)^{1/2}$$

It is then predicted that increasing the aspect ratio, the band is shifted to lower energies. The ratio A / B is known as the aspect ratio R (a.r).

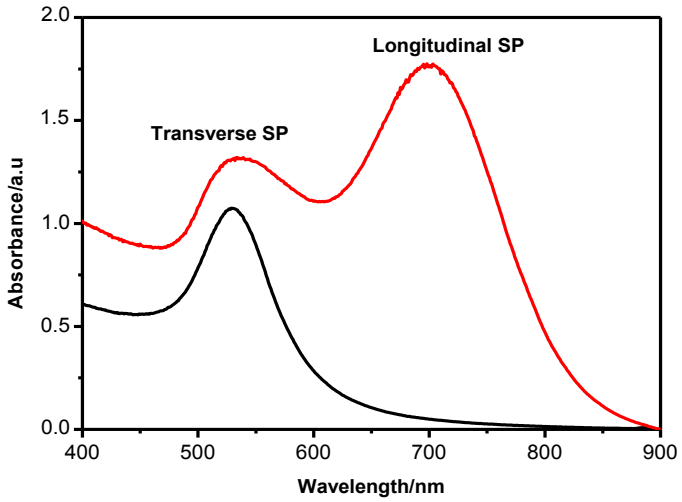

Figure 1-12: Absorption spectra of spherical and rod shape nanoparticles.

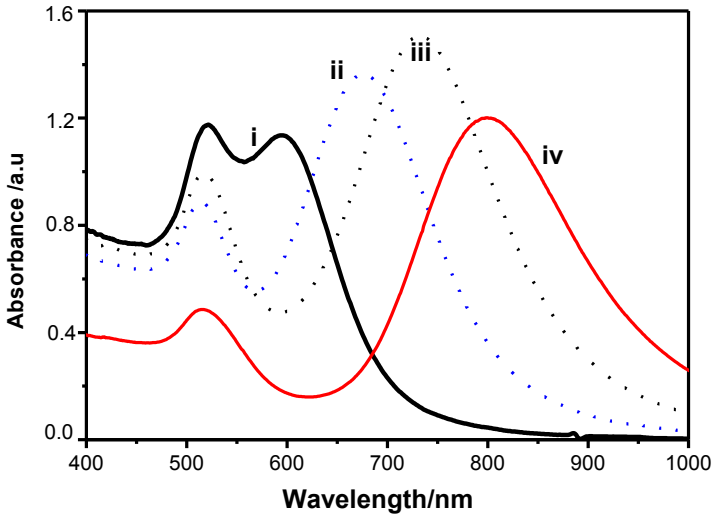

Figure 1-13: Absorption spectra showing the dependence of SP_L of the gold nanorods on the aspect ratio.

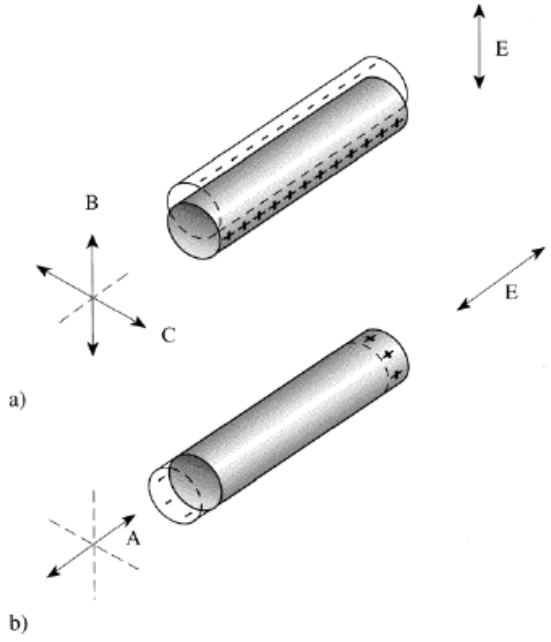

Figure 1-14: A representation diagram illustrating the optical response of rod-like nanoparticles to an electric field E. Two oscillating modes can be possible: (a) the transverse oscillation along the B or C axis and (b) the longitudinal oscillation along the A axis.

As it was previously mentioned, the plasma resonance for nanorods splits into two bands. In the case of nanoprisms[55,56], the plasmon resonance splits into three bands, a transverse mode, a longitudinal mode and a band between them. The third band and the longitudinal band depend on the length of the three axes of the prism. As the size (length and thickness) of these particles increases, these bands shift to lower energy. The higher energy bands are assigned to oscillation along the C3 axis perpendicular to the triangular faces and the broad low energy band is assigned to the in-plane oscillation on the triangular faces.

1-5: Applications of Gold Nanoparticles (nanorods).

The longitudinal surface plasmon wavelengths (LSPWs) of gold nanorods are tunable from the visible to infrared regions. Their absorption cross sections are at least five orders larger than those of conventional dyes, and the light scattering by Au nanorods is several orders larger than the light emission from strongly fluorescent dyes[109-111].The tunability of the LSPW, together with the strongly enhanced scattering and absorption at the LSPW, makes GNRs useful for the formation of many functional composite materials, for example, with hydrogels[112,113], polymers[114,115], silica[116], and bacteria[117]. The axial (transversal) surface Plasmon resonance (SSPR), though one-third that of the LSPR, is still many orders of magnitude greater than quantum dots and nanoshells, which can also be used for the described purposes. GNRs also offer advantages of good biocompatibility, facile preparation, and conjugation with a variety of biomolecular ligands, antibodies, and other targeting moieties[118]. They have therefore found wide applications in biochemical sensing[119], biological imaging, medical diagnostics, and therapeutics[120-124]. Further, GNRs have found application in materials and optics, including polarizers, filters, and to improve the storage density in compact disks.

The effectiveness of GNRs as scattering-based biomedical imaging contrast agents and as photothermal therapeutic agents is strongly dependent on their scattering and absorption cross sections. In general, high scattering cross sections are favorable for cellular and biological imaging based on dark field microscopy, while large absorption cross sections with small scattering losses allow for photothermal therapy with a minimal laser dosage. In addition, the LSPWs of GNRs are strongly desired because of their tunability in the spectral range of 650–900 nm. Light irradiation in this region can penetrate deeper in tissues and cause less photodamage than UV–visible irradiation[125]. Therefore, the ability to tailor both scattering and absorption of GNRs with different LSPWs is of ultimate importance for practical *in vivo* biomedical imaging and therapeutic applications[126-128]. Recent results show that laser writing can also be readily applicable to PVA films containing gold nanorods of various aspect ratios, and thus expanding the possibilities for practical applications of such films[129]. Further applications related to the nonlinear optical response of the nanorods can also be envisaged, but still need to be developed. However, the main use of GNRs is in electronics, catalysis and biomedical applications, which will be discussed in more in details below.

1-5-1: Electronics.

Gold is the material of choice in many electronic applications, especially in telecommunications, information technology and other high performance and safety critical applications. In the early 2000s it was estimated that around 200 tons of gold found its way into electronics and electrical components. Where the voltages are small, the circuitry complex or the required reliability is high; gold is usually the preferred choice. Gold-plated connectors are an integral part of plugs and sockets for cable terminations, integrated circuit sockets and printed circuit boards. In general, the more sophisticated the equipment and the greater the need for reliability, the

greater the requirement to exploit the advantages of gold as the material of choice. This means that in telecommunications, computers, automotive electronics and defense systems where safety is critical, gold is indispensable[130].

Gold's other main electronic use is in fine wires to connect parts of semi-conductors such as transistors and integrated circuits to ensure reliable connections between components. This bonding wire is specially refined to high purity (99.99 % gold) and would typically be thinner than a human hair (10 - 200 microns). Gold's use in electronics is based upon its high electrical conductivity along with excellent tarnish resistance. Its main applications are as conductive pastes, bonding wires, connectors and low duty contacts. Where high quality, durable, safety and reliability critical applications operating in arduous environments are concerned, gold is the optimal material. Despite the substantial growth in electronics, growth in gold demand has not kept pace due to miniaturization of devices, coupled with the use of cheaper, competing materials in the low-end, high-volume consumable electronics. The use of palladium as a cheaper alternative to gold in connectors is a typical example of this trend. The growth in automotive electronics continues; here, the electronics operate in arduous under-bonnet conditions, necessitating the use of gold. With environmental restrictions on traditional lead-tin coatings increasing, the use of electro less nickel/immersion gold protective coatings for printed circuit boards is reported to be growing[131].

1-5-2: Catalysis.

Catalysts drive many reactions, with the ability to lower the activation energy of the reaction, and thus increase the rate of reaction and the yield of the desired products. The use of nanoparticles as catalysts has increased exponentially as nanoparticle properties and reactions are better understood. The possibility of using less material and having different

properties for different shapes of nanoparticles is very attractive. Nanoparticle catalysis has been investigated for both homogeneous and heterogeneous systems. In homogeneous catalysis, Narayanan and El-Sayed[132] have shown that shapes with more corners and edge atoms have a higher reactivity than similar nanoparticles with fewer corner and edge atoms. Thus shape and crystal structure differences can lead to different catalytic rates. Research continues to observe the connection between structure and function for nanoscale catalysts. Small clusters are also found to be very catalytically active, even for materials that display very limited reactivity on the bulk scale[133]. Bulk gold is considered a noble metal, and is very unreactive in the bulk state. However, small clusters (nanoparticles smaller than approx. 2 nm) of gold are found to be catalytically active. The explanations to this include the different electronic and chemical properties of clusters than bulk material and nanoparticles. The surface support of the catalysis is also suggested to have an important influence on the catalytic activity. The crystal structure of gold has also been proposed to be important in the catalytic properties. This demonstrates the appearance of new properties for nanoparticles, which are unexpected based on bulk (and even on nanoparticle) behavior, since bulk gold has no catalytic activity, and clusters are efficient catalysts, generating further interest in nanomaterials as new functionalities are present on the nanoscale[134].

Catalysts are important to the chemical industry, with over 90 % of all the chemicals manufactured using catalysts. Among other chemicals, gold has been traditionally viewed as the exception to the other precious metals in not being very catalytically active. All that changed in the mid-to-late 80's when Hutchings and Yamada et al. demonstrated that, when prepared properly, gold can be a very active catalyst[134]. The key to this is preparation of gold as nanosized particles of around 5 nm in diameter on an

oxide support material. A major attribute is that gold catalysts are active at low temperatures. For the oxidation of carbon monoxide, important in automotive pollution control, for example, gold can catalyze the reaction at temperatures as low as -77 ^{0}C. Gold can also catalyze a range of important reactions, like oxidations, hydrogenation, the water gas shift (WGS) reaction, reduction of NOx and many others. Importantly, its uniqueness allows it to open up new application opportunities, not available to other catalytical systems. The commercial future of gold catalysts is very promising if we consider the growth in patent activity. The main part of these patents is concerned with the chemical processing, but pollution control is also strong, where catalyst manufacture and fuel cell applications are also significant[135].

In the chemical processing field, the production of acetate monomers based on gold/palladium catalysts is already a commercial application of some importance. This monomer is used in the manufacture of paints and glues. Propylene oxide manufacture is another application nearing commercialization with gold catalyst. This product is used extensively in polyurethane for the automotive and construction markets. The *in-situ* manufacture of hydrogen peroxide at point of use is another application of interest, particularly to the gold mining industry in the destruction of cyanide. The ability to manufacture peroxide on-site will save considerable transport difficulties and costs[136]. As it has been remarked in the above context, pollution control is an exciting area for gold. The use of gold catalysts in diesel-engine vehicles is a possibility since diesel engines run at lower temperatures than petrol engines, at which gold catalysts should be stable. In petrol-engine vehicles, the use of gold as a cheaper replacement for platinum based catalysts is not considered viable due to the higher temperature of operation and the instability of gold at these temperatures. However, a major area of concern is cold-start conditions when platinum

catalysts are not active until the engine warms up. A dual-box system incorporating a low light-off gold catalyst for the short period when the engine is cold, switching to the platinum catalyst as the engine reaches higher temperature is an option as emission legislation tightens[135].

Fuel cells offer potential applications for gold in both the hydrogen processing systems and as electro-catalyst constituents in the fuel cell itself. The water gas shift reaction is an important stage in producing hydrogen from hydrocarbon fuels and gold catalysts are attractive here for both technical and economical reasons. Carbon monoxide impurities in the hydrogen stream tend to poison current platinum electro-catalysts in the fuel cell and the use of gold catalysts to oxidize CO selectively under wet, hydrogen-rich conditions is another attractive application. In the fuel cell itself, there is already development in portable alkaline fuel cells for both civil and military applications where gold on carbon electro-catalysts are being used in preference to platinum-based ones[137].

The growth in demand for platinum group metals in car catalysts over 2-3 decades illustrates the potential for gold catalysts in the industrial sector and such an off-take potential has been discussed. More excitingly, other applications for gold catalysts in pollution control are emerging. Mercury emissions from electrical power plants and other big plants have led to the possibility of gold catalysts as a solution, where gold catalytically oxidizes the mercury, making its collection possible. Ozone is also another contaminant of the air at ground level raising some concern; gold catalysts could be a solution to the problem. Toxins such as dioxins are also of concern and again gold catalysts are the preferred option in catalytic combustion technology over thermal incineration. One important area attracting considerable attention is safety related – use in gas masks for mines, fire-fighters, police, military, etc. In domestic situations, the next generation of room air fresheners is likely to incorporate gold catalysts as

well as fragrances. Finally, another unusual potential application is in the storage of fruit and other products. Ripening is accelerated by ethylene, which is slowly generated and emitted by the fruit. Catalytic removal of ethylene using gold catalyst should enable longer storage, with economical benefits[138].

1-5-3: Biomedical Applications.

From its early historical use in ancient cultures, gold is becoming increasingly important in many modern medical treatments, ranging from drugs to precision implants. The claims for the medical benefits of gold date back to many thousands of years. Many ancient cultures, such as those in Asia used gold-based medicinal preparations in the treatment of ailments such as smallpox, skin ulcers and measles. Apart from the obvious use of gold alloys in dental restorations, there are also a number of direct applications of gold in medical devices. As with dental applications, these are related to the excellent biocompatibility of gold. Applications include wires for pacemakers and gold plated stents used in the treatment of heart diseases. Gold-plated stents are used to help support weak blood vessels. Many surgeons prefer gold-plated stents because these have the best visibility under X-ray. Its X-ray opacity makes it of interest for stents and its ability to be electroformed into complex shapes is being exploited for implants such as myringtomy tubes[136]. Other recent interesting developments include the use of microscopic spheres of gold for the delivery of vaccines, pharmaceuticals, or DNA portions into the human body. Gold has the required adsorptive characteristics and biocompatibility for such applications. It has also been used in the detection of deadly poisons such as anthrax, the development of gold coated lasers to aid in skin rejuvenation and the testing of vaccines. Nano-scale gold particles are also used in biomedical diagnoses. Gold is the perfect raw material for rapid testing. A rapid test is an inexpensive, disposable, membrane-based

technique that provides visual evidence of the presence of an analyte in a liquid sample. Applications for rapid tests include clinical uses (fertility tests, tumor markers, toxicology, and allergies etc.), agricultural uses (food safety, plant and crop diseases) and environmental uses (biological and environmental contamination). Overall, the superior stability, sensitivity and reproducibility of manufacture, make gold a first class raw material component for a wide range of rapid test applications[(137)].

Gold's ability to be coated with specific organic ligands, including bio-ligands such as DNA, makes it possible to engineer nanostructures in 2-D or 3-D and to tailor properties for applications such as biosensors. The ability to control particle size and ligands enables tuning for specific sensing application. Pregnancy testing kits are already on the market, based on gold nanoparticles. The use of gold nanoparticles, located at tumors and then heated by X-rays to kill tumors, looks a promising technique for cancer treatment, whilst the use of gold on silica nanoshells tuned specifically for application in blood diagnostics and even use of gold nanoparticles to kill unpleasant odors in socks are examples of potential medical applications of significance.

Considering its long history, it is a little surprising that the chemistry of gold is not well developed compared to other precious metals, and hence its applications has been hindered. However, its chemistry is now being researched and interesting properties are emerging. Paramount amongst these are two phenomena–luminescence and anti tumor activity. The properties of the former are of interest in optoelectronics, non-linear optical materials, sensors and devices. Whilst gold compounds have been long used for treatment of arthritis, recent research has shown that some compounds exhibit anti-tumor activity, making them potentially suitable for the treatment of cancer. Gold is biocompatible and has anti-microbial properties, making its use in medical and related applications of increasing

interest. More interesting is the proposed use for targeted drug delivery, known as pharmacy on a chip, where an electronic chip containing microdoses of drugs encapsulated in gold are implanted under the skin. Activating the chip allows drug release in the right location at the right time[138].

1-5-4: Assembly of gold nanorods.

Crystal structure has a crucial role in determining the assembly of nanoparticles. The surface structure of spherical gold nanoparticles are isotropic, mostly consisting of either {111} or {100} planes. The surface structure of GNRs is well studied (Figure 1-15 A and B)[139,140]. The side-faces of GNR are composed of {110} and the tips are composed of either {111} or {100}. So, by the attachment of CTAB on to {110} due to its affinity, the conventionally less stable {110} gets extra stability and, hence, this facet becomes prominent in GNRs. Also the CTAB bilayer coverage on the side-faces will be thicker. Since CTAB has a lesser affinity to {111}/{100} faces, the amount of it present on the tip is less compared to the side-faces. Figure (1-15B) shows a lattice resolved image of a GNR showing the specific planes. Due to the anisotropic crystal structure and the resultant difference in surface reactivity, anisotropic nanoparticles can be selectively functionalized to bring forth specific interactions between the constituent nanostructures giving different types of assembled structures.

Because the amount of CTAB covering the end faces is less than the other faces, functionalizing this facet is easy and specific functionalization of the end-faces can trigger the interaction of ends of NRs resulting in their end-to-end assembly. Another kind of interaction possible is that in which the sides of the NRs are interacting with each other. The removal of CTAB from the side-faces comprising of {110} facet is considered to be difficult (the free energy of the bilayer stabilization between CTAB molecules is found to be ≈ 6 kJ/mol per two methylene groups). Therefore,

functionalization of this face is done through rigorous procedures. This functionalization results in the side-to- side assembly. The different interactions as well as different kinds of resultant assemblies are depicted in Figure (1-15C). It has been proven that a side-by-side assembly leads to a blue shift in the UV-Vis spectrum whereas the end-to-end assembly gives rise to a red-shift[141]. The extent of shift in the spectra depends also on the extent of assembly. In a 2D or 3D assembly, where multiple interactions can be formed, the resultant shift can be a combination of all these interactions.

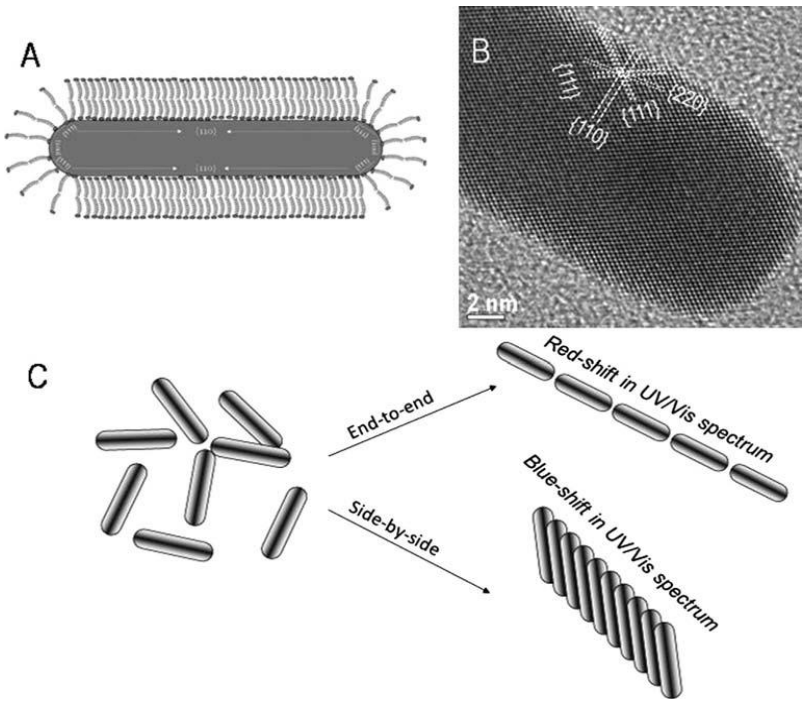

Figure 1-15 (A) Scheme of a single GNR. (B) HRTEM showing the different crystal planes and lattice structure. (C) Scheme showing the different ways of arranging the NRs.

When assembly happens without any external aid, it is called self-assembly. The GNRs are known to self assemble under optimum

conditions like concentration, pH, ionic strength, and so on. Self assembly can be modified by controlling the interactions between the constituents. This is usually done by regulating the environmental conditions such as pH and ionic strength and is often referred to as ¨programmed self-assembly¨. Chemical modifications or functionalization are usually done in order to control the assembly. Surface-functionalized GNRs, with specific molecular groups, can lead to precisely controlled self-assembled structures. It is generally observed that programmed self-assembly with functionalized NRs can be an efficient mean of nanofabrication owing to its simplicity, versatility, and low cost. The only drawback of this method is that normally provides ordered structures in small areas, and do not allow the control over large distances. Also the manipulation of the assembly after initiation is normally very difficult. But, with the advent of new techniques and with a better understanding of the system, these limitations are slowly getting overcome.

Depending upon the functionalizing molecules, the assembly can be formed through a wide variety of operating forces as covalent, hydrogen bonding, electrostatic, biochemical interaction, van der Waals and dipole interactions, and so on.

1-6: References.

1. Wagner F. E.; Haslbeck S.; Stievano L.; Calogero S.; Pankhurst Q. A.; Martinek K.-P., Nature, 2000, 407, 691.
2. Faraday M., Philosophical Transactions of the Royal Society, London, 1857, 147,145.
3. Gay-Lussac, Annalen der Physik, 1832. 101, 8, 629.
4. Berzelius, J. J., Annalen der Physik, 1831. 98, 6, 306.
5. Zsigmondy, Richard (December 11, 1926). "Properties of colloids". Nobel Foundation.http://nobelprize.org/nobel_prizes/chemistry/laureates/1925/zsigmondy-lecture.pdf. Retrieved 2009-01-23.
6. Vivek S.; Kyoungweon P.; Mohan S, Material Science and Engineering Reports, 2009, 65, 1-3, 1.
7. Norman T. J..; Kotov N. A.," Nanoparticles Assemblies and Superstructures", Ed, CRC Press, 2006, Ch.8.
8. Link S.; Mohamed M. B.; El-Sayed M. A., J. Phys. Chem. B, 1999, 103, 16, 3073.

9. Murphy C. J., Science, 2002, 298, 2139.
10. The Royal Society & The Royal Academy of Engineering. Nanoscience and Nanotechnologies, 2004. http://www.nanotec.org.uk/.
11. R. F. Service., Science, 2004, 304, 1732.
12. Rao C. N. R.; Cheetham A. K., J. Mater. Chem., 2001, 11, 2887.
13. Klabunde K. J., editor. Nanoscale Materials in Chemistry. John Wiley & Sons, Inc., 2001.
14. Kulkarni G. U.; Thomas P. J.; Rao C. N. R., Pure Appl. Chem., 2002,74, 9, 1581.
15. Turkevich J.; Stevenson P. C.; Hillier J., Discuss. Faraday Soc., 1951, 11, 55.
16. Turkevich J.; Kim G., Science, 1970, 169, 873.
17. Hirai H.; Nakao Y.; Toshima N., Chem. Lett., 1978, 545.
18. Hirai H.; Nakao Y.; Toshima N. J., Macromol. Sci. Chem., 1979, A13, 727.
19. Franke R.; Rothe J.; Pollmann J.; Hormes J.; Bonnemann H.; Brijoux W.; Hindenburg T., J. Am. Chem. Soc., 1996, 118, 12090.
20. Vidoni O.; Philippot K.; Amiens C.; Chaudret B.; Balmes O.; Malm J. O.; Bovin J. O.; Senocq F.; Casanove M., J. Angew. Chem. Int. Ed., 1999, 38, 3736.
21. Tanori J.; Pileni M. P., Langmuir, 1997, 13, 639.
22. Reetz M. T.; Lohmer G., Chem. Commun., 1996, 1921.
23. Kiwi J.; Gratzel M., J. Am. Chem. Soc., 1979, 101, 7214.
24. Sinzig J.; De Jongh L. J.; Bonnemann H.; Brijoux W.; Koppler R., Appl. Organomet. Chem., 1998, 12, 387.
25. Turkevich J.G.; Stevenson P.C., J. Colloid Sci. Suppl., 1954, 1, 26.
26. Turkevich J., Gold Bull., 1985, 18, 86.
27. Turkevich J., Gold Bull., 1985, 18,125.
28. Puntes V. F.; Zanchet D.; Erdonmez C. K.; Alivisatos A. P., J.Am. Chem. Soc., 2002, 124, 12874.
29. Puntes V. F.; Krishnan K.; Alivisatos A. P., Top. Catal., 2002, 19, 145.
30. Puntes V. F.; Krishnan K. M.; Alivisatos A. P., Appl. Phys. Lett., 2001, 78, 2187.
31. Puntes V. F.; Krishnan K. M.; Alivisatos A. P., Science , 2001, 291, 2115.
32. Murray C. B.; Norris D. J.; Bawendi M. G., J. Am. Chem. Soc., 1993, 115, 8706.
33. Henglein A., J. Phys. Chem., 1993, 97, 8457.
34. Henglein A., Chem. Rev., 1989, 89, 1861.
35. Tano T.; Esumi K.; Meguro K., J. Colloid Interface Sci., 1989, 133, 530.
36. Toshima N.; Takahashi T.; Hirai H., Chem. Lett., 1985, 1245.
37. Bronstein L.; Chernyshov D. ; Valetsky, P., *Langmuir*, 1999, 15 (1), 83.
38. Al-Sherbini E.-S.A.M., Materials Chemistry and Physics, 2010,121, 349.
39. Reetz M. T.; Helbig W., J. Am. Chem. Soc., 1994, 116, 7401.
40. Yu Y.; Chang S.; Lee C.; Wang C. R. C., J. Phys. Chem. B, 1997, 101, 34, 6661.
41. Lisieki I.; Pileni M. P., J. Phys. Chem., 1995, 99, 5077.
42. Taleb A.; Petit C.; Pileni M. P., Chem. Mater., 1997, 9, 950.
43. Barnickel P.; Wokaun A., Mol. Phys., 1990, 69, 1.
44. Chen Z. J.; Qu X. M.; Fang F. Q.; Jiang L., Colloids Surf. B, 1996, 7, 173.
45. Petit C.; Taleb A.; Pileni M. P., J. Phys. Chem. B, 1999, 103,1805.
46. Lopez-Perez J. A.; Lopez-Quintela M. A.; Mira J.; Rivas J.; Charles S. W., J. Phys. Chem. B, 1997, 101, 8045.
47. Sangregorio C.; Galeotti M.; Bardi U.; Baglioni P., Langmuir, 1996, 12, 5800.
48. Nagy J. B. Colloids Surf., 1989, 35, 201.
49. Lisieki I.; Billondet F.; Pileni M. P., J. Phys. Chem., 1996, 100, 4160.
50. Petit C.; Jain T. K.; Billoudet F.; Pileni M. P., Langmuir, 1994,10, 4446.

51. Shankar S. S.; Rai A.; Ankamwar B.; Singh A.; Ahmad A.; Sastry M., Nat Mater , 2004, 3, 482-8.
52. Shankar S. S.; Rai A.; Ahmad A.; Sastry M., Chem. Mater, 2005, 17, 566.
53. Ankamwar B.; Chaudhary M.; Sastry M., Synth React Inorg Me, 2005, 35, 19.
54. Link S.; Mohamed M. B.; El-Sayed M. A., J. Phys. Chem. A, 1999, 103, 1165.
55. Callegari A.; Tonti D.; Chergui M., Nano Lett., 2003, 3, 1565.
56. Jin R.; Cao Y.; Mirkin C. A.; Kelly K. L.; Schatz G. C.; Zheng J. G., Science, 2001, 294, 1901.
57. Chang S. S.; Shih C. W.; Chen C. D.; Lai W. C.; Wang C.R.C., Langmuir 15 ,1999, 701.
58. Foss Jr C.A.; Hornyak G.L.; Stockert J.A.; Martin C.R., J. Phys. Chem. 96, 1992, 7497.
59. Martin C.R., Science 266, 1994, 1961.
60. Martin C.R., Chem. Mater. 8, 1996, 1739.
61. Kim F.; Song J. H.; Yang P., J. AM. CHEM. SOC. 2002, 124, 14316.
62. Ahmed M.; Narain R., Langmuir, 2010, 26(23), 18392.
63. Zsigmondy R. The chemistry of colloids. New York: John Wiley; 1917.
64. Jana N.R,; Gearheart L.; Murphy C.J. , J Phys Chem B, 2001,105,4065.
65. Brown K.R.; Lyon L.A.; Fox A.P.; Reiss B.D.; Natan M.J., Chem.Mater. 12, 2000, 314.
66. Jana N.R.; Gearheart L.; Murphy C.J., Chem. Mater. 13, 2001, 2313.
67. Watzky M.A.; Finke R.G., J. Am. Chem. Soc. 119, 1997, 10382.
68. Murphy C.J.; San T.K..; Gole A.M.; Orendorff C.J.; Gao J.X.; Gou L.; Hunyadi S.E.: Li T., *J. Phys. Chem. B,* 2005,109,13857.
69. Canizal G.; Ascencio J. A.; Gardea-Torresday J.; Yacaman, M. J. *Journal of Nanoparticle Research,* 2001, *3,* 475.
70. Mieszawska A. J.; Zamborini F. P. *Chemistry of Materials,* 2005, *17,* 3415.
71. Pal A., Talanta, 1998, 46, 583.
72. Liz-Marzn L.M., Materials Today's, 2004, 26.
73. Mulvaney P., Langmuir, 1996, 12 , 788.
74. Freeman R. G.; Grabar K. C.; Allison K. J.; Bright R. M.; Davis J. A.; Guthrie A. P.; Hommer M. B.; Jackson M. A.; Smith P. C.; Walter D. G.; Natan M. J., Science, 1995, 267, 1629.
75. Kahl M.; Voges E.; Kostrewa S.; Viets C. ; Hill W., Sens. Actuator B Chem., 1998, 51, 285.
76. Dirix Y.; Bastiaansen C.; Caseri W. ; Smith P., Adv. Mat., 1999, 11, 223.
77. Maier S. A.; Brongersma M. L.; Kik P. G.; Meltzer S.; Requicha A. A. G. ; Atwater H. A., Adv. Mat., 2001, 13, 1501.
78. Maier S. A.; Kik P. G.; Atwater H. A.; Meltzer S.; Harel E.; Koel B. E. ; Requicha A. A. G., Nat. Mat., 2003, 2, 229.
79. Haes A. J., Van Duyne R. P., J. Am.Chem. Soc., 2002, 124, 10596.
80. Mucic R. C.; Storhoff J. J.; Mirkin C. A. ; Letsinger R. L., J. Am. Chem. Soc. , 1998, 120, 12674.
81. Hirsch L. R; Jackson J. B.; Lee A.; Halas N. J. ; West J. L., Anal. Chem., 2003, 75, 2377.
82. Mie G., Ann. Phys, 1908, 25, 329.
83. Kreibig U.; Vollmer M., "Optical Properties of Metal Clusters", Springer, Berlin, 1995.
84. Papavassiliou G.C., Prog. Solid State Chem., 1979, 12, 185.

85. Bohren C.F.; Huffman D.R., "Absorption and Scattering of Light by Small Particles", Wiley, New York, 1983.
86. Creighton J. A.; Eadon D. G., J. Chem. Soc., Faraday Trans., 1991, 87, 3881.
87. Link S.; El-Sayed M. A., Annu. Rev. Phys. Chem., 2003, 54, 331.
88. Ashcroft N. W.; Mermin N. D., Solid State Physics, Saunders College, Philadelphia, PA ,1976.
89. Schmid G.;" Metals. In Nanoscale Materials in Chemistry"; Klabunde K. J.; Ed., Wiley-Interscience, New York, 2001, Chapter 2, 15.
90. Van Duyne R. P.; HulteenJ. C.; Treichel D. A., J. Chem. Phys., 1993, 99, 2101.
91. Kahl M.; Voges E.; Hill W., Spectrosc. Eur., 1998, 10, 12.
92. Hornyak G. L.; Patrissi C. J.; Martin C. R.; Valmalette J. C.; Dutta J.; Hofmann H., Nanostruct. Mater, 1997, 9, 575.
93. Collier C. P.; Saykally R. J.; Shiang J. J.; Henrichs S. E.; Heath J. R., Science, 1997, 277, 1978.
94. Petroski J. M.; Wang Z. L.; Green T. C.; El-Sayed M. A., J. Phys. Chem. B, 1998, 102, 3316.
95. Michaels A. M.; Nirmal M.; Brus L. E., J. Am. Chem. Soc., 1999, 121, 9932.
96. Kreibig U.; Fragstein C., Z. Phys., 1969, 224, 307.
97. Kreibig U. Z., Phys., 1970, 234, 307.
98. Kreibig U.; Genzel U., Surf. Sci., 1985, 156, 678.
99. Shaw D. J., Introduction to Colloid and Surface Chemistry. Butterworths,3rd edition, 1989.
100. Alvarez M. M.; Khoury J. T.; Schaaff T. G.; Shafigullin M. N.; Vezmer I.; Whetten R. L., J. Phys. Chem. B, 1997, 101, 3706.
101. Kittel C.," Introduction to Solid State Physics", New York, Wiley, 1996.
102. Kawabata A.; Kubo R., J. Phys. Soc. Jpn., 1966, 21, 1765.
103. Persson N. J., Surf. Sci., 1993, 281, 153.
104. Yannouleas C.; Broglia R. A., Ann. Phys., 1992, 217, 105.
105. Cini M., J. Opt. Soc. Am., 1981, 71, 386.
106. Genzel L.; Martin T. P.; Kreibig U., Z. Phys. B, 1975, 21, 339.
107. Kraus W. A.; Schatz G. C., J. Chem. Phys., 1983, 79, 6130.
108. Kerker M.," The Scattering of Light and Other Electromagnetic Radiation", Academic, New York, 1969.
109. Mohamed M. B.; Ismael K. Z.; Link S.; El-Sayed M. A., J. Phys. Chem. B, 1998, 102, 9370.
110. Lee K.-S.; El-Sayed M. A., J. Phys. Chem. B, 2005, 109, 20331.
111. Jain P. K.; Lee K. S.; El-Sayed I. H.; El-Sayed, M. A., J. Phys. Chem. B, 2006, 110, 7238.
112. Chen W. R.; Adams R. L.; Carubelli R.; Nordquist R. E., Cancer Lett., 1997, 115, 25.
113. Karg M.; Pastoriza-Santos I.; Pérez-Juste J.; Hellweg T.; Liz-Marzán L. M, Small, 2007, 3, 1222.
114. Pérez-Juste J.; Rodríguez-González B.; Mulvaney P.; Liz- Marzán L. M., Adv. Funct. Mater., 2005, 15, 1065.
115. Murphy C. J.; Orendorff C. J., Adv. Mater, 2005, 17, 2173.
116. Chon J. W. M.; Bullen C.; Zijlstra P.; Gu, M., Adv. Funct. Mater., 2007, 17, 875.
117. Berry V.; Gole A.; Kundu, S.; Murphy C. J.; Saraf R. F. , J. Am. Chem. Soc., 2005, 127, 17600.
118. Katz E.; Willner I , Angew. Chem., Int. Ed., 2004, 43, 6042.

119. Sudeep P. K.; Joseph S. T. S.; Thomas K. G., J. Am.Chem. Soc., 2005, 127, 6516.
120. Wang H. F.; Huff T. B.; Zweifel D. A.; He W.; Low P. S.; Wei A.; Cheng J.-X. , Proc. Natl. Acad. Sci. U.S.A., 2005, 102, 15752.
121. Durr N. J.; Larson T.; Smith D. K.; Korgel B. A.; Sokolov K.; Ben-Yakar A. , Nano Lett., 2007, 7, 941.
122. Huang X. H.; El-Sayed I. H.; Qian W.; El-Sayed M. A., Nano Lett., 2007, 7, 1591.
123. Huang X. H.; El-Sayed I. H.; Qian W.; El-Sayed M. A. , J. Am. Chem. Soc., 2006, 128, 2115.
124. Chen C.-C.; Lin Y.-P.; Wang C.-W.; Tzeng H.-C.; Wu C.-H.; Chen Y.-C.; Chen C.-P.; Chen L.-C.; Wu Y.-C. , J. Am.Chem. Soc., 2006, 128, 3709.
125. Weissleder R. A, Nat. Biotechnol. , 2001, 19, 316.
126. Hirsch L. R.; Stafford R. J.; Bankson J. A.; Sershen S. R.; Rivera B.; Price R. E.; Hazle J. D.; Halas N. J.; West J. L. , Proc. Natl. Acad. Sci. U.S.A,. 2003, 100, 13549.
127. Loo C.; Lowery A.; Halas N.; West J.; Drezek R., Nano Lett., 2005, 5, 709.
128. Chen J. Y.; Saeki F.; Wiley B. J.; Cang H.; Cobb M. J.; Li Z.- Y.; Au L.; Zhang H.; Kimmey M. B.; Li X. D.; Xia Y. N. , Nano Lett. , 2005, 5, 473.
129. P´erez-Juste J.; Pastoriza-Santos I.; Liz-Marz´an L. M.; MulvaneyP., Coordination Chemistry Reviews, 2005, 249, 1870.
130. Bauer L. A.; Birenbaum N. S.; Meyer G. J., *J. Mater. Chem*., 2004, 14, 517.
131. Hutchings J., *Gold Bull*., 2004, 37, 3.
132. Narayanan R.; EI-Sayed M.A., *J. Phys. Chem. B*, 2005, 109, 12663.
133. Knosp H.; Holliday R.J., Corti C.W., *Gold Bull*., 2003, 36, 93.
134. Haruta M.; Kobayashi T.; Sano H.; Yamada N., *Chem Lett*., 1987, 4, 405.
135. Pattrick G.; van der Lingen E.; Corti C.W.; Holliday R.J.; Thompson D.T., *Topics Catalysis*, 2004, 30, 273.
136. Corti C.W.; Holliday R.J., *Gold Bull*., 2004, 37, 20.
137. Corti C.W.; Holliday R.J.; Thompson D.T., *Appl. Catalysis A: General*, 2005, 291,253.
138. Corti C.W.; Holliday R.J., *Materials World*, 2003, 11, 12.
139. Johnson C.J.; Dujardin E.; Davis S.A.; Murphy C.J.; Mann S., J Mater Chem., 2002, 12, 1765-70.
140. Perez-Juste J.; Liz-Marzan L.M.; Carnie S.; Chan DYC.; Mulvaney P., Adv Funct Mater, 2004, 14, 571.
141. Sau T.K.; Murphy C.J., Langmuir, 2005, 21, 2923.
142. Nikoobakht B.; El-Sayed M. A., Chem. Mater. 2003, 15, 1957.

Chapter Two
Experimental Chapter

Chapter II
General Experimental section

In this chapter, we will describe the different preparation methods for the production of gold nanoparticles with different sizes and shapes. The experimental methods used for the characterization of these particles will be also discussed in this chapter together with the explanation of the different methods used to study the thermal and photostability of these particles. We will start firstly writing the materials used in the preparation methods.

2-1: Materials.

The materials used were:

1- Surfactants:

- Cetyltrimethylammonium bromide (CTAB, Fluka, 99%)
- Cetyltrimethylammonium bromide (CTAB, Aldrich, ≥ 98%)

2- Gold (III) chloride hydrate, (Aldrich, 99.999% metal basis).

3- Reducing agents:

- Sodium borohydride (($NaBH_4$), Riedel-de Haën, 95%)
- L-ascorbic acid (Sigma-Aldrich, 99%)

4- Trisodium citrate (Sigma-Aldrich, 99%)

5- Silver nitrate ($AgNO_3$, Aldrich, A.C.S. reagent, 99%)

6- Polyvinyl pyrrolidone (PVP-K30, with an average molecular weight = 30000 to 40000, Fluka)

7- Silver atomic quantum clusters dispersed in water at a concentration of 1 mg/l (Ag-clusters, NGAP AQC Ag-1102-W, Nanogap, Spain).

The details of the characterizations and the properties of these silver clusters, provided by the supplier, are :

Ag-1102-W	*Size distribution*	*Product Form*	*Concentration*	*Colour*
	-	Water solution	1 mg/L (determined by FAAS)	Greenish; clear
	Volume	*Density*	*Density of particles*	*Storage*
	5 ml	1,0 g/ml	-	Refrigerated (4°C – 8°C) and protected from light
Observations: Contains NaCl (< 11 mM)				

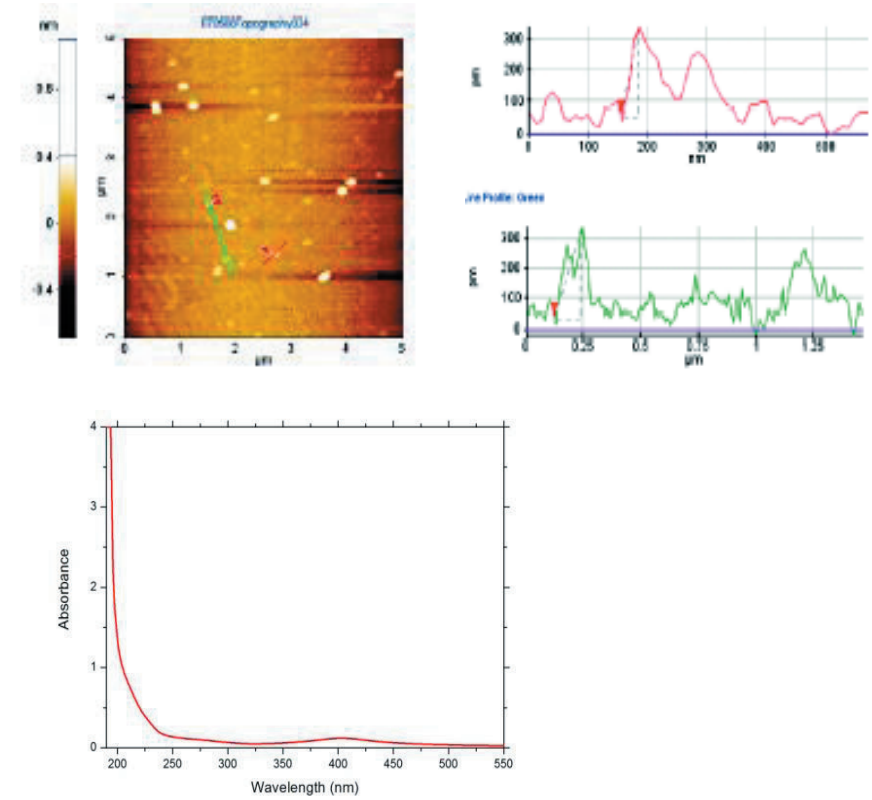

Figure 2-1: Absorption spectra showing the Nanogap Ag-clusters with an AFM picture of the clusters deposited on mica (mean square roughness ~150 pm) and the profiles throughout the red and green lines depicted on the AFM picture.

Distilled water (18 MΩ) was used in all the experiments. All glassware was firstly washed with aqua regia (3:1 ratio by volume of HCl and HNO_3), and then several times with distilled water before using.

2-2: Instrumentation.

2-2-1: Nanoparticle characterization and optical absorption.

One of the significant challenges in the gold nanoparticle synthesis is the right characterization in order to establish the average size and shape, ligand shell composition and impurity profile of the synthesized material. Developing an accurate picture of the formed gold nanoparticles allows for a greater understanding of the optical and electronic properties and assists in the development of structure-function relationships. To determine the size and shape of the produced gold nanoparticles, transmission electron microscopy (TEM) and UV-Visible spectroscopy (UV-Vis) were used. Atomic Force Microscopy (AFM) was also used to determine the size of the clusters and seeds of gold and silver particles.

Thermal gravimetric analysis (TGA) and Differential scanning calorimetry (DSC) were used to determine changes in the heat flow and weight of Au NRs capped with CTAB.

Using this string of characterization techniques, it is possible to develop a fairly accurate picture of the gold nanoparticle samples, though the development of new characterization methods is an active area of research.

A) Absorption spectra were recorded with a Perkin-Elmer Lambda 40 spectrometer, Thermo Evolution300 UV-Visible spectrophotometer and Hewlett-Pack 8452A Diode - Array spectrophotometer to analyze the optical properties of gold nanoparticles, primarily through the plasmon resonances. For spherical particles the plasmon band is located at ~520 nm; however, the location is shifted due to changes in the dielectric constant of the solvent, ligand shell, core

size and aggregation of particles. In the case of nonspherical particles, there is typically more than one plasmon resonance peak due to the asymmetry, allowing for the assessment of the shape as well. Because of the convenience of the technique, UV-Vis spectrophotometry allows for a rapid and qualitative assessment of the shape of the formed particles, and was used throughout the thesis.

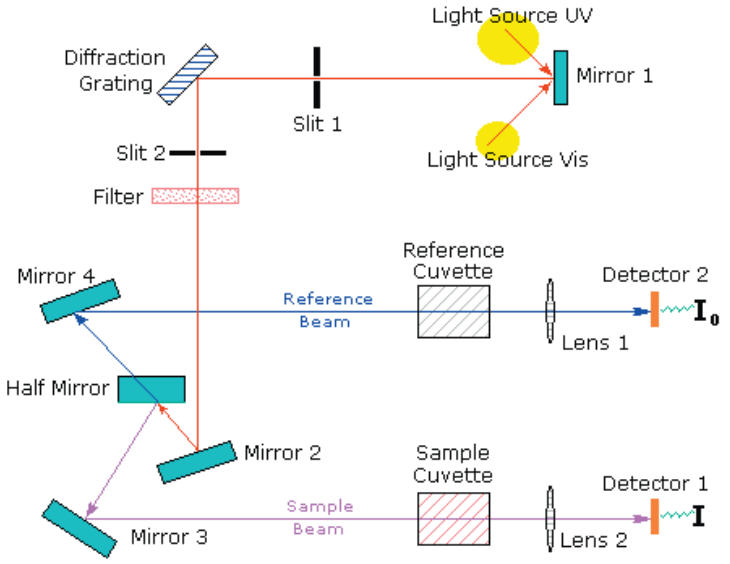

Figure 2-2: A diagram showing the components of a typical UV-Vis spectrometer.

B) The size and shape of the nanoparticles were determined by Transmission Electron Microscopy (TEM) with a Philips CM20 microscope, operating at an accelerating voltage of 200 kV. For this purpose, a drop from a diluted sample solution was deposited onto an amorphous carbon-copper grid and left to evaporate at room temperature. TEM allows for a quantitative determination of those characteristics including the direct visualization of the metallic core. Additionally, electron diffraction experiments can also be carried out, allowing for an assessment of the atomic packing and orientation. In order to ensure that there is no bias in the size

analysis, several images representing diverse regions of the TEM grid and several hundreds to thousands of nanoparticles were counted to obtain the size distribution of the NPs. This helps to avoid artificial size separation or skewing as a result of drying effects or aggregation.

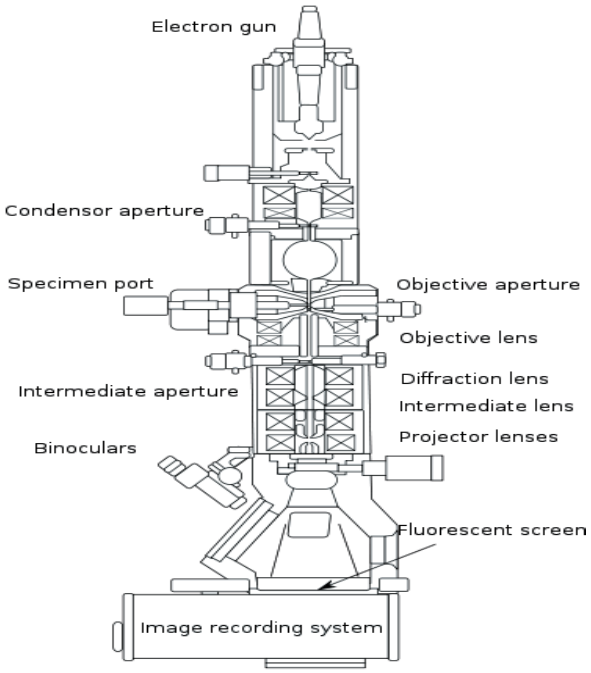

Figure 2-3: A diagram showing the components of a typical TEM.

C) The size of the seeds and clusters was determined by Atomic Force Microscopy (AFM). AFM measurements were conducted in normal atmosphere at room temperature using a XE-100 instrument (Park Systems) in non-contact mode. Scanning tips were aluminum-coated silicon ACTA from Park Systems with a resonance frequency of 325 kHz. For AFM imaging, 10 µL of a diluted sample was dropped onto a fresh mica sheet (SPI Supplies, Grade V-1 Muscovite), thoroughly washed with milli-Q water and dried under nitrogen flow.

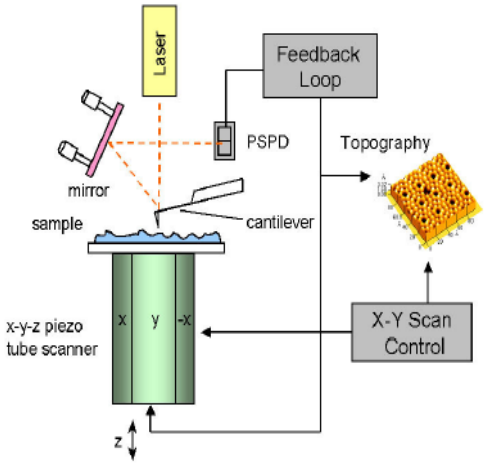

Figure 2-4: A diagram showing the components of a typical AFM.

D) Mass spectrophotometry with electrospray ionization (ESI-MS) was also used in the characterization of gold nanoclusters. ESI-MS has the ability to directly analyze and provide high mass measurement accuracy for the estimation of cluster sizes.

2-2-2: Thermal and photostability of gold nanoparticles.

To study the thermal- and photo-stability of different shapes of gold nanoparticles and their shells the following procedure was carried out:

The change in the absorption spectrum of a solution of nanorods (3ml) was determined at five temperatures ranging from 40 to 100 ^{0}C in a water bath (Transonic 46 O/H, USA). At each temperature, the change in the absorption spectrum was followed as a function of time after the sample solution was immersed into the thermostatted bath at a fixed temperature. The rate constant of the change of the shape, at each of temperature, was determined by following the changes in the absorption and wavelengths of the surface plasmon bands. From the values of the rate constants at different temperatures, the activation energy of the shape transformation

was determined. To heat the water samples above 100ºC few drops of glycerol were added to the sample immersed in an oil bath.

Photostability of gold nanoparticles was tested by exposure of 3ml of the solutions in a quartz cuvette to UV light source (UVP LIGHT SOURCES, 254nm, Ultra-Violet Products Ltd, UK) and measuring the changes of the absorption spectra using the UV-Vis Spectrophotometer.

The effect of laser on gold nanoparticles was tested by exposure of 3ml of the solutions in a quartz cuvette to three different nanosecond laser beams:

2-2-2-1. Pulsed Nd:YAG laser, working in Q-switch regime.

The laser used was a spectra-physics laser (model Quanta-Ray GCR-130) with a repetition frequency of 50 Hz, pumped by lamps. The diameter of the beam is around 1cm in the fundamental mode and 0.8cm in the second and third harmonic.

Wavelength	Pulse width (FWHM)
1064 nm (fundamental)	8-9 ns
532nm (second harmonic)	6-7 ns
355 nm (third harmonic)	5-6 ns

Table 2-1: Physical specifications of the pulsed Nd:YAG laser.

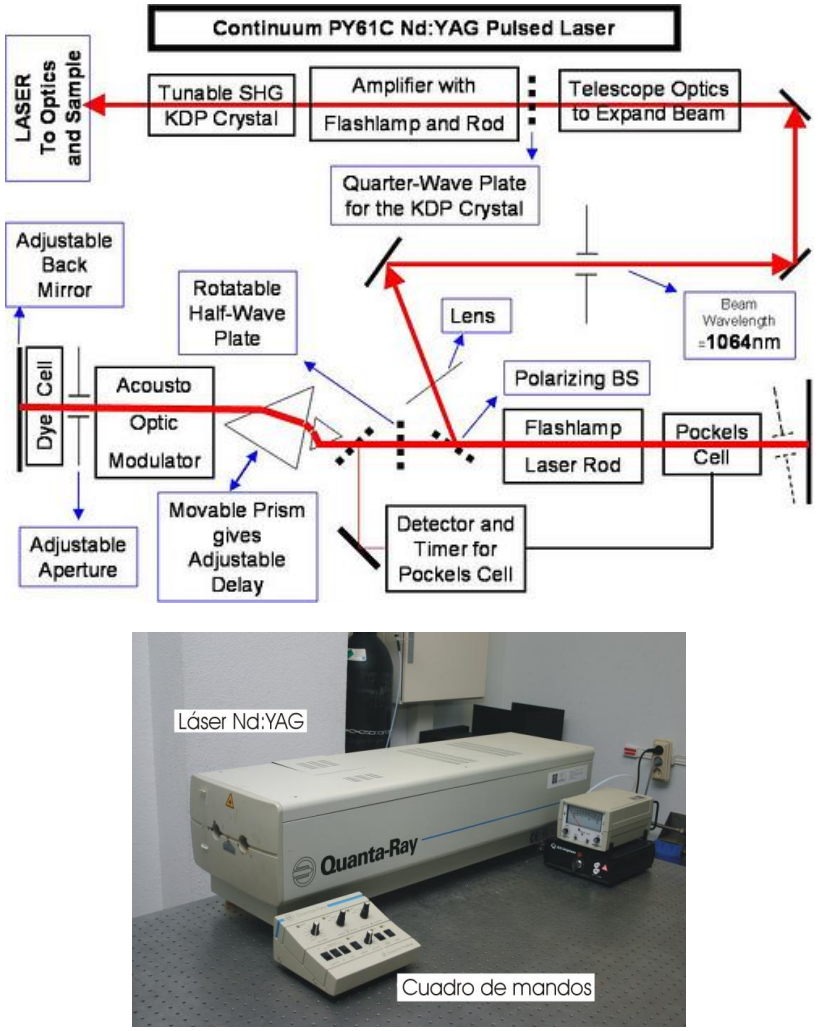

Figure 2-5: A diagram showing the pulsed Nd:YAG laser setup**.**

2-2-2-2: Pulsed Nd: YVO_4 laser, working in Q-switch regime.

The laser used was a ROFIN laser (model RSM Poweline 20E/LP), pumped by diode in the back part. The working parameters of the laser beam are controlled by commercial software. It is possible to change the power, repetition frequency (number of pulses by second),…etc. The nominal value of the laser beam diameter is 30 mm, approximately. In order to address the output beam as desired, the beam is deflected

continuously by two galvanometric mirrors. The laser is emitting at the fundamental wavelength (1064nm) and the pulse width has a value of 12 ns (FWHM). The beam power, the repetition rate and the scanning velocity of the galvanometers, can be adjusted by a commercial software tool, which allows an accurate control of the process. The beam is focused on the sample by a lens with 100 mm focal length, which assures a homogeneous density of the power in an area of 80 x 80 mm^2. Other parameters can be adjusted by the software, such as the superposition of continuous beam scans (the angle of beam scans). Also the same laser was used in CW-mode (at zero frequency).

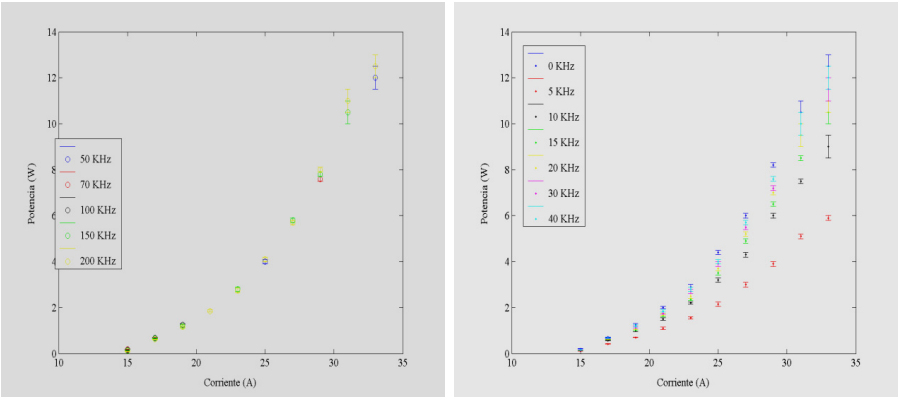

Figure 2-6: Relation between the applied intensity ("corriente") and the output power.

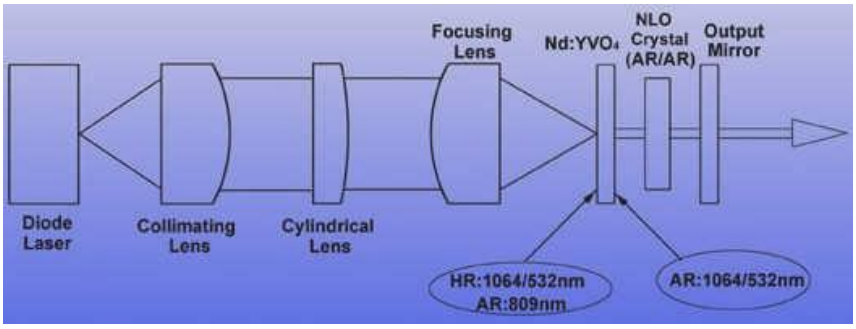

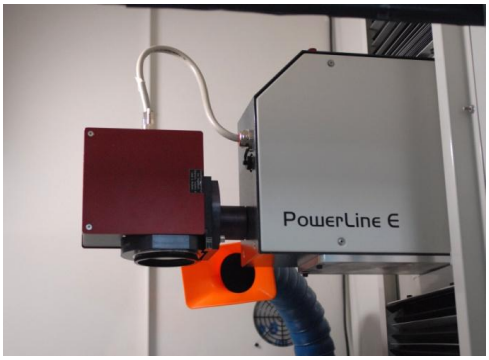

Figure 2-7: A diagram showing the pulsed Nd: YVO_4 laser setup.

2-2-2-3: Nd: YAG laser (continuum SLI-10).

The laser (10 Hz) generated from the second harmonic generation of the Nd-YAG laser (continuum SLI-10) at $\lambda = 1064/2 = 532$ nm were focused onto a quartz cell containing the sample solution of gold nanoparticles. The energy of the Nd-YAG laser was 100mJ measured with a power energy meter (molectron-EPM 2000:Tar5).

The photostability of the gold nanoparticles was followed by measuring the changes in absorption spectra as a function of time.

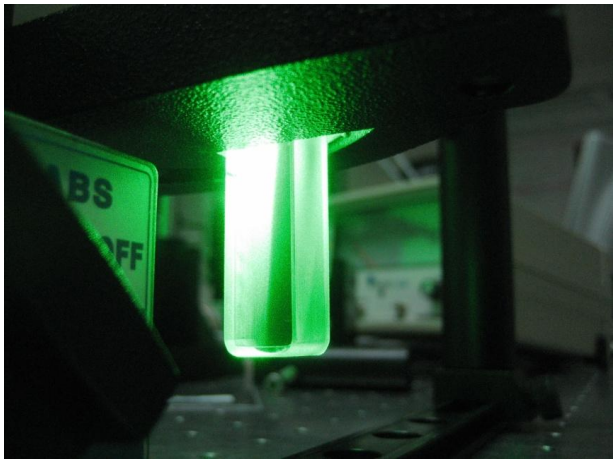

Figure 2-8: A picture showing the exposure of the gold nanoparticles in a quartz cuvette to laser radiation.

2-3: Preparation methods.

2-3-1: Preparation of spherical gold nanoparticles using the citrate method.

Spherical gold nanoparticles in aqueous solution were prepared according to the method described by Turkevich. Simply, the method is a chemical reduction of gold ions by sodium citrate in aqueous solution. Sodium citrate serves also as a capping material to prevent aggregation and further growth of the particles. 5 ml of 1 % sodium citrate solution were added to 40 ml of a boiling solution of chlorauric acid ($HAuCl_4$) containing 5 mg of gold ions. The solution was boiled for 30 minutes and was then left to cool down to room temperature. The produced gold particles have an average diameter of 15 nm as determined by TEM analysis. The standard deviation of the average particle diameter was found to be about 10 % or less.

2-3-2: Preparation of different shaped gold nanoparticles.

Different shaped gold nanoparticles were prepared by a modified version of the seed-mediated method. In order to study the effect of Ag-ions and seed concentration, the seed and the growth solutions were made as described below:

I- Influence of $AgNO_3$ concentration.

Seed Solution:

A CTAB solution (2.5 ml, 0.20 M) was mixed with 2.5 ml of $5x10^{-4}$ M $HAuCl_4$. To the stirred solution, 0.3 ml of ice-cold 0.01 M $NaBH_4$ was added, which resulted in the formation of a brownish yellow solution. Vigorous stirring of the seeds was continued for 2 min. Then, after the solution was stirred, it was kept at 25 ^{0}C.

Growth Solution:

A CTAB (2.5 ml, 0.20 M) was added to specific amounts (0 - 400µl) of $4x10^{-3}$ M $AgNO_3$ solution at 25^0C. To this solution, 2.5 ml of 10^{-3}M $HAuCl_4$ was added and, after gentle mixing of the solution, 35 µl of 0.0788 M ascorbic acid (freshly prepared) was added. The color of the growth solution changed from dark yellow to colorless.

The final step was the addition of 6 µl of the seeds to the growth solution at 27-30 ^{0}C. The color of the solution gradually changed within 10-20 minutes. For lower concentration of Ag-ions, the change in color took place more slowly. The temperature of the growth medium was kept constant at 27-30 ^{0}C in all the experiments.

II- Influence of the seed solution concentration on the growth process.

Seed Solution:

A CTAB solution (2.5 ml, 0.20 M) was mixed with 2.5 ml of $5x10^{-4}$ M $HAuCl_4$. To the stirred solution, 0.3 ml of ice-cold 0.01 M $NaBH_4$ was added, which resulted in the formation of a brownish yellow solution. Vigorous stirring of the seeds was continued for 2 min. After the solution was stirred, it was kept at 25 ^{0}C.

Growth Solution:

A CTAB (2.5 ml, 0.20 M) was added to 100µl of $4x10^{-3}$ M $AgNO_3$ solution at 25^0C. To this solution, 2.5 ml of 10^{-3}M $HAuCl_4$ was added and, after gentle mixing of the solution, 35 µl of 0.0788 M ascorbic acid (freshly prepared) was added. The color of the growth solution changed from dark yellow to colorless.

The final step was the addition of (2 µl - 14 µl) of the seeds to the growth solution at 27-30 ^{0}C. The color of the solution gradually changed within

10-20 minutes. The temperature of the growth medium was kept constant at 27-30 ^{0}C in all the experiments.

2-3-3: Influence of aging of the seeds.

In the method 2-3-2, the final step for the addition of the seeds was to use this solution aged at different times.

2-3-4: Influence of CTAB suppliers.

To study the effect of CTAB supplier, two sources of CTAB (one from Fluka and other from Aldrich) were used in the 2-3-2 method.

2-3-5: Influence of Ascorbic acid on the growth of gold nanoparticles.

The effect of ascorbic acid concentration was studied using the same method of preparation (2-3-2):

Seed Solution:

A CTAB solution (2.5 ml, 0.20 M) was mixed with 2.5 ml of $5x10^{-4}$ M $HAuCl_4$. To the stirred solution, 0.3 ml of ice-cold 0.01 M $NaBH_4$ was added, which resulted in the formation of a brownish yellow solution. Vigorous stirring of the seeds was continued for 2 min. After the solution was stirred, it was kept at 25 ^{0}C.

Growth Solution:

A CTAB (2.5 ml, 0.20 M) was added to 100µl of $4x10^{-3}$ M $AgNO_3$ solution at 25^{0}C. To this solution, 2.5 ml of 10^{-3}M $HAuCl_4$ was added and, after gentle mixing of the solution, different amount (25, 35, 50, 70, and 100 µl) of 0.0788 M ascorbic acid (freshly prepared) was added. The growth solution color changed from dark yellow to colorless.

The final step was the addition of different amounts (2, 6, and 12 µl) of the seeds to the growth solution at 27-30 ^{0}C. The color of the solution gradually changed within 10-20 minutes.

2-3-6: Effect of the nature of the capping agent in the seed solution using trisodium citrate.

I- Change of the concentration of the seeds.

Seed Solution:

A trisodium citrate solution (10 ml, $2.5x10^{-4}$ M) was mixed with 10 ml of $2.5x10^{-4}$ M $HAuCl_4$. To the stirred solution, 0.6 ml of ice-cold 0.1 M $NaBH_4$ was added, which resulted in the formation of a pink solution. This solution was aged and used after 10 minutes and 3 hours of addition of $NaBH_4$. It was kept at 27 ^{0}C.

Growth Solution:

A CTAB (2.5 ml, 0.20 M) was added to 100 µl of $4x10^{-3}$ M $AgNO_3$ solution at 25^{0}C. To this solution, 2.5 ml of 10^{-3}M $HAuCl_4$ was added and, after gentle mixing of the solution, 35 µl of 0.0788 M ascorbic acid (freshly prepared) was added. The growth solution color changed from dark yellow to colorless.

The final step was the addition of different amounts (6, 12, 25, 50, 100, 250, 500, 1000 12 µl) of the seeds to the growth solution at 27-30 ^{0}C. The color of the solution gradually changed within 5-25 minutes.

II- Change of the silver ions concentration.

Seed Solution:

A trisodium citrate solution (10 ml, $2.5x10^{-4}$ M) was mixed with 10 ml of $2.5x10^{-4}$ M $HAuCl_4$. To the stirred solution, 0.6 ml of ice-cold 0.1 M $NaBH_4$ was added, which resulted in the formation of a pink solution. This solution was aged and used after 10 minutes and 3 hours of addition of $NaBH_4$. It was kept at 27 ^{0}C.

Growth Solution:

A CTAB (2.5 ml, 0.20 M) was added to different solutions (0 - 400µl) of $4x10^{-3}$ M $AgNO_3$ at 25^{0}C. To this solution, 2.5 ml of 10^{-3}M $HAuCl_4$ was

added and, after gentle mixing of the solution, 35 µl of 0.0788 M ascorbic acid (freshly prepared) was added. The growth solution color changed from dark yellow to colorless.

The final step was the addition of 50µl of the seeds to the growth solution at 27-30 ^{0}C. The color of the solution gradually changed within 10-20 minutes.

2-3-7: Preparation of large volume of gold nanoparticles.

The method to prepare gold nanorods in large volumes (up to 500ml) was as follows:

Seed Solution:

A CTAB solution (2.5 ml, 0.20 M) was mixed with 2.5 ml of $5x10^{-4}$ M $HAuCl_4$. To the stirred solution, 0.3 ml of ice-cold 0.01 M $NaBH_4$ was added, which resulted in the formation of a brownish yellow solution. Vigorous stirring of the seeds was continued for 2 min. After the solution was stirred, it was kept at 25 ^{0}C.

Growth Solution:

(2.5, 5, 10, 25, 50 and 250 ml) of 0.20 M CTAB were added to (0.1, 0.2, 0.4, 1, 2, 10 ml) of $4x10^{-3}$ M $AgNO_3$ solution at 25^{0}C. To this solution, (2.5, 5, 10, 25, 50 and 250 ml) of 10^{-3}M $HAuCl_4$ were added and, after gentle mixing of the solution, (35, 70, 140, 350, 700 and 3500µl) of 0.0788 M ascorbic acid (freshly prepared) were added. The color of the growth solution changed from dark yellow to colorless.

The final step was the addition (6, 12, 24, 60, 120 and 600µl) of the seeds to the growth solution at 27-30 ^{0}C. The color of the solution gradually changed within 10-50 minutes. The temperature of the growth medium was kept constant at 27-30 ^{0}C in all the experiments.

2-3-8: Preparation of different shaped gold nanoparticles using silver clusters.

The effect of commercial Ag-clusters on the growth process of gold nanoparticles was carried out as described below:

Seed Solution:

A CTAB solution (2.5 ml, 0.20 M) was mixed with 2.5 ml of $5x10^{-4}$ M $HAuCl_4$. To the stirred solution, 0.3 ml of ice-cold 0.01 M $NaBH_4$ was added, which resulted in the formation of a brownish yellow solution. Vigorous stirring of the seeds was continued for 2 minutes. After the solution was stirred, it was kept at 25 ^{0}C.

Growth Solution:

A CTAB (2.5 ml, 0.20 M) was added to varied amounts of 1 mg/l of Ag-clusters (Nanogap, Spain) to have a final concentration ranging from 6.65 x 10^{-11} to $9.5x10^{-7}$ M at 25^{0}C. To this solution, 2.5 ml of 10^{-3}M $HAuCl_4$ was added and, after gentle mixing of the solution, 35 µl of 0.0788 M ascorbic acid (freshly prepared) was added. Ascorbic acid changed the growth solution color from dark yellow to colorless.

Finally, 6 µl of the seeds added and the color of the solution gradually changed within 2-10 minutes.

2-3-9: Effect of [Cl⁻] on the growth of gold nanoparticles.

The effect of NaCl on the growth process was studied in the absence and the presence of Ag-clusters (Nanogap, Spain) as follows:

Seed Solution:

A CTAB solution (2.5 ml, 0.20 M) was mixed with 2.5 ml of $5x10^{-4}$ M $HAuCl_4$. To the stirred solution, 0.3 ml of ice-cold 0.01 M $NaBH_4$ was added, which resulted in the formation of a brownish yellow solution. Vigorous stirring of the seeds was continued for 2 minutes. After the solution was stirred, it was kept at 25 ^{0}C.

Growth Solution:

A CTAB (2.5 ml, 0.20 M) was added to varied amounts of 0.0973 M of NaCl to get a final concentration [Cl^-] ranging from 10^{-7} to $3.14x10^{-3}$ M at 25^0C. To this solution, 2.5 ml of 10^{-3}M $HAuCl_4$ was added and, after gentle mixing of the solution, 35 µl of 0.0788 M ascorbic acid (freshly prepared) was added. Ascorbic acid changed the growth solution color from dark yellow to colorless.

Finally, 6 µl of the seeds added and the color of the solution gradually changed within 30-120 minutes.

2-3-10: Preparation of different shaped gold nanoparticles using gold clusters.

For the preparation of gold nanorods of different aspect ratios, seeds, clusters and growth solutions were made as described below:

Cluster solution:

5 ml of 0.2 M CTAB solution was mixed with 5 ml of $5x10^{-4}$ M $HAuCl_4 \bullet 3H_2O$. To the stirred solution, 60 µl of ice-cold freshly prepared 0.1M $NaBH_4$ was added, which results in the formation of a solution with brownish yellow color. Vigorous stirring of the clusters was continued and used after 10 sec., 30sec., 1min. and 5min. of preparation.

Seed solution:

2.5 ml of 0.2 M CTAB solution was mixed with 2.5 ml of $5x10^{-4}$ M $HAuCl_4 \bullet 3H_2O$. To the stirred solution, 30 µl of ice-cold freshly prepared 0.1M $NaBH_4$ was added, which results in the formation of a solution with brownish yellow color. Vigorous stirring of the seed solution was continued for 2 minutes. The seeds were used after 10 minutes of preparation.

Growth solution:

5 ml of the gold clusters solution was added to 2.5 ml of deionized water at 25 ^{0}C. To this solution, 2.5 ml of 10^{-3}M $HAuCl_4 \cdot 3H_2O$ was added and, after gentle mixing of the solution, 35 µl of 0.0788 M ascorbic acid was added. The color of growth solution changed from pale yellow to colorless within few seconds. After that, the color of the solution changed gradually within 20-30 minutes. For comparison experiments, 6 µl of the seeds were added at the same time of the addition of ascorbic acid to the growth solution. The color of the solution gradually changed within 10-20 minutes.

Chapter III

Chapter III

Template catalysis by silver clusters: a key missing point in the anisotropic growth of gold nanoparticles by the seed mediated method

Abstract:

The possibility that small Ag clusters play an important role in the formation of different anisotropic structures (rods, triangular shapes, bipyramids, …) of gold nanoparticles was explored by studying different modifications of the seed-mediated method. It is found that the relative concentrations of Ag-clusters or Ag^+ ions to the seeds concentration is one of the key factors for obtaining the anisotropic shape control of gold nanoparticles. A novel mechanism for the shape control, based on the formation of catalytic small silver clusters supported on the micelle surface, is proposed. The mechanism is further confirmed by using externally synthesized Ag clusters instead of Ag^+ ions, giving to the formation of different shapes depending on the ratio of Ag clusters/seeds concentration.

Introduction:

Based on the fact that the absorption features of the gold particles is very sensitive to any change on average size, shape and dielectric constant, recording the absorption spectra is one of the best tools to monitor any change in the morphology and the chemical composition during the particle preparation and to test their stability as well. Recording TEM images is also important to test the quality of the sample regarding the size distribution and to determine the exact shape and size of the particles. For these reasons, the absorption spectroscopy was the main tool to follow the growth of the particles and to study the different factors that affect this

growth and the final shape of the particles; and TEM was the technique used for determining the exact structure of the particles.

3-1: Controlled Synthesis of Gold Nanoparticles: Nanospheres, Nanorods and Nanoprisms

As it was described in the Introduction section, a wide range of techniques for the synthesis of gold nanoparticles were developed with the objective of controlling the size and shape of the nanoparticles, and to prepare monodisperse metal nanorods[1,2], multipods[3], nanoprisms[4,5], nanocubes[6], nanotetrahedra[7], or nanodisks[8]. Among these techniques, one of the most important ones to control the shape of gold nanocrystals is the seed-mediated growth method. This method, mainly developed by Murphy's group[1], was improved by El-Sayed and co-workers[9], who made two significant modifications to increase the monodispersity and yield: a) replacement of the sodium citrate with cetyltrimethylammonium bromide (CTAB) in the seed formation step; and b) adjustment of the silver content of the growth solution to grow nanorods with controlled aspect ratios. Cetyltrimethylammonium bromide (CTAB) is used to form the precursor, a gold-surfactant complex, which has a lower redox potential and is able to influence the kinetics of the reduction reaction.

Gold nanoparticles of different shapes were prepared using the seed-mediated growth method previously developed[10-13] to prepare metallic nanospheres, nanorods and nanowires in aqueous solution. We developed further this method in order to achieve more control on the particle shape and to study the different factors which could affect the growth, the particle final shape and their stability. In particular, the main parameters which have been varied in this work were: the silver nitrate concentration, concentration of the seeds and the pH of the growth solution.

3-1-i: Synthesis without $AgNO_3$.

High aspect ratio cylindrical gold nanorods were synthesized by Murphy et al. through optimization of the concentration of CTAB and ascorbic acid, and by applying a two- or three-step seeding process. The primary nuclei were 3.5nm gold seeds prepared by borohydride reduction of gold salt in the presence of citrate as capping agent. The growth steps were carried out in aqueous surfactant media. Secondary nucleation during the growth stage was inhibited by carefully controlling the growth conditions, and in particular by using ascorbic acid as a weak reducing agent, that cannot reduce the gold salt in the presence of the micelles if the seed is not present. A summary of this process is described in the schemes (3-1 and 3-2).

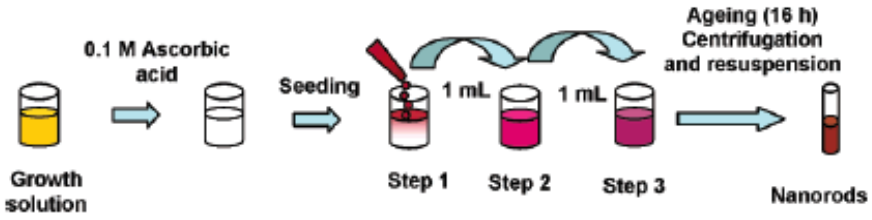

Scheme 3-1: Scheme showing the general methodology for the generation of gold nanorods.

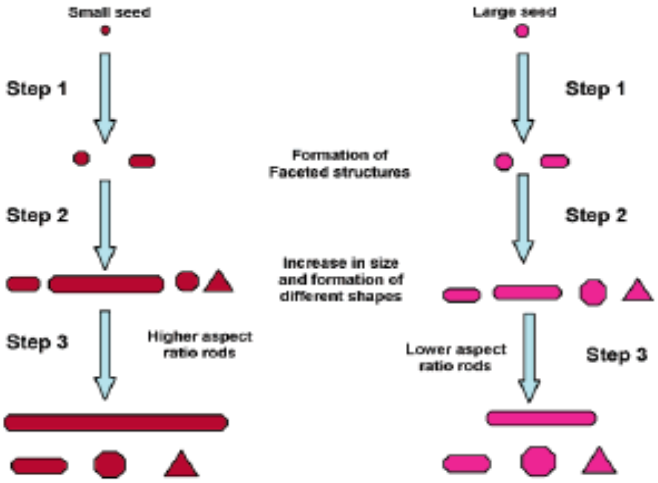

Scheme 3-2: Scheme showing the different stages of the growth of gold nanorods using small (5.5 nm) and big (8 nm) seed particles.

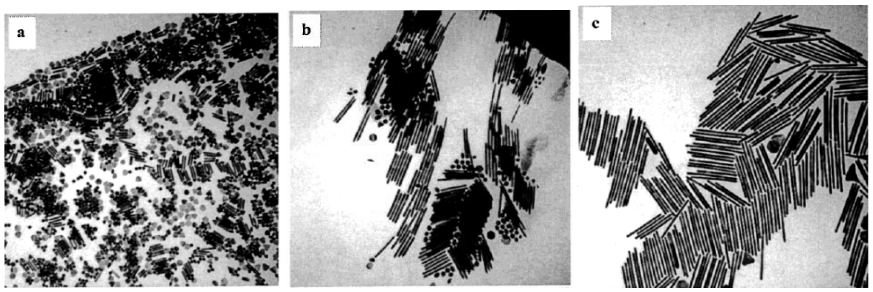

Figure 3-1: TEM images of gold nanorods, prepared by the Murphy's method (a) a.r.= 4.6; (b) a.r.=13; (c) a.r.=18. The scale bar (100 nm) applies to all three images.

The yield of the nanorods synthesized by this method is only about 4 %[14]. In order to increase this percentage the long rods can be concentrated and separated from the spheres and excess surfactant by many successive centrifugations. Later, the same group reported an improved method to produce monodisperse gold nanorods of high aspect ratio in ~90% yield[1], just through pH control. They found that changing the pH of the growth solution from 2.8 to 3.5 and 5.6, leads to the formation of gold nanorods of aspect ratio 18.8 ± 1.3 and 20.2 ± 1.2 respectively, with a dramatic increase in the relative proportion of nanorods to nanospheres. This reduced the number of the separation steps necessary to remove smaller particles through centrifugation.

Up to this point, the mechanism of formation of rod-shaped nanoparticles in aqueous surfactant media remains unclear. Murphy and co-workers proposed a mechanism to explain the growth of the rod shape particles based on the idea that CTAB adsorbs onto gold nanorods forming a bilayer with the trimethylammonium headgroups of the first monolayer facing the gold surface [15]. They proposed that the CTAB headgroup preferentially binds to the crystallographic faces of gold existing along the sides of pentahedrally twinned rods, as compared to the faces at the tips. The growth of gold nanorods would thus be governed by preferential adsorption of CTAB to different crystal faces during the growth rather than acting as a

soft micellar template[16]. HRTEM and selected area electron diffraction analysis have shown that the gold nanorods prepared in the absence of silver ions are pentatetradedral twins, where the cubic symmetry of the native gold face-centered cubic lattice is broken by twinning[16]. The cross sectional view of these rods is pentagonal; each end of the rod consists of five triangular facets that are Au {111} faces, and the sides of the rods are either Au {100} or Au {110}[14]. More specifically, they postulated that CTAB adsorbs preferentially on the side of rods, Au{100} or Au{110}, via chemisorbed bromide counter ions, leaving free the ends of the rods, which display Au{111} faces. This preferential binding mechanism agrees with the large size of the quaternary ammonium head groups, which are better accommodated over the larger binding sites available on the {100} and {110} faces of the crystalline rods[14,16]. The binding of CTAB, ultimately as a bilayer[17], on the side of the rod blocks hinders the deposition of further gold to the side and promotes the growth at the ends of the rods[17].

Liz-Marzán et al. proposed that the CTAB micellar structure also promoted the deposition of metal at the tips of gold seed particles that are also surrounded by CTAB[2]. Specifically, they proposed that $AuCl_4^-$ ions first displace Br^- ions and then tightly bind to CTA^+ micelles. Addition of ascorbic acid then reduce Au^{3+} to Au^+ at the micelle surface, and the rate of growth of the different nanorod facets would be determined by the approach of the micelle and thus gold species toward the facets of the gold seed particles that are also covered with CTAB. After calculating the surface potential of metal ellipsoids in 1 mM NaCl, Liz-Marzán et al. showed that this potential decays more rapidly at the nanorod tip than along its length, and thus the micelle can approach more easily to the tips of the rods than the sides allowing deposition of gold in the tips. It was noted by this group, however, that an asymmetry in the seed must be present to

create an asymmetric electric field initially, possibly in the form of a twinning plane or stacking fault[2,18].The influence of C_nTAB analogues, in which the length of the hydrocarbon tails was varied, keeping the headgroup and the counter ion constants, was also studied[19]. It was found that the length of the surfactant tail is critical for controlling not only the length of the nanorods but also the yield. Shorter chain lengths produce shorter nanorods, whereas longer chain lengths lead to longer nanorods in higher yields. Considering the preferential adsorption of $C_{16}TAB$ to the different crystal faces forming a bilayer[15,16,18,19], a "zipping" mechanism was proposed taking into account the van der Waals interaction between surfactant tails within the surfactant bilayer, that may promote the formation of longer nanorods from more stable bilayers[18].

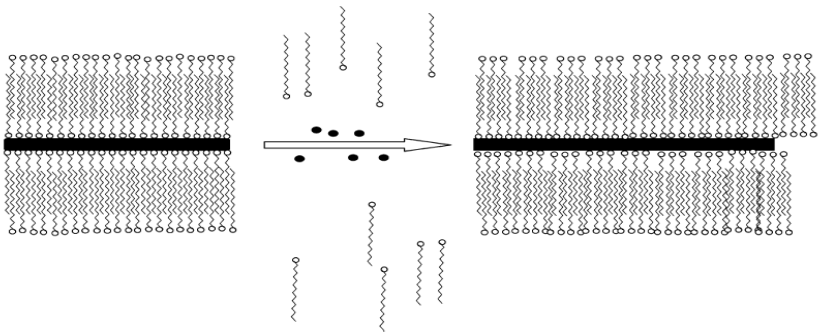

Figure 3-2: A cartoon illustrating the “zipping” mechanism: the formation of a bilayer of C_nTAB (squiggles) on the nanorod (black rectangle) surface may assist the growth of the nanorod as more gold ions (black dots) are introduced [16].

The group of Liz-Marzán also investigated the factors affecting the nucleation and growth of gold nanorods under similar conditions[2]. They showed that when temperature and CTAB concentration are reduced, it is also possible to synthesize short gold nanorods of aspect ratios ranging up to six with a yield up to ~ 50%. The control of the aspect ratio, as well as the monodispersity and the yield were demonstrated to be influenced by a number of factors, such as the stability of the seed, temperature and the

nature and concentration of surfactant. It is observed that the yield of nanorods prepared from CTAB capped seeds is much higher than that from naked (or citrate stabilized) seeds. This indicates that the more colloidally stable the gold seed nanoparticles are, the higher the yield of rods. As expected, the lower the amount of seeds added the higher the aspect ratio of the nanorods formed. In addition, the authors proposed another mechanism for the nanorod growth, which is based on a series of observations related to the binding of the gold salt ions to the cationic micelles, which are summarized below:

i. The yield of rods improves with increasing the colloidal stability of the seeds; hence dimmers or coalescent seeds are not good precursors to the rod formation.

ii. Bromide ions are much better than chloride ions as rod-inducing agents in the presence of C_nTA^+. As the length of the surfactant tail, C_n, increases the yield and the aspect ratio of the nanorods increase [18]. The addition of NaCl, $NaNO_3$, or NaBr reduces the aspect ratio of the nanorods, being this effect similar for each ion. An increase in the ionic strength produces a decrease in the yield of rods.

iii. Under optimal conditions, the aspect ratio can be controlled through the ratio of seeds to the $HAuCl_4$ concentration. An increase in the amount of seeds gives rise to a decrease in the aspect ratio of the rods because of the nuclei increase.

iv. Both $AuCl_4^-$ and $AuCl_2^-$ are quantitatively adsorbed to CTAB[20]. The optimal CTAB: $HAuCl_4$ concentration ratio is in a narrow window since precipitation of CTAB-$HAuCl_4$ occurs at < 10:1 ratio. This can be avoided by increasing the temperature. However, the yield of rods decreases gradually at higher temperatures.

v. The presence of CTAB not only directs Au ions to the tips, but also drastically retards the rate of metallic gold formation compared with

the absence of CTAB[18]. The higher the curvature of the gold surface, the faster the rate of growth.

The proposed mechanism can be summarized in the following steps:

$AuCl_4^- + 2e^- \leftrightarrow AuCl_2^- + Cl^-$ (1)

$3AuCl_2^- \leftrightarrow AuCl_4^- + 2Au^0 + 2Cl^-$; (2)

$AuCl_2^- + e^- \leftrightarrow 2Au^0 + 2Cl^-$ (3)

$AuCl_2^- - CTAB_{mic} + Au_m \leftrightarrow Au_{m+1} - CTAB_{mic} + CTAB_{mic} + 2Cl^-$ (4)

In the presence of CTAB, ascorbic acid reduces Au(III) to Au(I) via reaction (1). However, no colloidal gold is formed, i.e., disproportionation of $AuCl_2^-$ −CTAB does not occur (reaction 2). In fact, it is possible to prepare solutions of $AuCl_2^-$ - CTAB by adding $HAuCl_4$ to colloidal gold in the presence of CTAB. Consequently, the reduction of Au(I) can proceed through electron transfer at the surface of the electron–rich gold seeds (reaction 3). In the presence of CTAB, the reduction can be described by reaction (4).

During the typical microelectrode-type deposition[21], electrons are transferred to the gold particle while adsorbed $AuCl_2^-$ ions may pick up electrons at any favorable adsorption site. Usually spherical growth is obtained under these circumstances[21,22], but in the case of CTAB containing solutions, the gold seeds are encapsulated in CTAB, and the gold ions are likewise bound to CTAB [21]. It was postulated that the rate of nanorod formation is determined by the frequency of collisions of $AuCl_2^-$ laden cationic micelles with the cationic gold seed particles. The following sketch might explain this mechanism:

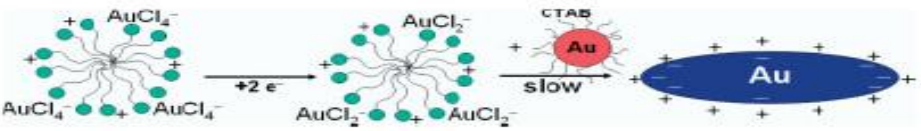

Figure 3-3: Sketch showing the mechanism for gold nanorod formation. The transport of the gold ions bound to the CTAB micelles to the growing seed particles is controlled by the double layer interaction[21].

This interaction will be controlled by the electrical double layer interaction between micelles and gold nanorods. The rate of the reaction is then controlled by the collision of the micelles. A faster rate of collision of the micelles at the tips than at the sides will induce rod formation which was confirmed through calculations of the potential distribution and potential gradient around an ellipsoid[2]. These calculations showed that the potential decays more rapidly near the tip which means that it will be easier for a micelle to approach to a given distance at the tip rather than from the sides of the rods. The initial change in morphology could only be explained assuming that a stacking fault or twinning plane in the seeds should be present to create an initial electric field asymmetry.

Zubarev found that Au(III)–CTAB complexes are capable of dissolving gold nanostructures in a shape-dependent manner; this process can be used to purify gold high aspect ratio nanorods and greatly improve their monodispersity[23].

There were many groups working on different ways in the chemically synthesis of gold nanorods, or nanowires; for example, Giersig and Liz-Marzán reported that $HAuCl_4$ can be reduced with oleylamine, followed with thermal and solvent processing, to yield 1.6 nm diameter single-crystalline gold nanowires that can have lengths up to 4 μm[24]. In this case the control of aspect ratio was limited, and the growth mechanism was, like for CTAB, attributed to preferential adsorption of oleylamine to different crystal facets of the growing nanorod/nanowire[24]. Murray et al. used a gold(I) precursor, AuCl, with oleylamine and carbon monoxide as a reducing agent in a related manner to produce gold nanowires that are 2.5 nm in diameter and up to several microns long, albeit with limited control over aspect ratio[25].

3-1-ii: Synthesis with $AgNO_3$.

The presence of silver nitrate allows a better control of the shape of gold nanorods synthesized via the electrochemical method[26]. In the seed-mediated growth method, Murphy and co-workers modified their initial procedure for long nanorods by adding a little amount of $AgNO_3$[14] in order to increase the yield of rod-shaped nanoparticles (up to 50%) and to control the aspect ratio of shorter nanorods and spheroids[27]. Under identical experimental conditions, a small amount of silver nitrate is added prior to the growth step. The aspect ratio of the spheroids and nanorods can be controlled by varying the ratio of seed to metal salt. They found that the presence of the seed particles is crucial in the growth process and that is an increase in the aspect ratio when the concentration of seed particles is decreased.

The mechanism by which Ag^+ ions modify the metal nanoparticle shape is not really understood. It has been hypothesized that Ag^+ adsorbs at the particle surface in the form of AgBr (Br^- coming from CTAB) and restricts the growth of the AgBr passivated crystal facets[27]. The possibility that the silver ions themselves are reduced under these experimental conditions (pH ~ 2.8) was neglected since the reducing power of ascorbic is too positive at low pHs[28].

Nikoobakht and El-Sayed modified the seed-mediated growth method to overcome its drawbacks and limitations, such as the formation of noncylindrical nanorods, unshaped particles and contamination by spherical particles. Their modification essentially consisted in the use of CTAB-capped seeds rather than the citrate-capped ones[9]. This resulted in the formation of 99% gold nanorods with aspect ratios, which could be turned from 1.5 to 5. The replacement of sodium citrate with CTAB in the seed´s formation step produces small spherical particles (<4nm)[9]. Differences in yield and shape of nanorods could be due to the slightly

different size of the CTAB and sodium citrate capped seeds, but it may also be attributed to different crystal structure in the two kinds of seed particles. By simply adjusting the amount of silver ions in the growth solution, a fine-tuning of the aspect ratio of the nanorods can be achieved so that an increase in silver concentration (keeping the amount of seed solution constant) leads to a red-shift in the longitudinal plasmon band indicating an increase of the aspect ratio. There is a critical silver ion concentration above which the aspect ratio of the nanorods decreases again[9]. The aspect ratio can be controlled by adjusting the amount of the seeds added to the growth solution in the presence of constant Ag^+ concentration. Contrary to expectations, an increase in the amount of seeds produces a red-shifted in the longitudinal plasmon band position pointing towards an increase in aspect ratio. With the increase of the concentration of seeds the length of the nanorods decreases slightly while the width decreases[29,30]. A similar trend is observed when the gold ion concentration is increased[30]. Nanorods with higher aspect ratios could be obtained for gold ion concentrations up to $[Au^{3+}] \sim 6 \times 10^{-4}$ M. The concentration of ascorbic acid has also been shown to influence the morphology with decreasing length and rod yield when the ascorbic acid concentration is increased maintaining other parameters constant. By adjusting the silver ion or gold seed concentrations in this single-component surfactant (CTAB) solution, the longitudinal plasmon band can be tuned up to 825nm corresponding to an aspect ratio of ~ 4.5.

Nikoobakht and El-Sayed proposed the use of a binary surfactant mixture containing CTAB and benzyldimethylammoniumchloride (BDAC) to grow gold nanorods with larger aspect ratios (>5)[9]. Two different approaches have been proposed for explaining this fact: firstly, by changing the BDAC: CTAB ratio from 16 to 2, the aspect ratio of the nanorods can be tuned from 5 up to 8. The process in this binary mixture is complex. There

is an initial fast growth stage that occurs over the first hour. This is followed by a much slower growth step that takes place over one week. The approach presents two main disadvantages related to the ageing of the solutions, namely the low reproducibility and the formation of a large amount of spherical particles as the surfactant ratio is increased. A second approach, which employs a low BDAC: CTAB surfactant ratio, has been used to ensure that few nanospheres are formed. After the first stage of the growth is completed (fast growth step), different amounts of the growth solution are added gradually. These gradual additions result in a red-shift of the longitudinal plasmon band position, which means that the length of the nanorods is increased after each addition. The mechanism in this case must be related to the presence of silver nitrate, since this is essential for the preparation of nanorods in high yields. Two mechanisms have been proposed to account for the gold nanorod formation although the role of silver ions is not clearly understood at this moment. In the first one, the surfactant forms a soft template with a certain size that depends on surfactant concentration and ionic strength of the solution[(9)]. The growth solution contains a mixture of gold and silver ions and when ascorbic acid is added only gold ions are reduced since it is assumed that silver ions can only be reduced at basic pH values[(31)]. Nikoobakht and El-Sayed proposed that silver ions located between the headgroups of the capping surfactant (CTAB) can be considered as Ag-Br pairs, decreasing the charge density on the bromide ions and, therefore, the repulsion between neighboring headgroups on the gold surface giving rise to NRs with lower aspect ratios[(9)]. This possibility is supported by the stronger affinity of CTAB monomers for the side facets compared to the end facets[(32)]. High-resolution TEM images show that nanorods have four facets[(33)]. In the case of the BDAC: CTAB surfactant mixtures, the template is considered to be more flexible than the single component surfactant. Due to the larger affinity of

CTAB monomers for the side facets, it has been assumed that there is a higher probability of having BDAC monomers bound to the end facets of the nanorods promoting a faster growth in the longitudinal direction due to the weaker bonding in Ag-Cl pairs relative to that in Ag-Br pairs[9].

The second mechanism considers a rigid structure of CTAB monomers, which helps maintain an one-dimensional growth but also serves to control the rate of gold reduction[9], in a similar way to the mechanism previously proposed for the formation of long rods in the absence of silver ions[32]. Again, it is assumed in this mechanism that silver ions are not being reduced by ascorbic acid, but will form silver bromide during the synthesis. Murphy and co-workers proposed the adsorption of silver bromide to the facets of the gold nanocrystals, which slow down the gold reduction and induces the single crystalline growth of the nanorods.

In spite of the large amount of literature about the chemical synthesis of anisotropic structures the mechanisms that determine the crystal habit and morphology[34] are not well-understood and even subtle changes in the experimental conditions, like surfactant supplier[35], seems to have a large influence in the final nanoparticle shape. As we discussed in the introduction part, two main mechanisms are accepted at this moment as the more relevant ones, although a complete understanding is still lacking [36].

The critical nature of the silver species formed during the synthesis has been even more heavily discussed, and several groups have proposed different reasons of why silver species can assist in the anisotropic growth of gold nanorods. One possibility is that silver bromide complexes play a critical role in this mechanism[37]. In the Murphy´s group mechanism, the deposition of AgBr on a specific facet of gold nanorods during seed-mediated growth stabilizes the rods and directs their growth by allowing a more rapid incorporation of gold onto the less hindered facets. The presence of silver bromide species is further evidenced by XPS data

suggesting the presence of Ag(I) . Also it was observed that 1H NMR spectra of CTAB capped gold nanorods was identical to those of pure AgBr–CTAB[37]. However, the presence of free silver bromide (as the reaction occurs above the Ksp of AgBr) could lead to spurious NMR spectra interpretation. Other authors found mass spectrometric evidence that $AgBr_2^-$, as well as $AuBr_2^-$, exist at the gold surface for well-purified nanorods that result from the photochemical synthesis method [38,39]. Hafner reported Raman evidence of the Au–Br bond formation at 180 cm^{-1}, which disappears if thiols replace the adsorbed bromine on the gold nanorod surface[40]. Other groups, however, propose that silver bromide complexes may not explain the anisotropic growth, and instead argue that underpotential deposition (UPD) of a monolayer or a submonolayer of elemental silver on the gold nanorod surface is of significance[41]. Guyot-Sionnest and colleagues proposed that, in the seed-mediated synthesis, underpotential deposition of silver preferentially occurs on the {110} gold facets compared to the {111} and {100} facets[41]. In this model, a silver monolayer strongly protects the {110} facet, and, although the silver may be oxidized and replaced by gold, other facets grow fastest due to the fact that they are less covered with silver. Differing degrees of silver passivation on the {110} facets should lead to varying ratios of growth on this facet and the nanorod's end facets, and this is consistent with what is observed for the standard silver-assisted growth technique (figure 3-4). Inductively coupled atomic emission spectroscopy has been used to quantify the amount of silver in the rods after synthesis, and it was estimated that four monolayers of silver are present in the rods, though the technique does not differentiate between Ag (0) and Ag (I)[42]. Extended X-ray absorption fine structure (EXAFS) studies[43] have suggested that Ag(0) is the final form of silver for rods grown via a photochemical method, consistent with the possibility that elemental silver is of crucial importance

not just for the standard technique, but for the variety of synthetic methods available to produce gold nanorods.

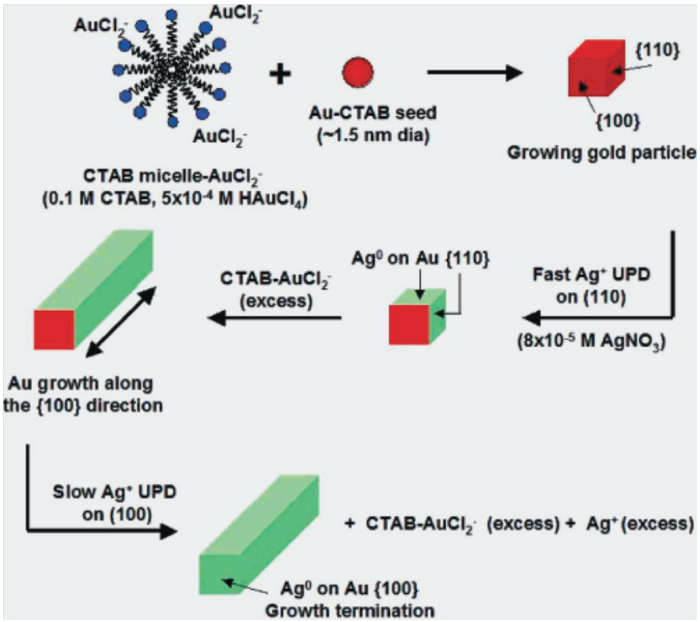

Figure 3-4: A cartoon illustrating of the mechanism of nanorod growth from CTAB protected gold seed particles in the presence of Ag^+.

To clarify the mechanisms involved in the growth of gold NRs, and to achieve a better understanding of the role of $AgNO_3$ we undertook a systematically study of the effect of the Ag^+ ions and the seed concentration on the final shape of gold particles. This would allow to prepare gold nanostructures in high yields and to get a more precise control on the final particle shape.

Because the experimental conditions used in many of the above mentioned methods are particularly suitable to produce metal clusters (kinetic control[44]), we investigate in this work the possibility that metal clusters may play a role in the anisotropic growth of nanoparticles.

For this purpose, we firstly studied the influence of some factors, which mainly affect the nanoparticle directed growth, such as Ag^+, seed and

CTAB concentration on the formation of gold anisotropic nanoparticles (mainly nanorods and nanoprisms) by using the seed-mediated method. Based on these results a novel mechanism is proposed, which takes into account the template catalysis by "in-situ" formation of Ag clusters. The proposed mechanism is further confirmed by using externally prepared Ag clusters. This result opens a new way of thinking in the interpretation of the mechanisms of anisotropic growth, which could be used to explain not only the gold anisotropic growth by the seeds-mediated method, but also the synthesis of other anisotropic materials by this and other related methods.

Experimental Section:

The preparation methods and characterization methods were already described in Chapter II.

Results and Discussion:

3-2: Effect of $AgNO_3$ concentration.

The effect of using different concentration of silver ions on the shape of the produced gold nanoparticles was first studied. For this purpose, under identical experimental conditions ([seeds] = 0.048μM), different amounts of $AgNO_3$ concentrations ranging from 40 to 320 μM were added into the growth solutions of the same composition. Figure 3-5 shows the change in UV-Vis absorption spectra of gold seeds after addition of $NaBH_4$. As it can be seen in figure 3-6, the size of the seeds, after 10 min of their preparation, estimated from AFM is s = 0.6 ± 0.2 nm. This size agrees with the fact that no Plasmon resonance is observed, which is characteristic for sizes ≈ ≤ 1.7nm. Concentration of seeds was calculated from this estimated size using the density (59 atom/nm^3) of bulk fcc-gold:

[seeds] = [Au atoms]/N_{Au}, being $N_{Au} = 59(\pi/6)\ s^3 \approx 6$ (2-16), the approximate number of atoms per cluster[25]. Then,

[seeds] ≈ 41.6 (125-15.6) μM.

Inside the parenthesis it is shown the size range of Au seeds (or concentration range) taking into account the standard error in the size estimated from AFM. This seed solution was used after 10 minutes of preparation. Au seeds are generally unstable at room temperature and grow to spherical particles with a uniform diameter after 24 hours (figure 3-7C).

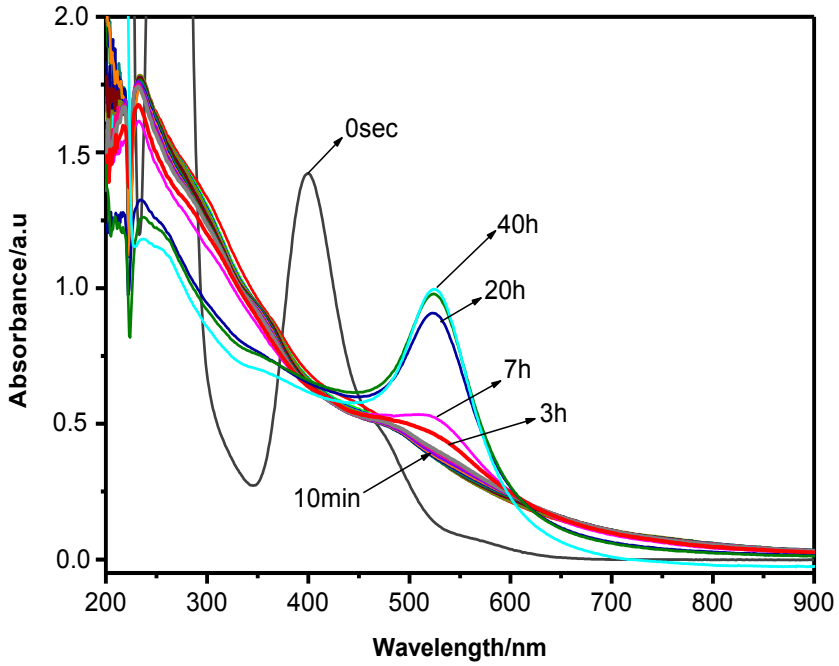

Figure 3-5: Absorption spectra of gold seeds after 10 min, 3h, 7h, 20h and 40h of preparation. Please note that the Au plasmon band is absent even at 3h from preparation.

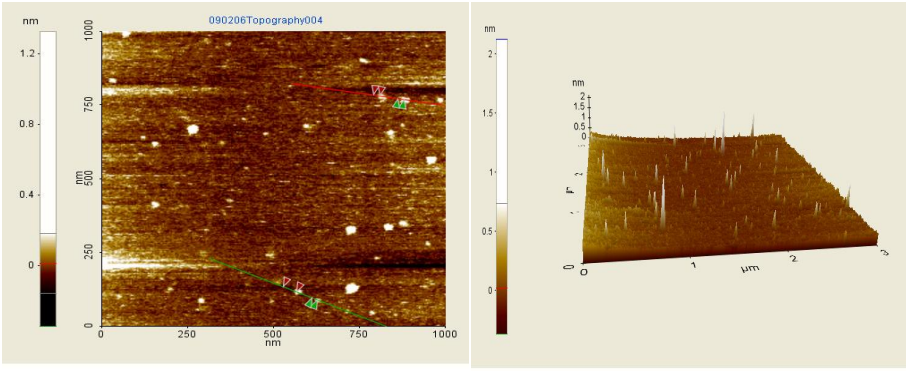

Figure 3-6: AFM images of the Au seeds after 10 min of preparation. Average size: 0.6±0.2nm.

Figure (3-7) shows the TEM images and the absorption spectra of gold nanoparticles produced without the addition of $AgNO_3$ at different addition times of the seed solution. It is observed that, under these conditions, only spherical particles with a size of 5±2 nm are obtained. For comparison purposes, the UV-Vis spectrum of Au nanospheres of approximately the same size prepared by the citrate method is also shown. It can be seen that there is a broadening and a small red shift (from 518 nm to 528 nm) of the plasmon absorption band for the particles prepared by the seed-mediated method, which can be attributed to a bigger polydispersity and a difference in the dielectric constant of the capping materials.

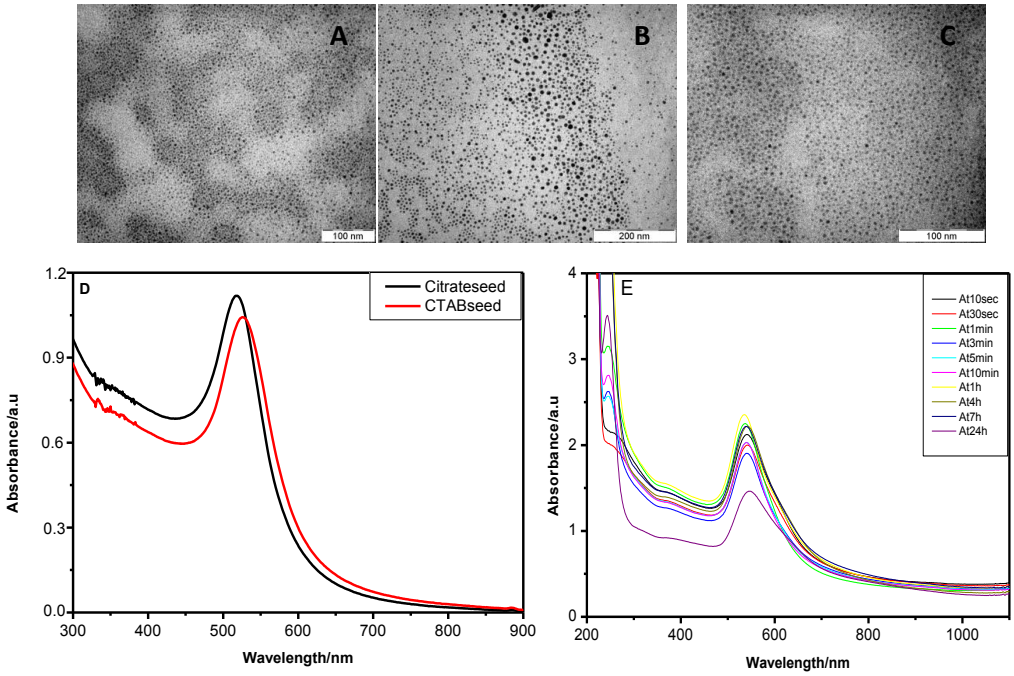

Figure 3-7: TEM images of gold nanoparticles prepared by the citrate method (A), for gold nanoparticles produced without $AgNO_3$(B) and using gold seeds after 24h (C), (D) UV-Vis absorption spectra of gold nanoparticles prepared by the citrate method (red line) and by the CTAB method without addition of $AgNO_3$ (black line). (E) UV-Vis absorption spectra of gold nanoparticles prepared without addition of $AgNO_3$ at different addition times of the seed solution.

In the presence of the smallest amount of Ag^+ ions i.e. 40 µM, rod shaped particles start to grow, which is characterized by the appearance of the longitudinal surface plasmon band. Increasing the amount of Ag^+ ions, does not increase the rod length, but increase the intensity of the longitudinal surface plasmon absorption due to the increasing amount of rods in the solution. At a critical concentration of Ag^+ ions (160 µM), a new absorption feature starts to appear, which is not characteristic to neither gold spheres nor gold nanorods. This band is located at the red side compared to the transverse plasmon resonance of the spheres and rods, and on the blue side of the longitudinal surface Plasmon band. Figure (3-8) shows the absorption spectra of the obtained gold particles using different concentrations of silver ions.

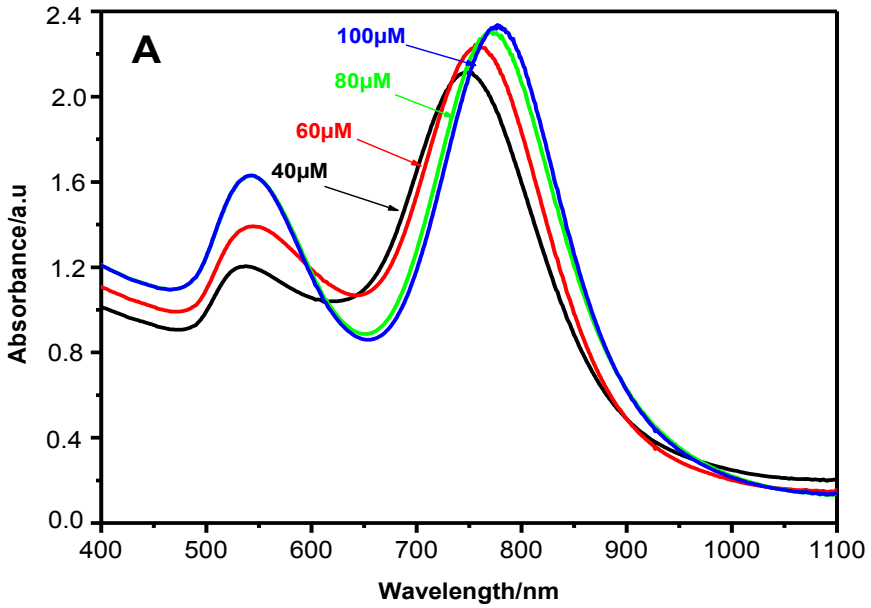

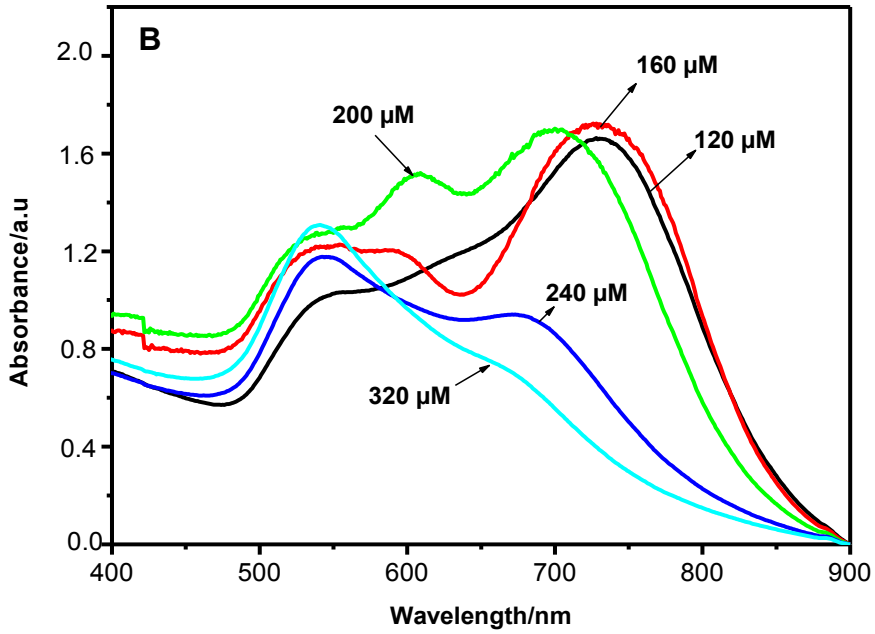

Figure 3-8: Absorption spectra showing the effect of Ag ions on the growth of gold nanoparticles, (A) from 40 to 100µM $AgNO_3$ and (B) from 120 to 320µM $AgNO_3$.

To understand the nature of this new absorption band, one drop of the solution was placed on a carbon-copper TEM grid and TEM images of this sample were recorded. The TEM images show the presence of new shapes such as prisms and snapped prisms in the solution. Increasing the concentration of Ag^+ ions more than 200 µM, leads to the formation of aggregated gold nanoparticles. Figure (3-9) shows the TEM images of gold nanoparticles produced when different amounts of Ag ions are introduced in the reaction media, showing the presence of rods (A - C) of different aspect ratios (a.r.:2.9 - 5.5) , and also the presence of new shapes, such as prisms and snapped prisms (D-F) and aggregated gold nanoparticles(G and H).

.

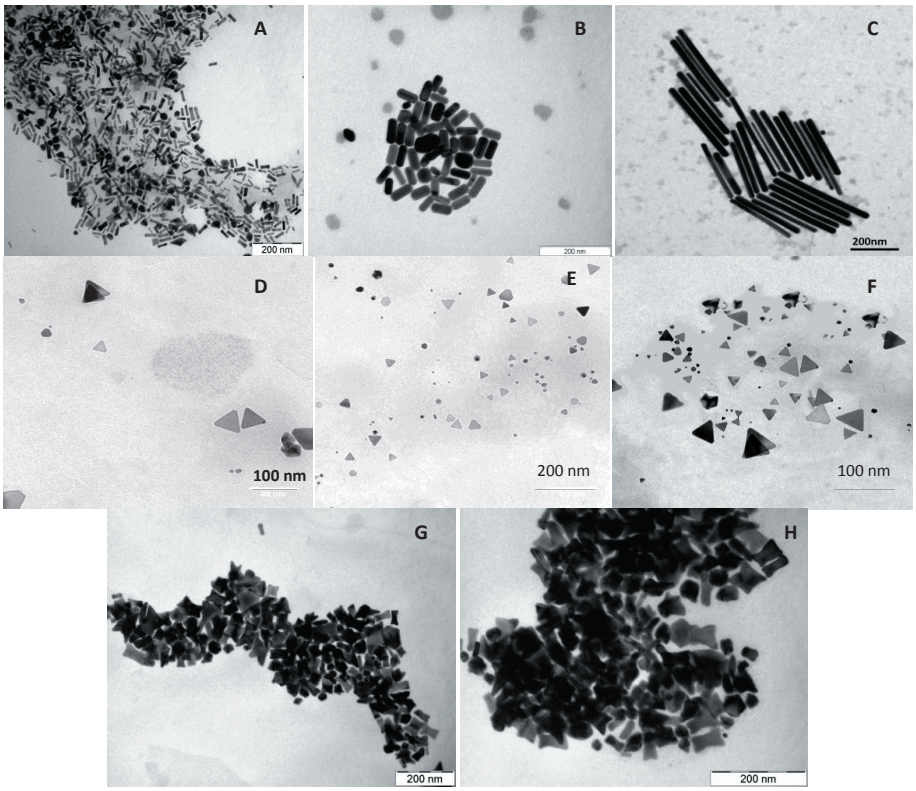

Figure 3-9: TEM images of gold nanorods produced with (A) 40µM, (B) 80µM and (C) 100µM of $AgNO_3$, respectively. Gold nanoprisms produced for 120µM $AgNO_3$ (D); 160µM $AgNO_3$ (E); 200µM $AgNO_3$ (F). Aggregated particles produced for 240µM $AgNO_3$ (G) and 320µM $AgNO_3$ (H).

Using the same technique (see figure 3-10), we succeeded to prepare large volume of gold nanorods (0.5 L). It was observed that, as the volume increased from 5ml to 20 ml at constant concentration of Ag-ions (80µM) and CTAB (0.1M), the intensity of the rods increased, but with decreasing the aspect ratio; while increasing the volume from 20 to 500 ml, the intensity decreased with increasing the aspect ratio.

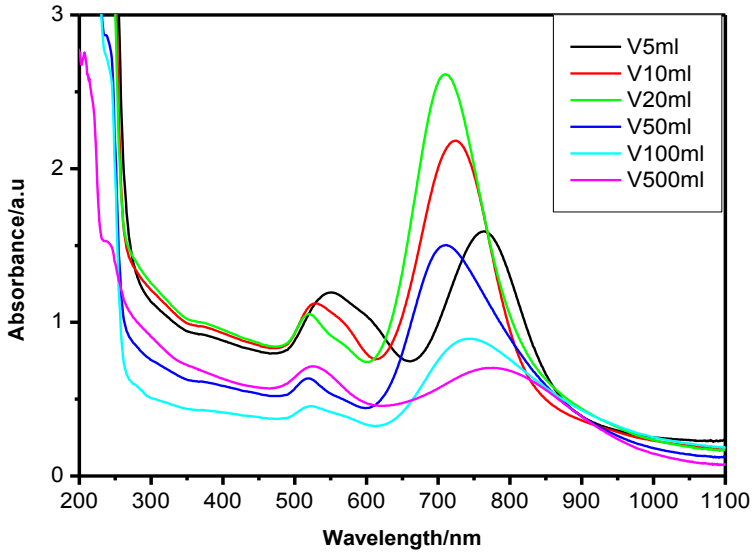

Figure 3-10: Absorption spectra for large volume synthesis (5-500 ml) using 80µM $AgNO_3$ and 0.1 M CTAB.

We also prepared large volumes (20 ml) of different shaped gold nanoparticles by changing the concentration of $AgNO_3$ with constant concentration of CTAB and the other reagents, as it is shown in figure (3-11). We found similar results than those obtained with 5ml (figure 3-8): prisms are produced when the Ag-ion concentration is increased.

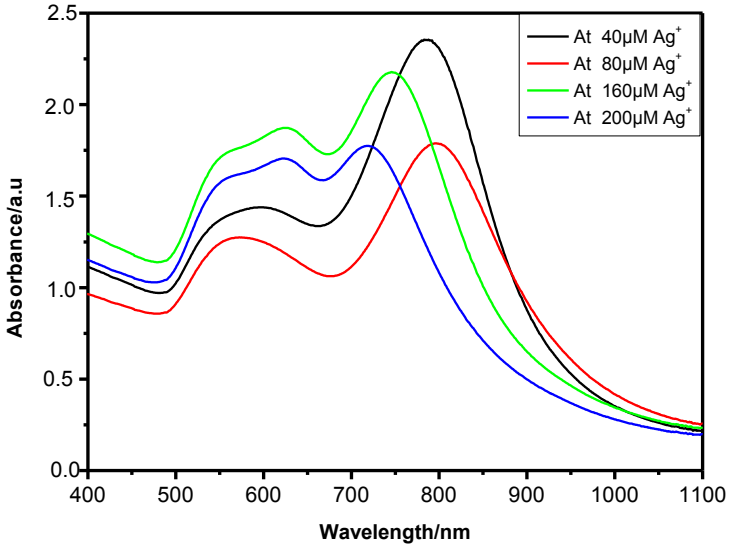

Figure 3-11: Absorption spectra for large volume synthesis (20 ml) with different concentrations of $AgNO_3$ (40, 80, 160, and 200 µM).

The growth of the gold nanoparticles after addition of AA and seeds to the growth solution containing different concentrations of $AgNO_3$, was followed spectrophotometrically, and the results are shown in the figures (3-12 to 3-15).

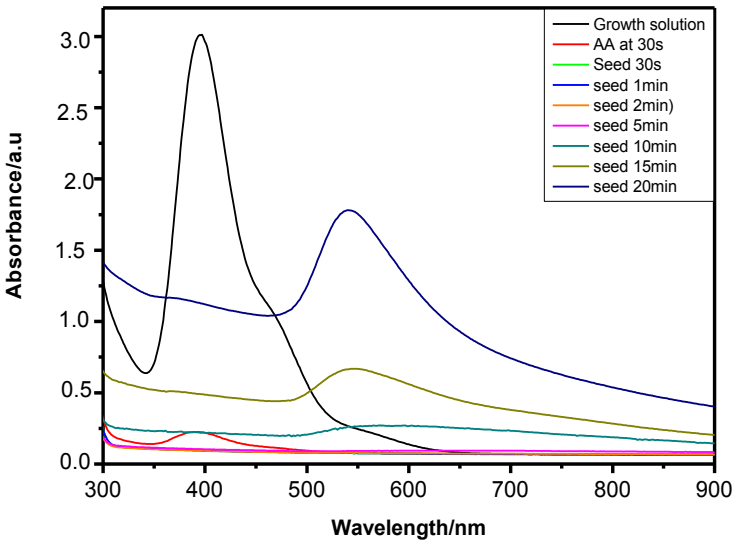

Figure 3-12: Absorption spectra showing the growth of the formed particles after addition of AA and the seeds to the growth solution without $AgNO_3$.

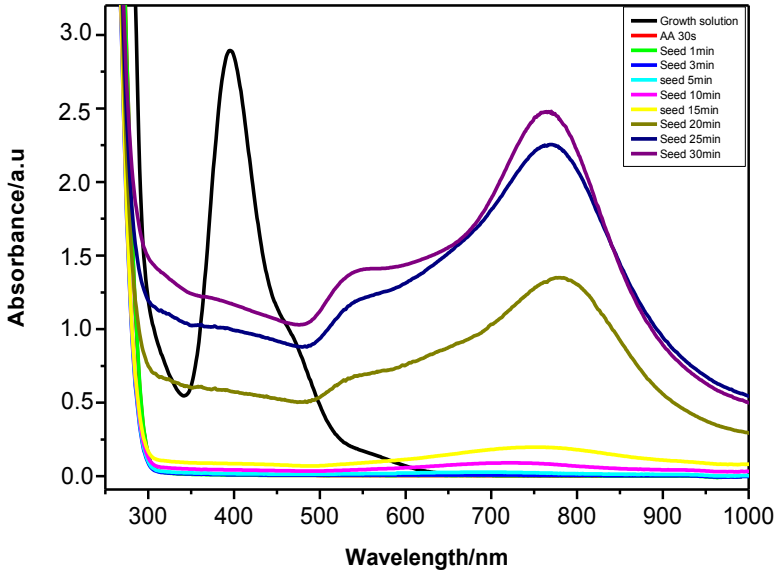

Figure 3-13: Absorption spectra showing the growth of the formed particles after addition of AA and the seeds to the growth solution with 40µM of $AgNO_3$.

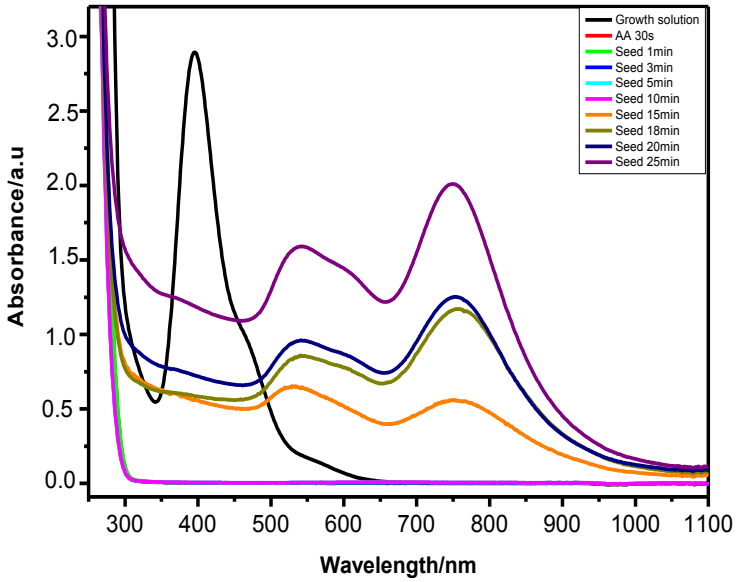

Figure 3-14: Absorption spectra showing the growth of the formed particles after addition of AA and the seeds to the growth solution with 80µM of $AgNO_3$.

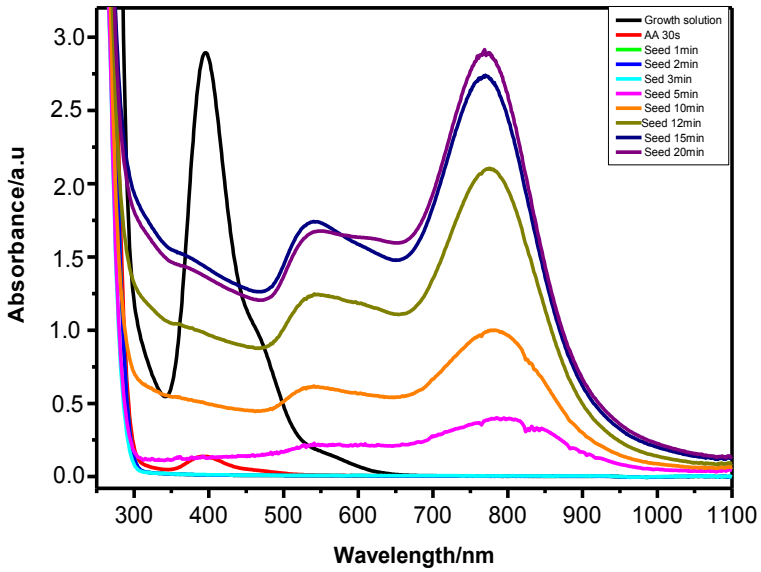

Figure 3-15: Absorption spectra showing the growth of the formed particles after addition of AA and the seeds to the growth solution with 160µM of $AgNO_3$.

It can be seen that the longitudinal band characterizing the rod´s shape appears faster with increasing $AgNO_3$ concentrations.

3-3: Effect of seeds concentration.

Figures (3-16 to 3-20) show the effect of the seed concentration on the nanoparticle shape. To emphasis the effect of the amount of silver ions concentration on the growth rate of the different facets of gold particles, and because we are mainly interesting in the gold nanorods formation, we used a fixed concentration of Ag^{+} ions (40, 60, 80, and 100 µM) and change the amount of the seed gold particles, which act as nuclei for the growing particles. We can see that, in the absence of Au seeds, the color remains transparent indicating that Au nanorods are not formed; while using the smallest amount of seeds nanoprisms are formed, as can be deduced from the presence of the 3rd band. Increasing the amount of seeds leads to the formation of gold rods. It is also to be noticed that, for high concentration of silver ions (100µM), gold nanorods are formed for all the concentrations of the seeds used.

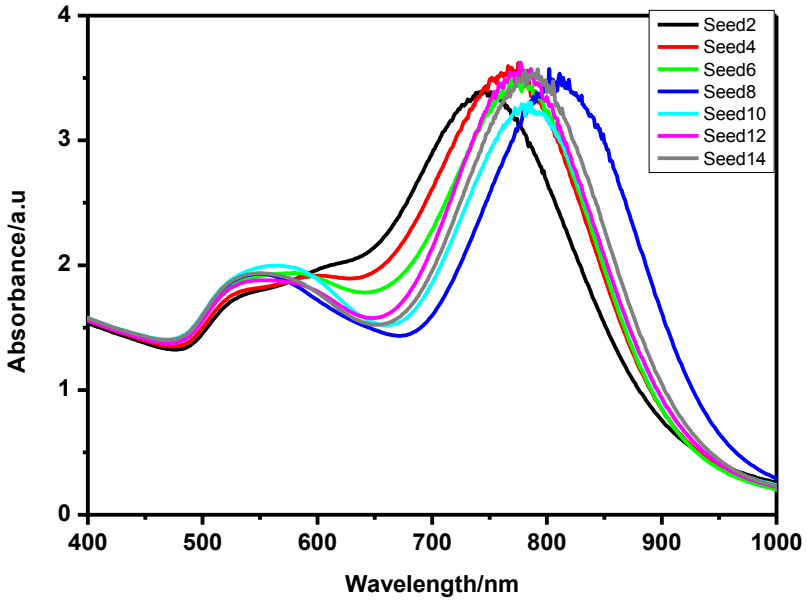

Figure 3-16: Absorption spectra showing the effect of the seed concentration using 40µM of $AgNO_3$.

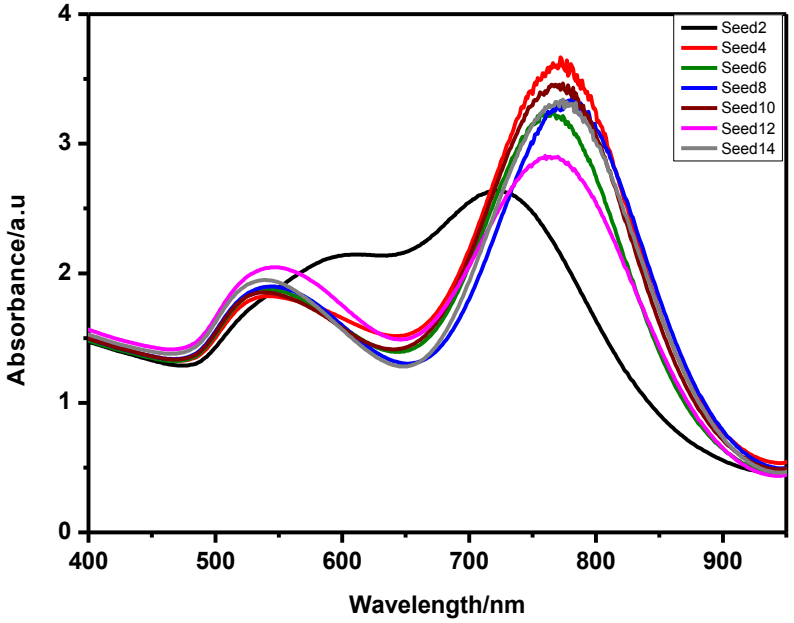

Figure 3-17: Absorption spectra showing the effect of the seed concentration using 60µM of $AgNO_3$.

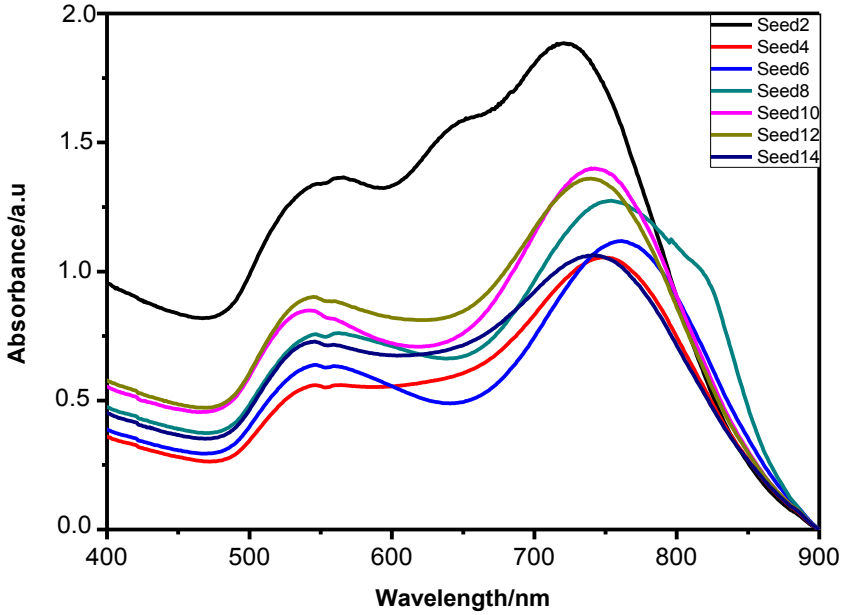

Figure 3-18: Absorption spectra showing the effect of the seed concentration using 80µM of $AgNO_3$.

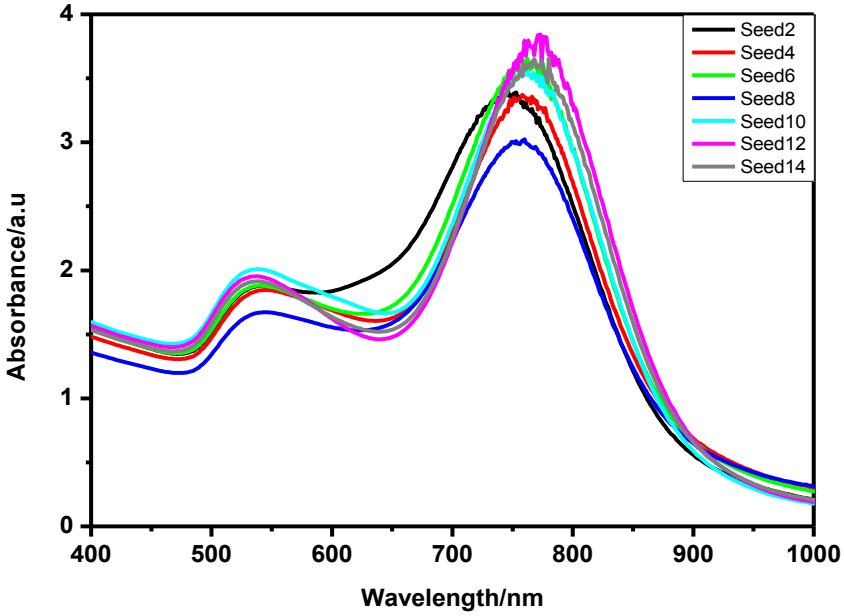

Figure 3-19: Absorption spectra showing the effect of the seed concentration using 100µM of $AgNO_3$.

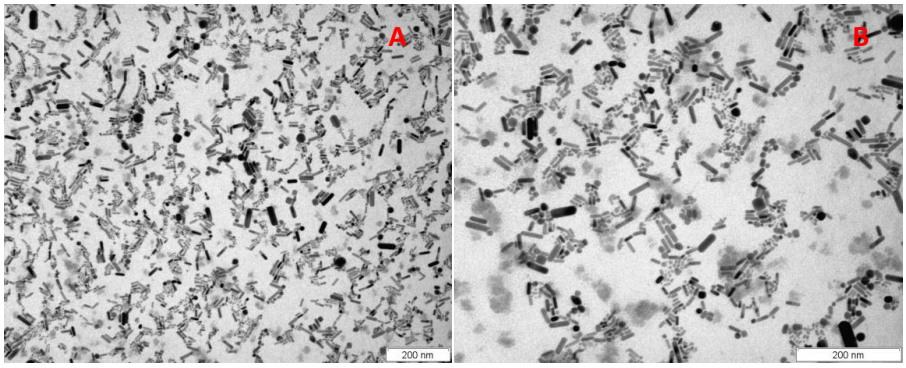

Figure 3-20: (A) TEM image of the NPs obtained using 0.113 µM of seeds and 40 µM $AgNO_3$ (a.r.= 3.4) and (B) TEM image for a similar synthesis using 80µM $AgNO_3$ (a.r.= 4.2).

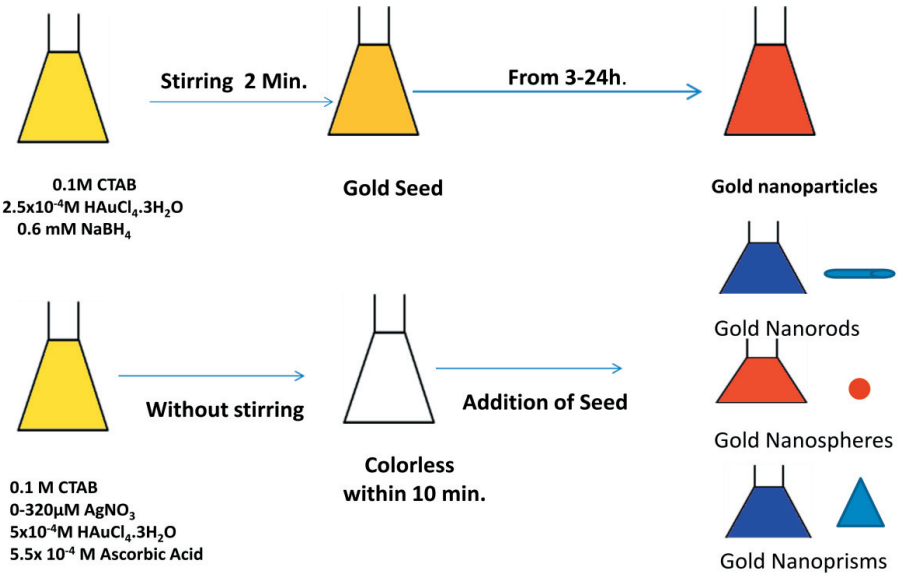

Scheme 3-3: Scheme showing a summary of the results obtained for the synthesis of the formation of gold nanoparticles with different shapes using different experimental conditions.

The effect of aging the seeds at different times (10 min., 4h, 7h, and 24 h.) were also studied with different concentration of $AgNO_3$. The following results were obtained:

In the absence of $AgNO_3$, spheres were produced for all the aging times (figure 3-21).

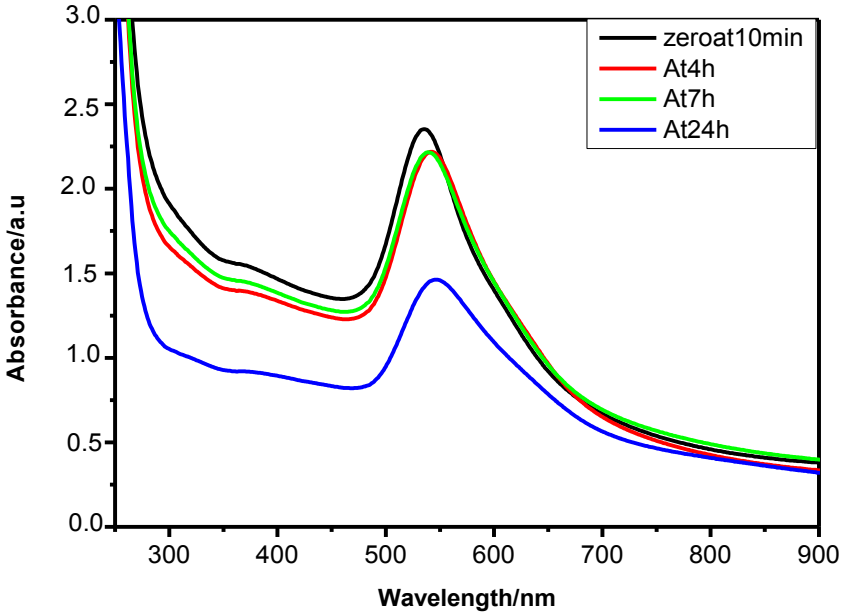

Figure 3-21: Absorption spectra showing the effect of the aging time of the seeds on the growth of NPs without $AgNO_3$.

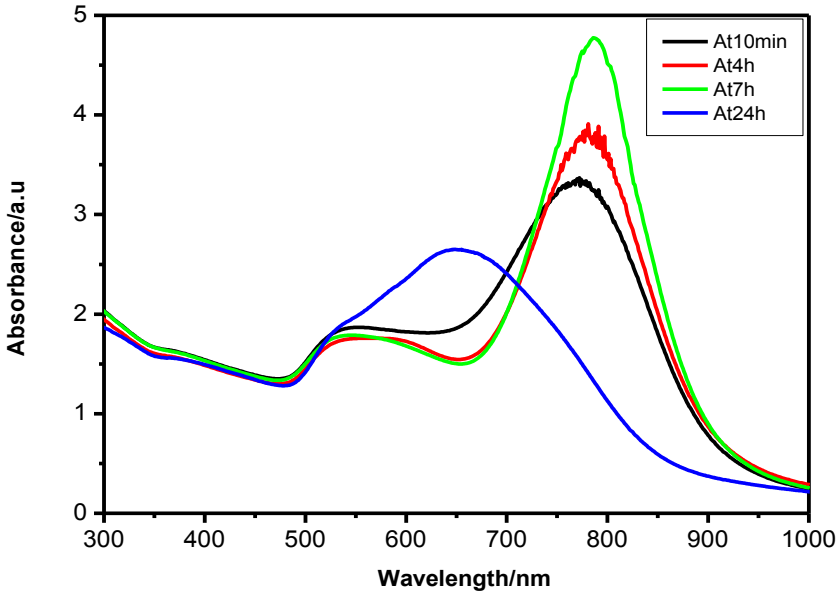

Figure 3-22: Absorption spectra showing the effect of the aging time of the seeds on the growth of NPs using 40µM $AgNO_3$.

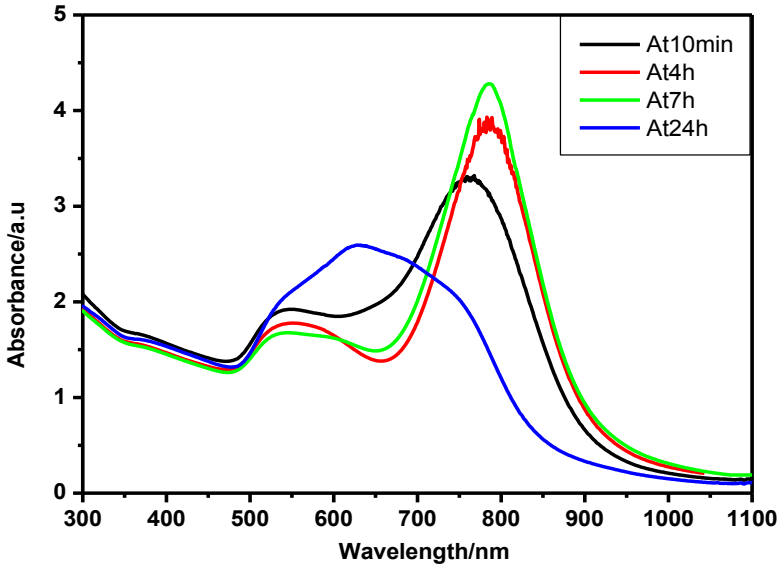

Figure 3-23: Absorption spectra showing the effect of the aging time of the seeds on the growth of NPs using 80µM $AgNO_3$.

The addition of the seeds aged for 10 min., 4h and 7h to the growth solution in the presence of $AgNO_3$ (40µM and 80 µM) yields to the formation of gold nanorods, while some snapped prisms and prisms mixed with spheres are formed using seeds aged for 24 hours.

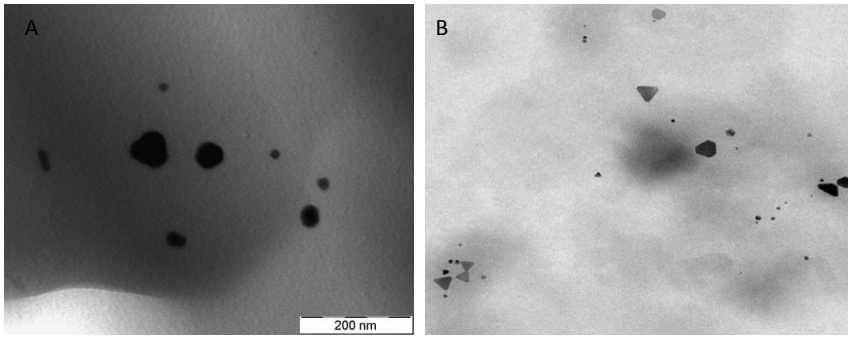

Figure 3-24: TEM images showing the produced nanoparticles with 40µM $AgNO_3$ (A) and 80µM $AgNO_3$ (B) using 24h aged seed solution.

Nanoprisms and snapped prisms mixed with gold nanorods are formed, when a high concentration of $AgNO_3$ (160µM) was added in the growth solution using seeds at different aging times (figure 3-25).

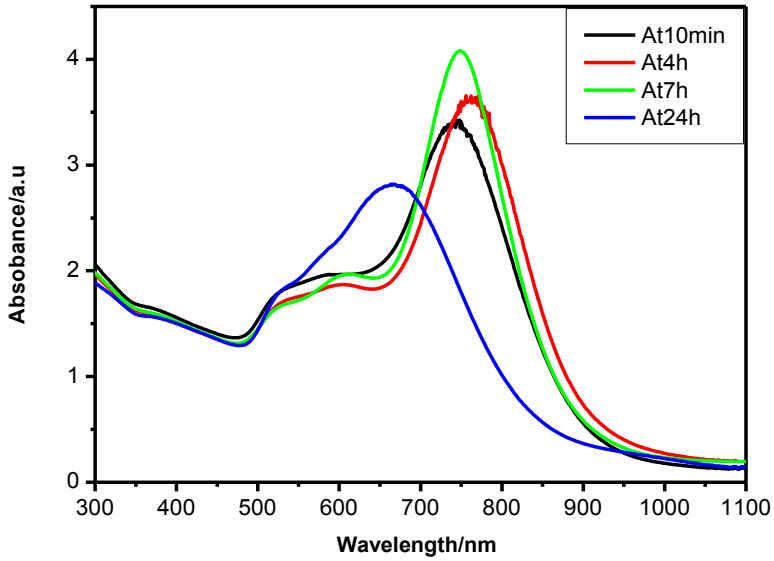

Figure 3-25: Absorption spectra showing the effect of the aging time of the seeds on the growth of NPs using 160µM $AgNO_3$.

One can then conclude that, at low aging times the seeds (from 10 min to 3h in which no Plasmon band appears in the UV-Vis absorption spectrum) well-shaped Au nanorods are produced with high yields (~90%) using low concentrations of $AgNO_3$, while largely snapped prisms are formed with 24h aging seeds. Therefore, the aged Au seeds at 24h are not suitable for the synthesis of well-defined Au nanorods.

Discussion:

In order to explain the results we propose here the following mechanism, which is different from those previously reported (see Scheme 3-4), based on the following facts:

1) We have checked that, under our experimental conditions, Ag^{+} ions are indeed reduced by ascorbic acid (see figure 3-26). UV-Vis spectra of Ag^{+} ions reduced by ascorbic acid, under similar conditions of the experiments, show the disappearance of the reactant bands (ascorbic acid: 264 nm and silver nitrate: 238nm). The absence of the Ag plasmon band after reduction can be associated with the formation of small silver clusters with sizes below ≈ 1-2 nm[45]. Moreover, the absence of bands above 275-300 nm shows that small and flat Ag_n clusters with n ≈ < 8-10 atoms are formed[46, 47]. Therefore, the formation of new Ag (0) species (Ag_n clusters), which may influence the growth mechanism, have to be taken into account.

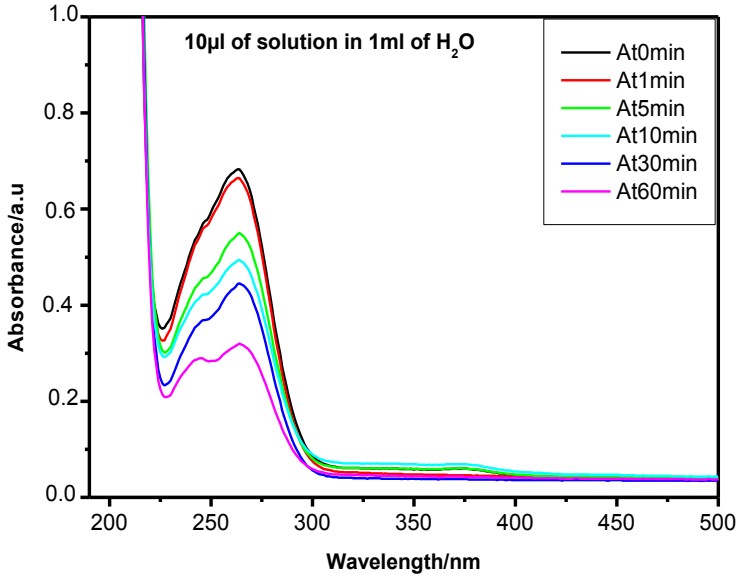

Figure 3-26: Absorption spectra showing the reduction of Ag^{+} ions at neutral pH by ascorbic acid. Please, note the absence of the Ag plasmon band even at 60 minutes.

By using AFM measurements, we tried to characterize the clusters. It was observed that the major size of the formed clusters is below 1 nm (see figure 3-27). Using HRTEM it was also observed the formation of some of larger particles with sizes in the range 2-4 nm, as it can be seen in figure (3-28). However, the fact that no plasmon band is observed in the UV-Vis spectrum indicates that, most probably, these particles are formed under the electron beam irradiation from some aggregation of clusters formed in the grids.

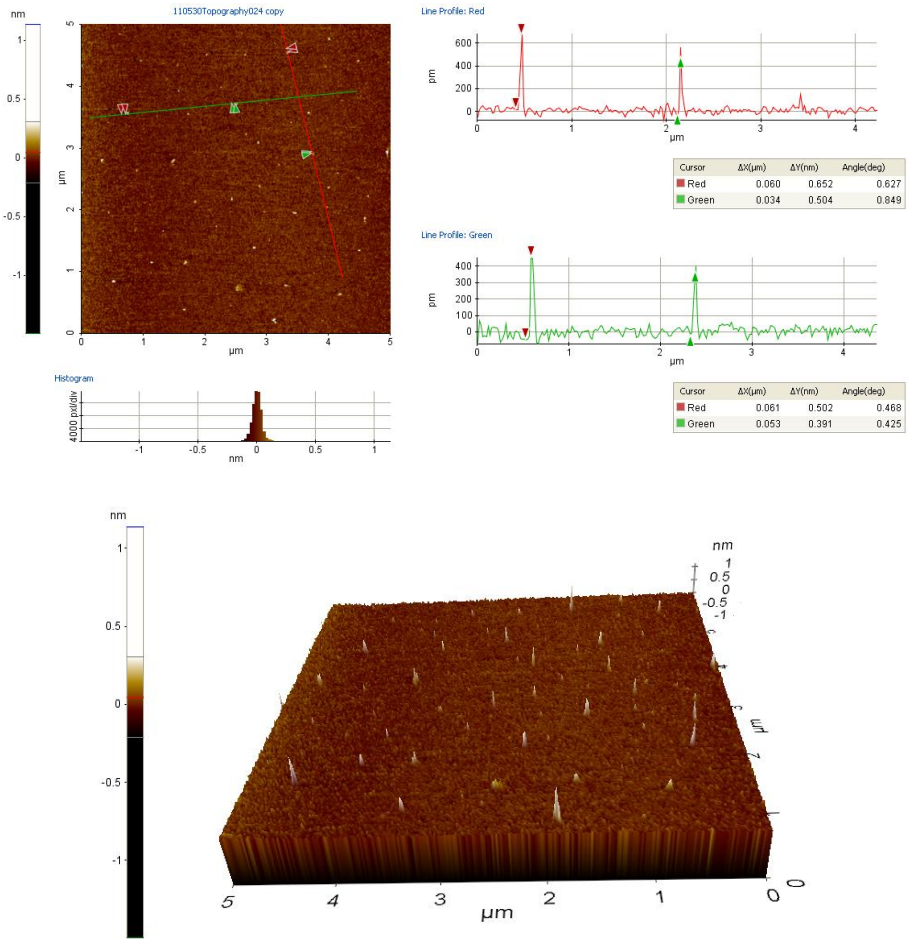

Figure 3-27: AFM picture of Ag-clusters (prepared in situ after 10 min. from the addition of ascorbic acid to the growth solution in the absence of Au salt) deposited on mica with the profiles throughout the red and green lines and 3D AFM picture showing that the size of Ag-clusters is below 1 nm.

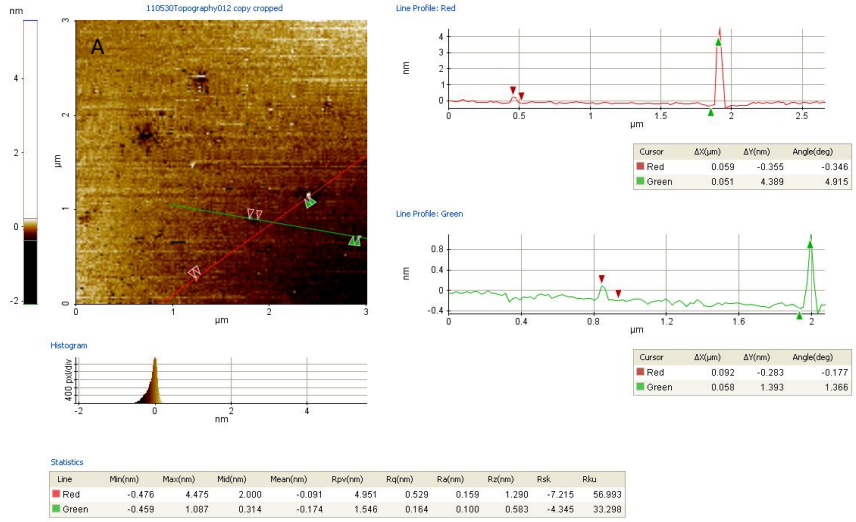

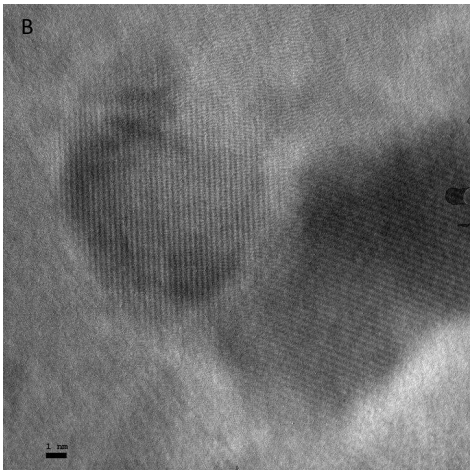

Figure 3-28: AFM picture of Ag-clusters deposited on mica with the profiles throughout the red and green lines (A) and, HRTEM for picture of Ag nanoparticles of approx.4nm with a pyramidal shape (B).

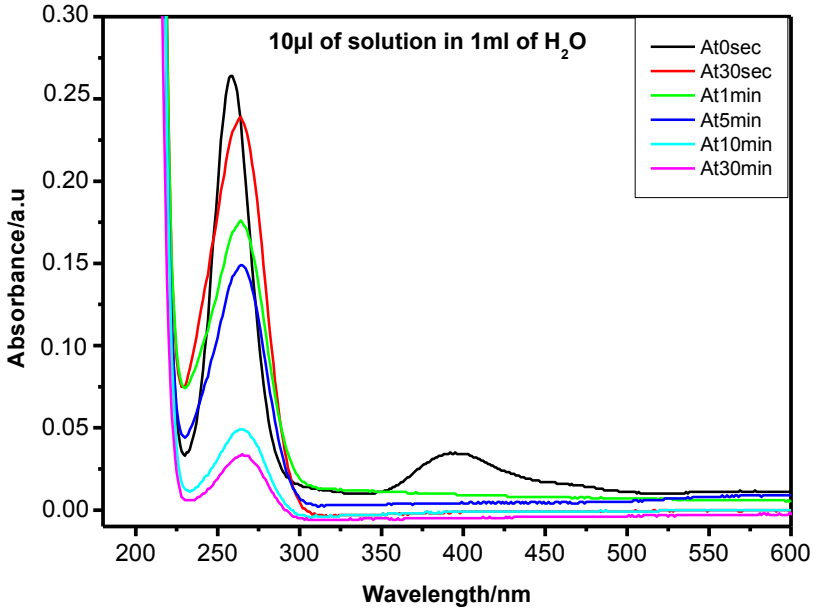

Figure 3-29: Absorption spectra showing the reduction by ascorbic acid (AA) of Au^{3+} to Au^{+} in the growth solution (without $AgNO_3$) at neutral pH.

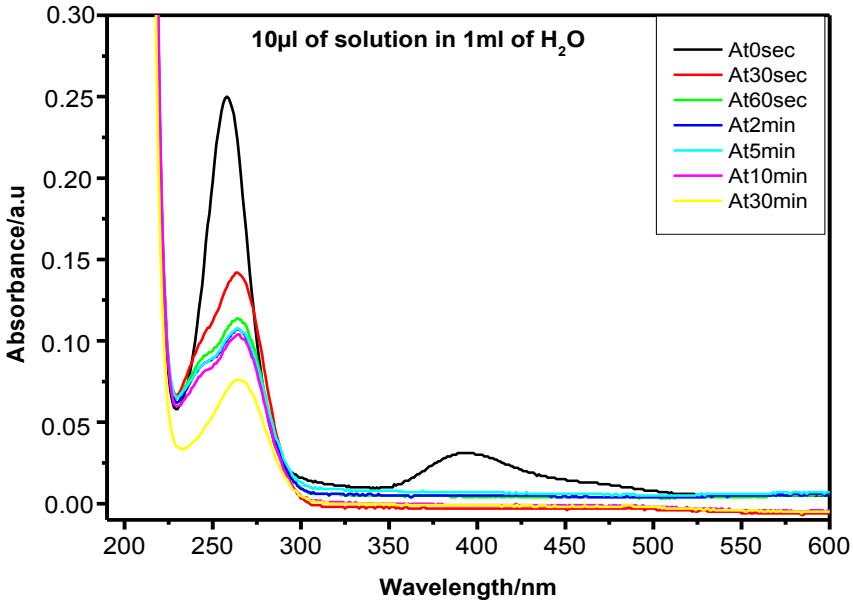

Figure 3-30: Absorption spectra showing the reduction of the growth solution by AA at neutral pH.

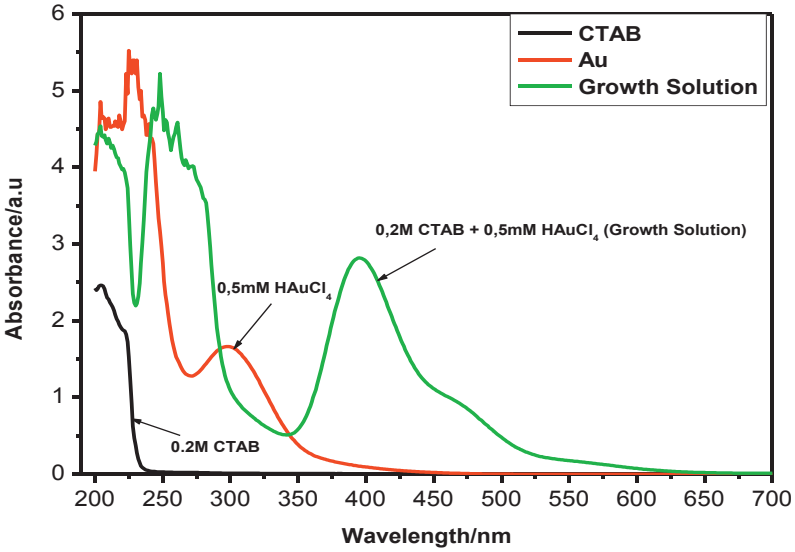

Figure 3-31: Absorption spectra showing the absorption of CTAB, $HAuCl_4$, and the growth solution.

2) We have also observed that the growth of gold nanorods is faster in the presence of Ag ions (see figure 3-33) suggesting a clear catalytic effect by either the silver ions or the new silver (0) species formed. From the increase in the intensity of the Plasmon bands one can estimate an approximate catalytic rate constant for Ag of $k_{cat} = 260 \pm 60\ M^{-1}s^{-1}$ (see figures 3-34 and 3-35).

Figure 3-32: A picture of the change in the color of the samples as the [$AgNO_3$] increases from 40µM to 240µM.

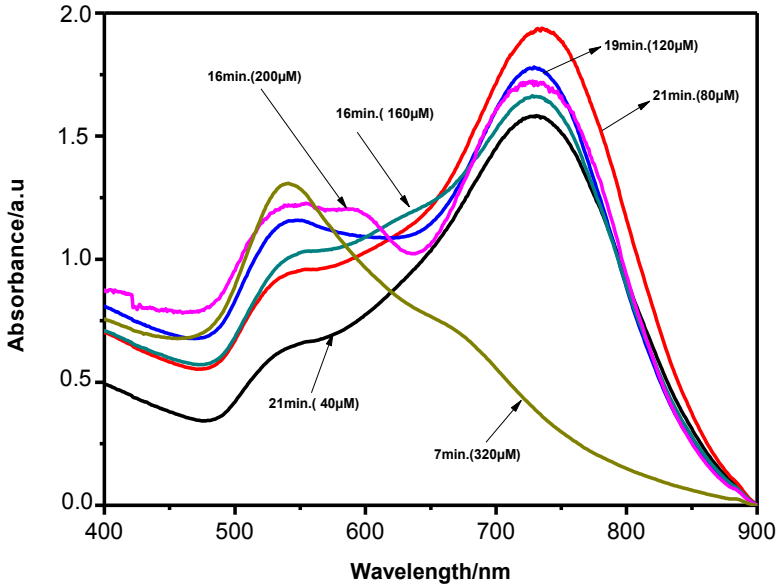

Figure 3-33: Absorption spectra showing the influence of the concentration of $AgNO_3$ on the formation of gold nanorods showing a faster growth with increasing concentration (only displayed the final spectra at the end of the reaction).

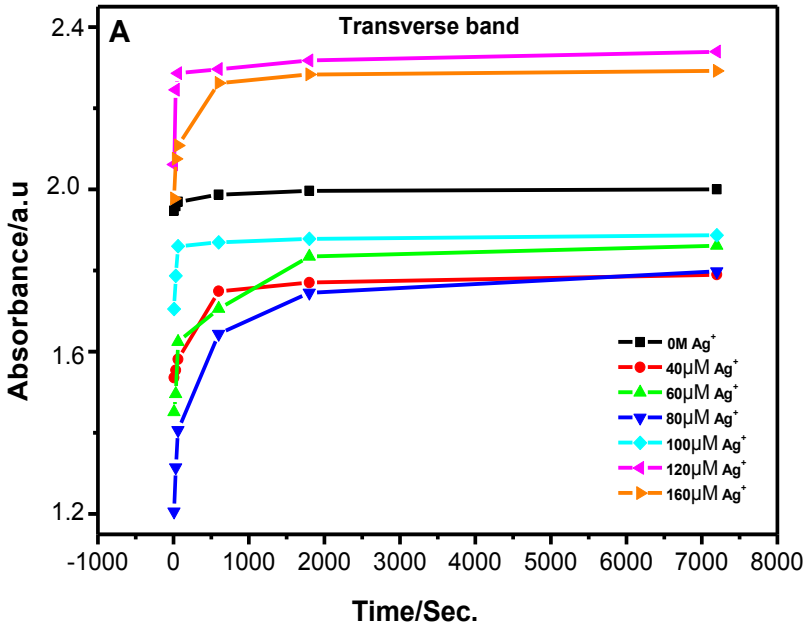

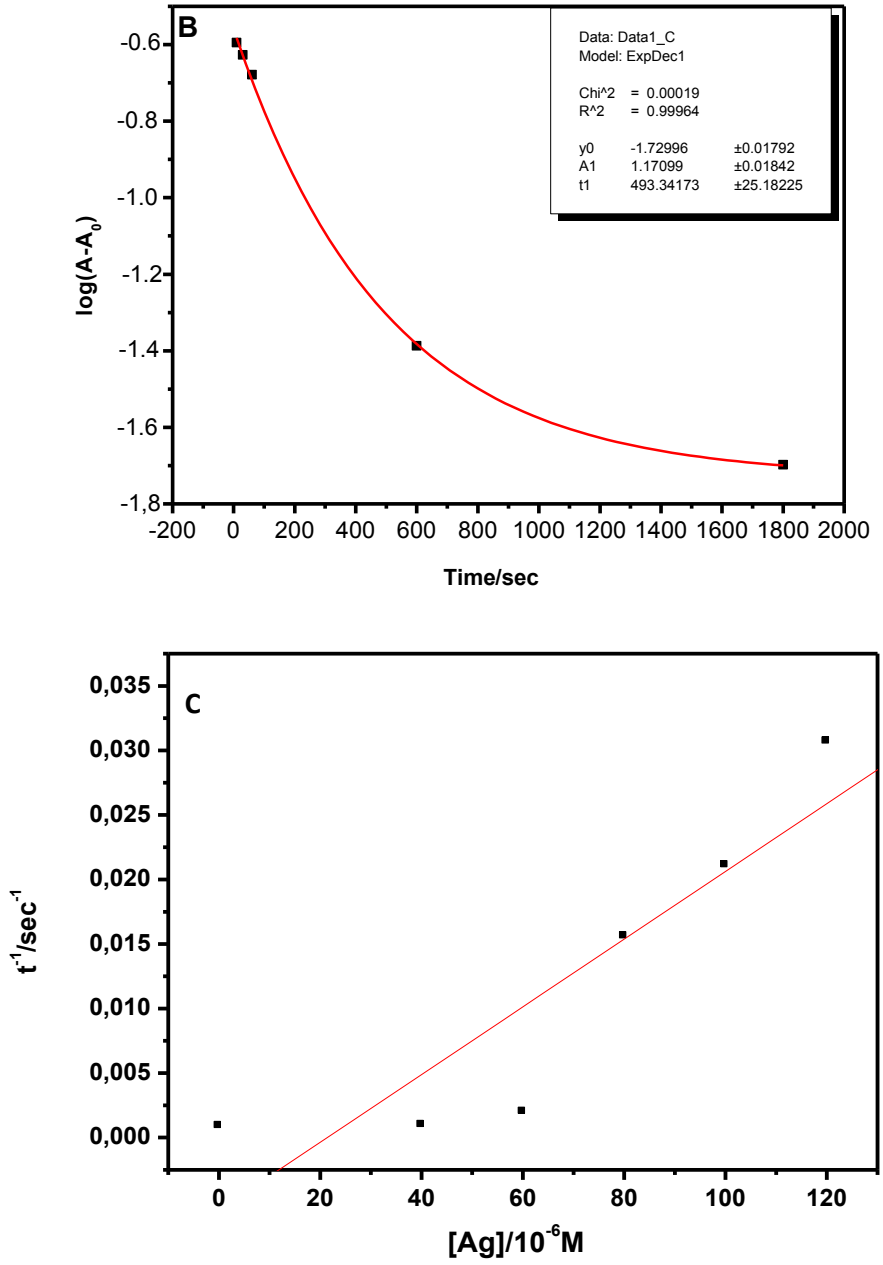

Figure 3-34: Catalytic effect of Ag-ions based on the increase of the transverse Plasmon band at different concentrations of $AgNO_3$. (A) Absorbance at λ = 538nm vs time. (B) Fitting to a pseudo-first order reaction: log ($A-A_0$) vs time. A_0: initial absorbance. (C) Linear dependence of the inverse of the relaxation time (τ^{-1} /s^{-1}) with the Ag^+ concentration. Slope = k_{cat} =(2.6±0.6)x10^2 $M^{-1}s^{-1}$

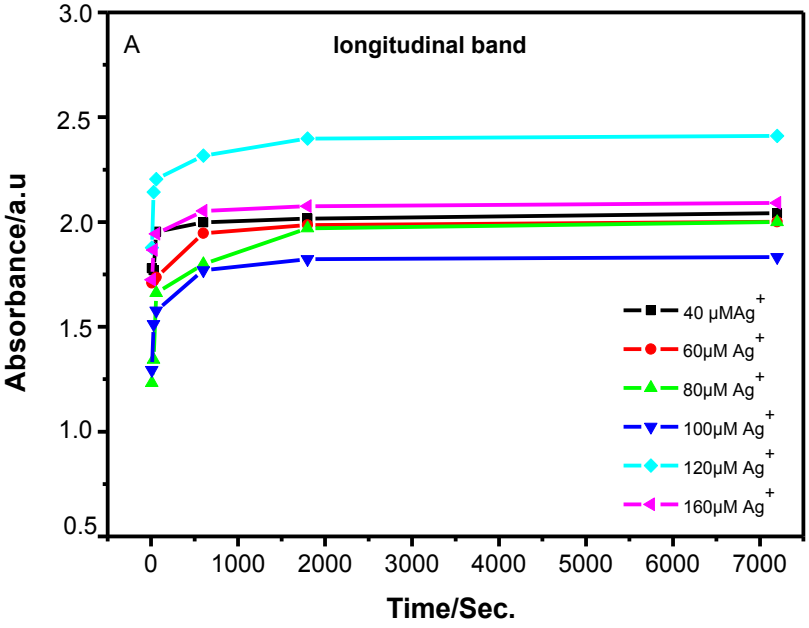
A
longitudinal band
Absorbance/a.u
Time/Sec.
40 μMAg+
60μM Ag+
80μM Ag+
100μM Ag+
120μM Ag+
160μM Ag+

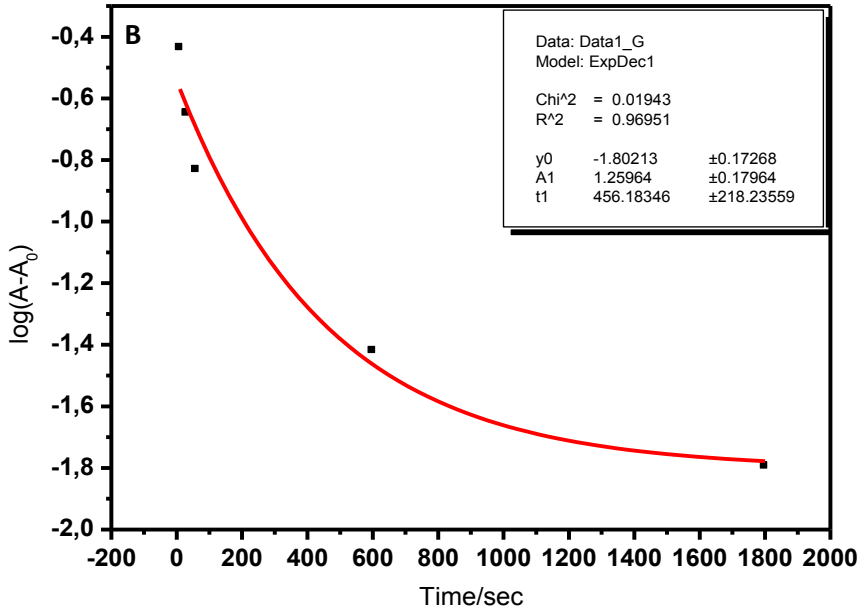
B
Data: Data1_G
Model: ExpDec1
Chi^2 = 0.01943
R^2 = 0.96951
y0 -1.80213 ±0.17268
A1 1.25964 ±0.17964
t1 456.18346 ±218.23559
log(A-A0)
Time/sec

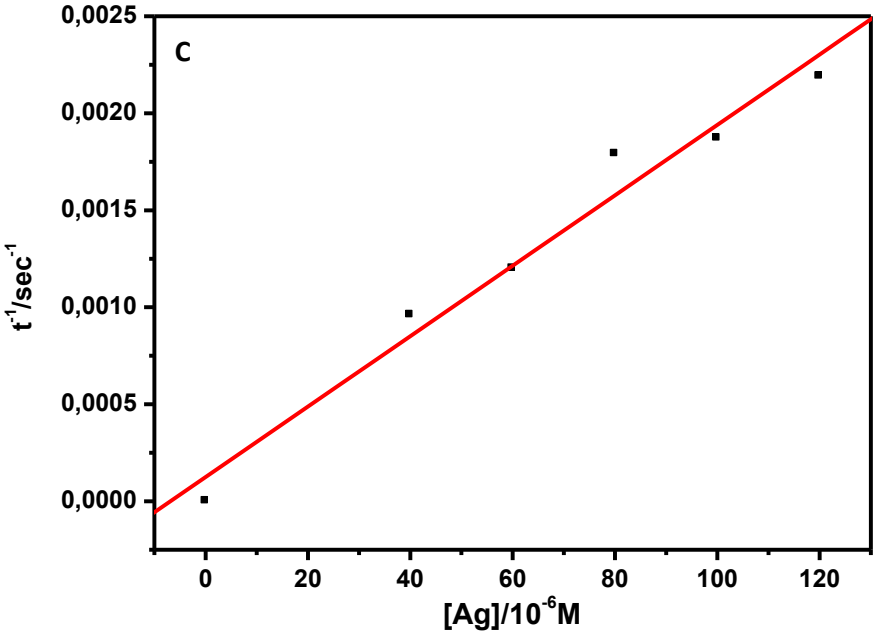

Figure 3-35: Catalytic effect of Ag-ions based on the increase of the longitudinal Plasmon band at different concentrations of $AgNO_3$. (A) Absorbance at λ = 724nm vs time. (B) Fitting to a pseudo-first order reaction: log ($A-A_0$) vs time. A_0: initial absorbance. (C) Linear dependence of the inverse of the relaxation time (τ^{-1} /s^{-1}) with the Ag^+ concentration. Slope = k_{cat} =18±2 $M^{-1}s^{-1}$

Our data clearly show that the amount of silver ions, needed to induce changes in the final nanoparticle morphology, is several orders of magnitude smaller than the CTAB used. Therefore, changes in the soft template provided by the CTAB, due to changes in the Ag ion concentrations, can be disregarded.

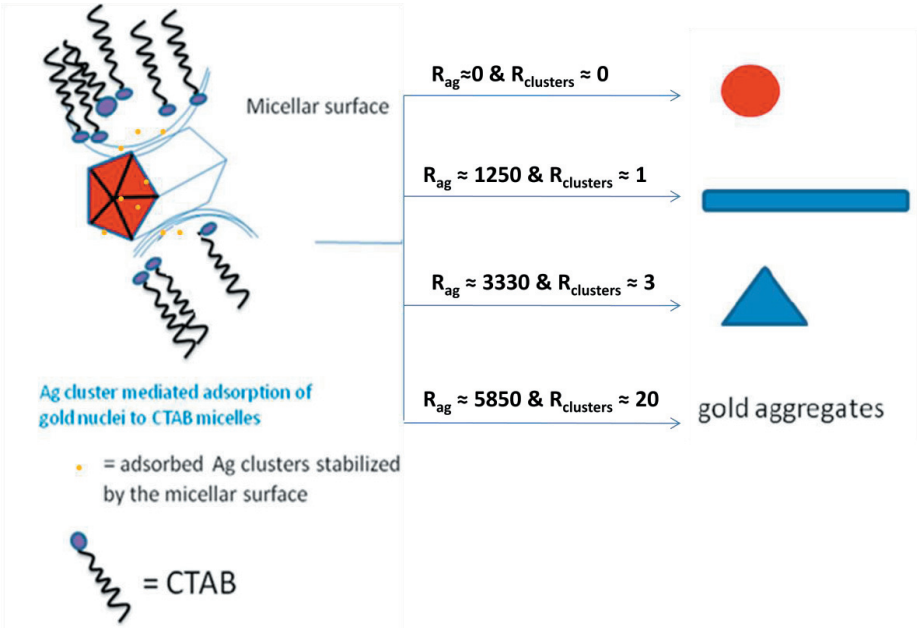

Scheme 3-4: Scheme showing the proposed mechanism of the formation of gold nanoparticles with different shapes.

R_{Ag} = [Ag^+] / [Au seeds]. $R_{clusters}$ = [Ag clusters] / [Au seeds].

According to the mechanism that we propose (scheme 3-4) to explain the experimental results, Ag^+ ions are reduced in the presence of ascorbic acid and adsorbed onto the surface of the gold seeds. This can happen because the oxidation potential of Ag^+/Ag (0.8V) is lower than the Au^{+3}/Au (1.5V) and, at the same time, there is a period of 10 minutes before the addition of the seed solution, which is enough for the formation of Ag clusters. The parallel reduction of Ag and Au ions will then lead to the formation of Ag clusters and Au seeds in different percentages depending on the experimental conditions. The produced silver atoms, probably forming stable clusters[47,48], can then act as a catalyst enhancing the growth of the gold nanorods (atomic metal clusters are now recognized as especially efficient catalysts[44]) since those clusters could be adsorbed on active sites on the surface of the formed gold nuclei (seeds). Gold particles with a cubic lattice have a tendency to grow forming cubes, or spheres, because

the rate of the growth of all facets is the same (result obtained when Ag^+ ions are not added). However, adsorption of silver clusters on one of these facets, leads to a breaking the symmetry of the growth, and enhance the growth of one of these facets much more than the others, which leads to the formation of rod shaped particles. This could happen when the ratio $R_{clusters}$ = [Ag clusters]/ [Au seeds] ≈ 1. It is difficult to estimate the amount of clusters produced because we do not know the amount of reacted Ag ions. But one can make some approximate calculations. Taking into account that [Ag clusters] = [reacted Ag ions]/N_{Ag}, being N_{Ag} < 10 –see above- the number of atoms per cluster, then we can deduce from Table (3-1) that the percentage of reacted Ag ions should be ≈ < 6% (0.2%-20%). From the results derived from the UV-Vis spectra for the direct reduction of Ag^+ ions by ascorbic acid (see figure 3-26) one can deduce that, after 10 minutes, ≈ 25% of the reaction has taken place. This result agrees with the largest estimation made from the mechanism described above (0.2-20%) and suggests, at the same time, that the size of Au seeds should be ≈ 16, with a 3D structure[49]. Then, one can assume that the formed Ag catalytic clusters, because they should have a flat structure[46], could be easily adsorbed on a flat facet of the 3D Au seeds, promoting the formation of rod shaped particles. When the amount of Ag^+ ions is increased, the corresponding amounts of Ag clusters produced should also increase and will be adsorbed in more than one facet. In this case, the rate of the growth of these facets will be different than the others leading to more anisotropic shapes, like prisms or triangles. According to table (3-1), this would happen when the ratio $R_{Ag}/R_{Ag\ rods}$ ≈ 2.7. Increasing further the Ag^+ ion concentration it will induce more and more the further growth of the particles in all directions, leading finally to the formation of gold aggregates, which happens for $R_{Ag}/R_{Ag\ rods}$ ≈ 4.7.

One can explain also the influence of the seed concentration because when a small amount of seeds are used, the concentration of Ag^+ ions is relatively high compared with the amount of gold seeds and, therefore, the amount of adsorbed Ag clusters on the surface of the seed facets is high, leading to the growth of prismatic shapes. But, when the amount of the seeds – relatively to the silver ions- increases, the smaller amounts of adsorbed clusters leads to the growth of only one facet and gives the formation of rods.

The final Shape	Spheres	Rods	Prisms & Hexagonal	Aggregated particles
R_{Ag}	0	≈ 1700 (50-6100)	≈3700 (110-13300)	≈6000 (180-21600)
$R_{Ag}/R_{Ag\ rods}$	0	≈ 1	≈ 2.7	≈ 4.7
$R_{clusters}$	0	≈ 1	≈ 3	≈ 20

Table 3-1: Summary of the results obtained for the dependence of the nanoparticle shape on the ratio R of the silver ions and clusters to the seeds concentration.

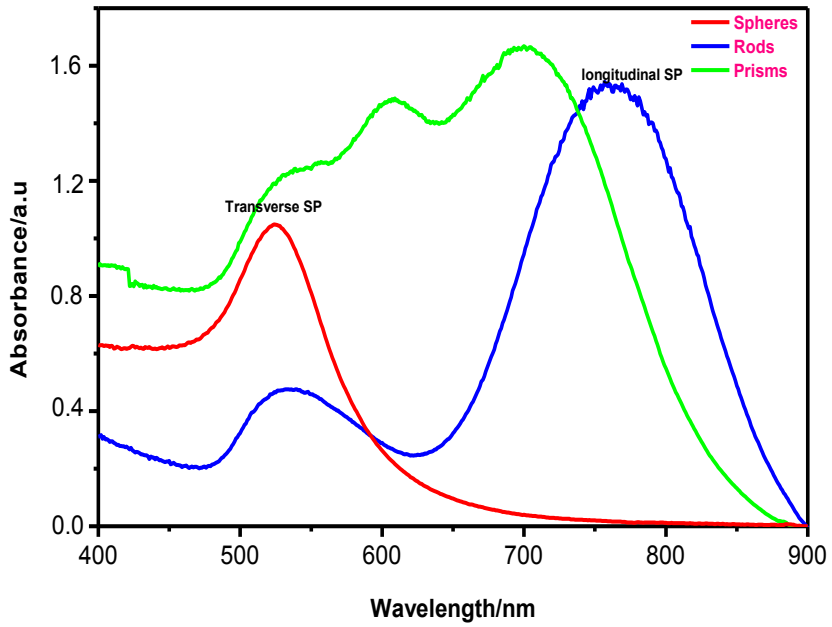

Figure 3-36: Absorption spectra of gold nanoparticles with different shapes at different concentration of silver ions: spheres ($R_{cluster}$≈0), rods ($R_{clusters}$≈1) and prisms ($R_{clusters}$≈3).

In order to confirm the mechanism here proposed, we decided to carry out a new set of experiments using external prepared clusters instead of Ag^+

ions. For this purpose, small Ag clusters from Nanogap, with Ag_3 as the main abundant clusters were employed.

3-4: Effect of using Ag-clusters.

Under identical experimental conditions (with [Seeds] = 0.048µM in all the solutions of this study), different amounts of 1 mg/l of Ag-cluster´s concentrations, ranging from 0.0665 nM to 0.95µM, were added into the growth solutions of the same concentrations as in previous experiments.

Figure (3-37) shows the TEM images and the absorption spectra of the gold nanoparticles produced when different amounts of Ag-clusters are introduced in the reaction media, showing mainly the formation of prisms and rods with different aspect ratios.

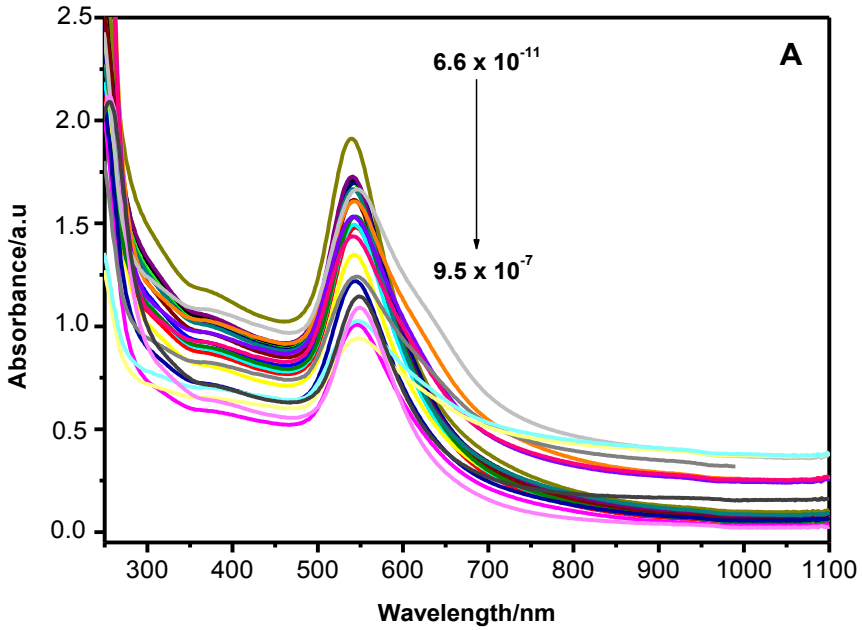

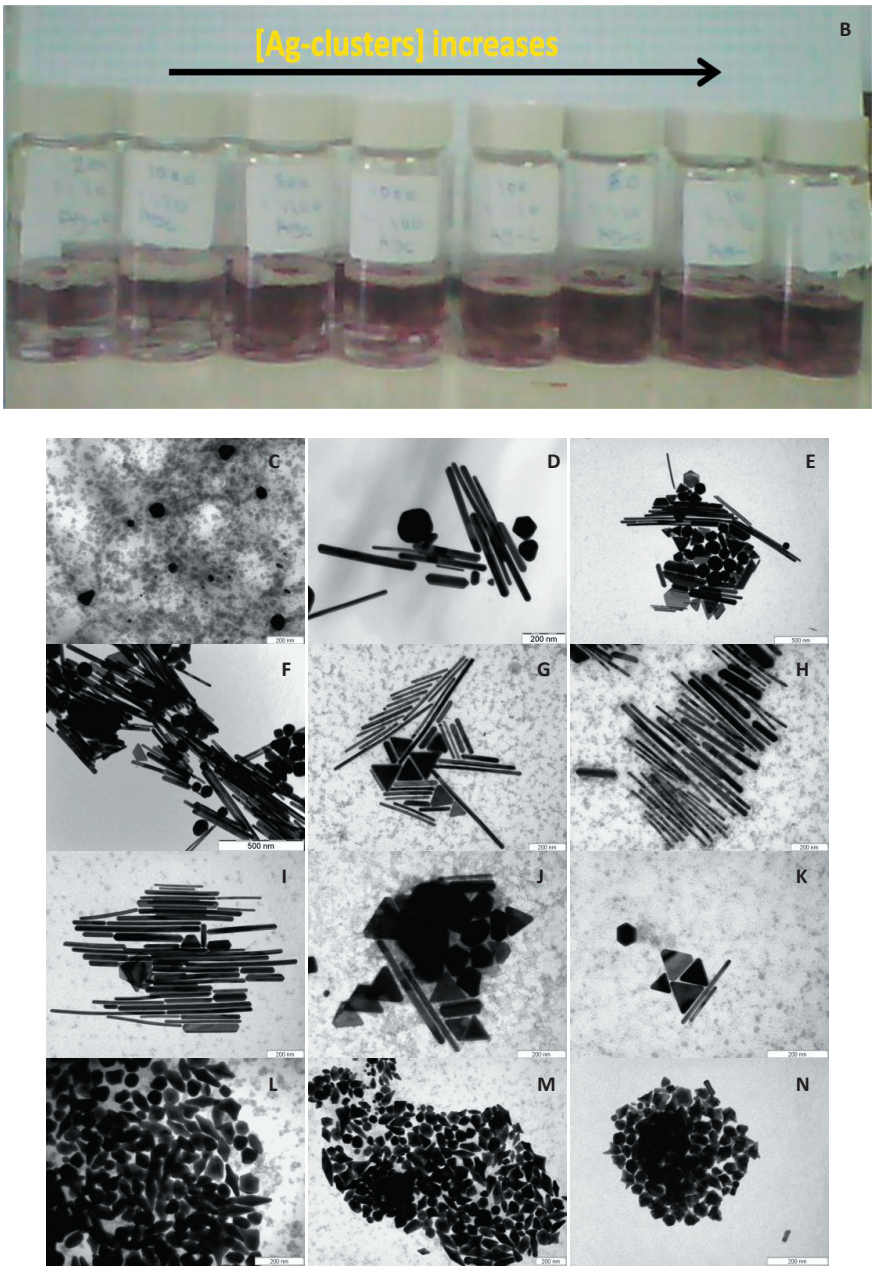

Figure 3-37: (A) Absorption spectra showing the effect of Ag-clusters at different concentrations ($6.6x10^{-11}$– $9.5x10^{-7}$M). (B) Picture showing the time for the appearance of the color in the samples, which is faster as the [Ag-clusters] increases. (C-N) TEM images of gold nanorods and nanoprisms obtained with different concentrations of Ag-clusters.

No. of samples	Ag-Clusters conc.	[NaCl]	Other shapes	Prisms	Rods	a.r.
C	$6{,}65x10^{-11}$	$2.2x10^{-7}$	90%(spheres)	7%(snapped)	3%	12.1±2
D	$3{,}3x10^{-10}$	$1.09x10^{-6}$	18%(hexagonal+spheres)	14%(snapped)	68%	15.6±1
E	$6{,}54x10^{-10}$	$2.16x10^{-6}$	16%(hexagonal+spheres)	11%	73%	17.2±1
F	$3{,}03x10^{-9}$	10^{-5}	4%(hexagonal+spheres)	18%	78%	19.8±1
G	$6{,}54x10^{-9}$	$2.16x10^{-5}$	1%(hexagonal+spheres)	15%(snapped)	84%	23.4±1
H	$1{,}28x10^{-8}$	$4.2x10^{-5}$	1%(hexagonal+spheres)	7%	92%	18.7±1
I	$3{,}3x10^{-8}$	$1.09x10^{-4}$	2%(hexagonal+spheres)	3%	95%	29.3±2
J	$6{,}54x10^{-8}$	$2.16x10^{-4}$	7%(hexagonal+spheres)	22%	71%	15.4±2
K	$1{,}28x10^{-7}$	$4.2x10^{-4}$	6%(hexagonal+spheres)	74%	20%	14.6±1
L	$3{,}03x10^{-7}$	10^{-3}	65%(bipyramids+tetrapods)	26%	9%	14.2±1
M	$5{,}56x10^{-7}$	$1.83x10^{-3}$	60%(bipyramids+tetrapods)	28%	12%	12.6±2
N	$9{,}5x10^{-7}$	$3.14x10^{-3}$	87%(aggregated + spheres)	8%(snapped)	5%	11.5±1

Table3-2: Summary of the results obtained by changing the silver cluster concentration maintaining all other parameters constant.

From the TEM-images one can see that the aspect ratio of the formed nanorods is a.r.: (~12-30). This a.r. is higher than the previous ones obtained using only Ag ions in the reaction media. This result is not surprising because the size (and concentration) of the used Ag clusters may not be exactly the same as the ones "in situ" produced by adding Ag ions. The observation of only one plasmon band in the UV-Vis spectra is due to the fact that the expected transverse plasmon band for these long rods will be located in the IR-region, as it can be predicted by the formula, $\lambda_{max}(nm) = 570 + 51(a.r.)$[26]: λ_{max} = 1200-2100 nm. The results, summarized in Tables (3-1 and 3-2), clearly show the expected effect of the parameter $R_{cluster}$ on the final shape of the Au nanoparticles, thus confirming the above proposed mechanism. It is worth to mention the formation of bipyramids with some tetrapod's shapes, which is observed at $R_{clusters} \approx 6$.

3-5: Effect of using NaCl.

From the data supplied of the commercial silver clusters prepared by NANOGAP-SPAIN, it can be observed that the sample of silver clusters

contains < ≈ 11 mM of NaCl. It is known that the presence of NaCl can affect the growth of gold nanorods. For example, Prasad and co-workers[50] found that the aspect ratio of gold nanorods increased in the presence of NaCl. However, there is a critical concentration, above which the aspect ratio decreased. Because of that we decided to study the effect of NaCl in the presence and absence of Ag- clusters.

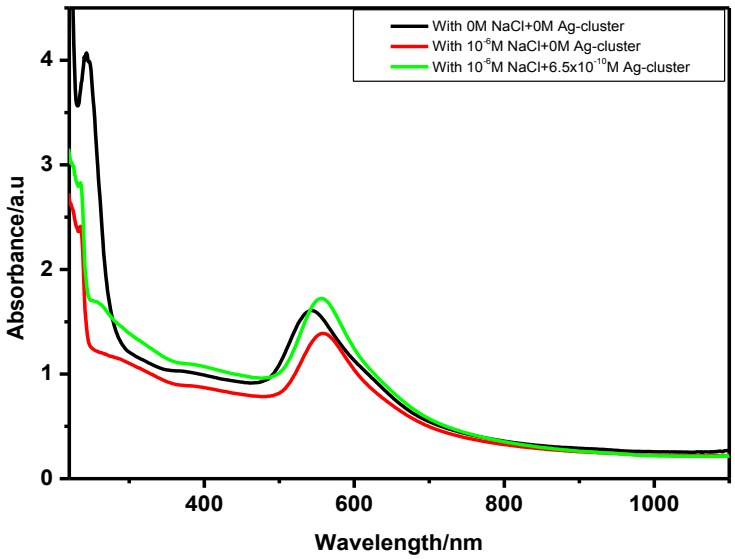

Figure 3-38: Absorption spectra showing the effect of NaCl in the absence and the presence of Ag-clusters.

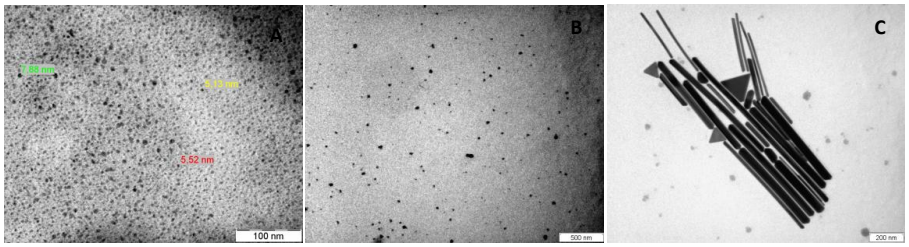

Figure 3-39: TEM images showing the samples without NaCl and Ag-clusters (A); with 10^{-6} M NaCl without Ag-clusters (B); and with 10^{-6} M NaCl in the presence of $6.5x10^{-10}$M Ag-clusters (C).

It is clear from the TEM-images that the clusters are the responsible for the formation of gold nanorods with high aspect ratio (≥ 20) with some byproducts like prismatical shapes.

To complete the study of the effect of NaCl on the growth of gold nanoparticles, we added NaCl at different concentrations from 0 to 10^{-2} M in the absence of silver clusters or Ag-ions. We found the same results as Prasad and co-workers. The presence of NaCl increases the aspect ratio and also the yield, while by increasing further the NaCl concentration, the aspect ratio decreased and the formation of other shapes, like prisms, is promoted. However, it is observed that at the lower concentrations of NaCl, Ag-clusters are needed for the formation of gold nanorods.

Finally, it has to be mentioned that, as it was described in the Introduction, Perez-Juste et al.[(2)] showed that an increase in the ionic strength produced a decrease in the yield of rods[(2)]. From Figure (3-40) and Table (3-3), we observed the same phenomenon without Ag ions while, such a phenomenon was not observed, in the presence of silver clusters.

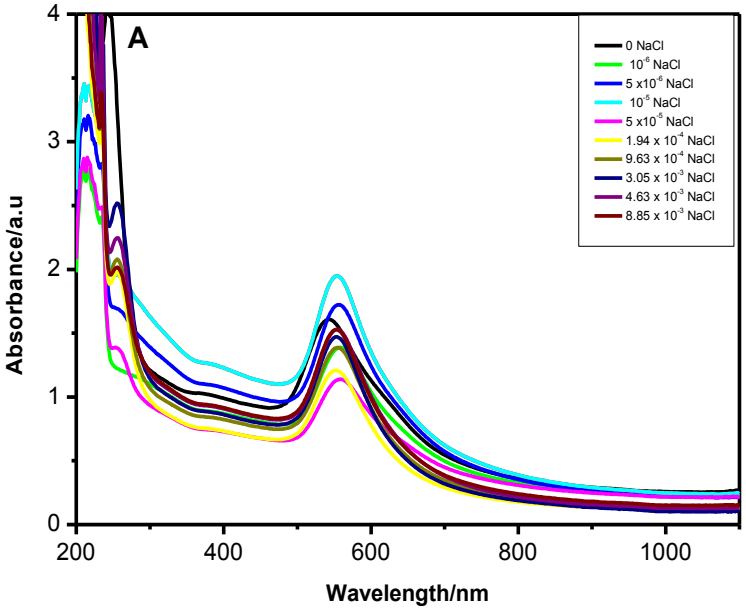

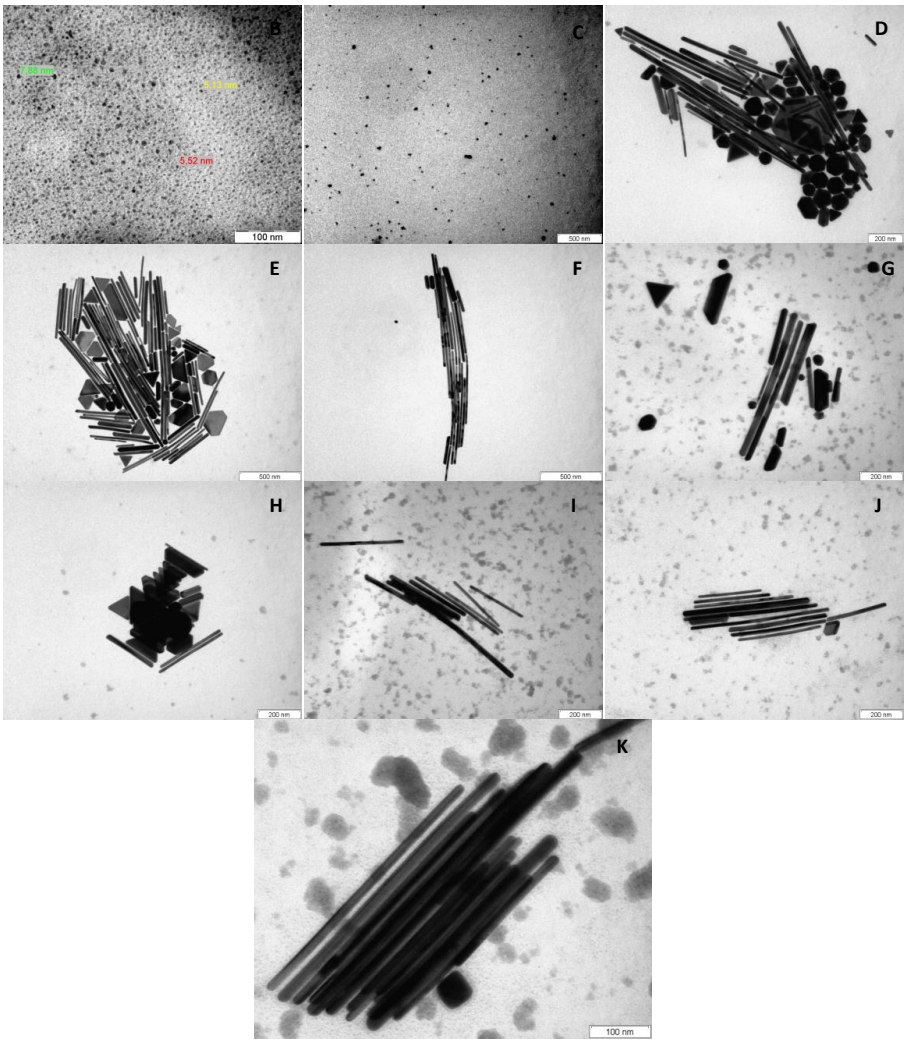

Figure 3-40: Absorption spectra showing the effect of NaCl with different concentrations (0 – $8.5x10^{-3}$ M) (A), and TEM images of the corresponding products (B-K).

	Samples	[Cl]	**Rods**	Prisms	Others
B	0M NaCl	$2.0012x10^{-3}$	0%	0%	100%
C	10^{-6} M NaCl	$2.0022x10^{-3}$	1%	0%	99%
D	$5x10^{-6}$ M NaCl	$2.0062x10^{-3}$	52%	13%	35%
E	10^{-5} M NaCl	$2.0112x10^{-3}$	75%	18%	7%
F	$5x10^{-5}$ M NaCl	$2.0512x10^{-3}$	40%	19%	41%
G	$1.94x10^{-4}$ M NaCl	$2.1952x10^{-3}$	46%	12%	42%
H	$9.63x10^{-4}$ M NaCl	$2.9642x10^{-3}$	58%	19%	23%
I	$3.05x10^{-3}$ M NaCl	$5.0512x10^{-3}$	45%	14%	41%
J	$4.63x10^{-3}$ M NaCl	$6.6312x10^{-3}$	52%	15%	43%
K	$8.85x10^{-3}$ M NaCl	$10.8512x10^{-3}$	53%	12%	35%

Table 3-3: Summary of the results showing the effect of different concentrations of NaCl on the growth of gold nanoparticles.

The mechanism that we discussed for the formation of gold nanoparticles with different shapes using $AgNO_3$ or Ag-clusters, so far did not take into account the influence of CTAB on the final nanoparticle shape. But, the reported results are only possible in the presence of CTAB. Without CTAB no change in the shape of the Au nanoparticles could be observed under our experimental conditions. It has to be noticed that Smith and Korgel[35] reported that not only the presence of Ag^+ ions is one of the key parameters for obtaining the anisotropic shape of gold nanoparticles, but also that the supplier of the CTAB is one significant factor for controlling the nanoparticle shape. Although those authors stated that different shapes of gold nanoparticles could be only produced when CTAB from certain suppliers (CTAB from Aldrich was anyone of them) was used, our results obtained using CTAB from Aldrich (95%) are in disagreement with such conclusions.

sample	supplier	product #	nanorods?[a]	catalog purity	actual lot purity
A	Sigma	H6269	yes	~99%	100.0%
B	Sigma	H9151	yes	~99%	100.3%
C	Fluka	52365	yes	≥99%	99.4%
D	Fluka	52367	yes	≥99%	99.7%
E	Fluka	52369	yes	≥99%	99.7%
F	Fluka	52370	yes	≥96%	97.1%
G	MP Biomedicals	194004	yes	>98%	98.9%
H	Acros	22716V	no	≥99%	99.0%
I	Sigma	H5882	no	≥99%	100%
J	Aldrich	855820	no	95%	100.3%

Table 3-4: Table showing the purity of CTAB described in the supplier's catalog and the actual lot purity of CTAB from several different suppliers that were used to synthesize gold nanorods in Korgel studies[35].

In order to investigate the reasons for such differences, and because we used higher concentrations of CTAB (0.1M) than the concentrations used by Korgel`s group (0.05M), we carry out some experiments to see the influence of the CTAB concentration (see figures 3-41 to 3-43). A clearly change from nanorods to spheres by reducing the CTAB concentration was observed, indicating that a minimum concentration of CTAB (which is above the CMC) is needed to get different shapes. The concentration of CTAB determines the shape of the nanoparticles. Below CMC, the reduction primarily results in nanospheres. Only above CMC, anisotropic shapes develop as the major products. It seems that this minimum concentration depends on the CTAB supplier but, in principle, any supplier could be used to produce different nanostructures provided that the right conditions are used. Although it remains to be clarified if there are some main impurities in the CTAB from different suppliers, which could induce such changes in the experimental conditions, from the above results one can say that they have only a minor influence on the minimum concentration needed to achieve the CMC.

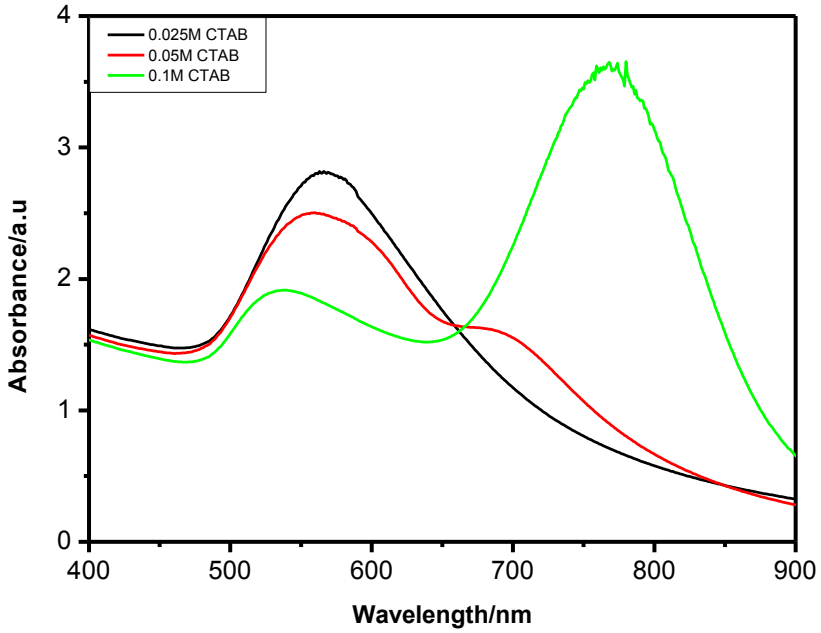

Figure 3-41: Absorption spectra showing the effect of the concentration of CTAB (from Aldrich) on the growth of gold nanorods.

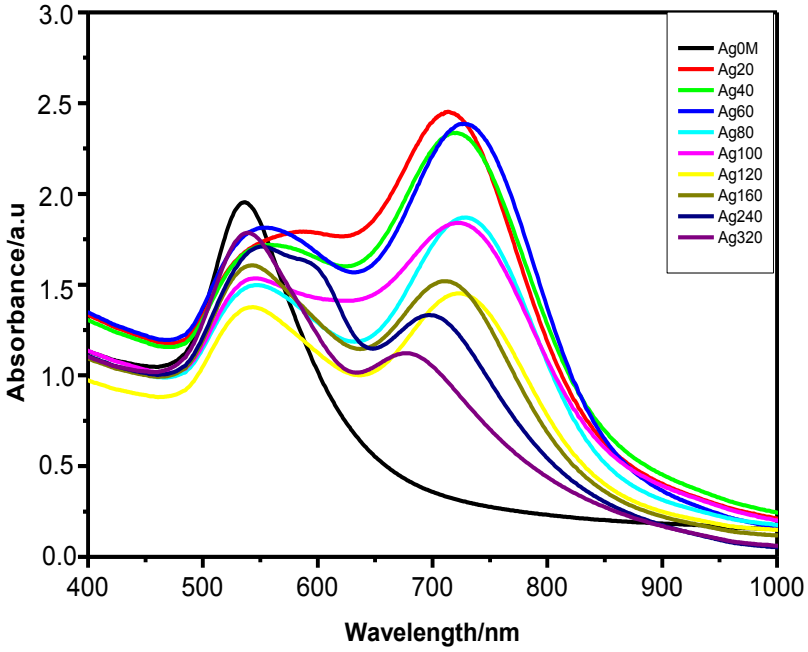

Figure 3-42: Absorption spectra showing the effect of the concentration of $AgNO_3$ on the growth of gold nanorods using CTAB from Fluka.

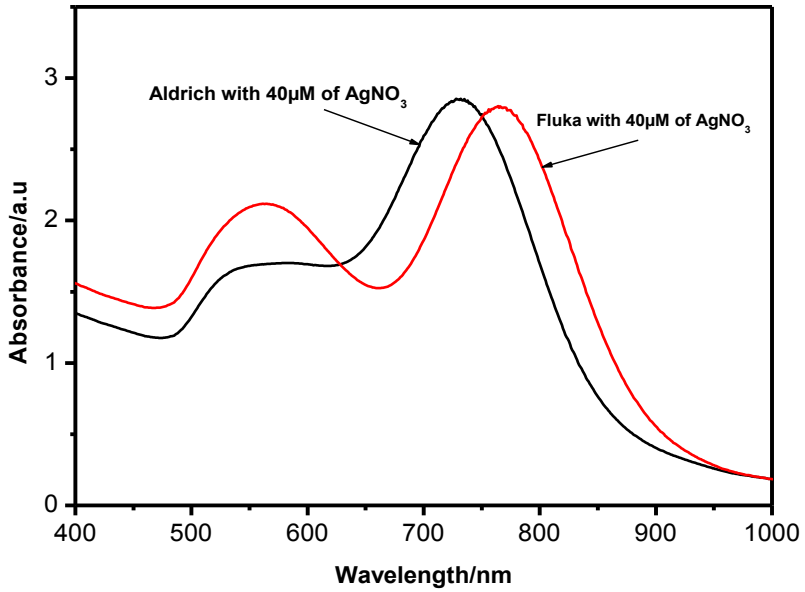

Figure 3-43: Absorption spectra showing the formation of gold nanorods at the same experimental conditions using CTAB from Aldrich and Fluka.

CTAB was used as stabilizer in all the experiments carried out in this study. This surfactant was chosen because it has been shown to be the most effective to produce longer NRs in high yields among other alkyltrimethylammonium bromide surfactants having different hydrocarbon tails[18]. We observed that Hexadecyltrimethylammonium chloride (CTAC) was used only for the UV-irradiation method to produce NRs in minor[20]. Since this surfactant has never been used as a single component in other reduction paths, we decided to check the influence of the counter ions in the final morphology of the NPs. The interaction between CTAB and $HAuCl_4$ in aqueous solution yields to the formation of [CTA]-$[AuBr_4]$ complexes, while CTAC and $[AuCl_4]^-$ form a complex without the change of ligand. This organic salt is solubilized by the surfactant micelles to produce "metallomicelles".

$[AuCl_4]^- + 4\ CTAB \leftrightarrow CTA\text{-}\ [AuBr_4] + 4Cl^- + 3CTA^+$

The main question is now, "why it seems to be important to have $[AuBr_4]^-$, instead of $[AuCl_4]^-$, and metallomicelles for the formation of NRs?. One can guess that if metallic species are involved in the formation of solute complexes or compounds, the standard redox potential of gold may play an important role, because such redox potential will be lower in the case of using any surfactant since the complex is more stable than the gold ions. In Table (3-5), the standard potentials of gold ions and gold complexes are shown[51] for the different ions involved in the discussion. It can be observed that the redox potential of gold complexes is lower than that of gold ions. Moreover, it can be also observed that $[AuBr_4]^-$ has a lower potential compared to $[AuCl_4]^-$ and the same can be said for $[AuBr_2]^-$ in comparison to $[AuCl_2]^-$. It can be then deduced that reduction is harder for the Br complexes than Cl complexes. In the growth solution, $[AuBr_4]^-$ exists as CTA-$[AuBr_4]^-$, which is expected to be even more stable. We can then conclude that a weak reducing agent, such as the ascorbic acid (AA) used in the experiments, cannot reduce the complex to form gold (0), while AA can easily reduce the $[AuCl_4]^-$ to gold (0) giving rise to the formation of nanoparticles. However, AA can only reduce $[AuBr_4]^-$ in the metallomicelles to $[AuBr_2]^-$. Therefore, the nucleation will be hindered until the seed solution is added. With the catalytic action of the seeds, Au^+ ions formed in the previous step, in the metallomicelles, are then reduced to gold (0). Therefore, the effectiveness of CTAB can be attributed to the lower redox potential of their gold complexes in comparison with the Cl complexes.

Half reaction	Standard potential(V)
Au(III)/Au(I)	
$Au^{3+} + 2e^- \rightarrow Au^{1+}$	+1.40
$AuCl_4^- + 2e^- \rightarrow AuCl_2^- + 2Cl^-$	+0.926
$AuBr_4^- + 2e^- \rightarrow AuBr_2^- + 2Br^-$	+0.805
Au(I)/Au(0)	
$Au^+ + e^- \rightarrow Au$	+1.71
$AuCl_2^- + e^- \rightarrow Au + 2Cl^-$	+1.154
$AuBr_2^- + e^- \rightarrow Au + 2Br^-$	+0.962
Ascorbic acid $C_6H_6O_6 + 2H^+ + 2e^- \rightarrow C_6H_8O_6$	+0.13

Table 3-5: Standard redox potentials of gold ions and gold complexes in aqueous solutions.

Therefore, we can conclude the role of the surfactant in the formation of gold NRs as follows:

I) to make complexes with the gold salt, which are more stable than the gold ions alone, so that the reduction becomes slower.

II) to capture the complexes inside the micelles, so that gold ions can be protected from being instantly reduced.

III) to adsorb on the surface of growing NRs, so that it can help in the direction of growth.

In the seed-mediated method ascorbic acid (AA) is often used as a reducing agent. As it was stated AA is able to reduce the gold ions from Au^{+3} to Au^{+1}. The reduction to Au^0 begins only when the seed solution is added (when a strong reducing agent ($NaBH_4$) is used, the growth solution becomes deep purple within several minutes and in this case, because the reaction is very fast, only nanospheres are produced). When the stoichiometric ratio of AA is added without the seeds, there is no color

change even after 24 hrs. The amount of AA added in the seed mediated method was not the same in the different reports, so that the variation in the size and shape of the nanoparticles produced is not trivial to work out. In order to clarify this aspect we studied the effect of [AA] by changing the concentration of ascorbic acid in the growth solution (0.4 – 1.6 m M) using 80μM of $AgNO_3$, with 0.048 and 0.097 μM seeds.

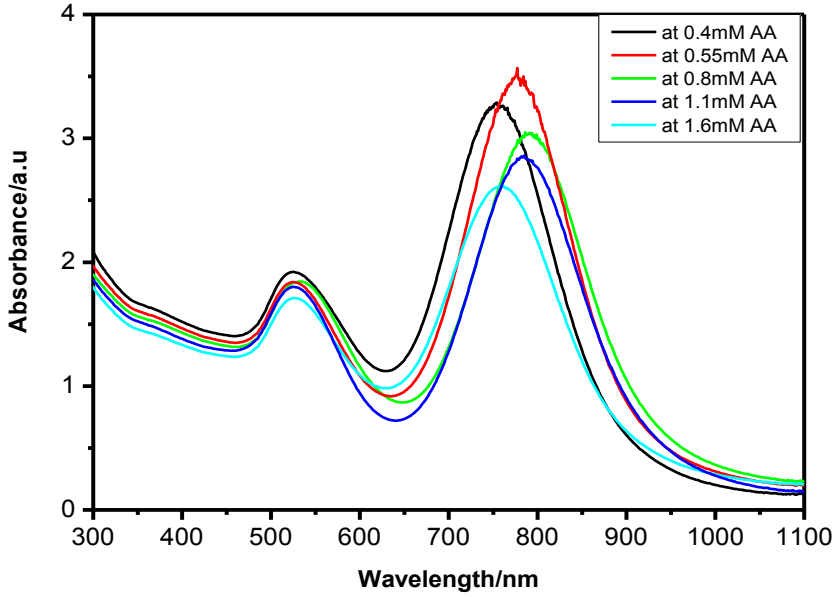

Figure 3-44: Absorption spectra showing the effect of AA concentration with 0.048 μM seed solution.

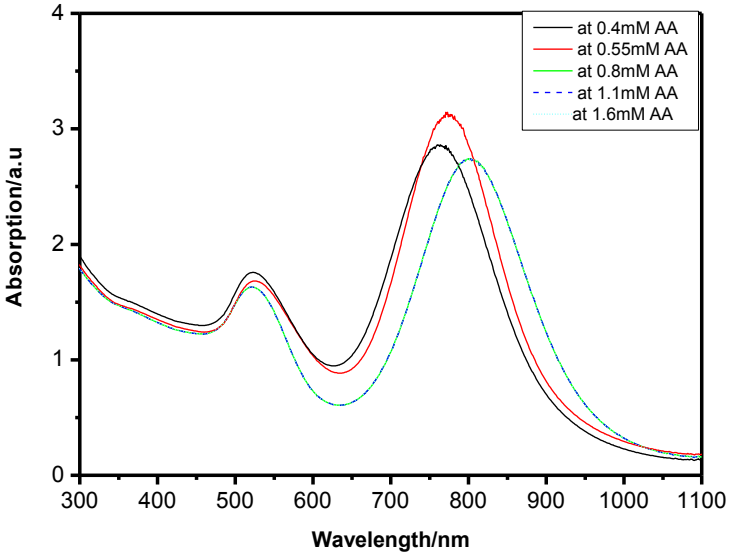

Figure 3-45: Absorption spectra showing the effect of [AA] with 0.097 µM seed solution.

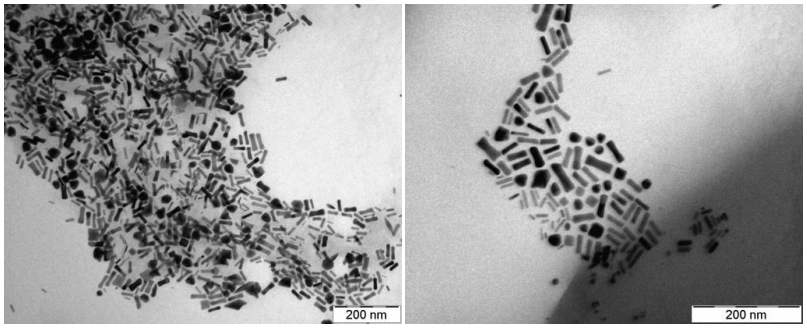

Figure 3-46: TEM images showing the effect of AA concentration (0.4 – 1.6 mM). Gold nanorods with different aspect ratios (2.7 to 5.8) are observed.

Figures (3-44 to3-46) show the results obtained. It can be observed that, as the concentration of ascorbic acid increases, the aspect ratio also increases with a decrease of the yield of NRs. But, when high concentrations of ascorbic acid (1.1 and 1.6 mM) are used, a blue shift of the maximum absorption wavelength is observed, which indicates the formation of some pod shapes together with rods.

These data can be interpreted within the framework of the previously proposed mechanism as follows. As the ascorbic acid concentration

increases, the percentage of the Ag-clusters formed from this reducing agent (which we remember is able only to reduce Au(III) to Au(I) in parallel to the formation for Ag clusters) increases and therefore, promotes the increase of the aspect ratio of the formed rods. This seems to happen only until a certain concentration of AA, 1.1mM, (which is more than double the concentration of gold). At that concentration the [Ag-clusters] increases so much that they can be deposited on more than one surface of the gold seeds. Then, the breaking of the symmetry from more sites can occur with the formation of pod shapes and some aggregated particles. We believe that this deposition and the reduction are favored at the end (tips) of the nanorods more than the sides (we will justify this hypothesis in Chapter V). Similar results were found by Ahmadi et al.[52] when they studied the effect of ascorbic acid on the formation of gold nanorods by using a photochemical method. They found that both ascorbic acid [H_2A] and ascorbate ions [HA^-], could be used to increase the length of gold nanorods as long as the rodlike shapes of the micelles.

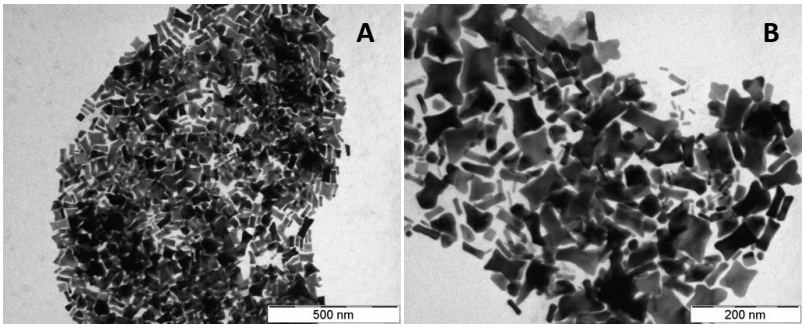

Figure 3-47: TEM images showing the effect of AA concentration; (A) 1.1mM ascorbic acid with 0.048µM seed concentration; (B) 1.1mM ascorbic acid with 0.097µM seed concentration.

From these experiments we can conclude that a weak reducing agent is essential for the formation of NRs. Also the seed solution is necessary as a way to induce the second reduction process. The reduction process of the gold ions by AA can be then summarized in the following way:

First reduction process: $Au^{+3} \rightarrow Au^{+1}$

$CTA{-}AuBr_4 + C_6H_8O_8 \rightarrow CTA{-}AuBr_2 + C_6H_6O_6 + 2H^+ + 2Br^-$

Second reduction process: $Au^{+1} \rightarrow Au^0$

$2CTA{-}AuBr_2 + C_6H_8O_6 \rightarrow 2Au + C_6H_6O_6 + 2CTA^+ + 2H^+ + 4Br^-$

The first reduction is confined in the metallomicelles. The second reduction only begins after the seed solution is added. The overall reaction is:

$2CTA{-}AuBr_4 + 3C_6H_8O_6 \rightarrow 2Au + 3C_6H_6O_6 + 2CTA^+ + 6H^+ + 8Br^-$

3-6: Effect of citrate-seeds on the growth of gold nanoparticles.

Finally, we investigate the use of seeds generated by citric acid instead of CTAB. For this purpose we studied the effect of these new seed concentrations, after aging the seed solution 10 minutes and 3 hours at a fixed concentration of $AgNO_3$ (80µM).

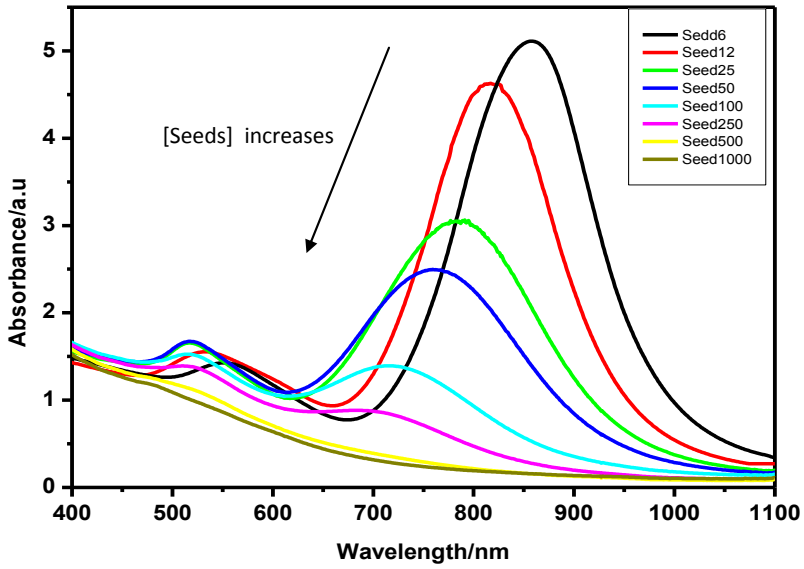

Figure 3-48: Absorption spectra showing the effect of citrate - seed concentrations aged 10 min.(6 to 1000 µl) using 80µM $AgNO_3$.

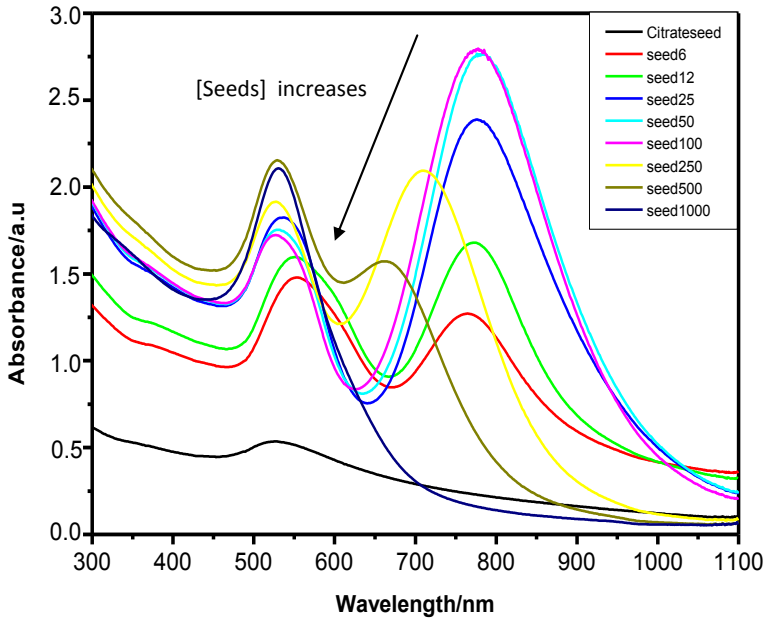

Figure 3-49: Absorption spectra showing the effect of citrate - seed concentration aged 3h (6 to 1000 µl) using 80µM $AgNO_3$.

From the absorption spectra (figures 3-48 and 3-49) one can observe that the aspect ratio of the prepared NRs decreases by increasing the concentration of the seeds, and finally, at very high concentrations, only nanospheres particles are formed. The effect of $AgNO_3$ concentration was also studied using the citrate seed solution (see figures 3-50 and 3.51).

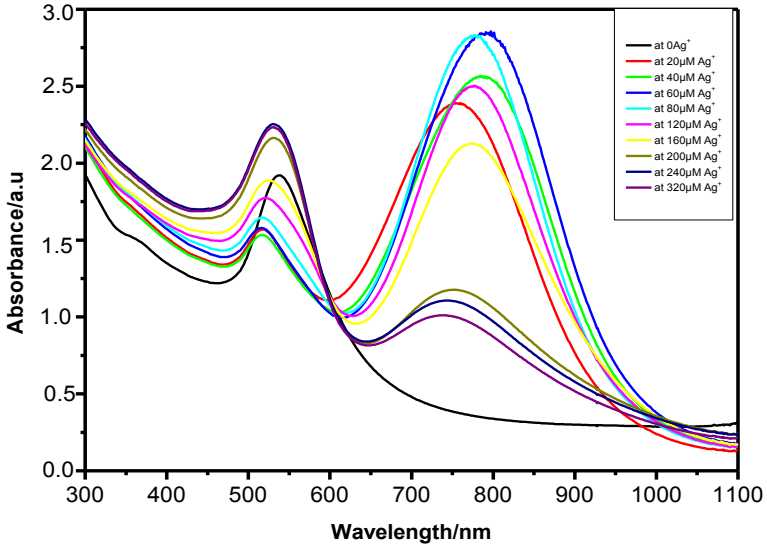

Figure 3-50: Absorption spectra showing the effect of $AgNO_3$ concentration from 0 to 320 µM using a fixed amount of 100µl of citrate - seeds (aged 10min.).

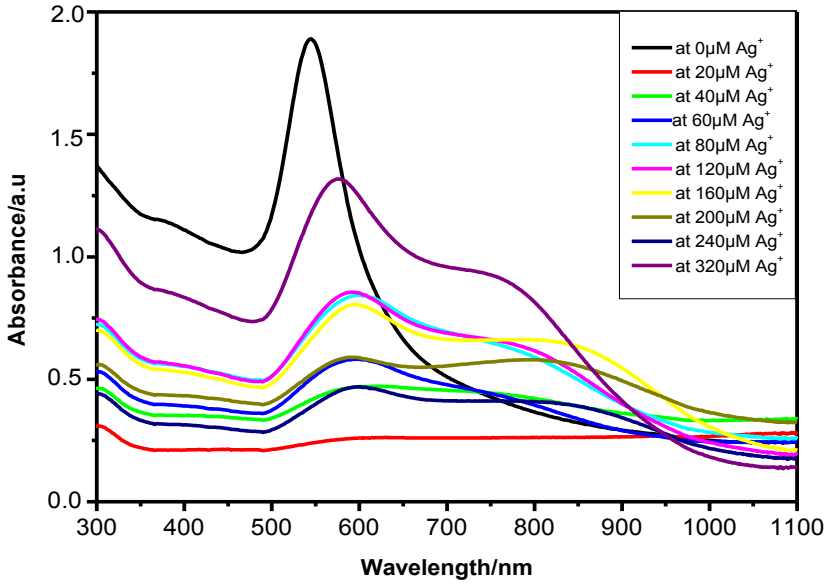

Figure 3-51: Absorption spectra showing the effect of $AgNO_3$ concentration from 0 to 320 µM using a fixed amount of 100µl of citrate - seeds (aged 3h.).

From the absorption spectra (figures 3-50 and 3-51) one can observe that the 10 min. aged seeds are optimal for formation of nanorods using different concentrations of $AgNO_3$.

One can also observe, from the comparison between these results those obtained using CTAB as a capping agent in the seed solution, the yield of gold nanorods using CTAB- seeds is higher than using citrate-seeds. Finally, we studied the effect of 1mg/l Ag-clusters from NANOGAP (Spain) using the citrate –seed solution aged at different times. Gold nanorods with low yields are formed using different concentrations of Ag-clusters.

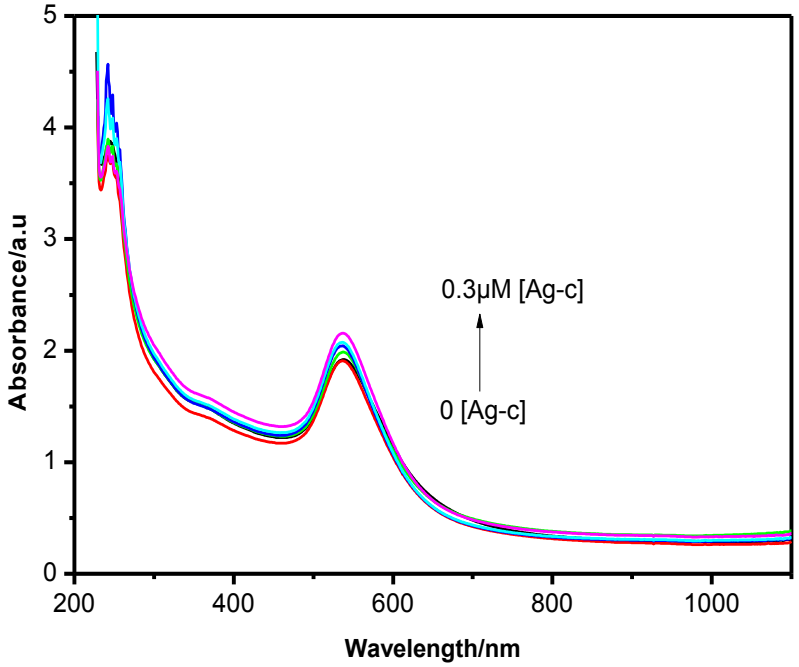

Figure 3-52: Absorption spectra showing the effect of [Ag-clusters] using 100µl of citrate - seeds (aging 10min.).

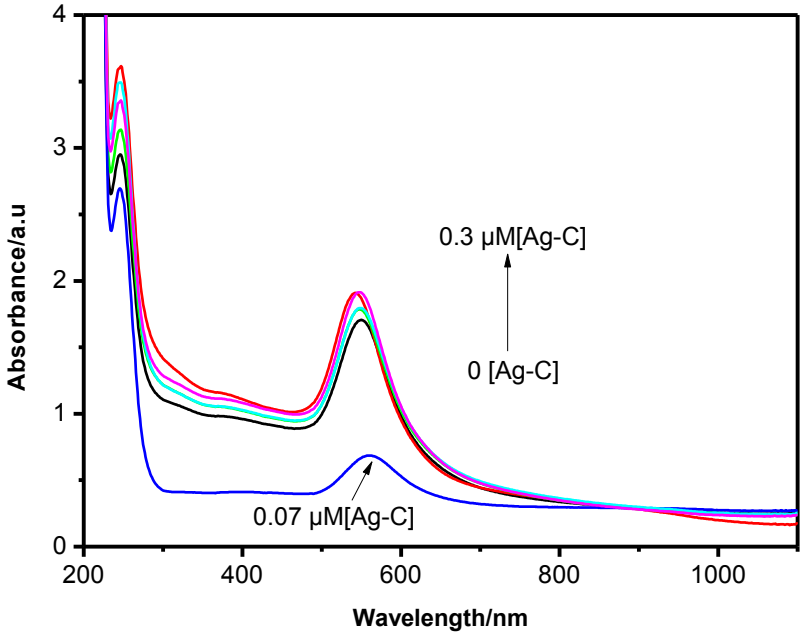

Figure 3-53: Absorption spectra showing the effect of [Ag-clusters] using 100µl of citrate - seeds (aging 3h.).

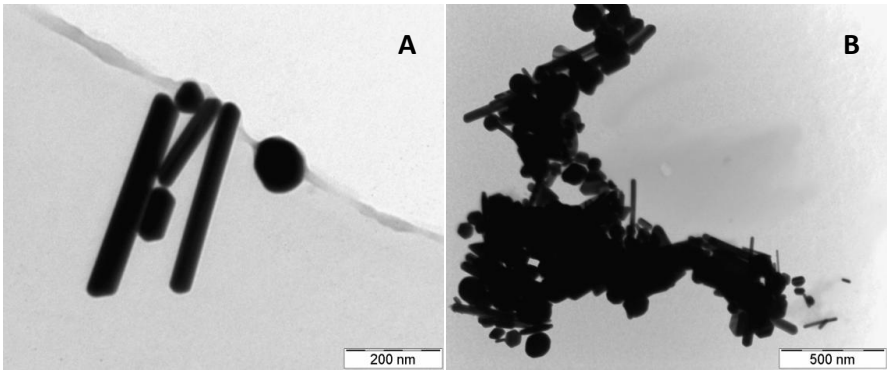

Figure 3-54: TEM images showing the effect of [Ag clusters] (0.175 µM); (A) citrate-seeds aged during 10 min and (B) citrate-seeds aged during 3h.

From the TEM images, it is observed that the formed particles are mainly nanospheres mixed with a very low yield of nanorods. Therefore, one can conclude that the presence of the more stable seeds (CTAB-seeds) is the best choice to form gold NRs.

3-7: Conclusion.

We described an improved seed mediated synthesis to prepare gold nanoparticles of different shapes (Spheres, Rods, Prisms,…..). New absorption features, different from those of the classical surface plasmon absorption bands of rods and spheres are found, which are associated with the appearance of nanoprisms, and snapped prismatic gold nanoparticles, as it was proved by TEM analysis. Gold nanorods with controlled aspect ratio were also prepared in large volumes by the modification to the seed-mediated method. The effect of [Ag-ions], [CTAB-seeds], [ascorbic acid], [citrate- seeds], [Cl^-] and the aging of the seed solution were studied in order to get more insight into the growth mechanism. Our results indicate that the ratio of [Ag^+] to [seed] is one of the key parameters for controlling the shape of the particles, e.g. rods, prisms or snapped prisms. We have proposed a mechanism for the different gold shapes that takes in account the reduction of Ag ions by ascorbic acid forming intermediate small Ag clusters, which can then act as a catalyst for the formation of gold nanoparticles. The mechanism has been proved using externally prepared Ag clusters instead of adding Ag ions. The results also indicate that, to get such different shapes, the used CTAB concentration should be above the CMC and is independent of the CTAB supplier. It seems therefore that, in order to be effective the catalytic behavior of clusters, they need to be stabilized on the micellar surface, which can be viewed as a kind of catalyst *nanosupport.* These results open a new way of thinking in the interpretation of the mechanisms involved in the anisotropic growth of nanoparticles.

The main question which remains to be clarified is why we need to have micelles in the system to achieve shape control by Ag ions. Although we do not have at this moment a conclusive explanation for this influence, it could be related with the fact that small flat clusters (like the ones proposed and used here for directing the formation of different shapes) are formed

and stabilized preferentially at interfaces, like the surfactant films in microemulsions[53]. In this case, the surface of the CTAB micelles could act as *nanosupports* for stabilization of the Ag cluster catalysts. More experiments were carried out to further clarify the mechanism, and will be described in the next chapters.

3-8: References:

1. Busbee B. D.; Obare S. O.; Murphy C., J. Adv. Mater., 2003, 15, 414.
2. Perez-Juste J.; Liz-Marzan L. M.; Carnie S.; Chan D. Y. C.; Mulvaney P., Adv. Funct. Mater., 2004, 14, 571.
3. Chen S.; Wang Z. L.; Ballato J.; Foulger S. H.; Carroll D. L., J. Am. Chem. Soc., 2003, 125,16186.
4. Pastoriza-Santos I.; Liz-Marzan L. M., Nano Lett., 2002, 2, 903.
5. Millstone J. E.; Park S.; Shuford K. L.; Qin L.; Schatz G. C.; Mirkin C. A., J. Am. Chem. Soc., 2005, 127, 5312.
6. Im S. H.; Lee Y. T.; Wiley B.; Xia Y., Ang. Chem. Int. Ed., 2005, 44, 2154.
7. Wiley B.; Herricks T.; Sun Y.; XiaY., Nano Lett., 2004, 4, 1733.
8. Maillard M.; Giorgio S.; Pileni M. P., J. Phys. Chem. B, 2003, 107, 2466.
9. Nikoobakht B.; El-Sayed M. A., Chem. Mater., 2003, 15, 1957.
10. Jana N. R.; Gearhert L.; Murphy C. J., Chem. Commun., 2001, 617.
11. Jana N. R.; Gearheart L.; Murphy C. J., J. Phys. Chem. B, 2002, 13,1389.
12. Murphy C. J.; Jana N. R., Adv. Mater., 2002, 14, 80.
13. Jana N. R.; Gearheart L.; Murphy C. J., Adv. Mater., 2001, 13, 1389.
14. Jana N.R.; Gearheart L.; Murphy C.J., J. Phys. Chem. B, 2001, 105, 4065.
15. Nikoobakht B.; El-Sayed M. A., Langmuir, 2001, 17, 6368.
16. Johnson C. J.; Dujardin E.; Davis S. A.; Murphy C. J.; Mann S., J.Mater. Chem., 2002, 12, 1765.
17. Murphy C. J.; Sau T. K.; Gole A. M.; Orendorff C.J.; Gao J. X.; Gou L, J Phys Chem. B, 2005, 109, 13857.
18. Gao J.; Bender C.M.; Murphy C.J., Langmuir, 2003, 19, 9065.
19. Nikoobakht B.; Wang Z.L.; El-Sayed M.A., J. Phys. Chem. B, 2000,104, 8635.
20. Torigoe K. ; Esumi K., Langmuir, 1992, 8, 59.
21. Henglein A. ; Meisel D., Langmuir, 1998, 14, 7392.
22. Brown K. R. ; Natan M. J., Langmuir, 1998, 14, 726.
23. Khanal B. P.; Zubarev E. R., J Am Chem. Soc., 2008, 130, 12634.
24. Pazos-Perez N.; Baranov D.; Irsen S.; Hilgendorff M.; Liz-Marzan L.M.; Giersig M., Langmuir, 2008, 24, 9855.
25. Kang Y.; Ye X.; Murray C.B., Angew Chem. Int Ed, 2010, 49, 6156.
26. Mohamed M. B.; Ismael K. Z.; Link S.; El-Sayed M. A., J. Phys. Chem.B, 1998, 102, 9370.
27. Cao Y. W.; Jin R.; Mirkin C.A., J. Am. Chem. Soc., 2001, 123, 7961.
28. Pal T.; De S.; Jana N. R.; Pradhan N.; Mandal R.; Pal A.; Beezer A. E.; Mitchell J. C., Langmuir, 1998, 14, 4724.
29. P´erez-Juste J.; Correa-Duarte M. A.; Liz-Marz´an L. M., Appl. Surf. Sci., 2004, 226, 137.

30. Sau T. K.; Murphy C. J., Langmuir, 2004, 20, 6414.
31. Alivisatos A. P., J. Phys. Chem., 1996, 100, 13226.
32. Wang Z. L.; Gao R. P.; Nikoobakht B.; El-Sayed M. A., J. Phys. Chem., B, 2000, 104, 5417.
33. Wang Z. L.; Mohamed M. B.; Link S.; El-Sayed M. A., Surf. Sci., 1999,440, 809.
34. Jin, R.; Cao, Y. C.; Hao, E.; Metraux, G. S.; Schatz, G. C.; Mirkin, C. A., Nature, 2003, 425, 487.
35. Smith, D.K.; Korgel, B.A., Langmuir, 2008, 24, 644.
36. P´erez-Juste, J.; Pastoriza-Santos, I.; Liz-Marz´an, L. M.; Mulvaney, P., Coordination Chemistry Reviews, 249, 2005, 1870.
37. Hubert F.; Testard F.; Spalla O., Langmuir, 2008, 24, 9219.
38. Liu X. H.; Luo X. H.; Lu S. X.; Zhang J. C.; Cao W. L., J Colloid Interface Sci., 2007, 307, 94.
39. Niidome Y.; Nakamura Y.; Honda K.; Akiyama Y.; Nishioka K.; Kawasaki H., Chem. Commun., 2009, 1754.
40. Liao H.; Hafner J. H., Chem. Mater., 2005, 17, 4636.
41. Liu M. Z.; Guyot-Sionnest P., J Phys Chem., B, 2005, 109, 22192.
42. Orendorff C. J.; Murphy C. J., J Phys Chem., B, 2006, 110, 3990.
43. Giannici F.; Placido T.; Curri M. L.; Striccoli M.; Agostiano A.; Comparelli R., Dalton Trans., 2009, 46, 10367.
44. Heiz U.; Landman U., ¨Nanocatalysis¨ Springer, New York, 2006.
45. Rodriguez-Sanchez M.L.; Rodriguez M.J.; Blanco M.C.; Rivas J.; Lopez-Quintela M.A., Phys. Chem. B, 2005, 109, 1183.
46. Hakkinen H.; Moseler M.; Landman U., Phys. Rev. Lett., 2002, 89,033401.
47. Ledo-Suarez A.; Rivas, J.; Rodriguez-Abreu C. F.; Rodriguez M. J.; Pastor E.; Hernandez-CreusA.; Oseroff S. B.; Lopez-Quintela M. A., Angew Chem. Int. Ed., 2007, 46, 8823.
48. Rodríguez-Vázquez M. J.; Blanco M. C.; Lourido R.; Vázquez-Vázquez C.; Pastor E.; Planes G.A.; Rivas J.; López-Quintela M.A., Langmuir, 2008, 24, 12690.
49. Koskinen P.; Hakkinen H.; Huber B.; von Issendorff B.; Moseler M., Phys. Rev. Lett., 2007, 98,015701.
50. Ken-Tye Y.; Yudhisthira S.; Mark T. S.; Paul M. S.; Paras N. P., Top Catal, 2008, 47, 49.
51. Bard A. J., vol. IV, Marcel Dekker: New York and Basel, 1975.
52. Miranda O. R. ; Dollahon N. R. ; Ahmadi T. S., crystal growth & design, 6, 2006,12, 2747.
53. War r G.G, Current Opinion in Colloid & Interface Science, 2000, 88.

Chapter IV

Chapter IV

Metal clusters: a key missing point in the synthesis of gold nanorods

Abstract:

We report in this chapter a very simple method to synthesize crystalline gold nanorods in water, in the absence of any surfactant or polymer in the growth solution to direct the anisotropic nanoparticle growth. We were able to obtain crystalline gold nanorods by just addition of gold clusters prepared and stabilized by CTAB to the growth solution that contains gold ions only and in presence / absence of externally added seed crystallites. It was found that the key point to produce gold nanorods with high aspect ratios is the addition of gold clusters, which confirms the important role of the clusters in the growth of gold nanorods. A new mechanism for the formation of high aspect ratio of gold nanorods is proposed depending on the presence of the catalytic gold sub-nm clusters, which supports the proposed mechanism described in chapter III.

Introduction:

A wide range of techniques for the synthesis of gold nanoparticles has been developed in recent years with the objective of controlling the size and shape of the nanoparticles[1-12]. Although good control over nanoparticle dimensions can be realized in these syntheses, removal of the template or directing agent from the nanoparticle surface generally requires harsh conditions or multiple washings to remove unwanted materials. Gold nanorods prepared by chemical synthesis methods require the use of surfactants like CTAB or polymers, like PVP (polyvinyl pirrolidone) in the growth solution to direct the nanoparticle growth and also the use of a seed solution.

We report here a simple method to synthesize crystalline gold nanorods in water, in the absence of any surfactant or polymer to direct the anisotropic nanoparticle growth in the growth solution. We were able to obtain crystalline gold nanorods in presence and also in absence of externally added seed crystallites. It was deduced that the key point to produce gold nanorods with high aspect ratios is the addition of gold clusters. This fact is in the line of the important role played by clusters in the growth process proposed and discussed previously in Chapter III. The reaction is carried out by reducing gold (III) to gold(I) with ascorbic acid in the presence of gold clusters stabilized by CTAB. By means of ESI mass spectrometry it was determined that the gold clusters, which catalyze the anisotropic growth, are in the range Au_2-Au_6 and, using atomic force microscopy, gold seeds have been identified as Au_{55} species. The concentration of the different gold species in solution was estimated from the kinetic data recorded during the first minutes of reaction at wavelengths close to the gold plasmon peak. From these studies it is concluded that the most important parameter to prepare monodisperse gold nanorods is the molar ratio between clusters and seeds.

Experimental section:

The experimental details methods and characterization were described in chapter II but, please note that the growth solution contains gold clusters and gold ions but there is no surfactant in the growth solution.

Results and discussion:

4-1: Preparation and characterization of gold clusters.

According to the results and the discussed mechanism in chapter III, Ag-clusters play the most important role in the growth of gold nanoparticles with different shapes. Therefore, we thought that clusters from other metals could play a similar role in the control of the formation of different shapes

of gold nanoparticles (especially nanorods). For this purpose we tried to prepare gold clusters by the reduction of $NaBH_4$ to gold (III) in the presence of CTAB aging this solution from 10 sec to 5 minutes, because in that time range we observed that the Au nanoparticles produced have no plasmon band, which indicates that the particles are below approx. 2 nm. We use such solutions to add to the growth solution in order to form anisotropic shapes of gold nanoparticles.

To check the formation of gold clusters at different aging times (from 0 to 5 min.) we used the ESI Mass Spectrometry technique. Mass spectra of the different samples and the identification of the most important fragments containing clusters are given below.

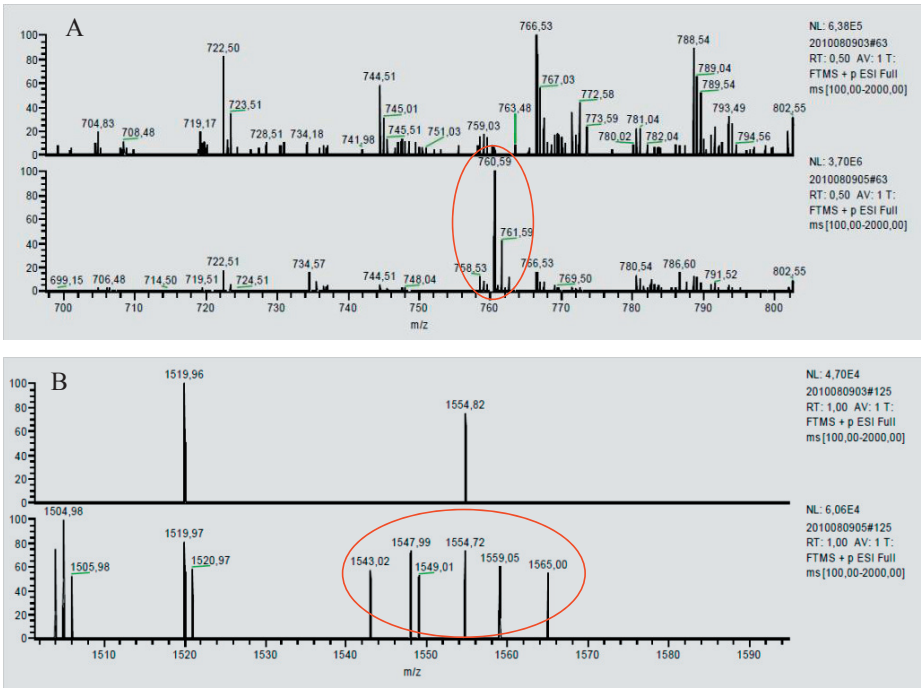

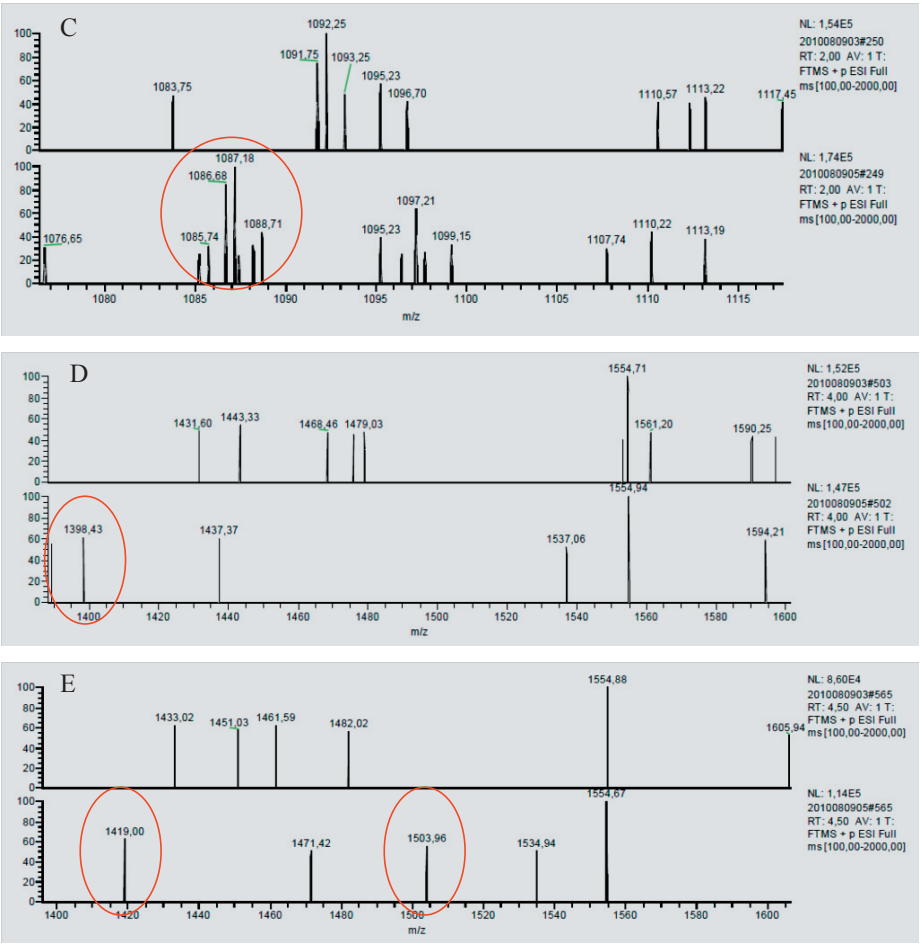

Figure 4-1: Mass spectra of the solutions aged at different times: 30, 60, 120, 240, and 300 s, respectively.

Figure (4-1) shows the mass spectra of the cluster solution aged at different times from 0 to 5minutes (in the bottom part of the spectra) compared to the mass spectra of a blank solution (in the upper part) that contains Au(III) ions in a CTAB solution.

Table (4-1) shows the type of clusters that could be identified in the fragments obtained by mass spectrometry for the samples prepared at different times. For this identification, we took only fragments that were

different from those found in the growth solution without $NaBH_4$ taken as a blank.

Time	Formula	Mass Theo.	Mass Exp.	Ints.
0.01min.	$Au_2C_{19}H_{42}N(C_2H_3N)_2$	760,31	760,58	H
	Au_6Na	1204,78	1205,77	L
	$Au_6C_2H_3N$	1222,82	1223,34	M
	$Au_6(CH_3CH_2)N(H_2)_2$	1228,87	1228,78	M
	$Au_6(CH_3)_3H_2O(H_2)$	1260,89	1260,94	M
	Au_7O_2	1410,75	1410,20	H
	$Au_7(CH_3CH_2)N(H_2)_2$	1425,83	1425,90	H
	$Au_7(CH_3)_3NH_2O$	1455,84	1456,00	M
	$Au_7(C_2H_3N)_2$	1460,80	1459,94	H
	$Au_7C_2H_3N(CH_3)_3NH_2O(H_2)$	1499,90	1499,02	M
	$Au_7(C_2H_3N)_3(H_2)$	1503,86	1503,97-1504.98-1505,98	M-H-M
	$Au_7(C_2H_3N)_4$	1542,87	1543,04	M
	$Au_7(C_2H_3N)_3(CH_3)_3H_2$	1548,93	1548,00	H
	$AU_7(C_2H_3N)_3(CH_3)_3H_2ONa(H_2)_2$	1591,94	1591,59	M
	$Au_8C_2H_3N(H_2O)_3$	1670,79	1670,65	L
	$AU_8(C_2H_3N)_3N(H_2O)$	1730,82	1730,52	L
	$Au_9(C_2H_3N)_3(CH_3)_3NNa(H_2)$	1979,85	1979,86	L
0,5MIN.	$Au_2C_{19}H_{42}N(C_2H_3N)_2$	760,31	760,58	H
	$Au_6(C_2H_3N)_3H_2ONa_2(H_2)_2$	1372,90	1373,36	M
	Au_7	1378,76	1378,78	M
	Au_7H_2O	1396,77	1396,92	M
	$Au_7(CH_3)_3NH_2O(H_2)_2$	1459,88	1459,95	M
1MIN.	$Au_2C_{19}H_{42}N(C_2H_3N)_2$	760,31	760,58	H
	$Au_6C_2H_3N(CH_3)_3NH_2O$	1299,90	1300,84	M
	$Au_6(C_2H_3N)_3H_2O$	1322,84	1321,95	M
	$Au_6C_2H_3N(CH_3)_3Na_2H_2O$	1331,88	1332,84	M
	$Au_6(C_2H_3N)_4$	1345,90	1346,39	M
	$Au_6(C_2H_3N)_2(CH_3)_3NaH_2OH_2$	1351,93	1351,85	M
	$Au_6(C_2H_3N)_2(CH_3)_3NaH_2O(H_2)_3$	1355,97	1355,90	M
	$Au_6(C_2H_3N)_3Na$	1327,86	1327,96	M
	$Au_7(C_2H_3N)_2H_2O(H_2)_2$	1482,86	1482,00	H
	$AU_7(C_2H_3N)_3H_2$	1503,86	1503,97-1504,98-1505,96	M-H-M
	$AU_7(C_2H_3N)_3Na_2$	1547,82	1547,99	H
	$Au_7(C_2H_3N)_3Na_3H_2$	1549,84	1549,01	M
	$Au_7(C_2H_3N)_3Na$	1565,86	1565,00	M
	$Au_8(C_2H_3N)_2H_2O(H_2)_4$	1683,85	1683,76	M
	$Au_8(C_2H_3N)_2Na_2H_2$	1719,78	1719,56	L

1,5MIN.	$Au_2C_{19}H_{42}N(C_2H_3N)_2$	760,31	760,58	H
	$Au_6C_2H_3N$	1222,82	1223,33	M
	$Au_6(CH_3CH_2)N(H_2)_2$	1228,87	1228,28	M
	$Au_6C_2H_3NNa$	1245,81	1245,34	H
	$AU_6(CH_3)_3NH_2O$	1258,88	1258,35	H
	$Au_6(CH_3)_3NH_2O(H_2)$	1260,89	1260,95	M
	$Au_6(CH_3)_3NH_2O(H_2)_2$	1262,91	1262,80	M
	$Au_6(C_2H_3N)_3(H_2O)_3H_2$	1360,40	1360,86	H
	$Au_6(C_2H_3N)_3H_2ONa_2(H_2)_2$	1372,90	1373,97	M
	$Au_7(H_2)_5$	1388,84	1388,89	M
	AU_7CH_3N	1393,78	1393,94	H
	$Au_7(C_2H_3N)_3H_2$	1503,86	1503,97	H
	$AU_7C_{12}H_{25}N$	1561,96	1562,45	M
	$Au_8(C_2H_3N)_3$	1698,81	1699,77	M
	$Au_8(C_2H_3N)_3Na$	1721,80	1721,88	M
	$Au_9CH_2CH_3$	1801,73	1801,06	M
	$Au_9(C_2H_3N)NH_2O$	1863,74	1863,25	L
2MIN.	$Au_2C_{19}H_{42}N(C_2H_3N)_2$	760,31	760,58	H
	$Au_4Br(H_2O)$	884,79	884,88	H
	$Au_4(C_2H_3N)_2H_2O$	887,92	888,07	H
	$Au_4(C_2H_3N)_2NaH_2O$	910,91	910,08	M
	$Au_4C_{14}H_{29}N(CH_3)_3H_2OH_2$	1064,19	1064,67	H
	$Au_5(C_2H_3N)_2H_2OH_2$	1086,91	1086,68	H
	$Au_5(C_2H_3N)_3$	1107,9	1107,74	M
	$Au_5C_{12}H_{25}H_2O$	1172,03	1173,82	H
	$Au_6(C_2H_3N)NaH_2$	1247,83	1247,50	M
	$Au_6(C_2H_3N)_2NaH_2$	1288,85	1288,88	M
	$Au_7(C_2H_3N)_2H_2O$	1478,82	1478,93	L
4MIN.	$Au_2C_{19}H_{42}N(C_2H_3N)_2$	760,31	760,58	H
	Au_6	1181,79	1181,53	M
	Au_6H_2	1183,81	1183,37	M
	$Au_6(H_2)_3$	1187,84	1188,39	M
	$Au_6(C_2H_3N)_3CH_3$	1319,90	1320,81	M
	$Au_6(C_2H_3N)_3NaH_2$	1329,88	1329,67	H
	$Au_7H_2O(H_2)$	1398,79	1398,42	H
	$Au_7C_2H_3NH_2O$	1437,80	1437,37	M
	$Au_7(C_2H_3N)_3(H_2O)_2$	1537,86	1537,06	M
	$Au_8(CH_2CH_3)(H_2)_2$	1608,80	1608,62	M
	$Au_8O_2(H_2O)(H_2)$	1627,74	1627,68	M
	$Au_9(H_2O)_3H_2$	1828,74	1828,61	L
	$Au_9C_2H_3NNa_2(H_2)_3$	1865,75	1865,85	L
4,5MIN.	$Au_2C_{19}H_{42}N(C_2H_3N)_2$	760,31	760,58	H
	$Au_5(C_2H_3N)_3H_2O(H_2)$	1127,93	1127,76	L
	Au_6	1181,79	1182,61	M

	$Au_6O_2Na(H_2O)_2$	1272,80	1272,81	H
	$Au_6(C_2H_3N)_2H_2O(H_2)_4$	1289,92	1289,88	M
	$Au_6C_2H_3N(CH_3)_3Na_2H_2OH_2$	1333,89	1333,88	H
	$Au_6(C_2H_3N)_3(H_2O)_3(H_2)$	1360,92	1360,40	H
	$Au_7C_2H_3N$	1419,79	1419,00	H
	$Au_7(C_2H_3N)(CH_2CH_3)Na$	1471,82	1471,42	M
	$Au_7(C_2H_3N)_3H_2$	1503,86	1503,96	M
	$Au_7(C_2H_3N)_2(H_2O)_4H_2$	1534,87	1534,94	M
	$Au_8C_2H_3N(H_2O)_2H_2$	1654,79	1654,16	L
	$Au_9CH_3(H_2O)$	1805,73	1805,34	L
	$Au_9C_2H_3N(H_2)_2$	1817,75	1817,59	L

Table 4-1: Mass spectra analysis of the fragments containing clusters for samples prepared at different times (H= high, M= medium and L= low).

Tables (4-2) summarizes the highest peaks obtained in the mass spectra of the samples at different times, showing that the cluster sizes are in the range Au_2-Au_6.

Time	Formula	Mass Theo.	Mass Exp.	Ints.
0.01min.	$Au_2C_{19}H_{42}N(C_2H_3N)_2$	760,31	760,58	H
	Au_7O_2	1410,75	1410,20	H
	$Au_7(CH_3CH_2)N(H_2)_2$	1425,83	1425,90	H
	$Au_7(C_2H_3N)_3(H_2)$	1503,86	1503,97- 1504.98- 1505,98	M- H-M
	$Au_7(C_2H_3N)_3(CH_3)_3H_2$	1548,93	1548,00	H
0,5MIN.	$Au_2C_{19}H_{42}N(C_2H_3N)_2$	760,31	760,58	H
1MIN.	$Au_2C_{19}H_{42}N(C_2H_3N)_2$	760,31	760,58	H
	$Au_7(C_2H_3N)_2H_2O(H_2)_2$	1482,86	1482,00	H
	$AU_7(C_2H_3N)_3H_2$	1503,86	1503,97- 1504,98- 1505,96	M- H-M
	$AU_7(C_2H_3N)_3Na_2$	1547,82	1547,99	H
1,5MIN.	$Au_2C_{19}H_{42}N(C_2H_3N)_2$	760,31	760,58	H
	$Au_6C_2H_3NNa$	1245,81	1245,34	H
	$AU_6(CH_3)_3NH_2O$	1258,88	1258,35	H
	$Au_6(C_2H_3N)_3(H_2O)_3H_2$	1360,40	1360,86	H
	AU_7CH_3N	1393,78	1393,94	H
	$Au_7(C_2H_3N)_3H_2$	1503,86	1503,97	H
2MIN.	$Au_2C_{19}H_{42}N(C_2H_3N)_2$	760,31	760,58	H
	$Au_4Br(H_2O)$	884,79	884,88	H
	$Au_4(C_2H_3N)_2H_2O$	887,92	888,07	H
	$Au_5C_{12}H_{25}H_2O$	1172,03	1173,82	H
	$Au_4C_{14}H_{29}N(CH_3)_3H_2OH_2$	1064,19	1064,67	H
	$Au_5(C_2H_3N)_2H_2OH_2$	1086,91	1086,68	H
4MIN.	$Au_2C_{19}H_{42}N(C_2H_3N)_2$	760,31	760,58	H

	$Au_6(C_2H_3N)_3NaH_2$	1329,88	1329,67	H
	$Au_7H_2O(H_2)$	1398,79	1398,42	H
4,5MIN.	$Au_2C_{19}H_{42}N(C_2H_3N)_2$	760,31	760,58	H
	$Au_6O_2Na(H_2O)_2$	1272,80	1272,81	H
	$Au_6C_2H_3N(CH_3)_3Na_2H_2OH_2$	1333,89	1333,88	H
	$Au_6(C_2H_3N)_3(H_2O)_3(H_2)$	1360,92	1360,40	H
	$Au_7C_2H_3N$	1419,79	1419,00	H

Table 4-2: Table shows the fragments of highest intensities for the samples prepared at different times.

From the ESI-MS mass spectrometry data, it can then be concluded that the gold clusters, which are formed in the solutions that were employed in this study, are mainly in the range Au_2-Au_6.

The concentration of the different gold species in solution was estimated from the kinetic data recorded during the first minutes of reaction at 520nm close to the gold plasmon peak, where there is a maximum change of the absorption with time.

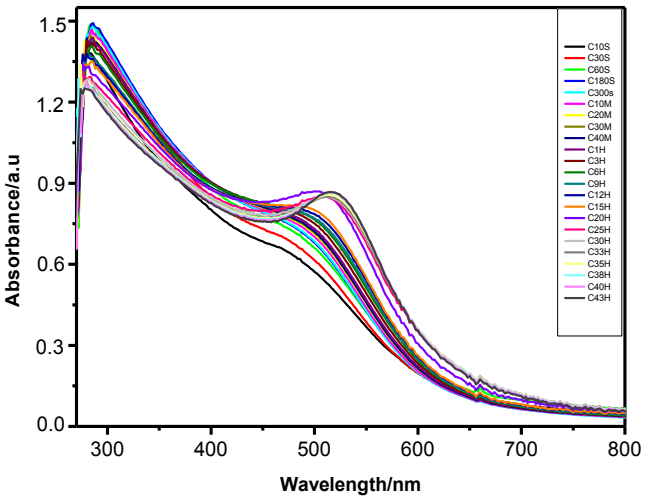

Figure 4-2: Absorption spectra showing the growing of gold clusters and seeds up to 43 h.

Determination of the rate constants of gold clusters and gold seeds were carried out using MATHCAD and Monte Carlo simulations. The results obtained for the concentrations of clusters and seeds, as well as the detailed calculations are given below.

The simulation data starts from 30s to 10000s; it is assumed that Au (III) transforms directly to Au_2 clusters and starting form this point: **Au_2 → Au_6 → seeds**

Z: = READPRN ("abs520nm from 30s to 10000s.dat")

Time(s) t:=$Z^{(0)}$ Absorbance at 520nm Abs:= $Z^{(1)}$

n:= last(t) n=108 i: = 0,1……n t_0= 30 s Abs_0 = 0,527

t_n= 9,6 x 102 Abs_n= 0,607

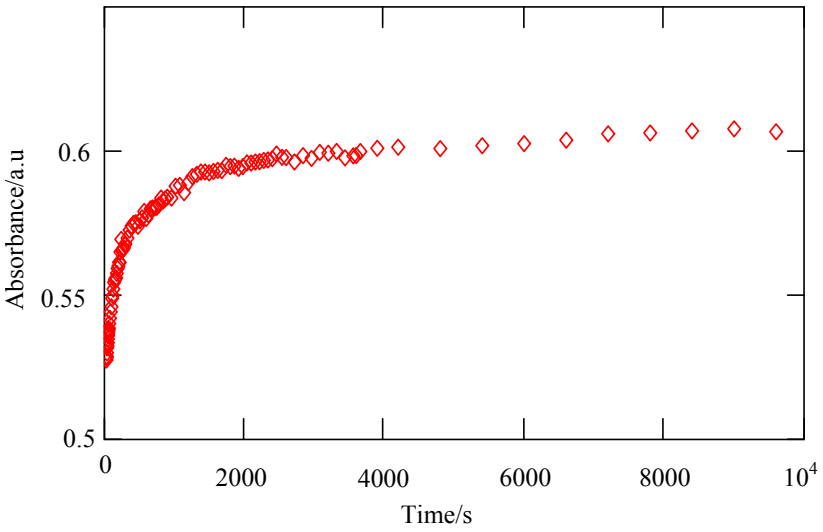

Figure 4-3: Absorbance intensity of gold clusters at λ= 520 nm from 30 to 10000 s.

Analysis of biexponential kinetic data, considering k_2 different than k_3:

Consecutive reactions: A --> I --> P $cA_t = [A]_t$, $cA_0 = [A]_0$, $cI_t = [I]_t$,

Instrument reading (absorbance): $cP_t = [P]_t$, y_A = molar fraction of species A

$Abs_t = y_A.cA_t + y_I.cI_t + y_P.cP_t \qquad cA_t = cA_0.\exp(-K2.t)$

$cI_t = \frac{K2.cA0}{K3-K2}.\left(exp(-K2.t) - exp(-K3.t)\right)$,

$cP_t = cA0.\left[1 - \frac{1}{K3-K2}.\left(K3.exp(-K2.t) - K2.exp(-k3.t)\right)\right]$

Since $Abs_{inf} = y_p.cA_0$,

It is obtained $Abs_t - Abs_{inf} = \beta.\exp(-K2.t) + \gamma.\exp(-K3.t)$

Where β and γ are constants:

$$\beta = \frac{(yI-yA).k2+(yA-yP).K3}{K3-K2}.cA0 \quad \text{and} \quad \gamma = \frac{(yP-yI).K2}{K3-K2}.cA0$$

$Abs_t(Abs_{inf}, Offset, \beta, k_2, \gamma, k_3, t) = Abs_{inf} + Offset + \beta\cdot(1 - \exp(-k_2\cdot t)) + \gamma\cdot(1 - \exp(-k_3\cdot t))$

In order to simplify the two offset limits: $Abs_o = Abs_{inf} + Offset$

$Abs_t(Abs_o, \beta, k_2, \gamma, k_3, t) := Abs_o + \beta\cdot(1 - \exp(-k_2\cdot t)) + \gamma\cdot(1 - \exp(-k_3\cdot t))$

$$SSE(Abs_o, \beta, k_2, \gamma, k_3) := \sum_i \left(Abs_i - Abs_t(Abs_o, \beta, k_2, \gamma, k_3, t_i)\right)^2$$

$Abs_{o1} := 0.52, \quad \beta 1 := 0.030, \quad \gamma 1 := 0.025, \quad k_{21} := 0.03271$ 1/s

$k_{31} := 0.01408$ 1/s

Given: $SSE(Abs_{o1}, \beta 1, k_{21}, \gamma 1, k_{31}) = 0 \qquad TOL \equiv 0.0001$

$Abs_{o1} > 0 \qquad \beta 1 > 0 \qquad \gamma 1 > 0$

$$\begin{pmatrix} Abs01 \\ \beta 1 \\ K21 \\ \gamma 1 \\ K31 \end{pmatrix} = \text{Minerr(Abs01, β1, K21,γ1,K31)} \quad \begin{pmatrix} Abs01 \\ \beta 1 \\ K21 \\ \gamma 1 \\ K31 \end{pmatrix} = \begin{pmatrix} 0{,}518 \\ 0{,}048 \\ 7{,}53xE-3 \\ 0{,}038 \\ 7{,}079xE-4 \end{pmatrix} 1/s \quad 1/S$$

SSE (Abs01, β1, K21, γ1, K31) = 2,106x10^{-4}

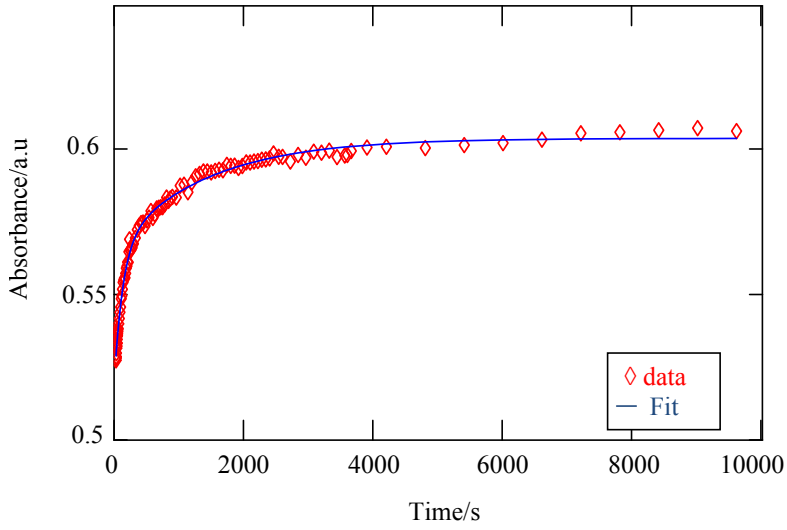

Figure 4-4: First fitting of the absorbance of gold clusters and seeds at λ= 520 nm with time, from 30 to 10000 s.

Second exponential: $fitexp2(t) := \beta 1 \cdot (1 - \exp(-k_{21} \cdot t))$

Third exponential: $fitexp3(t) := \gamma 1 \cdot (1 - \exp(-k_{31} \cdot t))$

2nd + 3rd exponentials: $fitexp(t) := fitexp2(t) + fitexp3(t)$

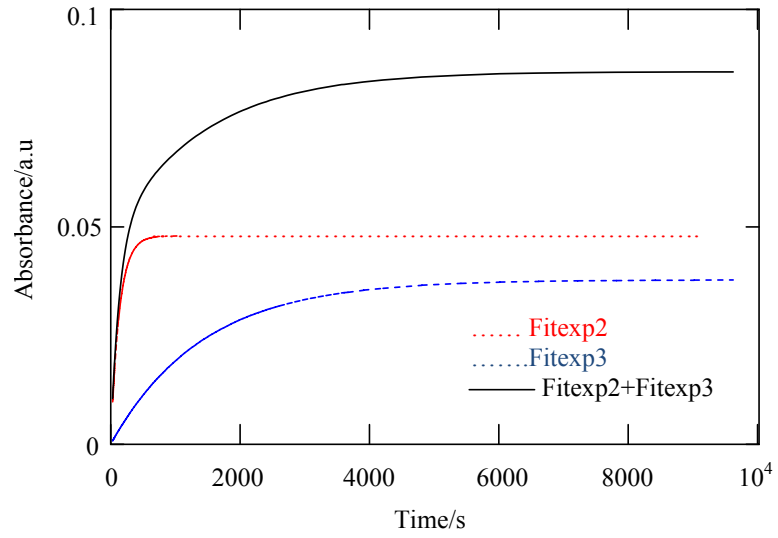

Figure 4-5: Three exponential fitting of the absorbance of gold clusters and seeds at λ= 520 nm with time, from 30 to 10000 s.

Determination of the concentration of different species present in the solution. Species present: A = Au_2 clusters =1/2* Au (III) or Au(I) ions; I = Au_6 clusters; P = seeds.

Initial concentration of Au(III) or Au(I) ions = 0.25 mM. It is assumed all are transformed to Au_2 clusters after 30s.

Seeds size:

The bond length in Au-Au is: 288.4 pm.

Considering the shell model and icosahedral geometry,

1 shell → Au_{13} → diameter = 865.2 pm

2 shells → Au_{55} → diameter = 1442 pm

3 shells → Au_{147} → diameter = 2018.8 pm

So, in first approximation, taking Au_{55} as seeds it can be calculated its concentration in the following way:

Initial conc. of Au_2 clusters: cA_0 = 0.125mM

Concentration of Au_6 clusters = 1/3 [Au_2 transformed] → $3Au_2 \rightarrow Au_6$

Concentration of Au_{55} seeds= [Au_2 transformed]*2/55 → $55/2Au_2 \rightarrow Au_{55}$

$cA_t(t) := cA_0 \cdot \exp(-k_{21} \cdot t)$

The analytical expressions of concentration of I and P have been modified accordingly to the stoichiometry.

$$cI_t(t) = \frac{cAo}{3} \cdot \left[\frac{K21}{K31-K21} \cdot \left(exp(-K21.t) - exp(-K31.t)\right)\right]$$

$$cP_t(t) = cA_0 - cA_t(t) - cI_t(t)$$

$$cPt(t) = \frac{cA0.\ 2}{55} \cdot \left[1 - \frac{1}{k31-K21} \cdot \left(K31.exp(-K21.t) - K21.exp(-K31.t)\right)\right]$$

Molar fractions (due to the stoichiometry, the concentrations of I and P must be modified):

$yA = \frac{cAt(t)}{cA0}$ $yA = exp(-K21.t)$ yA + yI + yP = I

$yI = 3.\frac{cIt(t)}{cA0}$ $yI = \frac{K21}{K31-K21}.\left(exp(-K21.t) - exp(-K31.t)\right)$

$yP = \frac{55}{2}.\frac{cPt(t)}{cA0}$ $yP = 1 - \frac{1}{K31-K21}.\left(K31.exp(-K21.t) - K21.exp(-K31.t)\right)$

Maximum concentration of the intermediate, I:

$$cI_{max} = \frac{cA0}{3} \cdot \left(\frac{K31}{K21}\right)^{\frac{K31}{K21-K31}}$$

Molar fraction: $\boldsymbol{yImax = 3.\frac{cImax}{cA0}}$

cI_{max} = 0.033mM yI_{max}= 0.782

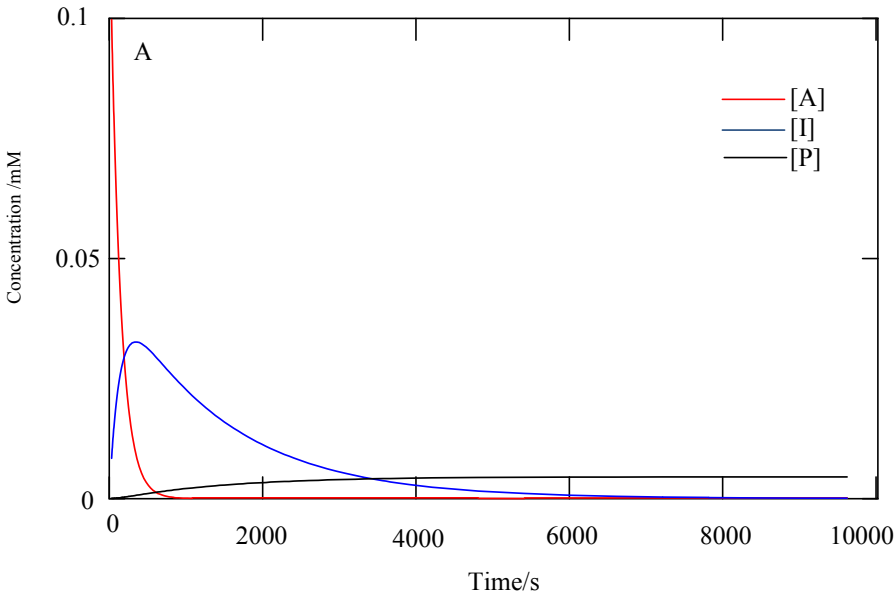

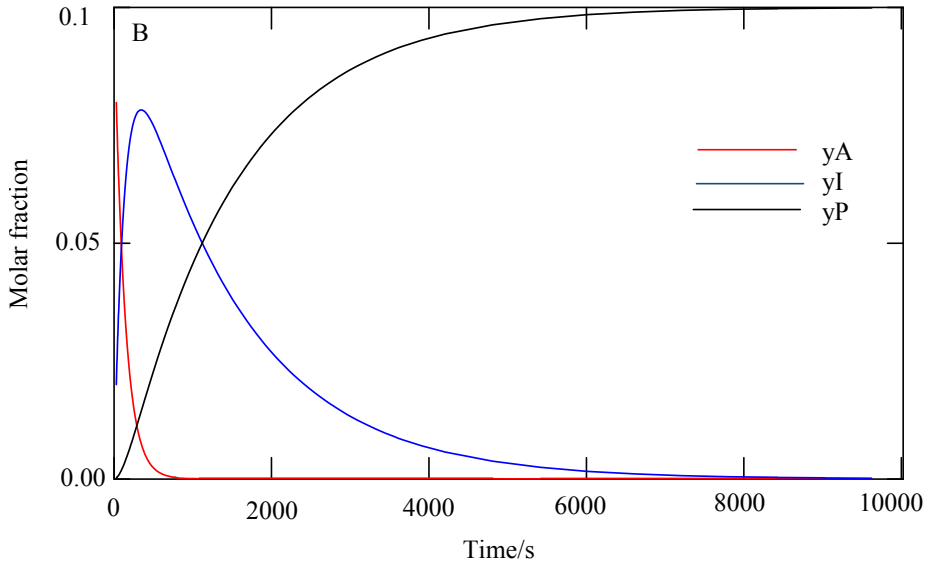

Figure 4-6: Relations of concentration and molar fractions of Au_2, Au_6 and Au_{55} with time (A and B, respectively).

The next table shows the calculated concentrations of [Au_2], [Au_6], and [Au_{55} (gold seeds)] according to the above Monte Carlo simulation.

	Time(sec)	[Au_2]=[A]	[Au_6]=[I]	[Au_{55}]=[P]
0	30	$9.973 \cdot 10^{-2}$	$8.333 \cdot 10^{-3}$	$1.005 \cdot 10^{-5}$
1	32	$9.823 \cdot 10^{-2}$	$8.818 \cdot 10^{-3}$	$1.138 \cdot 10^{-5}$
2	34	$9.677 \cdot 10^{-2}$	$9.294 \cdot 10^{-3}$	$1.278 \cdot 10^{-5}$
3	36	$9.532 \cdot 10^{-2}$	$9.763 \cdot 10^{-3}$	$1.425 \cdot 10^{-5}$
4	38	$9.390 \cdot 10^{-2}$	$1.022 \cdot 10^{-2}$	$1.579 \cdot 10^{-5}$
5	40	$9.249 \cdot 10^{-2}$	$1.068 \cdot 10^{-2}$	$1.741 \cdot 10^{-5}$
6	42	$9.111 \cdot 10^{-2}$	$1.112 \cdot 10^{-2}$	$1.909 \cdot 10^{-5}$
7	44	$8.975 \cdot 10^{-2}$	$1.156 \cdot 10^{-2}$	$2.084 \cdot 10^{-5}$
8	46	$8.841 \cdot 10^{-2}$	$1.199 \cdot 10^{-2}$	$2.266 \cdot 10^{-5}$
9	48	$8.708 \cdot 10^{-2}$	$1.241 \cdot 10^{-2}$	$2.455 \cdot 10^{-5}$
10	50	$8.578 \cdot 10^{-2}$	$1.283 \cdot 10^{-2}$	$2.650 \cdot 10^{-5}$
11	52	$8.450 \cdot 10^{-2}$	$1.324 \cdot 10^{-2}$	$2.851 \cdot 10^{-5}$
12	54	$8.324 \cdot 10^{-2}$	$1.364 \cdot 10^{-2}$	$3.058 \cdot 10^{-5}$
13	56	$8.199 \cdot 10^{-2}$	$1.404 \cdot 10^{-2}$	$3.272 \cdot 10^{-5}$
14	58	$8.077 \cdot 10^{-2}$	$1.442 \cdot 10^{-2}$	$3.492 \cdot 10^{-5}$
15	60	$7.956 \cdot 10^{-2}$	$1.481 \cdot 10^{-2}$	$3.718 \cdot 10^{-5}$
16	70	$7.379 \cdot 10^{-2}$	$1.662 \cdot 10^{-2}$	$4.932 \cdot 10^{-5}$
17	80	$6.844 \cdot 10^{-2}$	$1.828 \cdot 10^{-2}$	$6.280 \cdot 10^{-5}$
18	90	$6.347 \cdot 10^{-2}$	$1.980 \cdot 10^{-2}$	$7.752 \cdot 10^{-5}$
19	100	$5.887 \cdot 10^{-2}$	$2.119 \cdot 10^{-2}$	$9.335 \cdot 10^{-5}$

20	110	$5.460 \cdot 10^{-2}$	$2.246 \cdot 10^{-2}$	$1.102 \cdot 10^{-4}$
21	120	$5.064 \cdot 10^{-2}$	$2.361 \cdot 10^{-2}$	$1.280 \cdot 10^{-4}$
22	130	$4.697 \cdot 10^{-2}$	$2.467 \cdot 10^{-2}$	$1.467 \cdot 10^{-4}$
23	140	$4.356 \cdot 10^{-2}$	$2.562 \cdot 10^{-2}$	$1.661 \cdot 10^{-4}$
24	150	$4.040 \cdot 10^{-2}$	$2.649 \cdot 10^{-2}$	$1.862 \cdot 10^{-4}$
25	160	$3.747 \cdot 10^{-2}$	$2.728 \cdot 10^{-2}$	$2.070 \cdot 10^{-4}$
26	170	$3.475 \cdot 10^{-2}$	$2.799 \cdot 10^{-2}$	$2.283 \cdot 10^{-4}$
27	180	$3.223 \cdot 10^{-2}$	$2.863 \cdot 10^{-2}$	$2.502 \cdot 10^{-4}$
28	190	$2.989 \cdot 10^{-2}$	$2.920 \cdot 10^{-2}$	$2.725 \cdot 10^{-4}$
29	200	$2.772 \cdot 10^{-2}$	$2.972 \cdot 10^{-2}$	$2.953 \cdot 10^{-4}$
30	210	$2.571 \cdot 10^{-2}$	$3.018 \cdot 10^{-2}$	$3.184 \cdot 10^{-4}$
31	220	$2.385 \cdot 10^{-2}$	$3.058 \cdot 10^{-2}$	$3.419 \cdot 10^{-4}$
32	230	$2.212 \cdot 10^{-2}$	$3.094 \cdot 10^{-2}$	$3.656 \cdot 10^{-4}$
33	240	$2.051 \cdot 10^{-2}$	$3.126 \cdot 10^{-2}$	$3.897 \cdot 10^{-4}$
34	250	$1.903 \cdot 10^{-2}$	$3.153 \cdot 10^{-2}$	$4.139 \cdot 10^{-4}$
35	260	$1.765 \cdot 10^{-2}$	$3.177 \cdot 10^{-2}$	$4.383 \cdot 10^{-4}$
36	270	$1.637 \cdot 10^{-2}$	$3.197 \cdot 10^{-2}$	$4.630 \cdot 10^{-4}$
37	280	$1.518 \cdot 10^{-2}$	$3.214 \cdot 10^{-2}$	$4.877 \cdot 10^{-4}$
38	290	$1.408 \cdot 10^{-2}$	$3.228 \cdot 10^{-2}$	$5.126 \cdot 10^{-4}$
39	300	$1.306 \cdot 10^{-2}$	$3.239 \cdot 10^{-2}$	$5.376 \cdot 10^{-4}$
40	330	$1.042 \cdot 10^{-2}$	$3.258 \cdot 10^{-2}$	$6.128 \cdot 10^{-4}$
41	360	$8.311 \cdot 10^{-3}$	$3.259 \cdot 10^{-2}$	$6.884 \cdot 10^{-4}$
42	390	$6.630 \cdot 10^{-3}$	$3.246 \cdot 10^{-2}$	$7.637 \cdot 10^{-4}$
43	420	$5.290 \cdot 10^{-3}$	$3.222 \cdot 10^{-2}$	$8.387 \cdot 10^{-4}$
44	450	$4.220 \cdot 10^{-3}$	$3.189 \cdot 10^{-2}$	$9.129 \cdot 10^{-4}$
45	480	$3.367 \cdot 10^{-3}$	$3.150 \cdot 10^{-2}$	$9.864 \cdot 10^{-4}$
46	510	$2.686 \cdot 10^{-3}$	$3.106 \cdot 10^{-2}$	$1.059 \cdot 10^{-3}$
47	540	$2.143 \cdot 10^{-3}$	$3.059 \cdot 10^{-2}$	$1.130 \cdot 10^{-3}$
48	570	$1.710 \cdot 10^{-3}$	$3.009 \cdot 10^{-2}$	$1.201 \cdot 10^{-3}$
49	600	$1.364 \cdot 10^{-3}$	$2.957 \cdot 10^{-2}$	$1.270 \cdot 10^{-3}$
50	630	$1.088 \cdot 10^{-3}$	$2.904 \cdot 10^{-2}$	$1.338 \cdot 10^{-3}$
51	660	$8.681 \cdot 10^{-4}$	$2.850 \cdot 10^{-2}$	$1.404 \cdot 10^{-3}$
52	690	$6.926 \cdot 10^{-4}$	$2.796 \cdot 10^{-2}$	$1.470 \cdot 10^{-3}$
53	720	$5.525 \cdot 10^{-4}$	$2.742 \cdot 10^{-2}$	$1.534 \cdot 10^{-3}$
54	750	$4.408 \cdot 10^{-4}$	$2.688 \cdot 10^{-2}$	$1.597 \cdot 10^{-3}$
55	780	$3.517 \cdot 10^{-4}$	$2.635 \cdot 10^{-2}$	$1.658 \cdot 10^{-3}$
56	810	$2.806 \cdot 10^{-4}$	$2.582 \cdot 10^{-2}$	$1.719 \cdot 10^{-3}$
57	840	$2.238 \cdot 10^{-4}$	$2.529 \cdot 10^{-2}$	$1.778 \cdot 10^{-3}$
58	870	$1.786 \cdot 10^{-4}$	$2.478 \cdot 10^{-2}$	$1.836 \cdot 10^{-3}$
59	900	$1.425 \cdot 10^{-4}$	$2.427 \cdot 10^{-2}$	$1.893 \cdot 10^{-3}$
60	960	$9.068 \cdot 10^{-5}$	$2.328 \cdot 10^{-2}$	$2.003 \cdot 10^{-3}$
61	1020	$5.772 \cdot 10^{-5}$	$2.232 \cdot 10^{-2}$	$2.109 \cdot 10^{-3}$
62	1080	$3.674 \cdot 10^{-5}$	$2.140 \cdot 10^{-2}$	$2.210 \cdot 10^{-3}$
63	1140	$2.338 \cdot 10^{-5}$	$2.051 \cdot 10^{-2}$	$2.307 \cdot 10^{-3}$
64	1200	$1.488 \cdot 10^{-5}$	$1.966 \cdot 10^{-2}$	$2.400 \cdot 10^{-3}$

65	1260	$9.472 \cdot 10^{-6}$	$1.885 \cdot 10^{-2}$	$2.489 \cdot 10^{-3}$
66	1320	$6.029 \cdot 10^{-6}$	$1.806 \cdot 10^{-2}$	$2.575 \cdot 10^{-3}$
67	1380	$3.837 \cdot 10^{-6}$	$1.731 \cdot 10^{-2}$	$2.657 \cdot 10^{-3}$
68	1440	$2.442 \cdot 10^{-6}$	$1.659 \cdot 10^{-2}$	$2.735 \cdot 10^{-3}$
69	1500	$1.555 \cdot 10^{-6}$	$1.590 \cdot 10^{-2}$	$2.810 \cdot 10^{-3}$
70	1560	$9.895 \cdot 10^{-7}$	$1.524 \cdot 10^{-2}$	$2.883 \cdot 10^{-3}$
71	1620	$6.298 \cdot 10^{-7}$	$1.461 \cdot 10^{-2}$	$2.952 \cdot 10^{-3}$
72	1680	$4.009 \cdot 10^{-7}$	$1.400 \cdot 10^{-2}$	$3.018 \cdot 10^{-3}$
73	1740	$2.551 \cdot 10^{-7}$	$1.342 \cdot 10^{-2}$	$3.082 \cdot 10^{-3}$
74	1800	$1.624 \cdot 10^{-7}$	$1.286 \cdot 10^{-2}$	$3.142 \cdot 10^{-3}$
75	1860	$1.034 \cdot 10^{-7}$	$1.233 \cdot 10^{-2}$	$3.201 \cdot 10^{-3}$
76	1920	$6.579 \cdot 10^{-8}$	$1.181 \cdot 10^{-2}$	$3.257 \cdot 10^{-3}$
77	1980	$4.187 \cdot 10^{-8}$	$1.132 \cdot 10^{-2}$	$3.310 \cdot 10^{-3}$
78	2040	$2.665 \cdot 10^{-8}$	$1.085 \cdot 10^{-2}$	$3.362 \cdot 10^{-3}$
79	2100	$1.696 \cdot 10^{-8}$	$1.040 \cdot 10^{-2}$	$3.411 \cdot 10^{-3}$
80	2160	$1.080 \cdot 10^{-8}$	$9.968 \cdot 10^{-3}$	$3.458 \cdot 10^{-3}$
81	2220	$6.872 \cdot 10^{-9}$	$9.553 \cdot 10^{-3}$	$3.503 \cdot 10^{-3}$
82	2280	$4.374 \cdot 10^{-9}$	$9.156 \cdot 10^{-3}$	$3.547 \cdot 10^{-3}$
83	2340	$2.784 \cdot 10^{-9}$	$8.775 \cdot 10^{-3}$	$3.588 \cdot 10^{-3}$
84	2400	$1.772 \cdot 10^{-9}$	$8.410 \cdot 10^{-3}$	$3.628 \cdot 10^{-3}$
85	2460	$1.128 \cdot 10^{-9}$	$8.060 \cdot 10^{-3}$	$3.666 \cdot 10^{-3}$
86	2540	$6.175 \cdot 10^{-10}$	$7.617 \cdot 10^{-3}$	$3.715 \cdot 10^{-3}$
87	2600	$3.930 \cdot 10^{-10}$	$7.300 \cdot 10^{-3}$	$3.749 \cdot 10^{-3}$
88	2720	$1.592 \cdot 10^{-10}$	$6.705 \cdot 10^{-3}$	$3.814 \cdot 10^{-3}$
89	2840	$6.450 \cdot 10^{-11}$	$6.159 \cdot 10^{-3}$	$3.874 \cdot 10^{-3}$
90	2960	$2.613 \cdot 10^{-11}$	$5.658 \cdot 10^{-3}$	$3.928 \cdot 10^{-3}$
91	3080	$1.059 \cdot 10^{-11}$	$5.197 \cdot 10^{-3}$	$3.979 \cdot 10^{-3}$
92	3200	$4.288 \cdot 10^{-12}$	$4.774 \cdot 10^{-3}$	$4.025 \cdot 10^{-3}$
93	3320	$1.737 \cdot 10^{-12}$	$4.385 \cdot 10^{-3}$	4.067·10 -3
94	3440	$7.038 \cdot 10^{-13}$	$4.028 \cdot 10^{-3}$	$4.106 \cdot 10^{-3}$
95	3560	$2.851 \cdot 10^{-13}$	$3.700 \cdot 10^{-3}$	$4.142 \cdot 10^{-3}$
96	3600	$2.110 \cdot 10^{-13}$	$3.596 \cdot 10^{-3}$	$4.153 \cdot 10^{-3}$
97	3660	$1.343 \cdot 10^{-13}$	$3.447 \cdot 10^{-3}$	$4.169 \cdot 10^{-3}$
98	3900	$2.204 \cdot 10^{-14}$	$2.908 \cdot 10^{-3}$	$4.228 \cdot 10^{-3}$
99	4200	$2.302 \cdot 10^{-15}$	$2.352 \cdot 10^{-3}$	$4.289 \cdot 10^{-3}$
100	4800	0	$1.538 \cdot 10^{-3}$	$4.378 \cdot 10^{-3}$
101	5400	0	$1.006 \cdot 10^{-3}$	$4.436 \cdot 10^{-3}$
102	6000	0	6.577·10 -4	$4.474 \cdot 10^{-3}$
103	6600	0	4.301·10 -4	$4.499 \cdot 10^{-3}$
104	7200	0	2.812·10 -4	$4.515 \cdot 10^{-3}$
105	7800	0	1.839·10 -4	$4.525 \cdot 10^{-3}$
106	8400	0	1.203·10 -4	$4.532 \cdot 10^{-3}$
107	9000	0	7.865·10 -5	$4.537 \cdot 10^{-3}$
108	9600	0	5.143·10 -5	$4.540 \cdot 10^{-3}$

Table 4-3: Table shows all the calculation cluster atoms in the sample at different times.

4-2: Effect of gold cluster concentration.

Once we have identified the kind of clusters produced by reduction of gold ions by $NaBH_4$ in the presence of CTAB as stabilizer, and once we could estimate the concentration of the main species (clusters with 2, 6 and 55 atoms), then we can estimate the conditions at which the concentration of catalytic clusters are equal to the concentration of seeds. For this purpose we considered that Au_6 are the main clusters used in the production of gold nanorods due to the fact that it is the most abundant cluster found in the mass spectra analysis. Au_{55} was considered to be the seeds because of their estimated sizes (1.8±0.2 nm from AFM images).

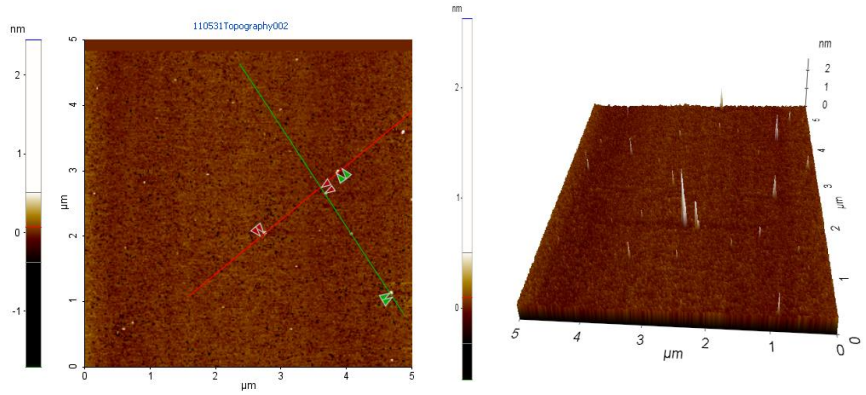

Figure 4-7: AFM images of the Au seeds after 10 min of preparation. Average size: 1.8±0.2nm.

After preparation and characterization of these gold clusters at different aging times that controlling the gold cluster´s concentration, the next step was to see if by using the appropriate conditions derived from the results shown in the previous chapter ([clusters] =[seeds]), one could control the formation of gold nanorods. Experiments were then carried out adding gold clusters aged at different times (10 sec, 30sec., 1min., and 5min.) to the growth solution. The results are shown in the following figures.

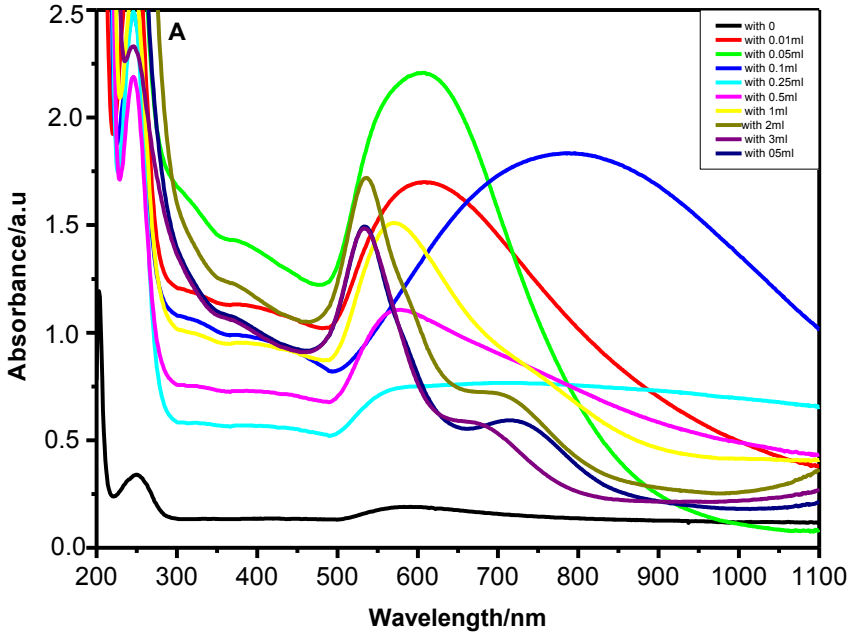
A
with 0
with 0.01ml
with 0.05ml
with 0.1ml
with 0.25ml
with 0.5ml
with 1ml
with 2ml
with 3ml
with 05ml
Absorbance/a.u
Wavelength/nm
0.0
0.5
1.0
1.5
2.0
2.5
200
300
400
500
600
700
800
900
1000
1100

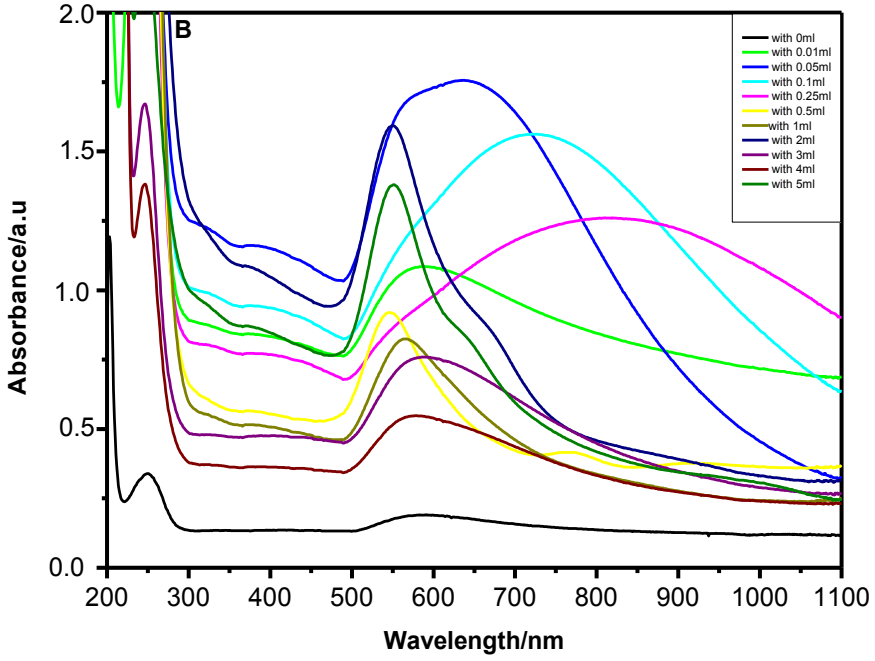
B
with 0ml
with 0.01ml
with 0.05ml
with 0.1ml
with 0.25ml
with 0.5ml
with 1ml
with 2ml
with 3ml
with 4ml
with 5ml
Absorbance/a.u
Wavelength/nm
0.0
0.5
1.0
1.5
2.0
200
300
400
500
600
700
800
900
1000
1100

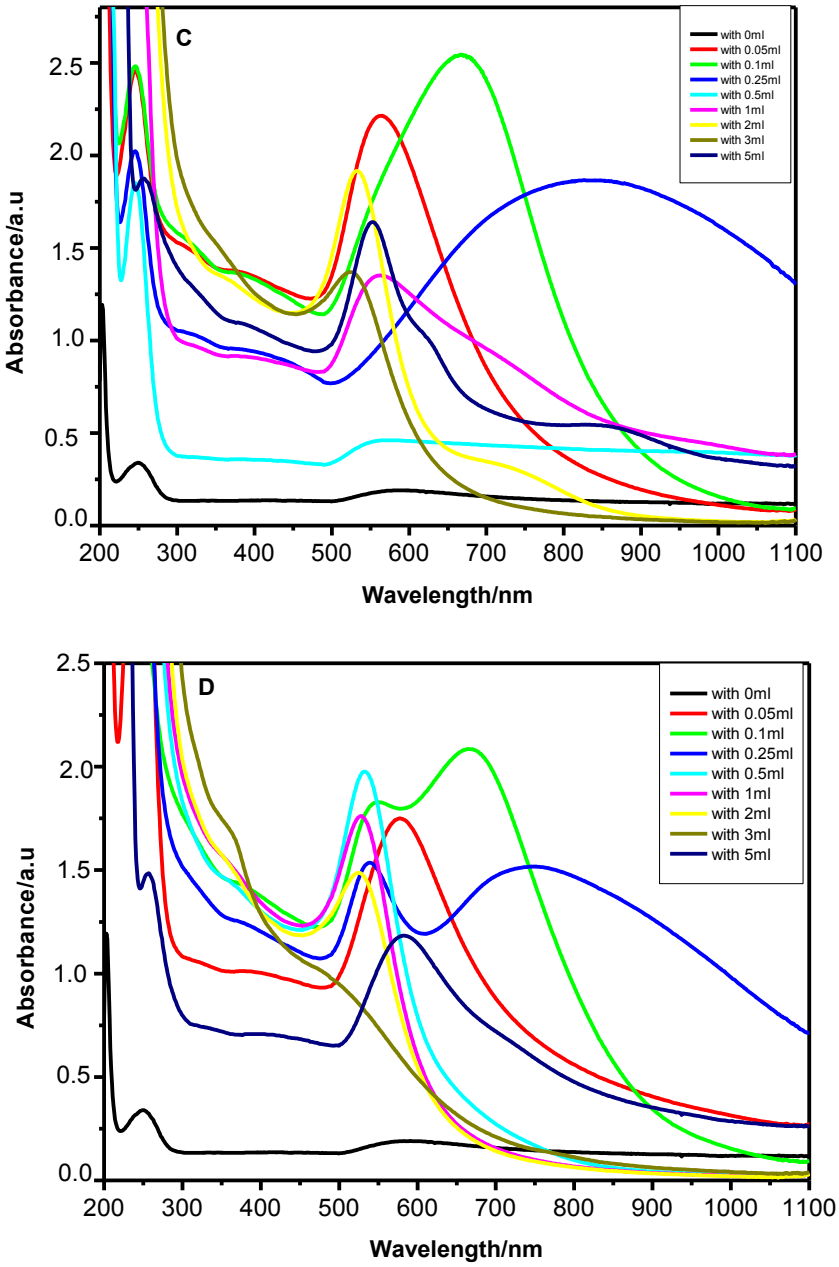

Figure 4-8: Absorption spectra showing the formation of high aspect ratio gold nanorods by the addition of gold clusters with different concentrations, i.e., aged at different times without addition of seeds; A) 10 s; B) 30 s; C) 1min; D) 5 min. Please note that without Au-clusters, only aggregated particles are formed.

For comparison purposes in the next figure (4-9) the final UV-Vis spectra, after addition of 5ml of gold clusters at different aging times (different concentrations), is shown.

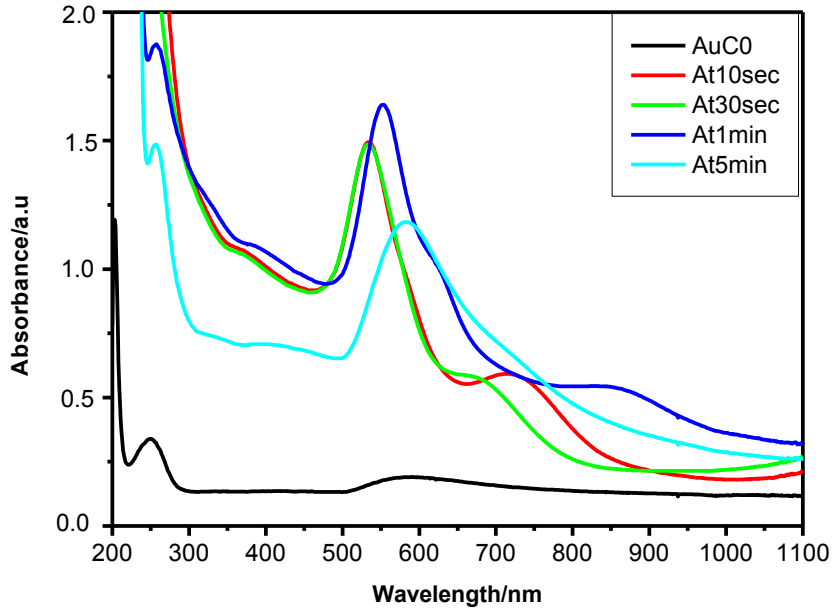

Figure 4-9: Absorption spectra showing the formation of high aspect ratio gold nanorods by the addition of 5 ml of gold clusters with different concentrations (different aging times) without addition of seeds. For comparison purposes the spectra of the same reaction without addition of gold clusters are included.

It can be seen in this figure the formation of gold nanorods with high aspect ratio, which are formed without addition of seeds solution. The growth solution without the addition of gold clusters, gives only aggregated and unshaped particles. It is also observed that the aspect ratio and the yield of gold nanorods increases from 10 sec to 1 min and then decreases using gold clusters at 5 min due to the formation of other shapes, like prisms and hexagonal shapes. In the next figures the absorption spectra adding different concentrations of gold clusters to the growth solution with the addition of seeds are shown, in order to compare the results with the previous spectra without addition of the seed solution.

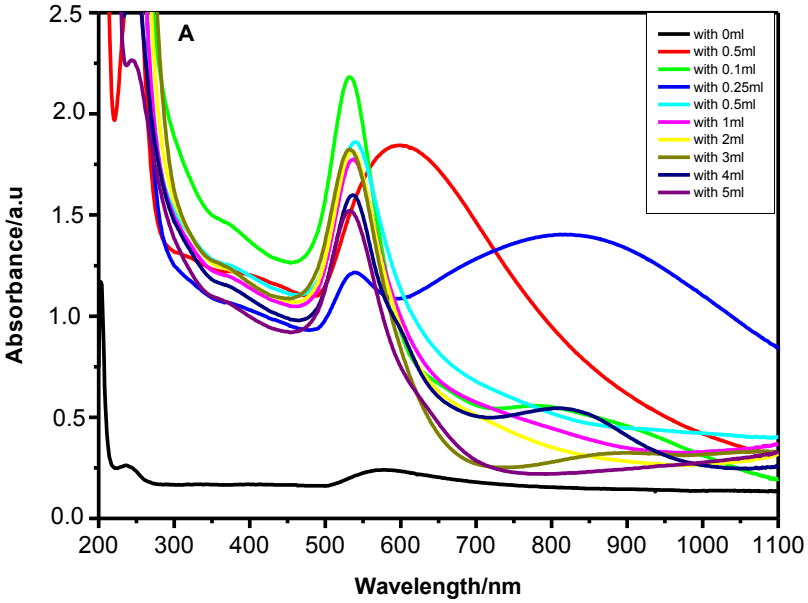
A
with 0ml
with 0.5ml
with 0.1ml
with 0.25ml
with 0.5ml
with 1ml
with 2ml
with 3ml
with 4ml
with 5ml
Absorbance/a.u
Wavelength/nm
0.0
0.5
1.0
1.5
2.0
2.5
200
300
400
500
600
700
800
900
1000
1100

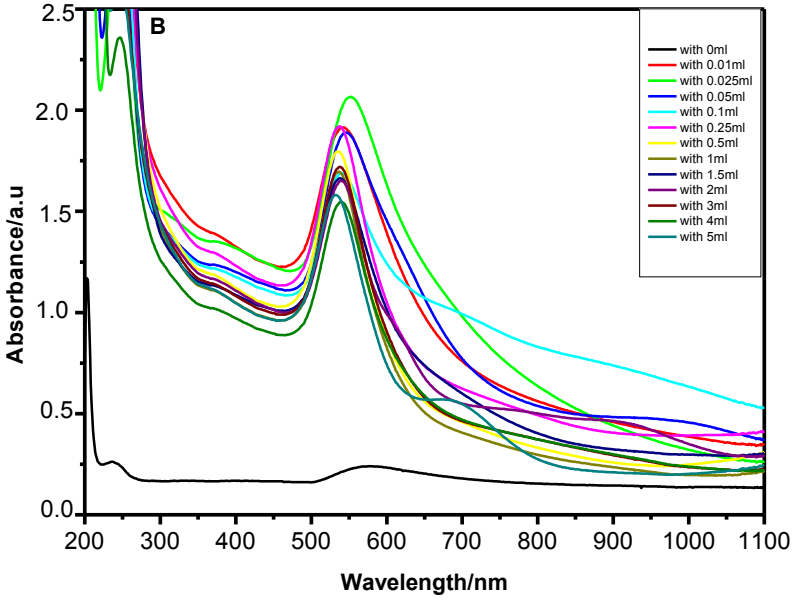
B
with 0ml
with 0.01ml
with 0.025ml
with 0.05ml
with 0.1ml
with 0.25ml
with 0.5ml
with 1ml
with 1.5ml
with 2ml
with 3ml
with 4ml
with 5ml
Absorbance/a.u
Wavelength/nm
0.0
0.5
1.0
1.5
2.0
2.5
200
300
400
500
600
700
800
900
1000
1100

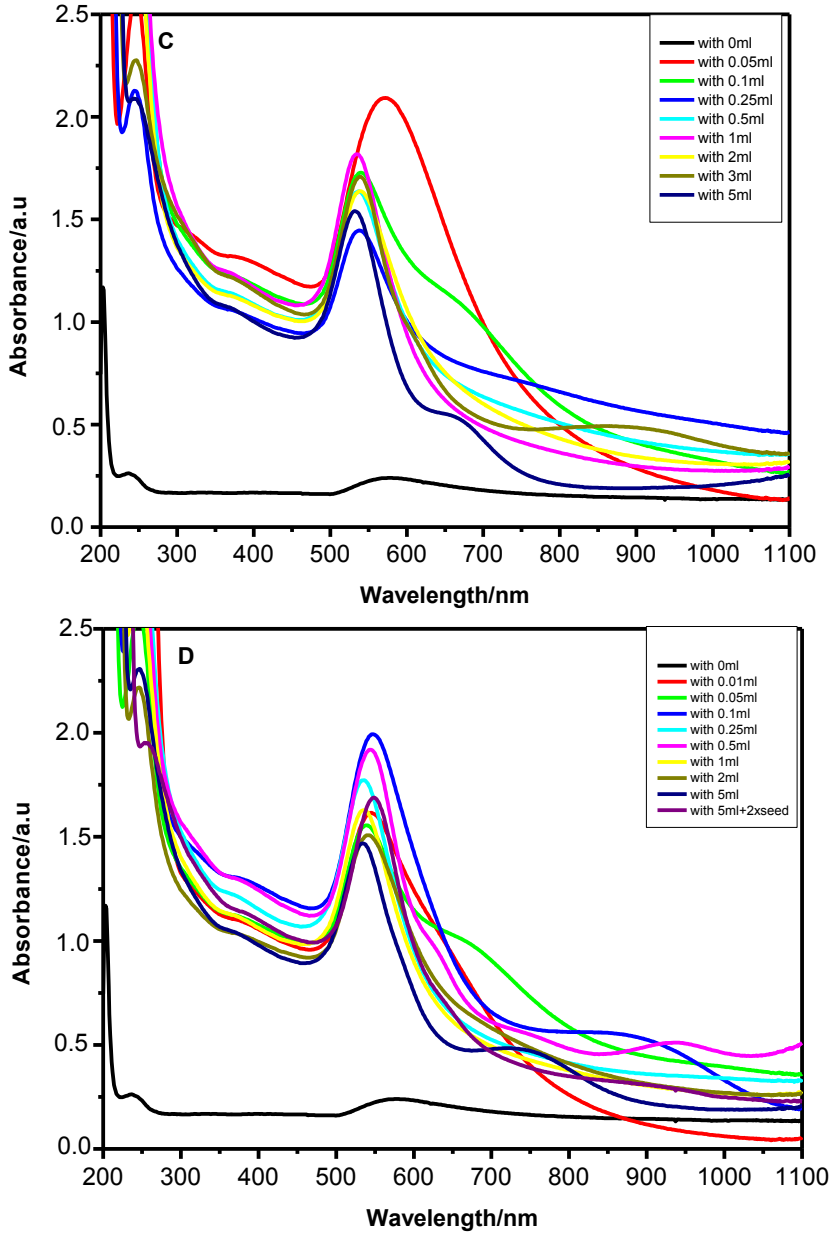

Figure 4-10: Absorption spectra showing the formation of high aspect ratio gold nanorods by the addition of 5 ml of gold clusters with different concentrations (different aging times) with addition of seeds. For comparison purposes the spectra of the same reaction without addition of gold clusters are included.

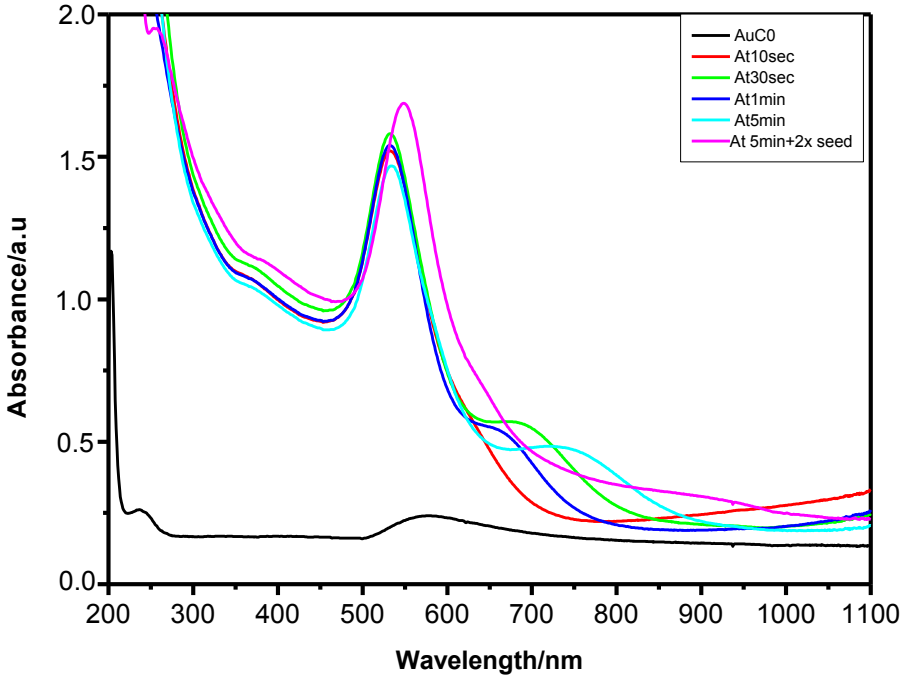

Figure 4-11: Absorption spectra showing the formation of high aspect ratio gold nanorods by the addition of 5 ml of gold clusters with different concentrations, (different times) in the presence of seeds.

TEM images of the formed particles using different concentrations of gold clusters in the absence and presence of the seed solution are shown in the next figure.

	Without seeds	With Seeds
10Sec.	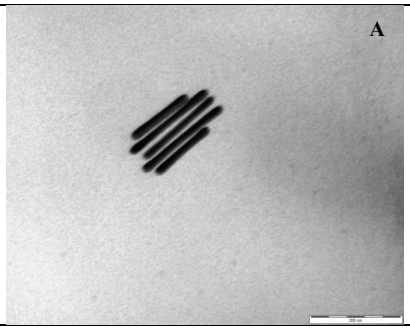	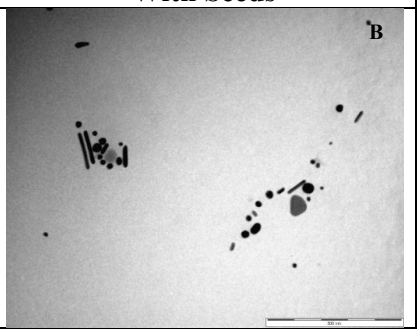

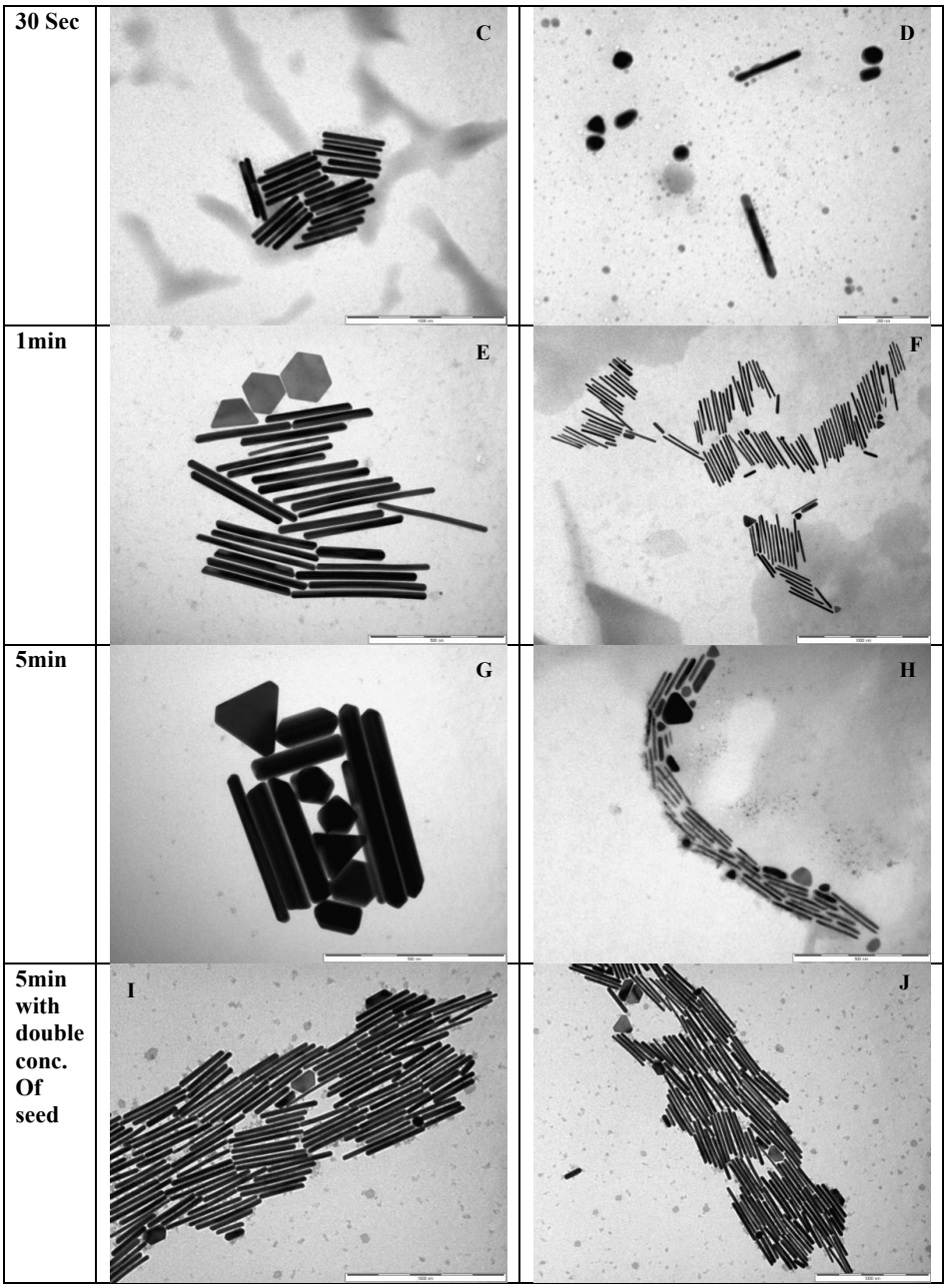

Figure 4-12: (A&B) TEM images showing the particles prepared using Au clusters aged during 10sec (without & with seeds, respectively); (C&D) with Au clusters aged during 30sec (without & with seeds, respectively); (E&F) with Au clusters aged during 60sec (without & with seeds, respectively); (G&H) with Au clusters aged during 5min (without & with seeds, respectively), and (I&J) with Au clusters aged during 5min (with double concentration of seeds).

Au-Clusters	Without seed		With seed		[Clusters]mM C_t	C_f	[Seed]mM	[AuC] /[Seed]
10Sec.	Long rods: Short rods: Others: alot of spheres+few prisms	18% 25% 57% (A)	Long rods: Short rods: Others:spheres+more prisms	**8% 20% 72% (B)**				
30Sec.	Long rods: Short rods: Others:few snapped prisms+spheres	83% 8% 9% (C)	Long rods: Short rods: Other shapes:spheres+snapped prisms	**15% 7% 78% (D)**	4.16×10^{-3}	4.16×10^{-7}	7.62×10^{-7}	R ≈ 0,55
1Min.	Long rods: Short rods: Others:snapped prisms+hexagonnal+spheres	**81% 11% 8% (E)**	Long rods: Short rods: Others:snapped +prisms+spheres	**89% 6% 4% (F)**	7.41×10^{-3}	7.41×10^{-7}	7.62×10^{-7}	R ≈ 1
5Min.	Long rods: Short rods: Others:hexagonal+snapped prisms+pentahydral+spheres	39% 13% 47% (G)	Long rods: Short rods: Others:spheres+snapped prisms	**34% 35% 30% (H)**	16.2×10^{-3}	16.2×10^{-7}	7.62×10^{-7}	R ≈ 2
5Min. Seed x 2			Long rods: Short rods: Others:snapped prisms	**90% 6% 3% (I&J)**	16.2×10^{-3}	16.2×10^{-7}	1.52×10^{-6}	R ≈ 1

Table 4-4: Table shows the summary of the results obtained by the TEM analysis.

From the table (4-4) and the TEM-images, it can be deduced that the yield of high aspect ratio gold nanorods increases in the samples prepared with Au clusters aged from 10sec to 30sec and then decreases from 30 sec to 5 min, without addition of the seed solution. But, with the addition of the seed solution the yield increases in the samples prepared with Au clusters aged from 10sec to 60sec and then decreases from 60 sec to 5 min. It can be also observed that after addition of a double concentration of the seed solution the yield increases again with gold clusters aged during 5min.

All these results support the idea of the important role of clusters in the formation of gold nanorods (chapter III). We have seen that Au-clusters are formed by the addition of $NaBH_4$ to gold salt in the presence of CTAB ($Au^{+3} \rightarrow Au^0$). These clusters are then added to the growth solutions that not contain any surfactant or polymer. According to the mechanism we proposed to explain the results, these clusters are adsorbed onto the gold surfaces and the reduction of Au^{+3}/Au^{+1} to Au(0) will happen after addition

of ascorbic acid to the growth solution. The adsorbed Au clusters can then act as catalysts enhancing the growth of the gold nanorods (atomic metal clusters are now recognized as especially efficient catalysts[13]) since those clusters could be adsorbed on any active site on the surface of the gold nucleus. Gold particles with a cubic lattice have a tendency to grow forming cubes, or spheres, because the rate of the growth of all facets is the same (result obtained when no Ag-clusters or ions are added). However, adsorption of gold clusters to one of these facets breaks the symmetry of the growth and enhances the growth of one of these facets much more than the others, leading to the formation of rod shaped particles. When the concentration of Au clusters increases more, gold clusters are adsorbed onto more than one active sites of the gold surface breaking the symmetry to form some triangular and hexagonal shapes. The reduction reaction of Au-ions to Au^0 happened without addition of external seed solution that started the reduction reaction in the previous mechanism described in Chapter III, and also without formation of the stable Au-CTAB complex because we assumed that Au_{55}(seeds) produced during the preparation of gold clusters and it can act as seeds.

As it was proposed in the previous chapter, the ratio [Au-clusters] / [seed] is the key factor in the production of gold nanorods with high aspect ratio. We can calculate the [Au-clusters] and [seeds] from the data shown in table (4-3). One can see that the concentration of clusters is much higher than the concentration of seeds for the aging times used in this study, which seems to be in disagreement with what was assumed in previous chapter, namely, that gold NRs are produced when the cluster/seed ratio is approx. 1. However, one has to consider that many clusters can be trapped inside the CTAB micelles, which are in this way not able to be attached to the active sites of the gold surface. We can then try to estimate the amount of free clusters in the following way:

$[Clusters]_f + [CTAB] \rightarrow [\ CTAB\text{-}Clusters]$

$K = \frac{[CTAB-Clusters]}{[Clusters]fx\,[CTAB]}$, $[clusters]_T = [clusters]_f + [CTAB\text{-}clusters]$

$\therefore [clusters]_T - [clusters]_f = K\,[CTAB][Clusters]_f$

$[Clusters]f = \frac{[Clusters]T}{K[CTAB]+1}$, if K>>1 then

$\therefore [Clusters]f = \frac{[Clusters]T}{K[CTAB]}$

The value of K can be estimated from the results obtained of the effect of [Ag-ions] and [seed] previously described in chapter III. From this value of K, the final concentrations of free gold clusters can be calculated and from this, the ratio [Au-Clusters] / [Seed] can also be calculated. These values are given in table (4-4). It can be seen that, in agreement with the results obtained in chapter III, when R ≈1 we get nanorods. Calculation of K:

Rod formation occurs when R=1, i.e.

$[clusters]_f = [seed]$. Therefore,

$K = [Clusters]_{Total} / [seed] \times [CTAB]$

From figures (3-16 to 3-19), we observe that NRs in high yield can be obtained with 0.1mM of Ag-ions and $5x10^{-9}$M of seed solution. Therefore, assuming that all the Ag ions transform into clusters, one can make an approximate estimation of K:

$K = 0.1 \times 10^{-3} / (5 \times 10^{-9}) \times 0.1$

$K = 2 \times 10^5$. This value has been used to obtain the data shown in Table (4-4). We can then explain the last results as follows: gold nanorods with high yield are produced when the ratio $R_{clusters}$ = [Au- clusters] / [Au seeds] is ≈ 1. When the amount of Au clusters is increased, the corresponding amounts of Au seeds should also increase to maintain the ratio between the

[Au clusters]/ [Au seeds] ≈ 1. For that purpose extra seed concentration (double concentration) was added to the Au-clusters solution at 5min, because the concentration of clusters is higher at this time (see Table 4-3). In this way, gold nanorods with high aspect ratio are also formed in these conditions. Therefore, these results further support the mechanism of the formation of different shapes of gold nanorods in the presence of $AgNO_3$ proposed in previous chapter and the catalytic activity of metal clusters, which play an important role in the anisotropic growth of nanoparticles. This important aspect was not recognized until now, and may be a key point in the interpretation of the complex mechanisms involved in the formation of nanoparticles with different shapes.

At the same time, the results also show that one can synthesize crystalline gold nanorods in water, in the absence of any surfactant or polymer to direct the anisotropic nanoparticle growth.

4-3 Influence of CTAB concentration.

We studied the influence of CTAB concentration in the clusters solution on the anisotropic growth gold nanoparticles.

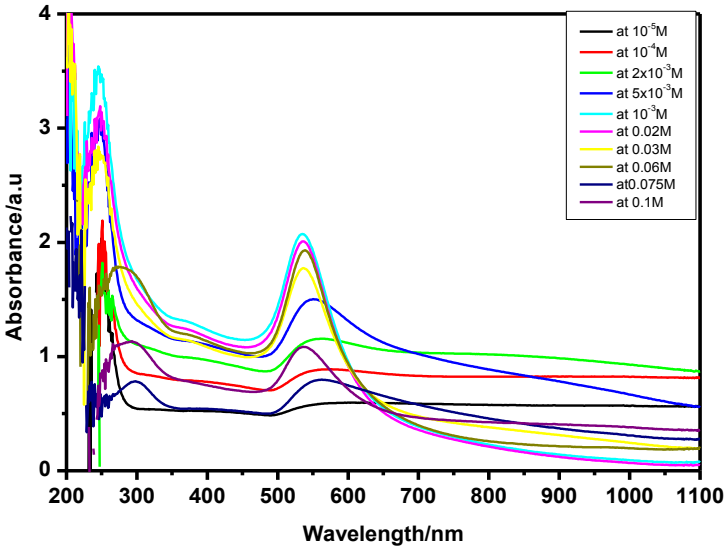

Figure 4-13: Absorption spectra showing the influence of CTAB concentration (10^{-5} to 0.1M) using gold clusters aged during 1 min on the growth of gold nanoparticles in the absence of seeds.

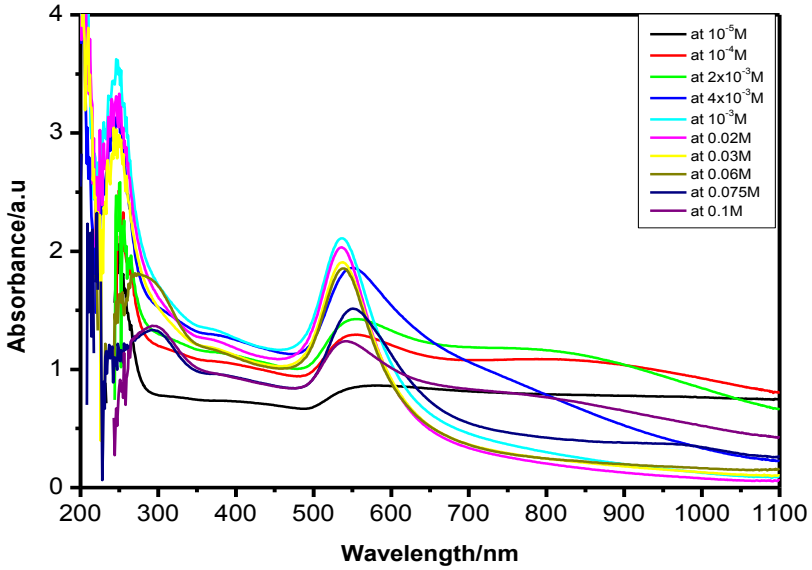

Figure 4-14: Absorption spectra showing the influence of CTAB concentrations (10^{-5} to 0.1M) using gold clusters aged during 1 min on the growth of gold nanoparticles in the presence of seeds.

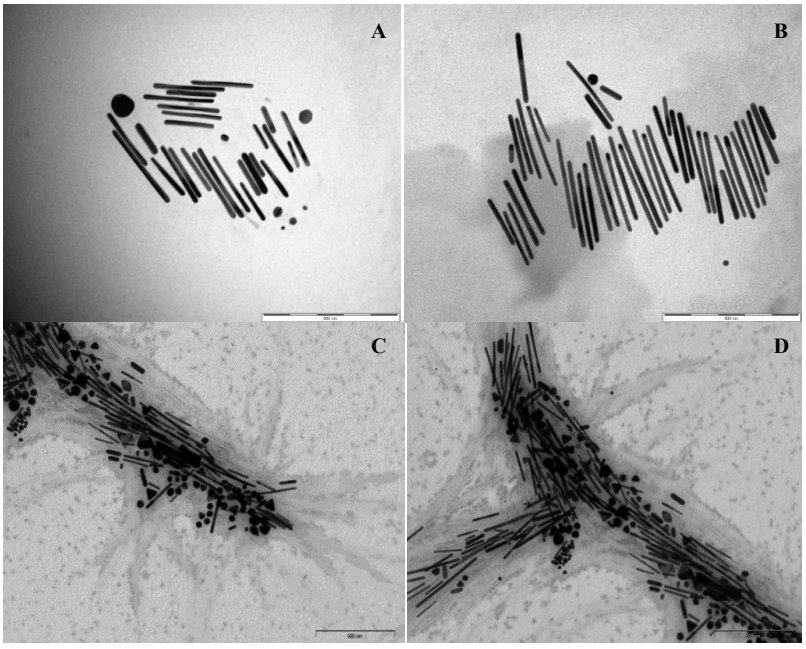

Figure 4-15: TEM images, showing the formation of gold nanorods with [CTAB] = 10^{-4} (A) and 8 x 10^{-4} M (B) using the gold clusters aged during 1 min without adding seeds, and formation of gold nanorods with [CTAB] = 10^{-4} (C) and 8 x 10^{-4} M (D) using gold clusters aged during 1 min with the addition of adding seeds.

From these results one can deduce that the role of CTAB in the clusters solution is to stabilize the formed clusters and also to slow the growth process, because gold nanorods are formed using CTAB concentrations lower than the CMC (~10^{-3} M) in the clusters solution.

4-4: Influence of the addition of diluted concentrations of seeds.

The effect of the addition of diluted concentrations of seeds to the growth solution that contains gold ions and gold clusters, is reported in the next section by added diluted concentrations of seeds (1:10, 1:100, and 1:1000) at different aging times (1, 3, and 5h).

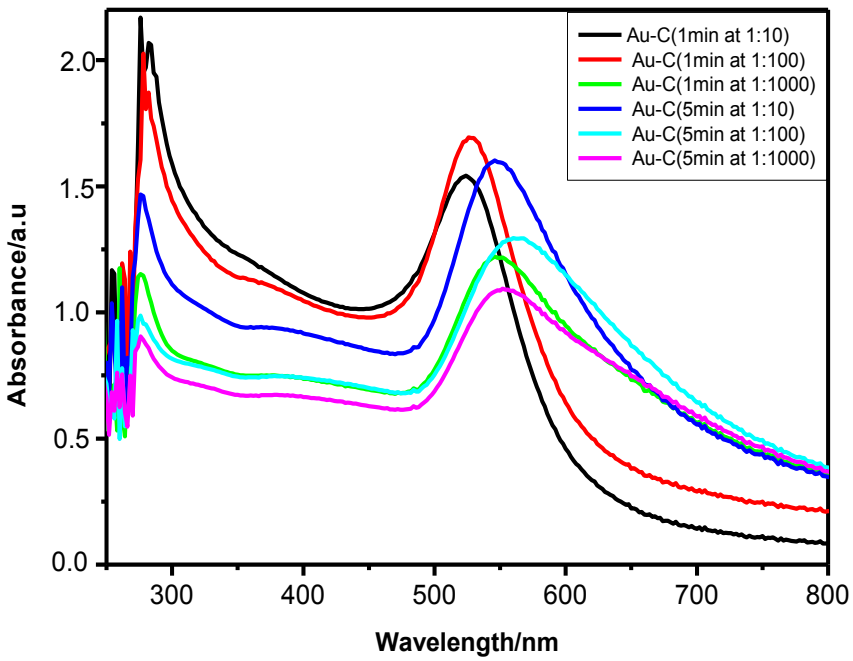

Figure 4-16: Absorption spectra showing the effect of diluted concentration of seeds aged during 1h on the growth of gold nanoparticles using gold clusters aged during 1min and 5min.

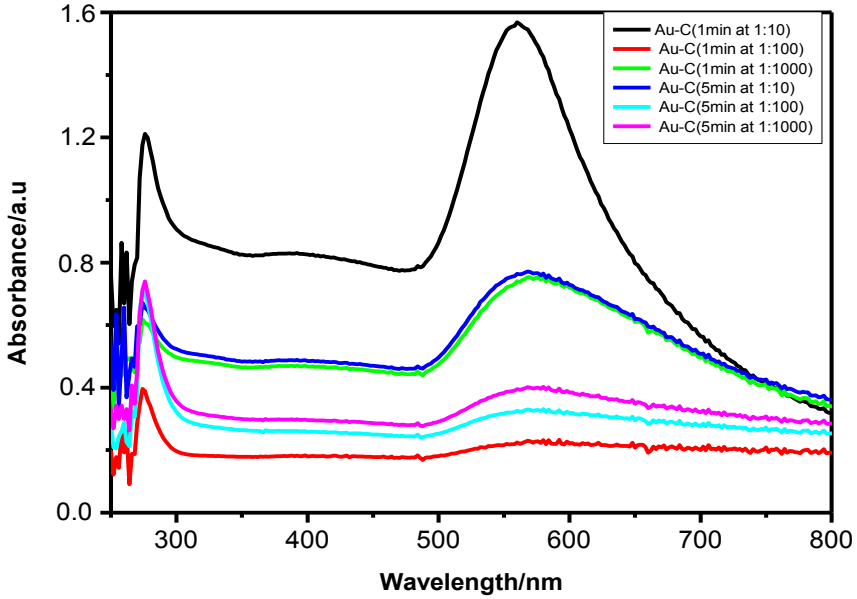

Figure 4-17: Absorption spectra showing the effect of diluted concentration of seeds aged during 3h on the growth of gold nanoparticles using gold clusters aged during 1min and 5min.

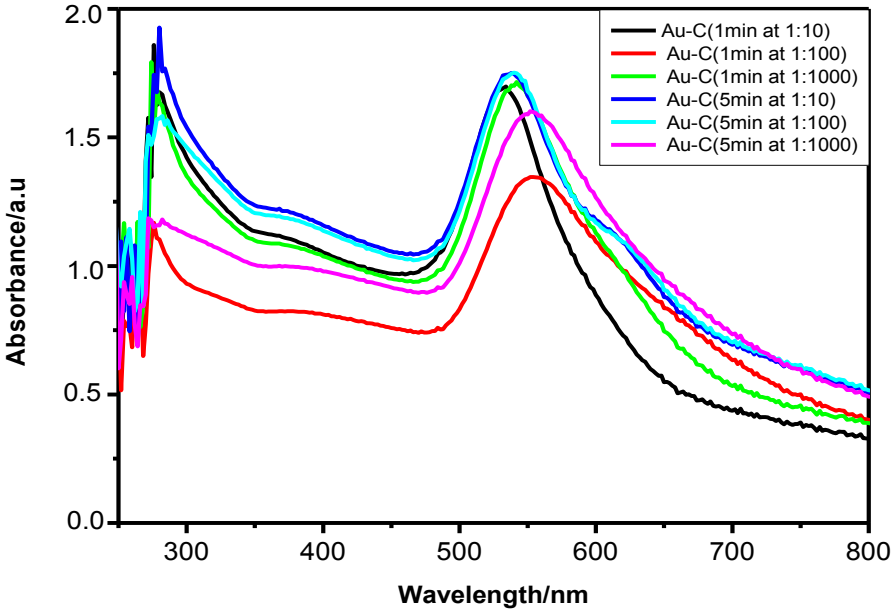

Figure 4-18: Absorption spectra showing the effect of diluted concentration of seeds aged during 5h on the growth of gold nanoparticles using gold clusters aged during 1min and 5min.

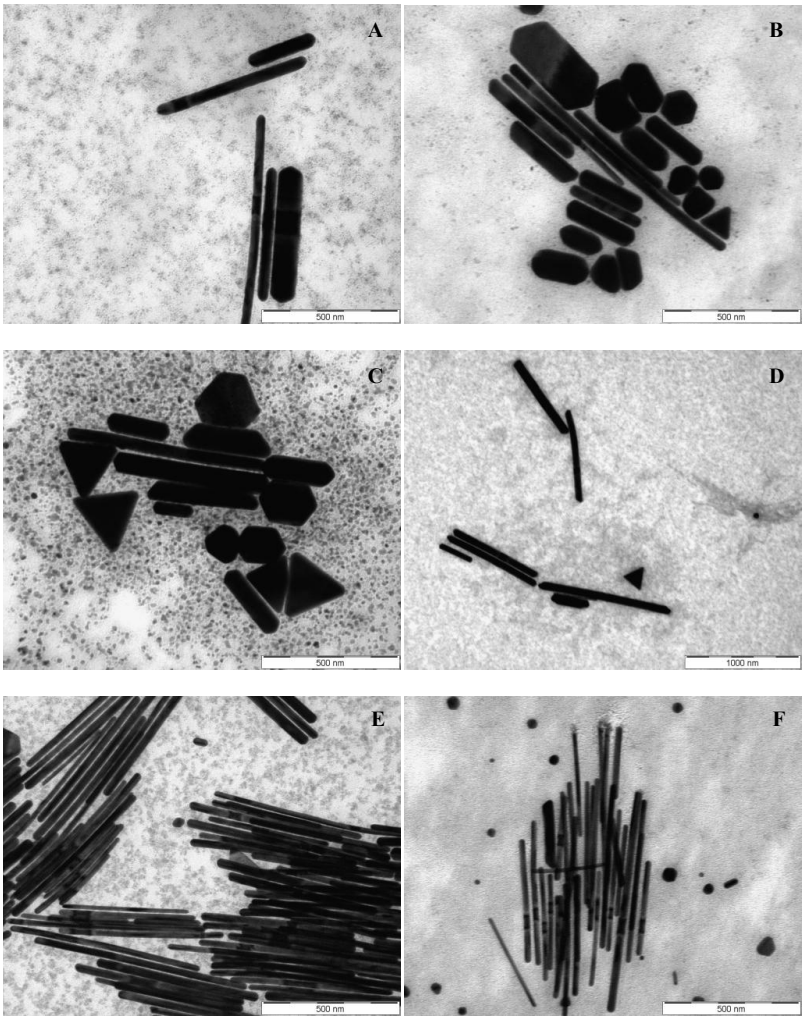

Figure 4-19: TEM-images of gold NRs prepared with seeds (aged during 1h) in a dilution 1:1000 using gold clusters aged during 1min (A) and 5min (B). TEM images of gold NRs prepared with seeds (aged during 3h) in a dilution 1:1000 using gold clusters aged during 1min (C) and 5min (D). TEM images of gold NRs prepared with seeds (aged during 5h) in a dilution 1:1000 using gold clusters aged during 1min (E) and 5min (F).

Gold nanorods with high aspect ratio are also produced with a 1:1000 dilution of the seeds prepared after 5h aging. The reason of the formation of gold nanorods with this high dilution will be the subject of a future work.

4-5: Influence of the nature of seeds.

Recent studies suggest that even in the absence of external addition of seeds, gold nanorods can be made. In 2010, Samal et al. synthesized gold nanorods by a one-step process, whereby the use of seed particles was eliminated[14]. The study suggests that the nature of the metal seed (seeds made using different metals having different crystal structures) does not affect the formation and monodispersity of gold nanorods. Further investigations revealed that sodium borohydride present in the seed solution played a critical role in the formation of gold nanorods; that is, gold nanorods can be synthesized by direct addition of sodium borohydride to the growth solution. In such method various metal seed particles with a size of 3-5 nm and different crystal structures, such as Fe (body centered cubic, bcc), Ru, and Cd (hexagonal close packing, hcp), Cu, Pb, Ag, and Au (cubic close packing, ccp), Hg (rhombohedral), In (tetragonal), and Sb (trigonal) were prepared from their salts by reduction with $NaBH_4$ and then added to the growth solution. All the seed particles produced nanorods with the same structures.

We also used seeds prepared from the reduction of Ni and Co salts by addition of $NaBH_4$ in the presence of CTAB. In this case, we studied the effect of $AgNO_3$ concentration using seeds from Ni and Co and the effect of the Ni & Co seeds concentration using a fixed concentration of $AgNo_3$ (80μM) on the growth of gold nanoparticles. Gold nanorods and nanoprisms are produced as it can be seen in the next figures.

Again it is observed that nanorods are formed when the ratio between Ag-clusters and seeds ≈1.

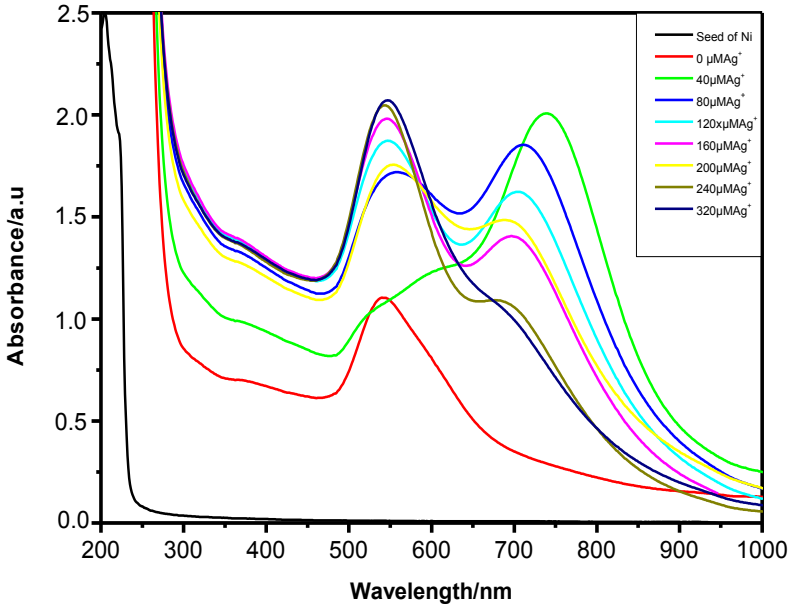

Figure 4-20: Absorption spectra showing the effect of different concentrations of $AgNO_3$ on the growth of gold nanoparticles using Ni-seeds.

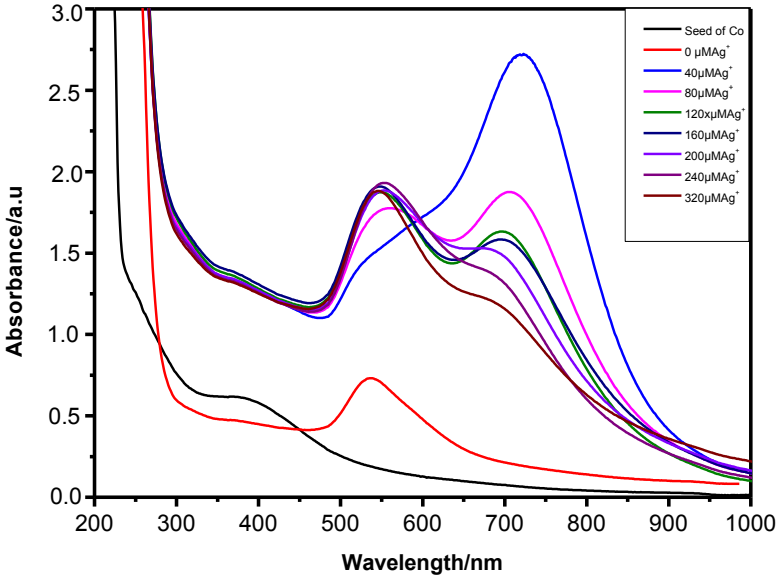

Figure 4-21: Absorption spectra showing the effect of different concentrations of $AgNO_3$on the growth of gold nanoparticles using Co-seeds.

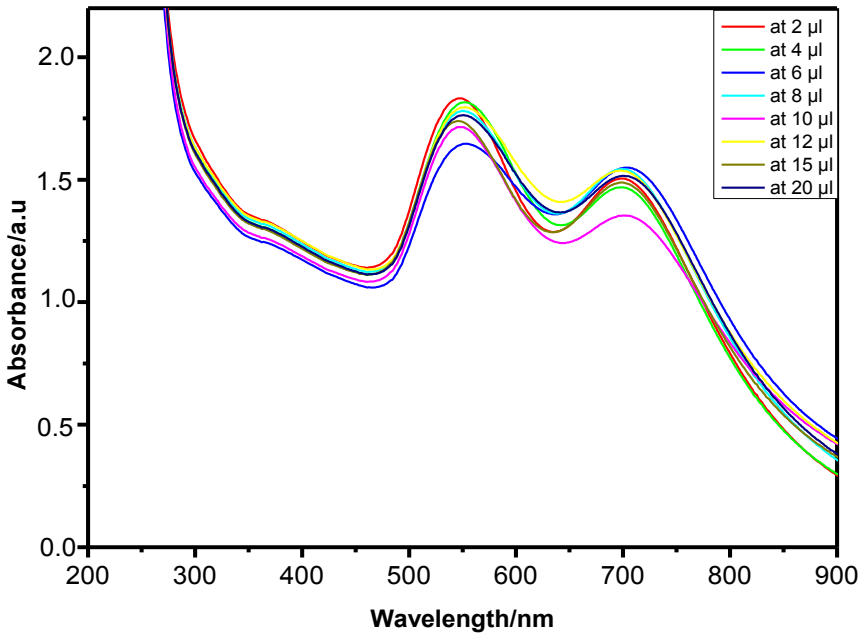

Figure 4-22: Absorption spectra showing the effect of different concentrations of Ni-seeds on the growth of gold nanoparticles using 80µM $AgNO_3$.

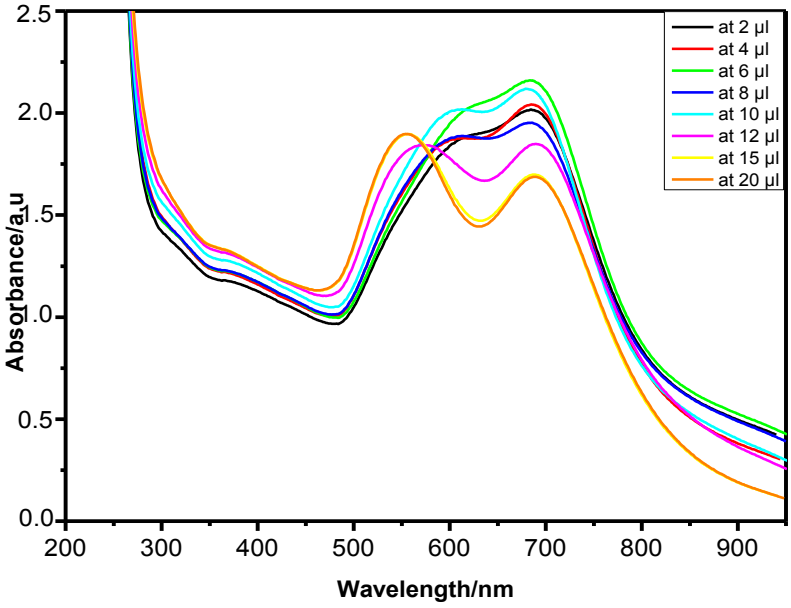

Figure 4-23: Absorption spectra showing the effect of different concentrations of Co-seeds on the growth of gold nanoparticles using 80µM $AgNO_3$.

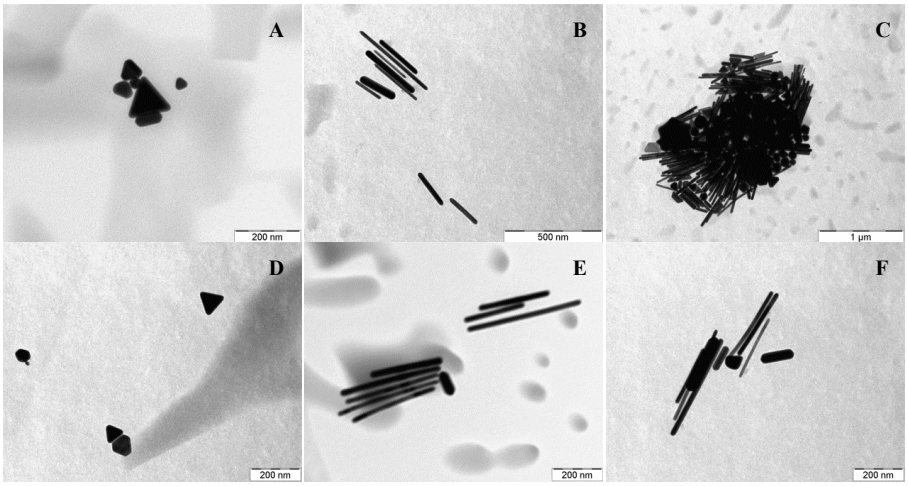

Figure 4-24: TEM images showing the effect of Ni-seeds on the growth of gold nanoparticles (A-C for 40, 100 and 200µM of $AgNO_3$, respectively); and (D-F) effect of Co-seeds on the growth of gold nanoparticles (40, 100 and 200µM of $AgNO_3$, respectively).

4-6: Conclusion.

By using a simple method, gold nanorods with high aspect ratios were prepared by just addition of prepared gold clusters stabilized with CTAB to gold ions in the growth solution without any surfactant or polymer. These results clearly show the importance of gold clusters in the growth mechanism. It seems that the deposition of Au clusters and the reduction reaction mainly occurs at the end (tips) of the nanorods. The prepared gold clusters were found to be mainly in the range Au_2-Au_6. The clusters were studied and characterized with different techniques. The effects of the dilution of CTAB in the clusters solution and the dilution of the seed solution on the growth of gold nanorods were also studied. The results show that gold nanorods can be formed without addition of the seeds.

4-7: References.

1. Busbee, B. D.; Obare, S. O.; Murphy, C., J. Adv. Mater., 2003, 15, 414.
2. Nikoobakht, B.; El-Sayed, M. A., Chem. Mater. 2003, 15, 1957.
3. Jin, R.; Cao, Y. C.; Hao, E.; Metraux, G. S.; Schatz, G. C.; Mirkin, C. A., Nature, 2003, 425, 487.
4. Smith, D.K.; Korgel, B.A., Langmuir, 2008, 24, 644.
5. P´erez-Juste, J.; Pastoriza-Santos, I.; Liz-Marz´an, L. M.; Mulvaney, P., Coordination Chemistry Reviews, 249, 2005, 1870.
6. Jana, N.R.; Gearheart, L.; Murphy, C.J., Adv. Mater. , 13, 2001, 1389.
7. Jana, N.R.; Gearheart, L.; Obare, S.O.; Murphy, C.J., Langmuir, 18, 2002, 922.
8. Pastoriza-Santos I.; Liz-Marzan L. M., Nano Lett., 2002, 2, 903.
9. Millstone J. E.; Park S.; Shuford K. L.; Qin L.; Schatz G. C.; Mirkin C. A., J. Am. Chem. Soc., 2005, 127, 5312.
10. Im S. H.; Lee Y. T.; Wiley B.; Xia Y., Ang. Chem. Int. Ed., 2005, 44, 2154.
11. Wiley B.; Herricks T.; Sun Y.; XiaY., Nano Lett., 2004, 4, 1733.
12. Maillard M.; Giorgio S.; Pileni M. P., J. Phys. Chem. B, 2003, 107, 2466.
13. Heiz U.; Landman U., ¨Nanocatalysis¨ Springer, New York, 2006.
14. Samal A.; Sreeprasad T.; Pradeep T., J Nanopart. Res., 2010, 12, 1777.

Chapter V

Chapter V

Stability of gold nanoparticles

Part I: Influence of the nanoparticle's shape on their thermal stability: nanorods vs nanoprisms

Abstract:

In this study, the modification of the seed-mediated method to prepare rods and triangular shapes of gold nanoparticles has been carried out to study their thermal and photo-stability. A mechanism which accounts for the different thermal and photo- reshaping of gold nanoprisms than gold nanorods has been proposed. Great enhancement of the thermal and photostability has been achieved by adding specific amount of polyvinyl pyrrolidone (PVP) to the gold particles of different shapes capped with cetyltrimethylammonium bromide (CTAB). Gold nanoprisms and nanorods under soft UV-irradiation showed totally unexpected a photocorrosion effect. The study of this effect showed that the photodissolution is due to the presence of semiconducting Ag clusters, mainly located at the tips of the nanostructures. With appropriate conditions oxygen and hydrogen evolution could be achieved, which implies that these systems can have important applications in photocatalysis and photovoltaics. The results further confirm the important role of the Ag-clusters in the formation mechanism of anisotropic nanostructures described in previous chapters. Finally, fragmentation and melting mechanisms were proposed for the effect of different types of nanosecond lasers (CW and pulsed at different lines) on gold nanorods with different aspect ratios.

Introduction:

It is well known that the electrical, thermodynamic, and chemical properties of gold nanoparticles depend sensitively on particle size and

shape, and thus these materials have been tagged for a wide range of applications, including catalysis, optoelectronics, film growth seeding, and others[1–6]. One of the desired goals is the challenge to control the morphology of the nanoparticles and to be able to fabricate and stabilize them in the desired form.

The thermal and photo- in/stability of gold nanorods have been reported before[7- 10]. El-Sayed´s group studied the thermal stability of gold rods (average aspect ratio=3.3) electrochemically prepared and encapsulated inside of rod shape micelles. It was found that the mean aspect ratio of the nanorods in solution decreases with increasing temperature, while the average width remains constant due to the difference in the thermal stability of micelles of different length. Following the observed change in the maximum of the longitudinal surface plasmon absorption with temperature, a kinetic study of the thermal reshaping was also carried out by those authors. The activation energy of micelle´s decomposition determined from such experiments, and also their decomposition temperature (Kraft temperature; 155^0C), was also reported.

Petrova H. et al.[9] observed that gold nanorods, at the highest temperature examined (250^0C), are transformed into spheres within one hour. However, no structural changes were observed in the laser-induced heating experiments up to temperatures of 700- 750 ^{0}C. Al-Sherbini et al.[8, 10] also studied the effect of thermal heating and UV-light on gold nanorods of different aspect ratios, in water/ glycerol mixtures. It is interesting to note here that other studies shown that the temperature of the growth solution can have an important influence on the final aspect ratio of gold nanorods[11-13].

In the presented work, we made a comparison study between different gold nanoparticle shapes (rods vs prisms) against the thermal and the photo-

in/stability. For this purpose we used gold nanorods and nanoprisms prepared by the method described in chapters II and III.

Experimental section:

Gold nanorods and nanoprisms were prepared as it was explained in the experimental chapter (chapter II and chapter III). The photo-and thermal stability studies were carried out as it was described in detail in chapter II. For convenience, a brief summary of the experimental details is summarized here.

For preparation of different shapes of gold nanoparticles, seeds and growth solutions were made as described below.

Seeds using CTAB:

2.5 ml of 0.2 M CTAB solution was mixed with 2.5 ml of $5x10^{-4}$ M $HAuCl_4$. To the stirred solution, 30 µl of ice-cold 0.1M $NaBH_4$ was added, which results in the formation of a solution with brownish yellow color. Vigorous stirring of the seed solution was continued for 2 minutes. We then used this seeds from 10 minutes to 3 hours after the addition of the reducing agent.

Seeds using citrate:

10ml of $2.5x10^{-4}$M $HAuCl_4$ was added to 10ml of $2.5x10^{-4}$M tri-sodium citrate.0.6ml of 0.1M ice-cold of $NaBH_4$ was added to that mixture without stirring. The color of the solution changed to pink and this solution could be used within 2-5 hours.

Growth solution:

Different amounts (50, 100,150, 200 and 250µl) of $4x10^{-3}$M $AgNO_3$ solution were added to 2.5 ml of 0.2 M CTAB. To this solution, 2.5 ml of 10^{-3}M $HAuCl_4$ was added and, after gentle mixing of the solution, 35 µl of 0.0788 M ascorbic acid was added. Ascorbic acid, as a reducing

agent, changes the growth solution from dark yellow to colorless within 10 minutes. The final step was the addition of the seeds to the growth solution. The color of the solution gradually changed within 10-20 minutes.

Thermal and photostability of gold nanoparticles:

To study the thermal stability of gold nanoparticles, the change in the absorption spectrum of solutions of nanorods and nanoprisms was determined at different temperatures ranging from 40 to 220 ^{0}C in a water bath. After the addition of a few drops of glycerol, the sample was heated above 100 ^{0}C in an oil bath in order to determine the decomposition temperature of the micelles capping the gold nanorods and nanoprisms. The same work was repeated with gold nanorods immersed in a polymer solution of PVP. Photostability of gold nanorods was tested by exposure 3ml of the colloidal solution of nanoparticles, which were put in a quartz cuvette, to different irradiation times with a UV light source (254nm). The thermal and photostability of gold particles were followed by measuring the changes in absorption spectra as function of time. The shape of the particles was characterized by TEM. Also, thermal gravimetric analysis (TGA) and differential scanning calorimetry (DSC) for gold nanorods capped with CTAB and free CTAB have been done in order to determine changes in heat flow and weight during the thermal annealing.

Results and Discussion:

5-1: Preparation of gold nanorods and gold nanoprisms:

Gold nanorods and nanoprisms were prepared using different concentrations of $AgNO_3$. At the lower concentrations (40, 80, and 120 μM), gold nanorods with different aspect ratio (a.r.= 2.2, 3.4, and 4.5) are formed, whereas at high concentrations (160 and 200μM), gold nanoprisms

are formed, as it can be seen from the corresponding UV-Vis spectra and TEM images.

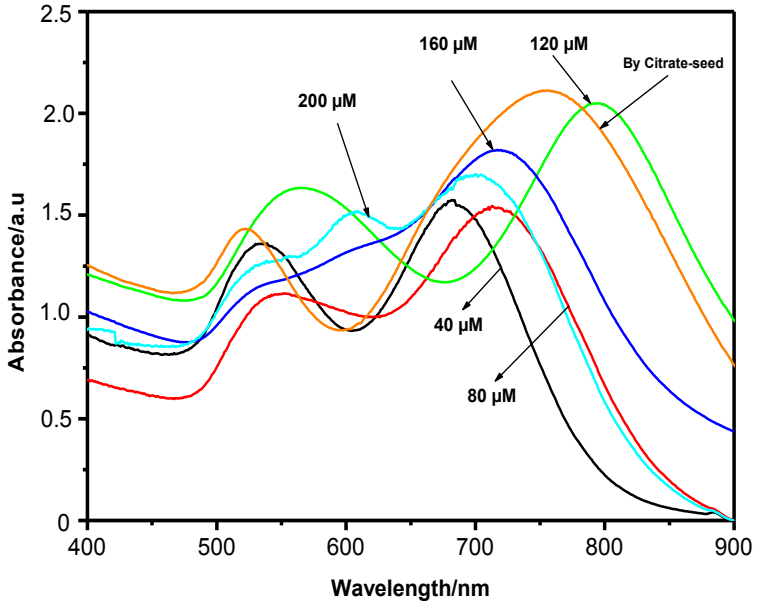

Figure 5-1: Absorption spectra of gold nanorods (40, 80 and 120µM of $AgNO_3$) with different aspect ratios and gold nanoprisms (160 and 200 µM of $AgNO_3$), using CTAB as a capping agent in the seed solution. Gold nanorods prepared with 80µM of $AgNO_3$ using citrate as capping agent in the seed solution are also shown by comparison.

From the UV-Vis spectra, one can see the existence of two plasmon bands corresponding to SP_L (located at higher wavelengths) and SP_T, (located at lower wavelengths). As the concentration of $AgNO_3$ increased the SP_L is shifted to longer wavelengths until a critical concentration (160µM) of $AgNO_3$, in which a third band, located between the SP_T and SP_L starts to appear showing the formation of nanoprisms. Figure (5-2) shows the TEM pictures of the nanoparticles at different $AgNO_3$ concentrations. The percentage of nanorods and nanoprims at the optimal concentrations are 87% for gold nanorods (at 40 µM $AgNO_3$) and > 90% for gold nanoprisms (at 200 µM $AgNO_3$).

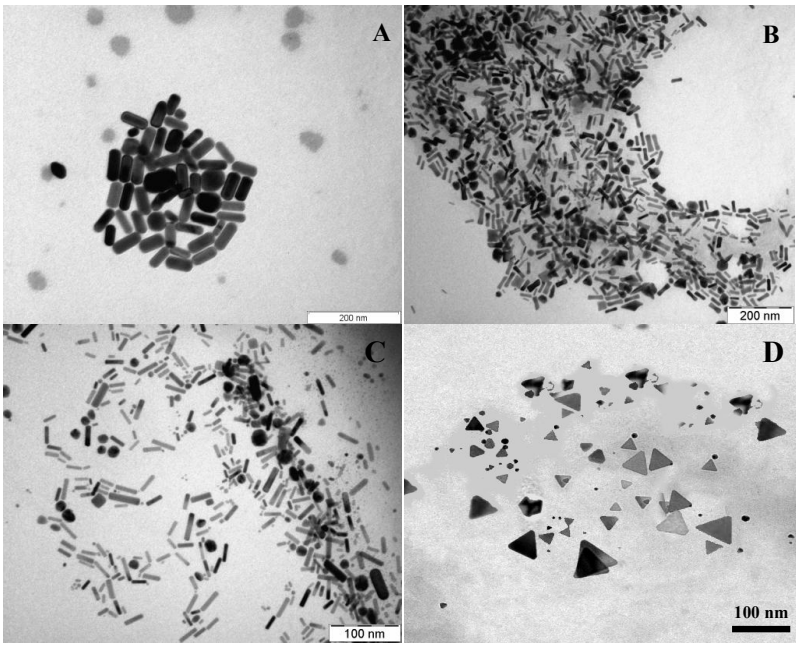

Figure 5-2: A and B: TEM images of gold nanorods prepared using 40 and 80µM of $AgNO_3$ respectively. C: gold nanorods prepared with 80µM $AgNO_3$ using trisodium citrate as capping agent in the seed solution. D: gold nanoprisms prepared with 200 µM $AgNO_3$.

5-2: Thermal stability of gold nanoparticles: nanorods vs nanoprisms

We studied the thermal stability of nanorods and nanoprisms to understand the effect of shape on their stability. Details are discussed below.

5-2-1: Effect of micelle's composition on the stability of gold nanorods.

As we have mentioned, the gold nanorods solution has an absorption maximum of the longitudinal surface plasmon band which mainly depends on the rod length. Therefore, the stability of Au nanorods of two different aspect ratios was first studied at room temperature by comparing the change in the absorption spectrum of the different gold nanorods at 30 min, 10h, 1 day and 90 days after addition of the seeds to the growth solution in the experimental preparation method.

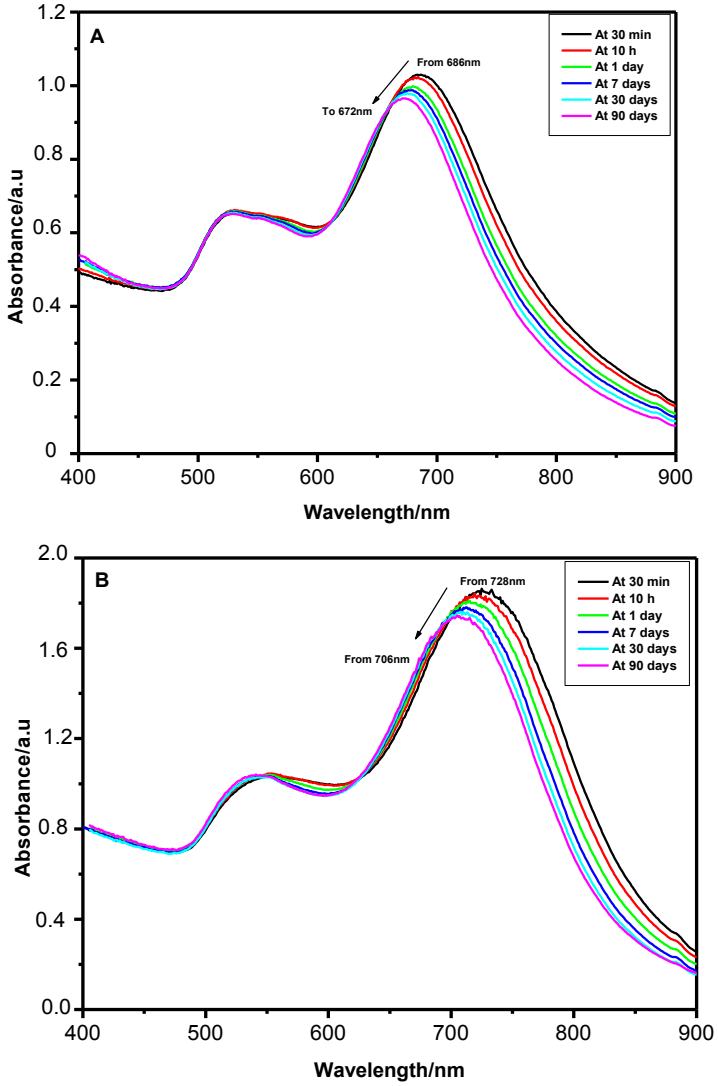

Figure 5-3: Change in the absorption spectra of gold rods of aspect ratio 2.27 (A) and 3.1 (B) at room temperature (27^0C) from 30 min to 90 days.

From the changes in the absorption spectra, we can conclude that the aspect ratio decreased from 2.27 to 2 (A) and from 3.1 to 2.67(B) by aging to 90 days at room temperature (27^0C). This decrease in the length of Au nanorods with the aging time could be due to atomic defects on the unstable {110} facets of the Au nanorods with a surface reconstruction of Au atoms. This is supported by Wang et al.[13] from which a detailed examination of the defect sites of both {100} and {110}

facets shows that, while the defective regions of the stable {100} facets show atom-height steps with no reconstruction, the less stable higher energy {110} surfaces show a reconstruction with a missing-row of atoms. However, because this experiment was carried out under atmospheric light, a possible photodecomposition of the rods cannot be disregarded, as it will be shown in section (5-3).

The thermal heating effect on gold nanorods was determined by the change in the absorption spectrum of a solution of nanorods at different temperatures ranging from 40 to 180 ^{0}C (few drops of glycerol were added for stabilizing the water solution at high temperatures).The absorption spectra of gold rods of aspect ratio 2.2, 3.4, 4.5 (A, B, and C) and 3.4(D) with citrate-seeds at different temperatures are shown in Figure (5-4).

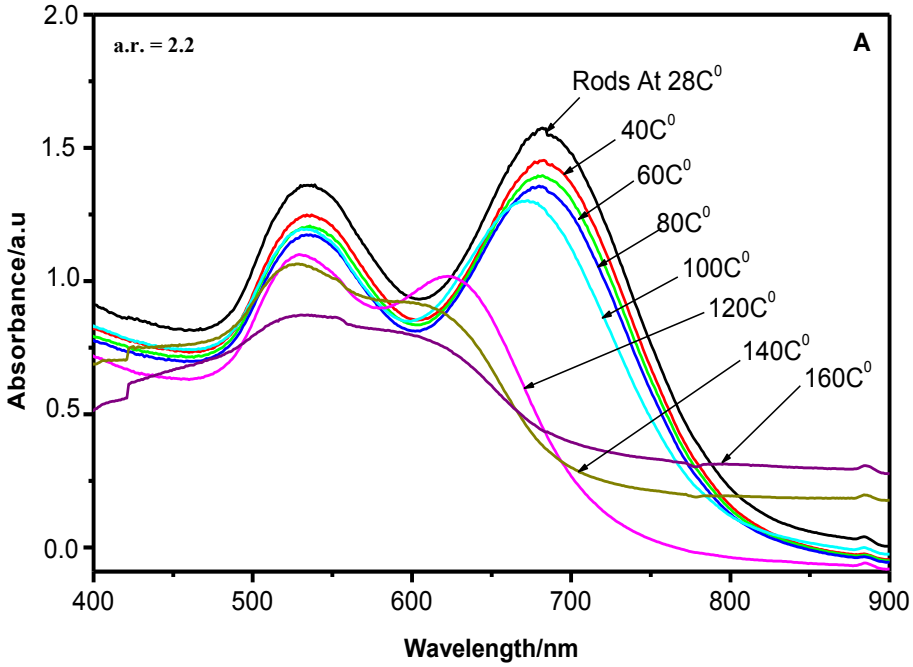

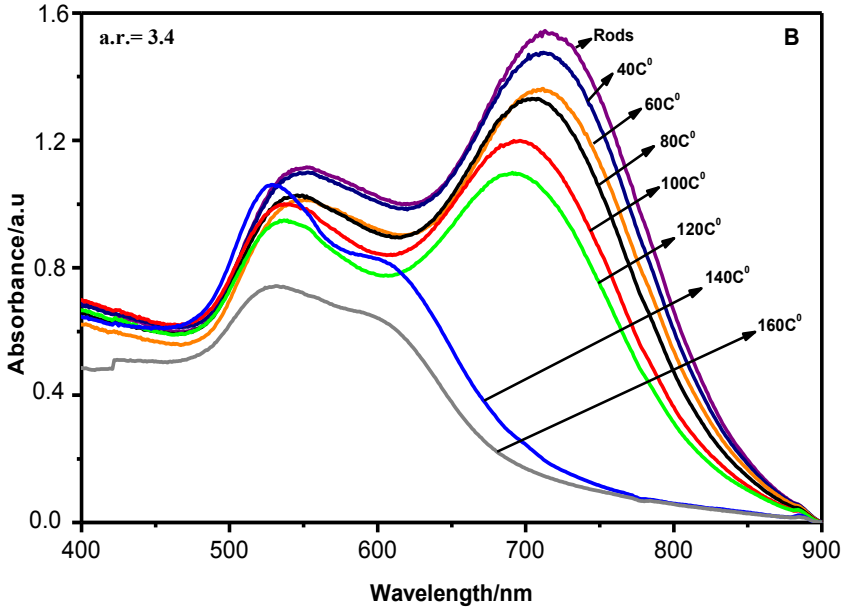
a.r.= 3.4
B
Rods
40C0
60C0
80C0
100C0
120C0
140C0
160C0
Absorbance/a.u
Wavelength/nm
1.6
1.2
0.8
0.4
0.0
400
500
600
700
800
900

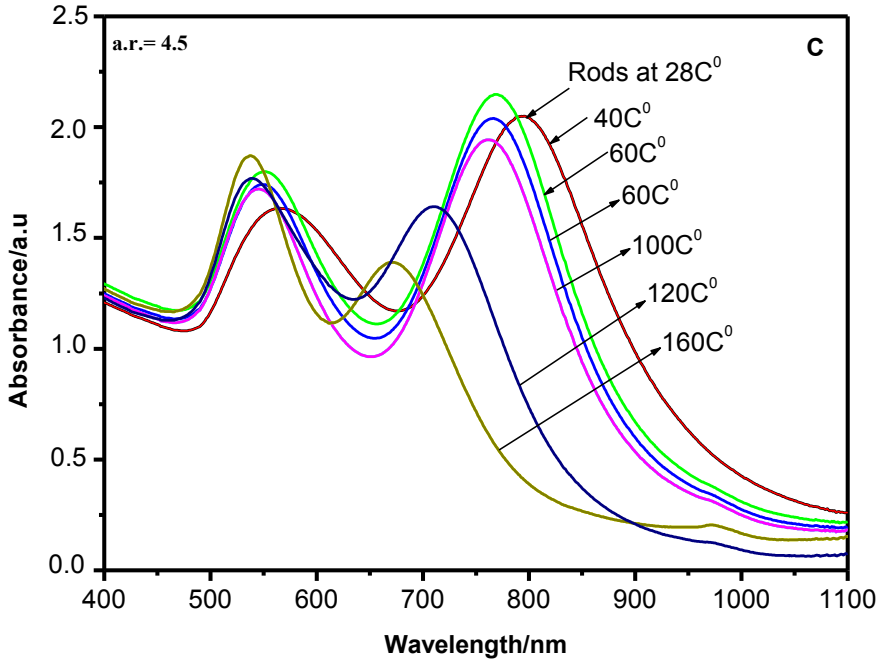
a.r.= 4.5
C
Rods at 28C0
40C0
60C0
60C0
100C0
120C0
160C0
Absorbance/a.u
Wavelength/nm
2.5
2.0
1.5
1.0
0.5
0.0
400
500
600
700
800
900
1000
1100

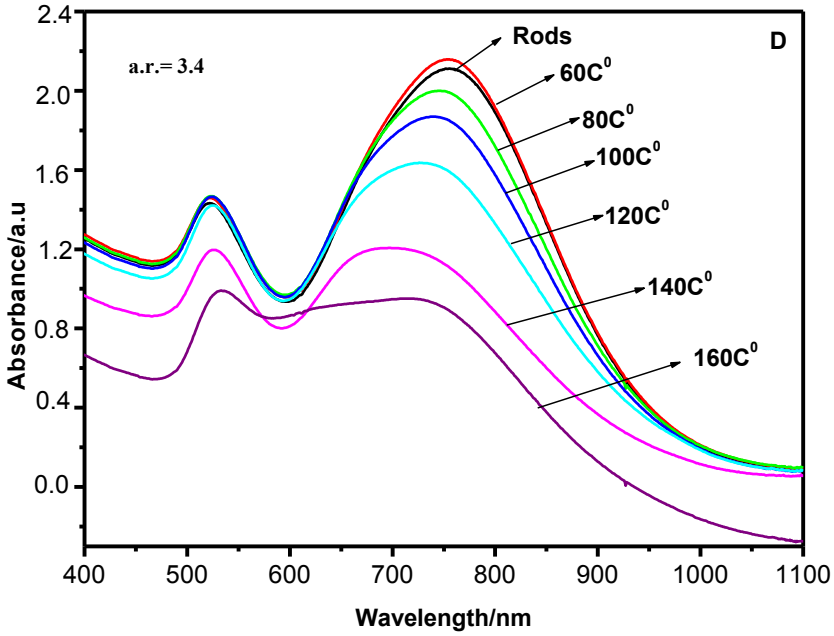

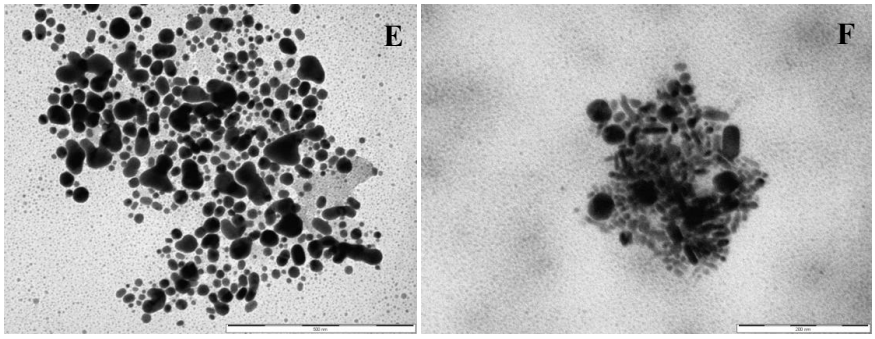

Figure 5-4: Absorption spectra showing the effect of thermal heating on gold nanorods of aspect ratio 2.2, 3.4, 4.5 (A, B, and C), and 3.4 (D) prepared with citrate-seeds at different temperatures. TEM images showing gold nanorods prepared using CTAB-seeds with a.r. =3.4 aged at 160^0C (E) and gold nanorods prepared by citrate-seeds with a.r. =3.4 aged at 160^0C (F).

Comparing these data with the data previously reported by El-Sayed et al.[7], one can observe that the Kraft temperature of the rod shape micelles formed from CTAB is higher than that for the rod shape micelles made of CTAB and tetraoctylammonium bromide (TDAB) as a co-

surfactant. The Kraft temperature for the rod mixed micelles of CTAB and TDAB has been reported to be 155 ^{0}C, while we observed that up to 180 ^{0}C the rod shape micelles of pure CTAB do not completely decomposed.

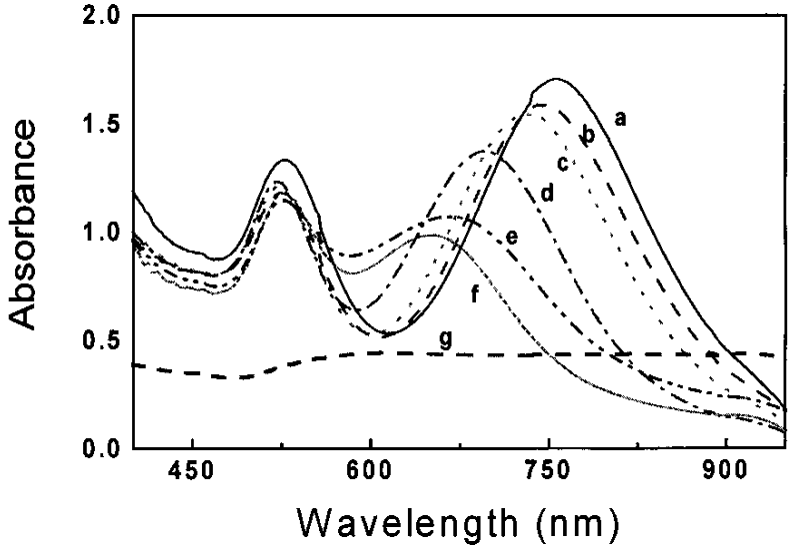

Figure 5-5: Absorption spectra showing the effect of temperature on the gold nanorod´s absorption of an aqueous solution sample with a few drops of glycerol: (a) 25 ^{0}C, (b) 110 ^{0}C, (c) 120 ^{0}C, (d) 140 ^{0}C, (e) 150 ^{0}C, (f) 155 ^{0}C, and (g) 160 ^{0}C. The disappearance of the transverse surface plasmon band (λ_{max} = 520 nm) at 160 ^{0}C suggests that even the spherical nanoparticles are not present, which indicates that the micelles have been decomposed at this temperature [7].

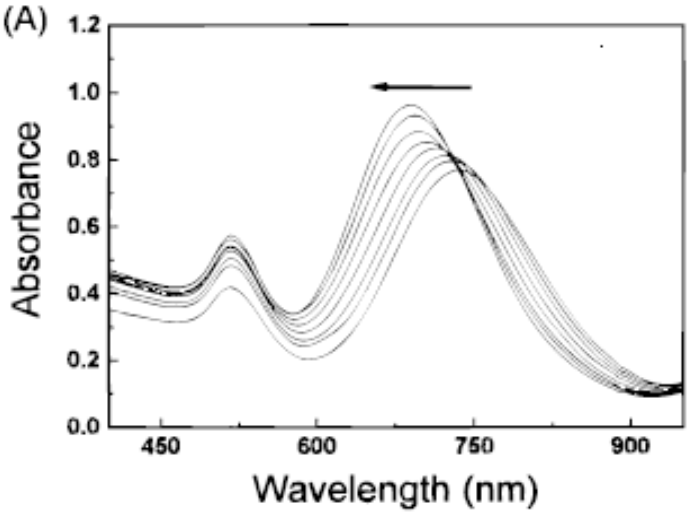

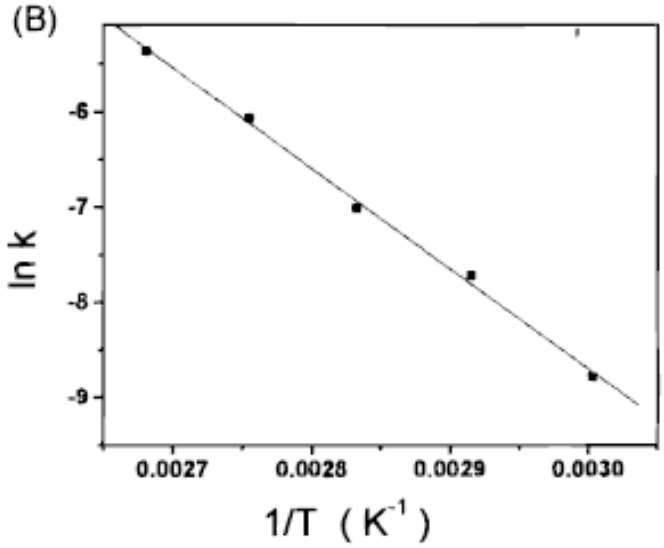

Figure 5-6: (A) Absorption spectra of a gold nanorod´s solution as a function of time after being placed in the thermostat at 100^0C; and (B) Arrhenius plot for the determination of the activation energy for the thermal reshaping of gold nanorods (21.0 ± 1.0 Kcal mol^{-1})[7].

At each temperature, the change in the absorption spectrum was followed as a function of time, after the original sample solution was immersed into the thermostatted bath at a fixed temperature. The rate constant of the change in the shape at each temperature was determined by following the rate of the absorbance´s change at the absorption maximum of the longitudinal surface plasmon band. From the values of the rate constants at different temperatures, the activation energy (E^{act}) of the shape transformation can be calculated. It can be seen that, for a.r. = 3.4, E^{act} = 7.4±0.1 $kJmol^{-1}$, which is slightly higher than that for a.r. =2.2 (E^{act} = 6.85±0.2 kJ mol^{-1})

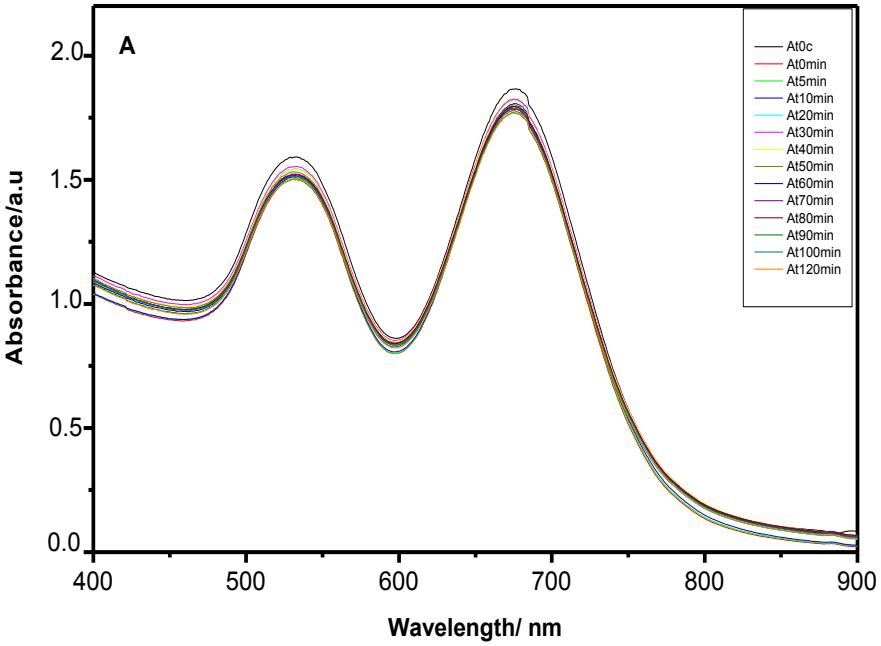
A
Absorbance/a.u
Wavelength/ nm
At0c
At0min
At5min
At10min
At20min
At30min
At40min
At50min
At60min
At70min
At80min
At90min
At100min
At120min

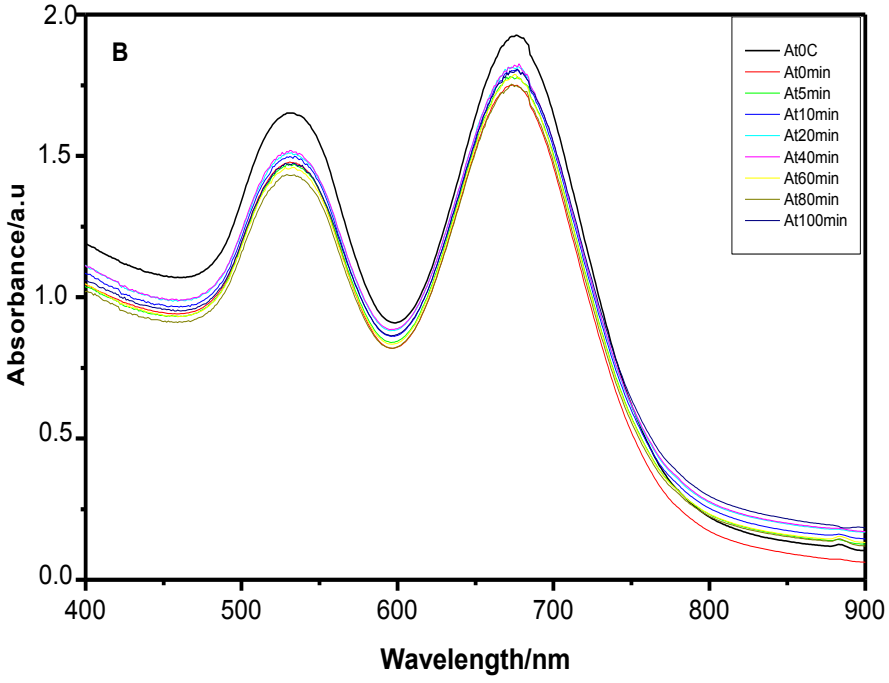
B
Absorbance/a.u
Wavelength/nm
At0C
At0min
At5min
At10min
At20min
At40min
At60min
At80min
At100min

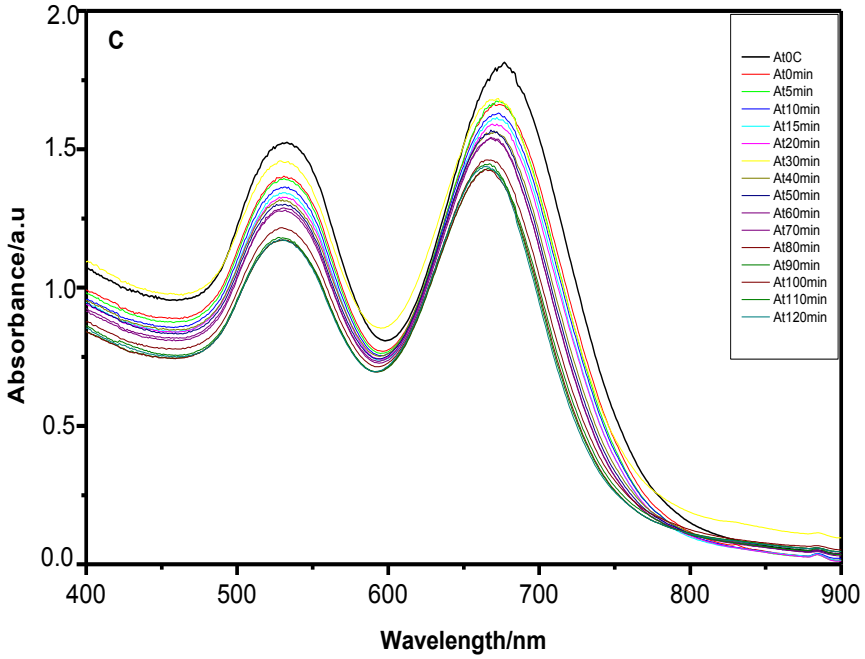
C
Absorbance/a.u
Wavelength/nm
2.0
1.5
1.0
0.5
0.0
400
500
600
700
800
900
At0C
At0min
At5min
At10min
At15min
At20min
At30min
At40min
At50min
At60min
At70min
At80min
At90min
At100min
At110min
At120min

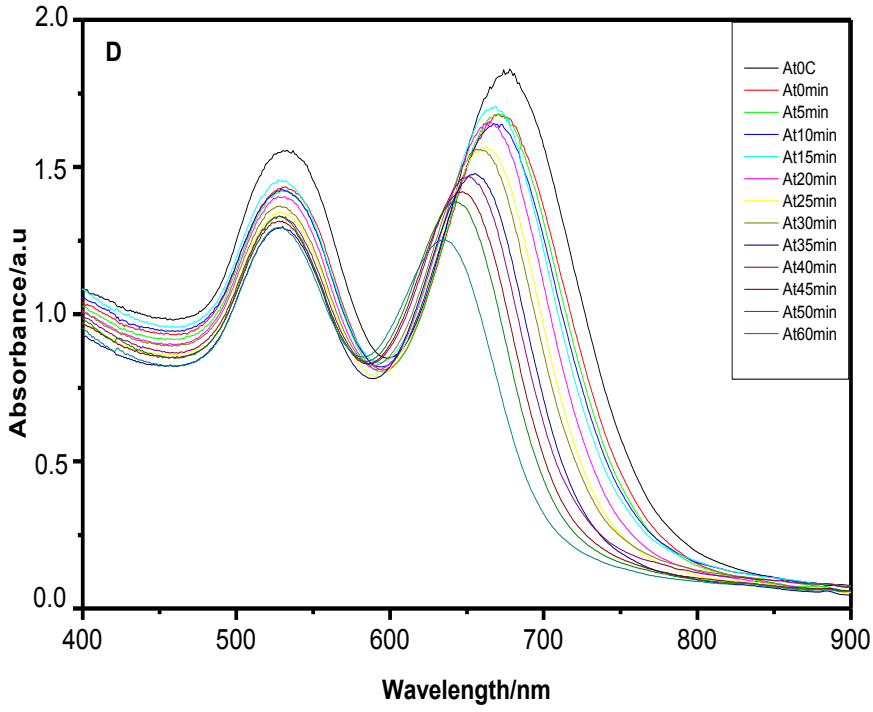
D
Absorbance/a.u
Wavelength/nm
2.0
1.5
1.0
0.5
0.0
400
500
600
700
800
900
At0C
At0min
At5min
At10min
At15min
At20min
At25min
At30min
At35min
At40min
At45min
At50min
At60min

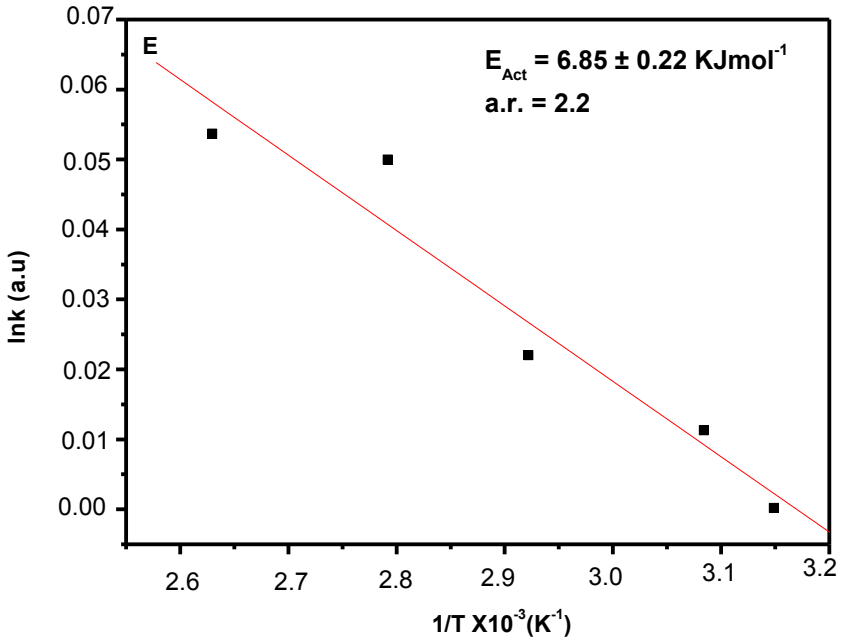

Figure 5-7: Absorption spectra showing the effect of thermal heating on the gold nanorods of a.r.= 2.2 at temperatures 40, 60, 80, and 100^{0}C with time (A-D, respectively). The activation energy for the decomposition of gold nanorods (a.r. = 2.2) is showing in (E).

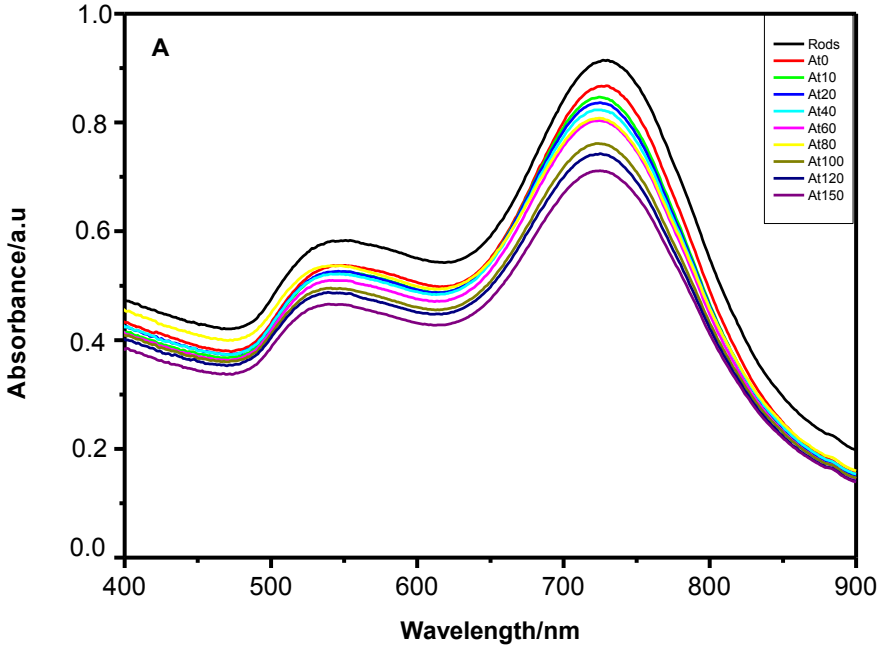

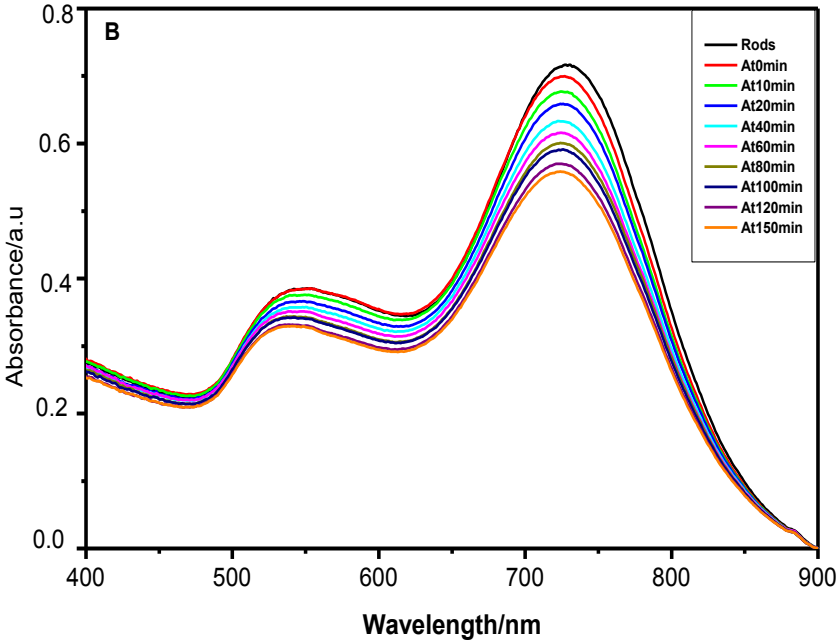
B
Rods
At0min
At10min
At20min
At40min
At60min
At80min
At100min
At120min
At150min
Absorbance/a.u
Wavelength/nm
0.0
0.2
0.4
0.6
0.8
400
500
600
700
800
900

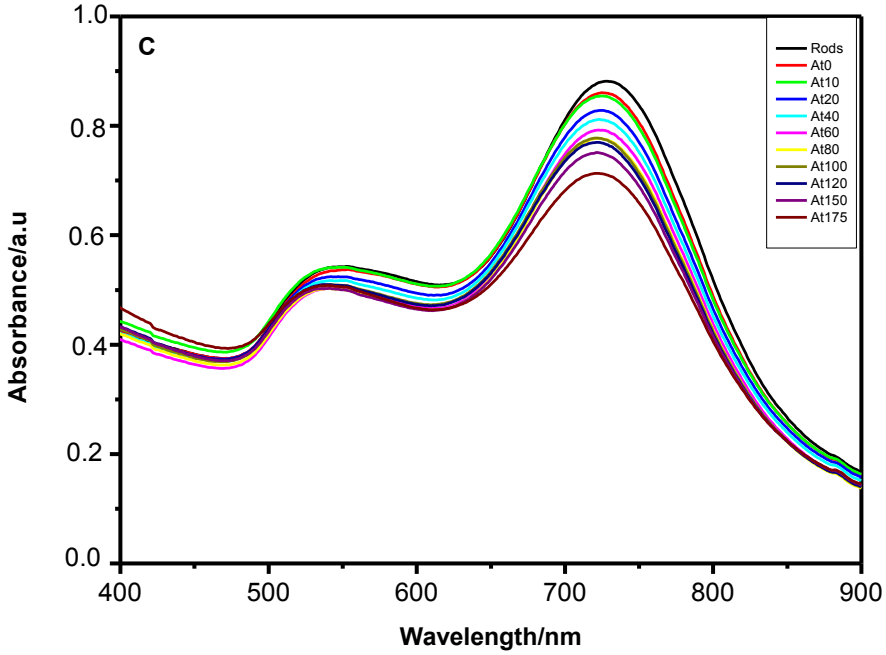
C
Rods
At0
At10
At20
At40
At60
At80
At100
At120
At150
At175
Absorbance/a.u
Wavelength/nm
0.0
0.2
0.4
0.6
0.8
1.0
400
500
600
700
800
900

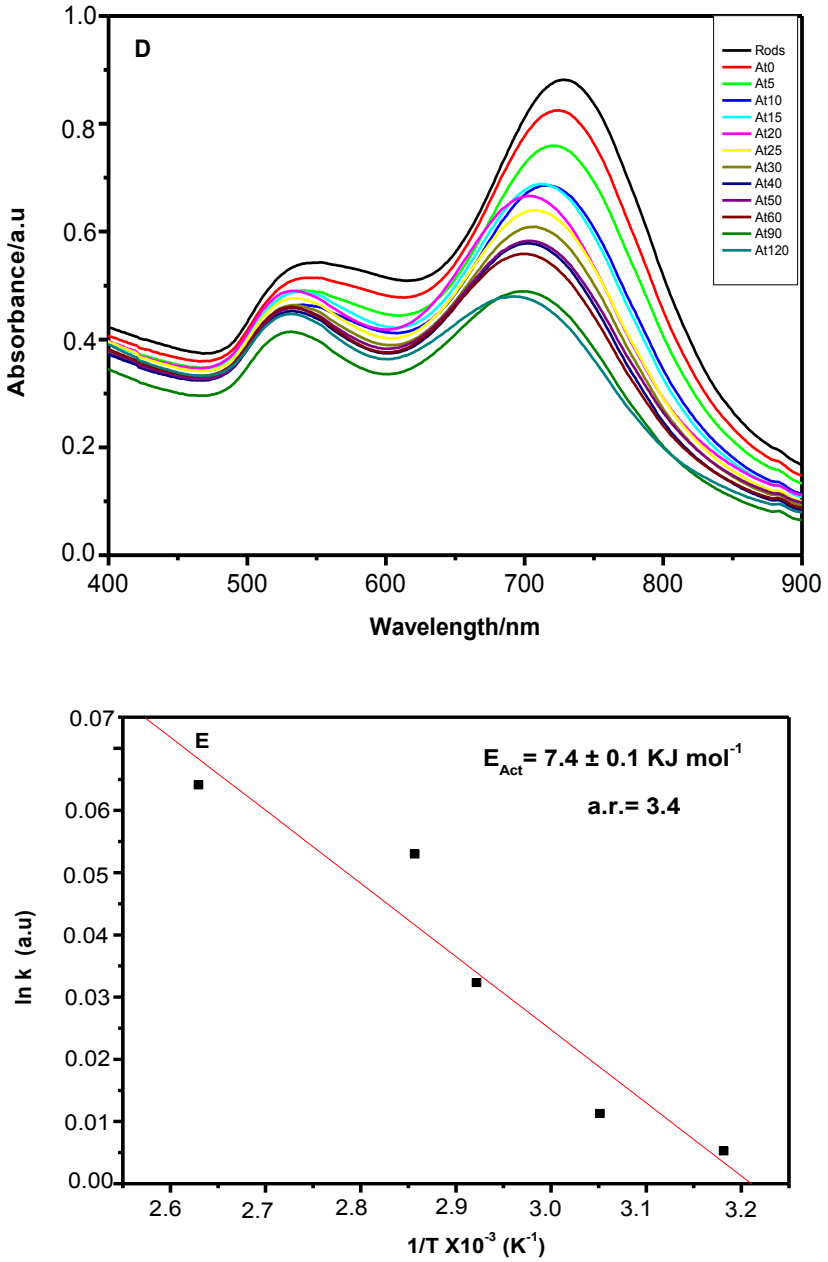

Figure 5-8: Absorption spectra showing the effect of thermal heating on the decomposition of gold nanorods of a.r. =3.4 at temperatures 40, 60, 80, and 100^{0}C (A-D, respectively). The activation energy for the decomposition of gold nanorods (a.r. = 3.4) is showing in (E).

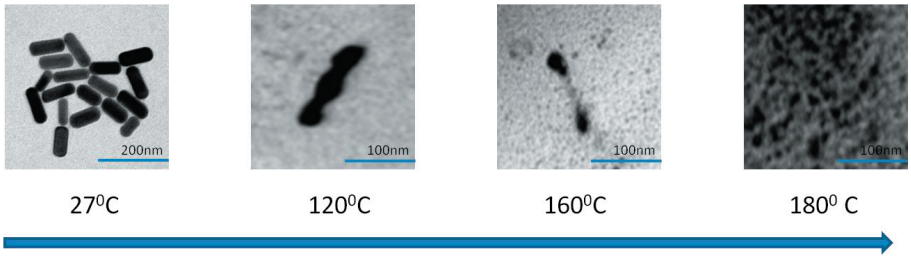

Figure 5-9: TEM images showing the decomposing of gold nanorods (a.r.= 2.2) at different temperatures 27, 120, 160 and 180 ^{0}C.

Thermogravimetric analysis (TGA) and differential scanning calorimetry (DSC) were employed to study the behavior of gold nanorods, CTAB and gold nanorods washed two times after centrifuged at 6000 rpm for 30min. All these samples were dried from water in desiccators.

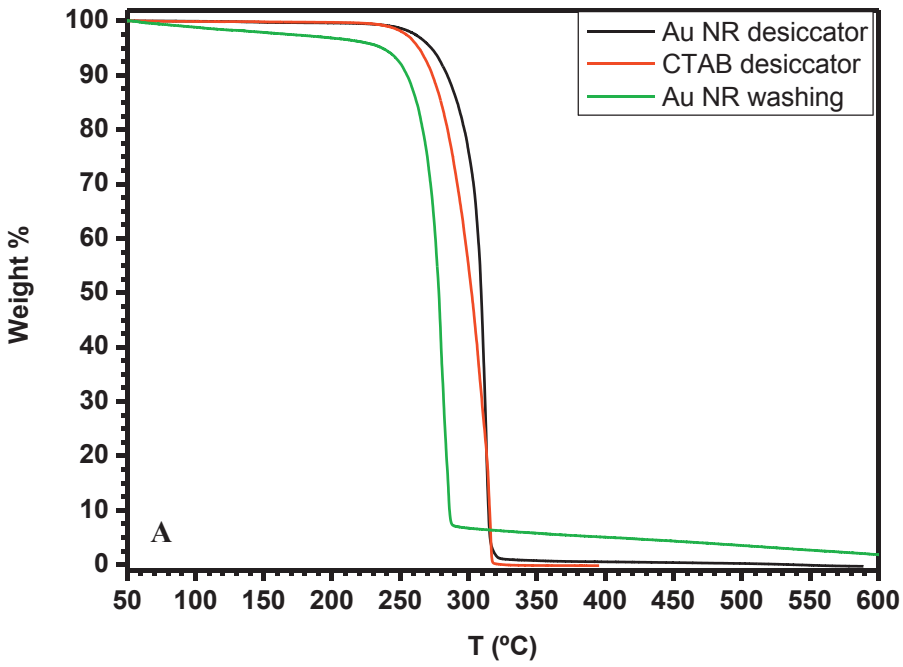

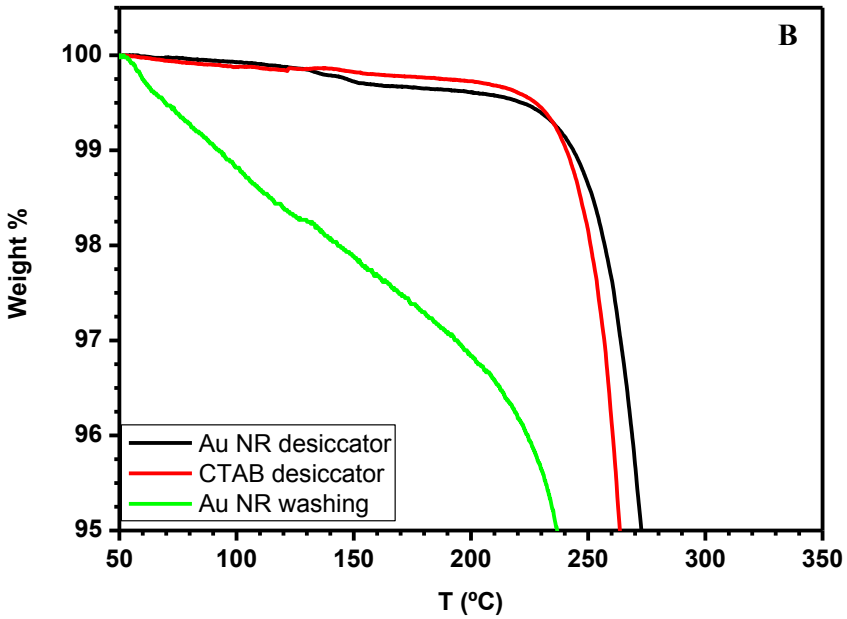

Figure 5-10: (A) TGA data showing GNRs, CTAB, and GNRs after washing 2 times at 6000 rpm for 30 min with distilled water and dried in desiccators under vacuum (green line) from 45^0C to 600^0C at 10^0C/min. (B) is the zooming of figure A from 50^0C to 350^0C.

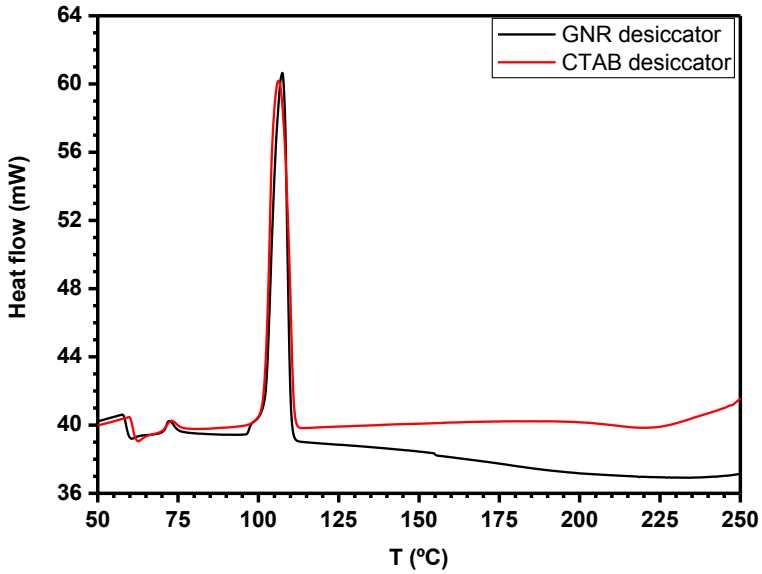

Figure 5-11: DSC data showing GNRs and CTAB dried in desiccators under vacuum.

It can be seen that the decomposition of GNRs and CTAB is similar. But, the decomposition of washed GNRs is much easier. This can be explained because CTAB binds preferentially to the {110} facets of the gold nanorods[14].

5-2-2: Influence of gold nanoparticle´s shape on their thermal stability: nanorods vs nanoprisms.

In this section we are compare the influence of the nanoparticle´s shape on their thermal stability. The results are shown in figures (5-12 to 5-14).

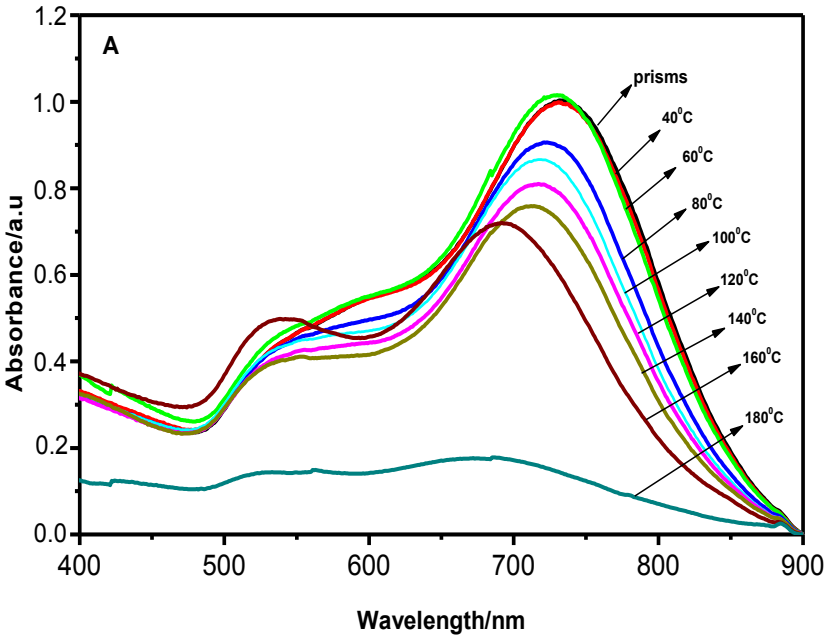

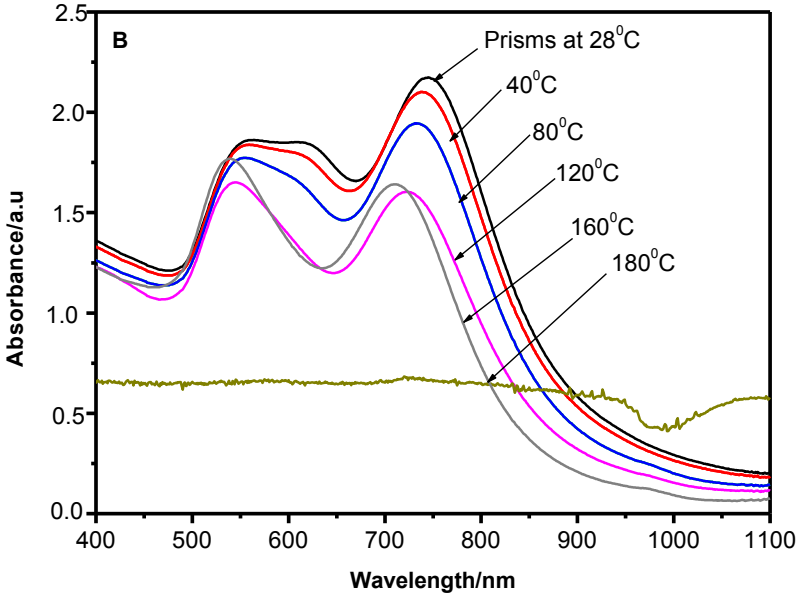

Figure 5-12: Absorption spectra showing the effect of thermal heating on gold snapped prisms and prisms from 40^0C to 180^0C (A and B, respectively).

The activation energy of gold nanoprisms under thermal heating at 40, 60, 80, and 100^0C was found to be 7.9kJ/mol, which is higher than the activation energy for nanorods 7.4kJ/mol.

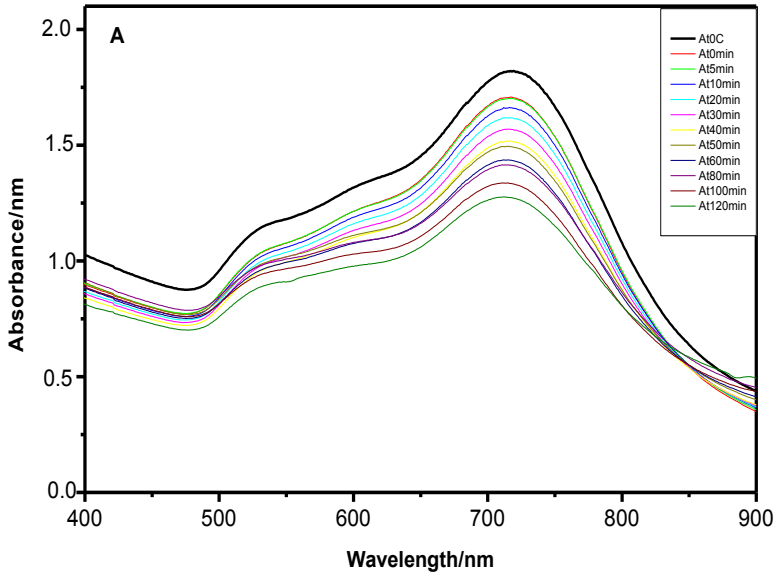

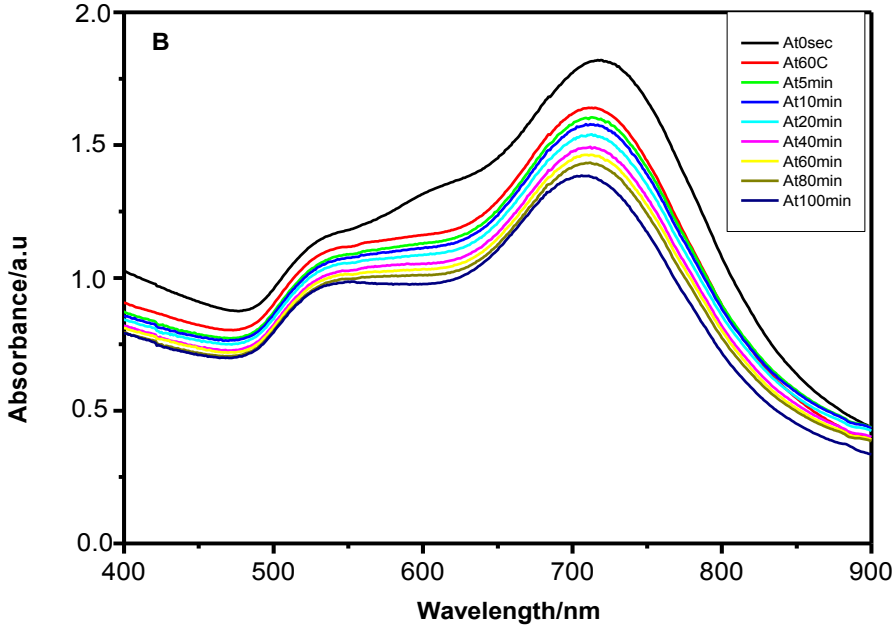
B
At0sec
At60C
At5min
At10min
At20min
At40min
At60min
At80min
At100min
Absorbance/a.u
Wavelength/nm
2.0
1.5
1.0
0.5
0.0
400
500
600
700
800
900

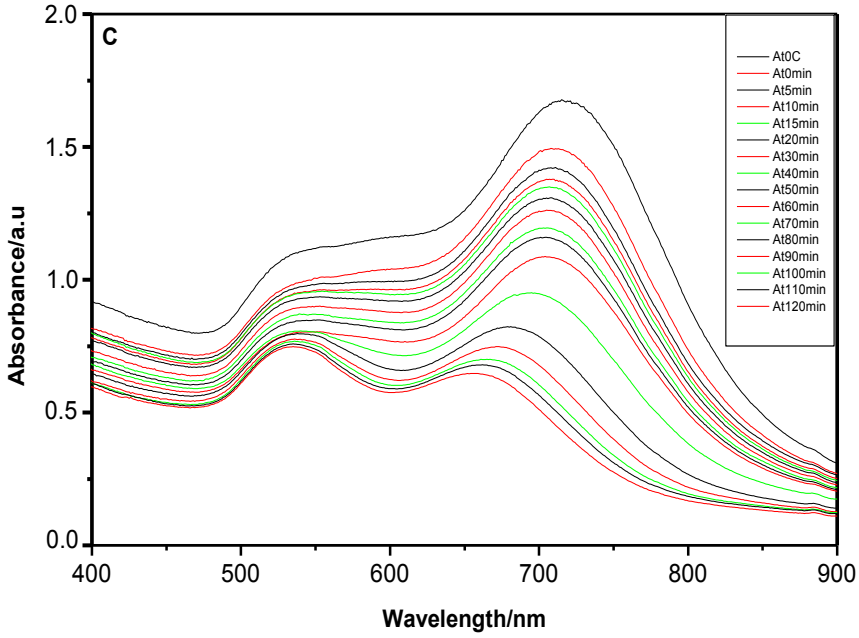
C
At0C
At0min
At5min
At10min
At15min
At20min
At30min
At40min
At50min
At60min
At70min
At80min
At90min
At100min
At110min
At120min
Absorbance/a.u
Wavelength/nm
2.0
1.5
1.0
0.5
0.0
400
500
600
700
800
900

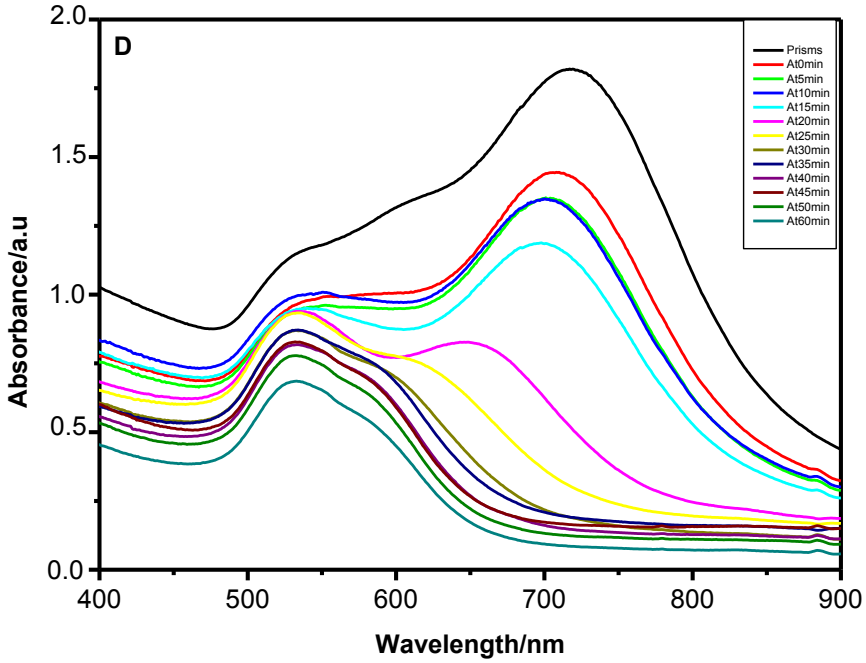

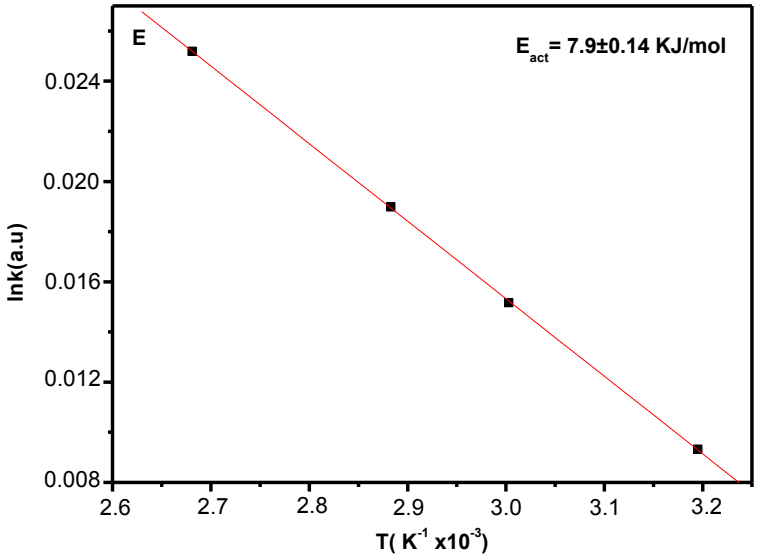

Figure 5-13: Absorption spectra showing the effect of the thermal heating on gold nanoprisms at temperatures 40 (A), 60 (B), 80 (C), and 100^0C (D) with time. The activation energy for the decomposition of gold nanoprisms is shown in (E).

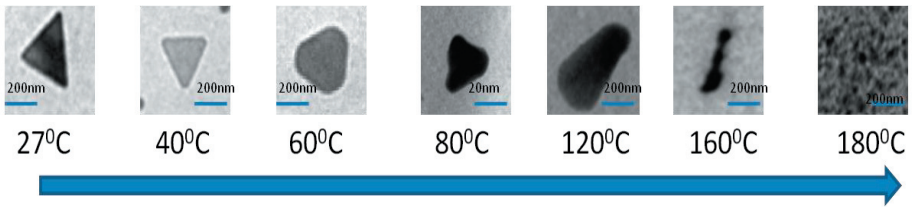

Figure 5-14: TEM images showing the decomposing of gold nanoprisms at different temperatures: 27, 120, 160 and 180 ^{0}C.

As it can be seen in figure (5-12), the temperature has different effect on nanoprisms than the previously observed for rods (see Figures 5-7 and 5-8). In the case of nanoprisms, the third absorption band, characteristic of the nanoprisms, disappears gradually giving rise to an absorption spectrum similar to the rods. Then, it is observed the absorbance and blue shift of the longitudinal surface plasmon, similar to what was observed for gold nanorods. The effect of temperature on nanoprisms can be summarized as follows: i) Dissolution of the tips of the prisms, which are thermodinamically unstable, giving rise to snapped prisms. ii) These snapped prisms change to rods, which are thermodynamically more stable. iii) The decomposition of the formed nanorods leads to a decrease in the absorbance intensity and a shift to higher wavelengths, but until 160 ^{0}C the particles are stable. iv) Suddenly, at 180 ^{0}C, the particles completely decompose, which is due to the fact that micelles also decompose at the Kraft temperature of circa 180ºC.

5-2-3: Enhancement of the thermal stability of gold nanoparticles.

We extend our thermal study trying to increase the stability of gold particles at high temperatures. For this purpose we added PVP as a protecting polymer to the pre-prepared gold particles capped with surfactant (CTAB), and then we studied their thermal stability as mentioned above.

5-2-3-1: Gold nanorods.

As it can be seen in Figure (5-15), the thermal stability of the rod shaped particles depends on the amount of added PVP. Adding 30 % by weight of PVP to the nanorod solution leads to very stable gold nanorods. Upon addition of PVP, a slight shift to the red (~ 4 nm) is observed due to the change of the dielectric constant of the surrounding medium and the absorbance is decreased slightly because of the dilution by adding PVP. Afterwards, there is no change in the absorption spectrum until 220 ^{0}C. For lower concentrations of PVP, the stability is greatly reduced as it can be observed in Figure (5-15B). The activation energy for the decomposition of these particles with the addition PVP, calculated in the temperature range 40-100^{0}C (see figure 5-16) is: 8.3kJ/mol.

.

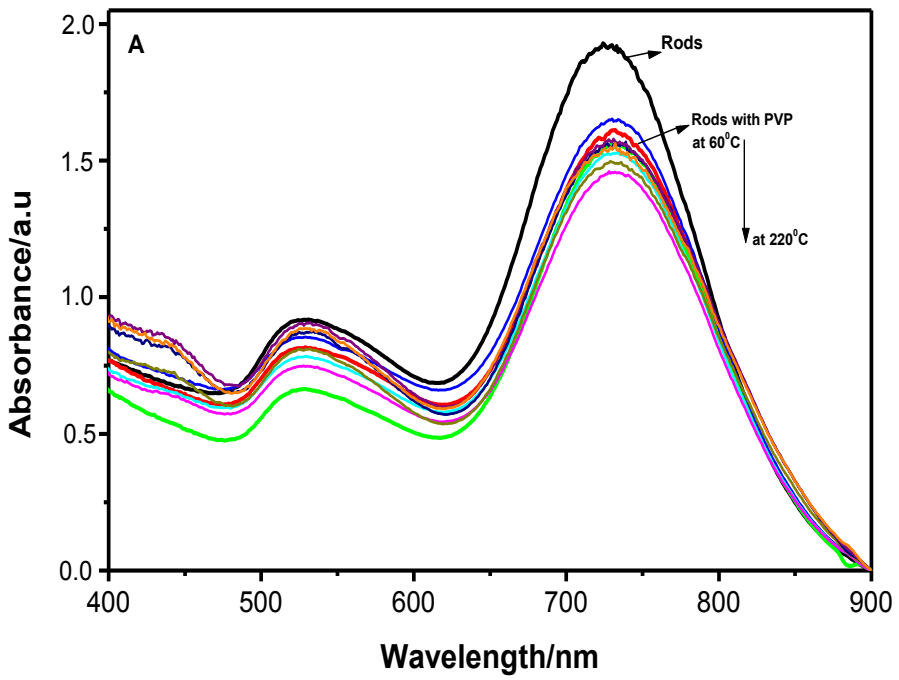

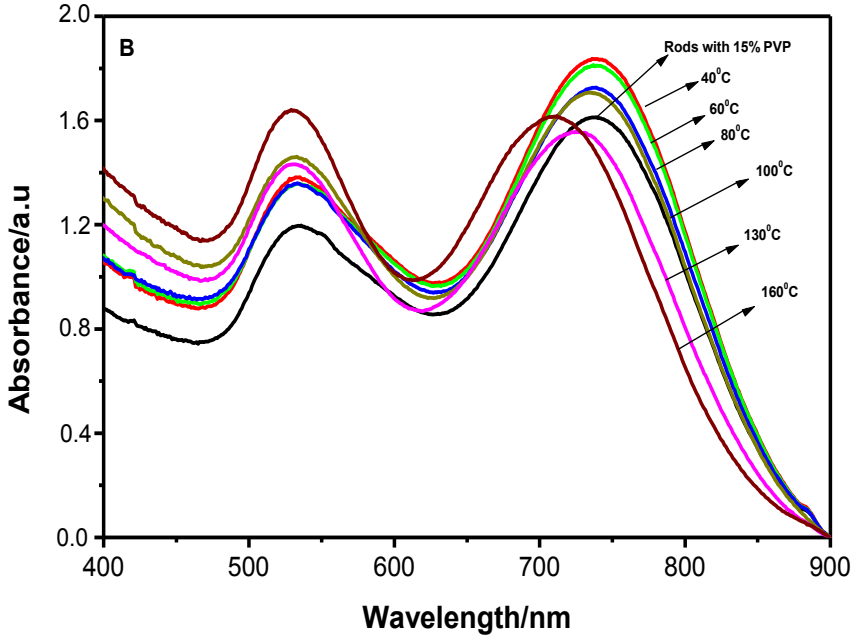

Figure 5-15: Absorption spectra showing the effect of thermal heating on gold nanorods with 30% PVP (A) and with 15% PVP (B) from 40^0C to 220^0C.

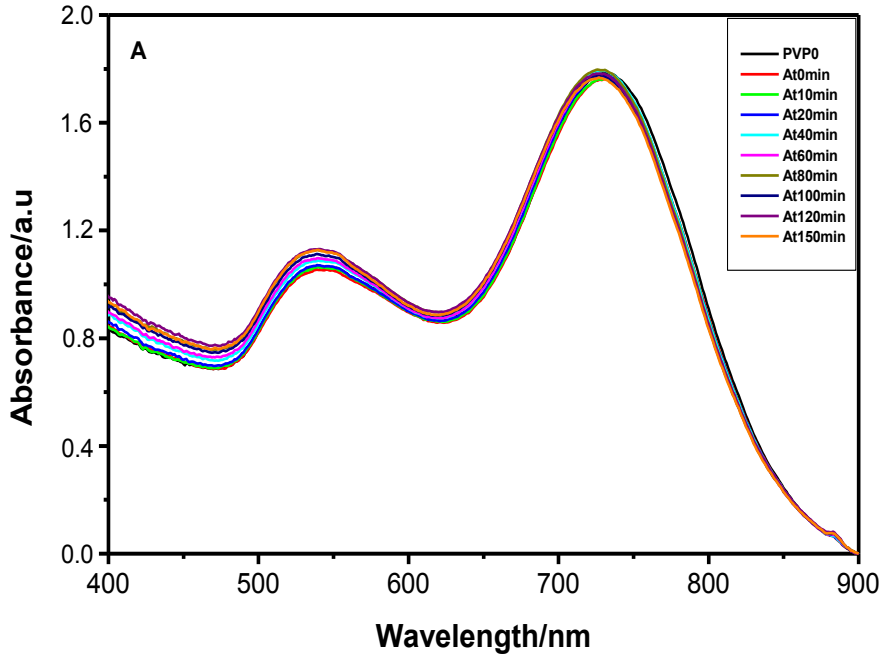

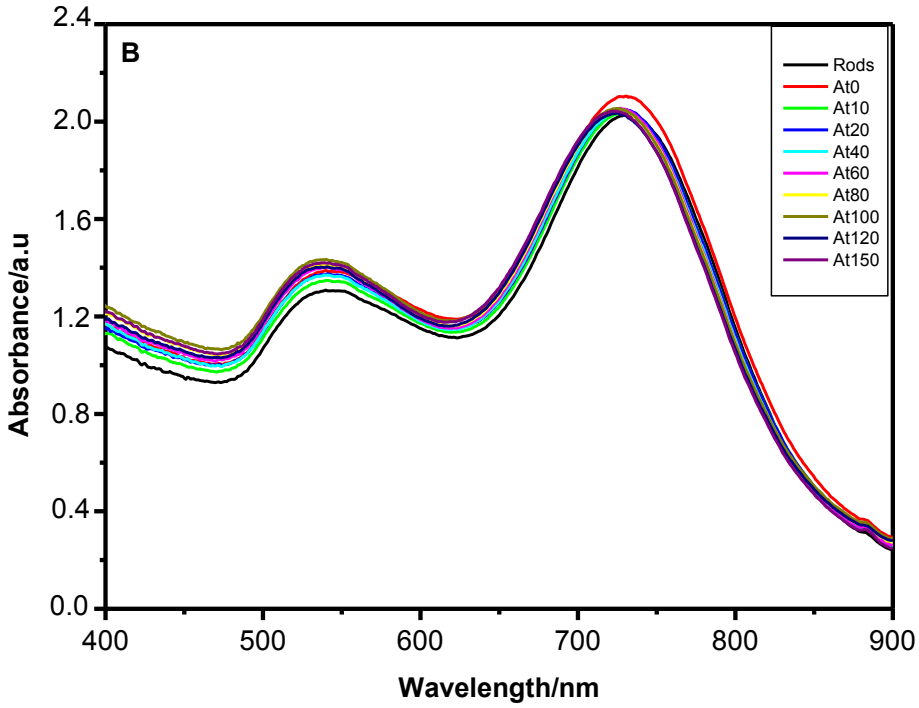
B
Rods
At0
At10
At20
At40
At60
At80
At100
At120
At150
Absorbance/a.u
Wavelength/nm
2.4
2.0
1.6
1.2
0.8
0.4
0.0
400
500
600
700
800
900

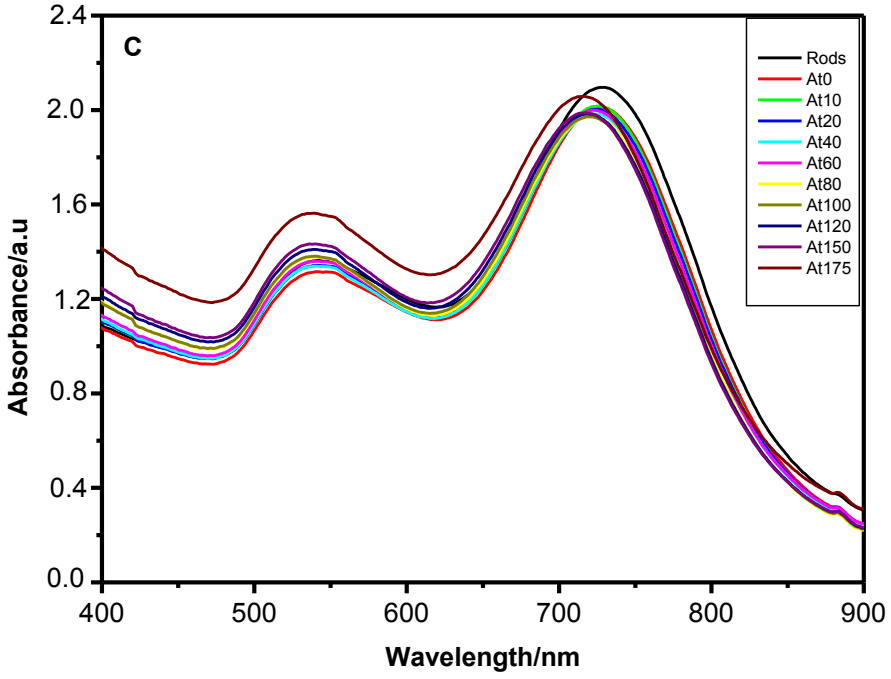
C
Rods
At0
At10
At20
At40
At60
At80
At100
At120
At150
At175
Absorbance/a.u
Wavelength/nm
2.4
2.0
1.6
1.2
0.8
0.4
0.0
400
500
600
700
800
900

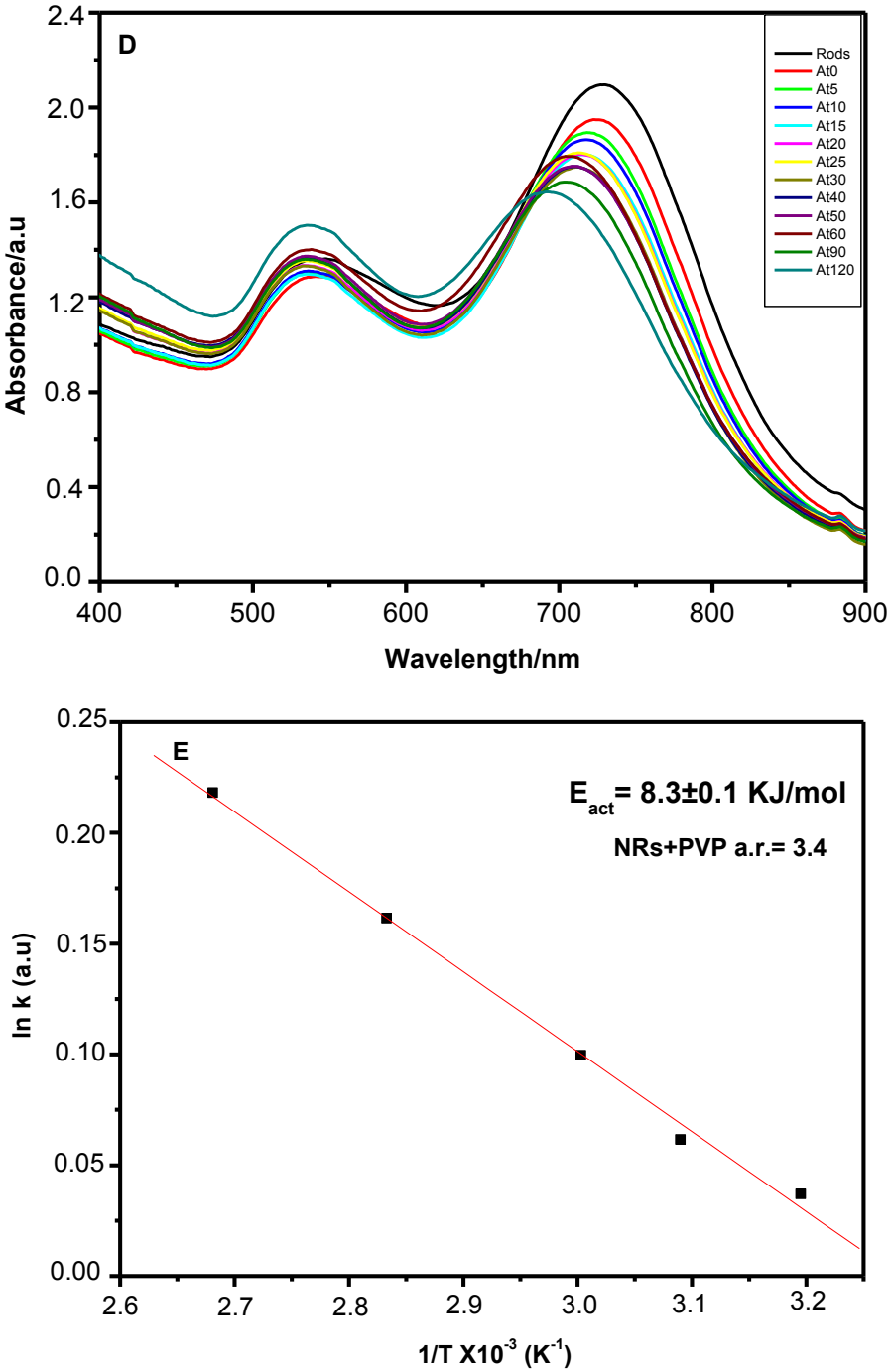

Figure 5-16: Absorption spectra showing the effect of thermal heating on gold nanorods containing 30% PVP with time, at temperatures 40-100^{0}C (A-D, respectively). The activation energy for the decomposition of gold nanorods containing 30% PVP is shown in (E).

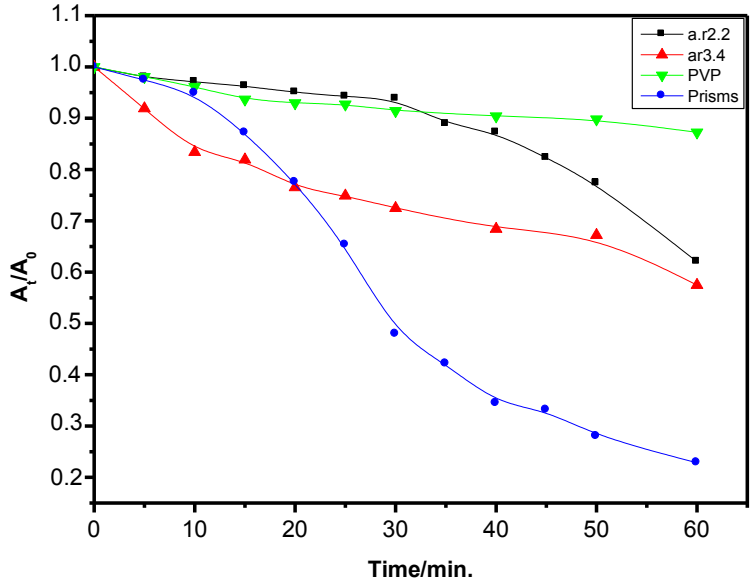

Figure 5-17: Normalized absorption spectra showing the effect of thermal heating on rods with different aspect ratios; rods containing 30%PVP; and nanoprisms.

5-2-3-2: Gold nanoprims.

In the case of nanoprisms, adding 30% of PVP, the particles are completely stable up to 100 ^{0}C. Then, a slight decrease in the absorbance is observed with almost no shift in the absorption band up to 140 ^{0}C. At 160 ^{0}C a large decrease of the intensity is observed, which corresponds to the aggregation of nanoparticles. A picture of the aggregated nanoparticles at 180^{0}C is shown in figure (5-18A). Using lower concentrations of PVP (15%), the thermal heating leads first to the dissolution of the tips of these prisms yielding snapped prisms. Then, particles decompose leading to a decrease in the absorbance intensity and a shift to higher wavelengths, but the particles remain stable after such reorganization until 180 ^{0}Csee figure (5-18B).

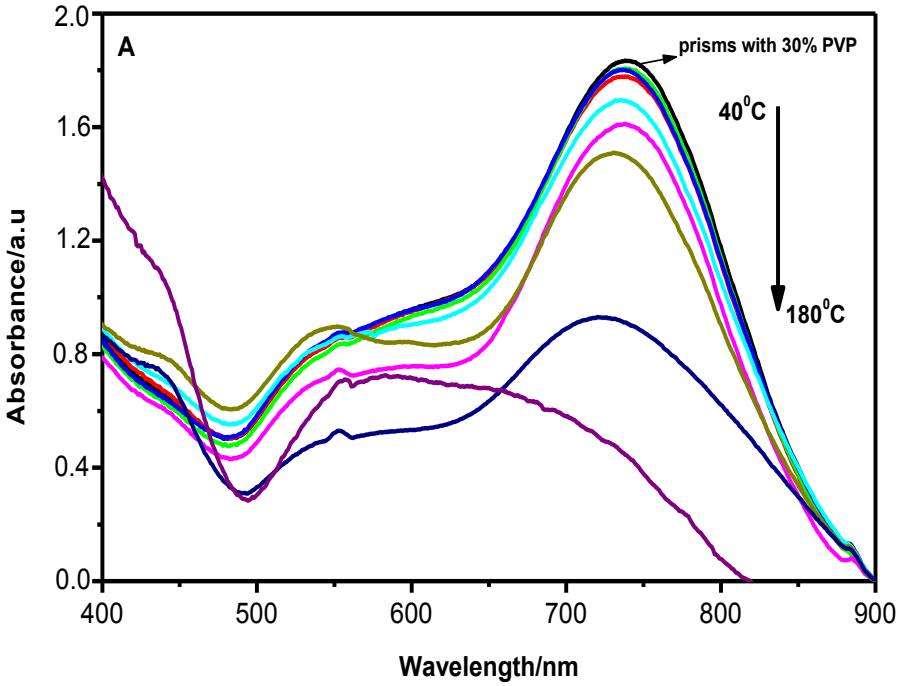
A
prisms with 30% PVP
40^{0}C
180^{0}C
Absorbance/a.u
Wavelength/nm
2.0
1.6
1.2
0.8
0.4
0.0
400
500
600
700
800
900

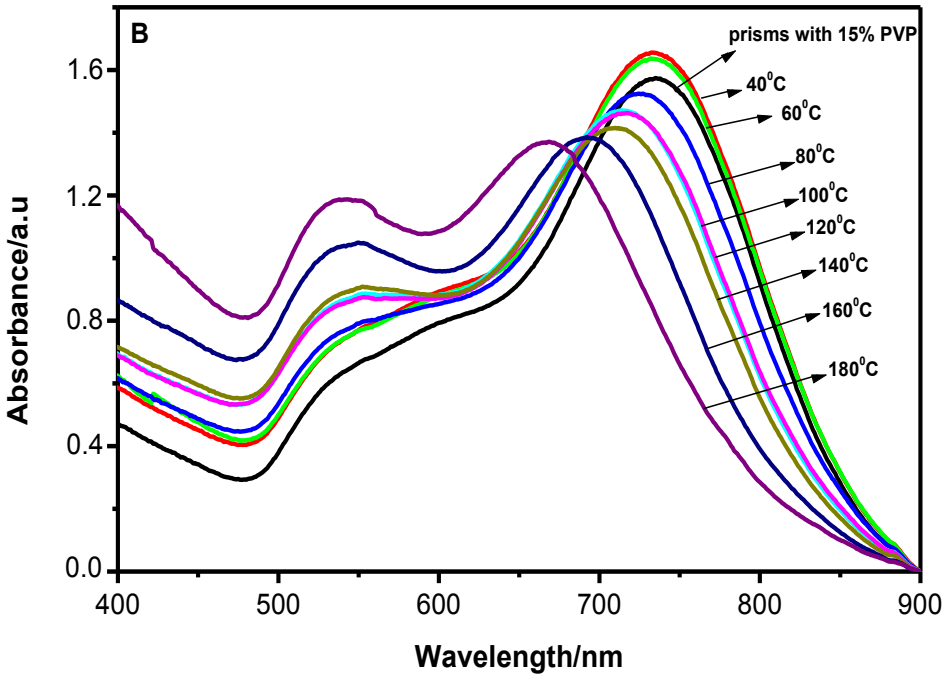
B
prisms with 15% PVP
40^{0}C
60^{0}C
80^{0}C
100^{0}C
120^{0}C
140^{0}C
160^{0}C
180^{0}C
Absorbance/a.u
Wavelength/nm
1.6
1.2
0.8
0.4
0.0
400
500
600
700
800
900

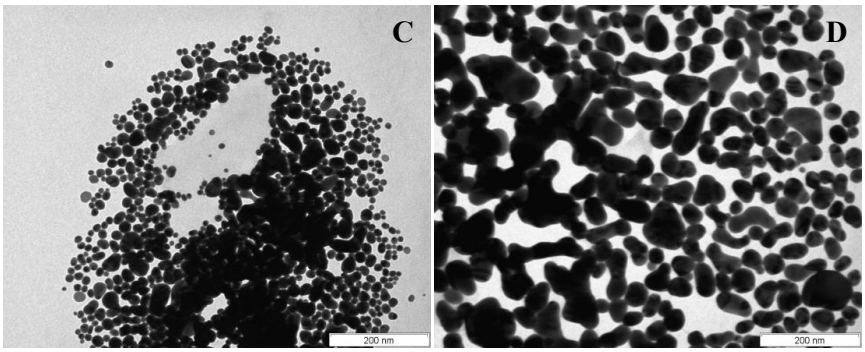

Figure 5-18: Absorption spectra showing the effect of addition of 30 % (A) and 15% (B) PVP on the thermal stability of the gold nanoprisms. TEM images (C and D) showing gold nanoprisms with 15% and 30 % PVP, respectively.

Part II: Photostability of gold nanoparticles.

5-3: Effect of UV irradiation.

In this section, we report the effect of UV-light and Laser on the shape of gold particles of different shapes.

5-3-1: Effect of UV-light irradiation on gold nanospheres.

As it can be seen in Figure (5-19), irradiation of spherical nanoparticles prepared in the absence of $AgNO_3$ shows only a very slight decrease without any remarkable shifts in the corresponding SP band. This implies that spherical particles are very stable against UV-light irradiation.

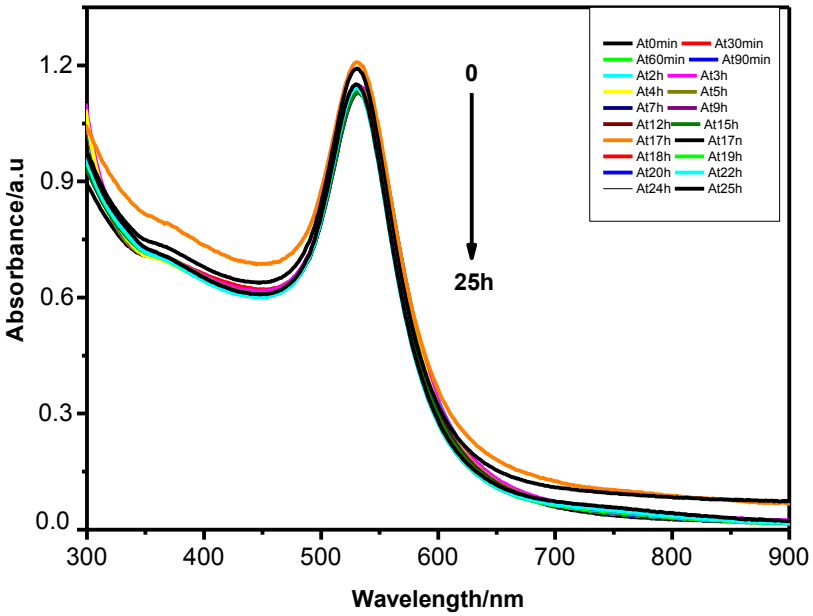

Figure 5-19: Absorption spectra showing that UV-irradiation of gold nanospheres prepared in the absence of $AgNO_3$ during 25h has almost no noticeable effect.

5-3-2: Effect of UV-light irradiation on gold nanoprisms.

As it can be seen in Figure (5-20), nanoprisms are also very stable towards UV light. After exposure for long times (about 24 hrs) only small changes - probably associated with the morphology change from prisms to snapped prisms are observed. The three absorption bands, characteristic of nanoprisms, are blue shifted. However, after 2 days of irradiation (see figure 5-21) almost all prisms are converted into rods, as it can be observed by the disappearance of the intermediate plasmon band.

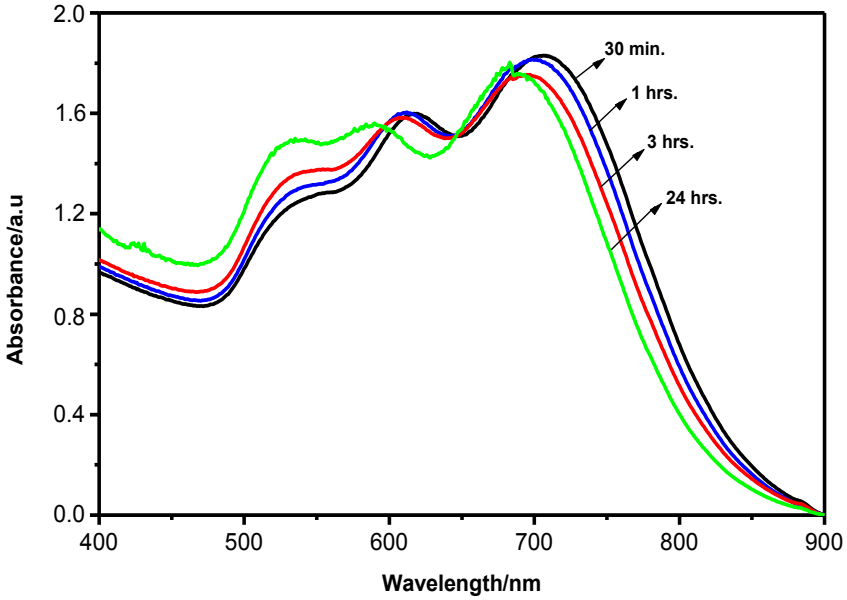

Figure 5-20: Absorption spectra showing the effect of UV-light on the gold nanoprisms at different times, from 0 to 24h.

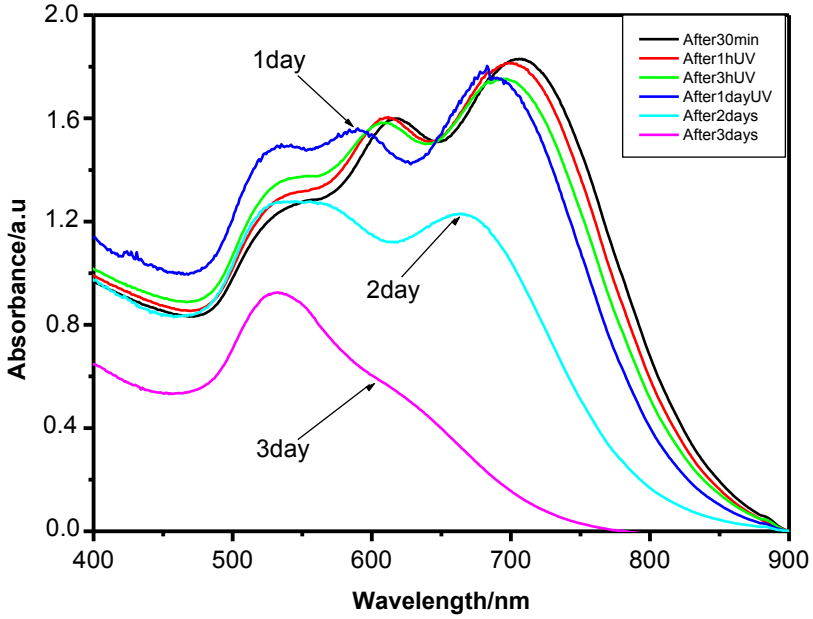

Figure 5-21: Absorption spectra showing the effect of UV-light on gold nanoprisms at different times: 1h, 3h, 1 day, 2 days, and 3 days.

5-3-3: Effect of UV-light irradiation on gold nanorods.

The effect of the irradiation on gold nanorods encapsulated in micelles, with average aspect ratios of a.r. =2.5 and 3.7, (with absorption maxima at 701and 762 nm, respectively), was investigated. Figures (5-22A and, 5-22B) show the absorption spectra of gold nanorods of a.r. = 2.5 before and after irradiation by UV-light. The optical density at both, longitudinal and transverse plasmon bands, decreases with increasing the irradiation time and the absorption maxima of the SP_L are gradually shifted to shorter wavelengths ($\lambda_{max.}$ = 672nm versus 700nm). The observed decrease in the absorption spectra-and the shift in SP_L- are mainly caused by the decrease in the length of the nanorods. Figure (5-22C) illustrates that the normalized absorption spectra changes almost linearly with time. This change may be due to the regular reshaping of the nanorods inside the capping micelles. Increasing the irradiation time (for the two types of gold nanorods), produces an increase of the decomposition of rods, decreasing their lengths. But, totally unexpected, it is also observed that exposure to UV-irradiation for longer times (24h), leads to almost the complete decomposition of the rods (see figure 5-22D).

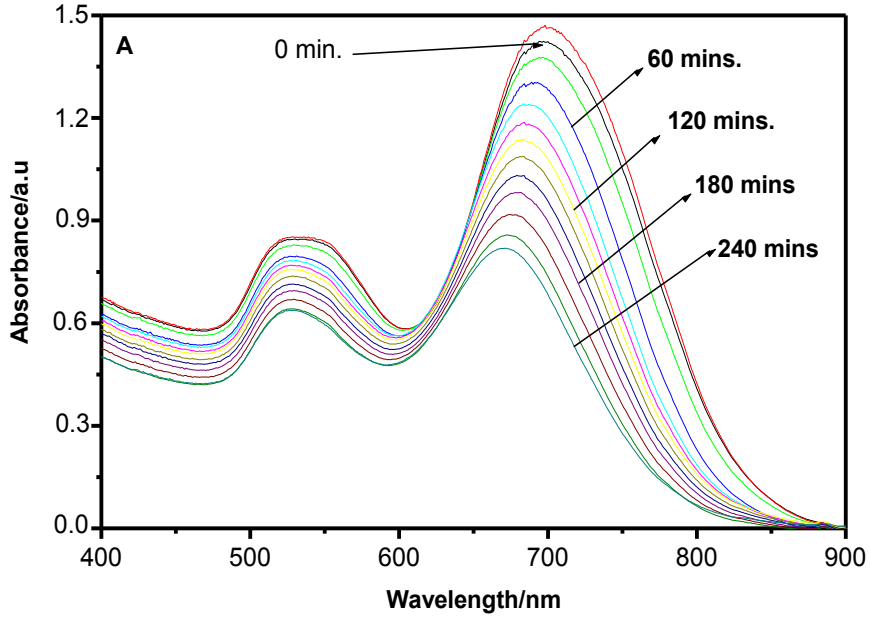
A
0 min.
60 mins.
120 mins.
180 mins
240 mins
Absorbance/a.u
Wavelength/nm
1.5
1.2
0.9
0.6
0.3
0.0
400
500
600
700
800
900

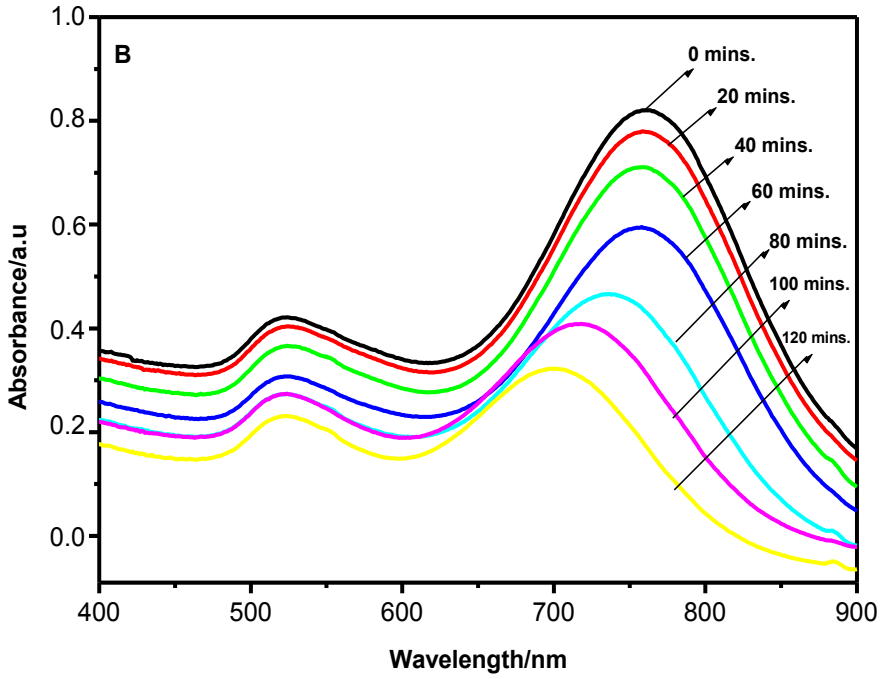
B
0 mins.
20 mins.
40 mins.
60 mins.
80 mins.
100 mins.
120 mins.
Absorbance/a.u
Wavelength/nm
1.0
0.8
0.6
0.4
0.2
0.0
400
500
600
700
800
900

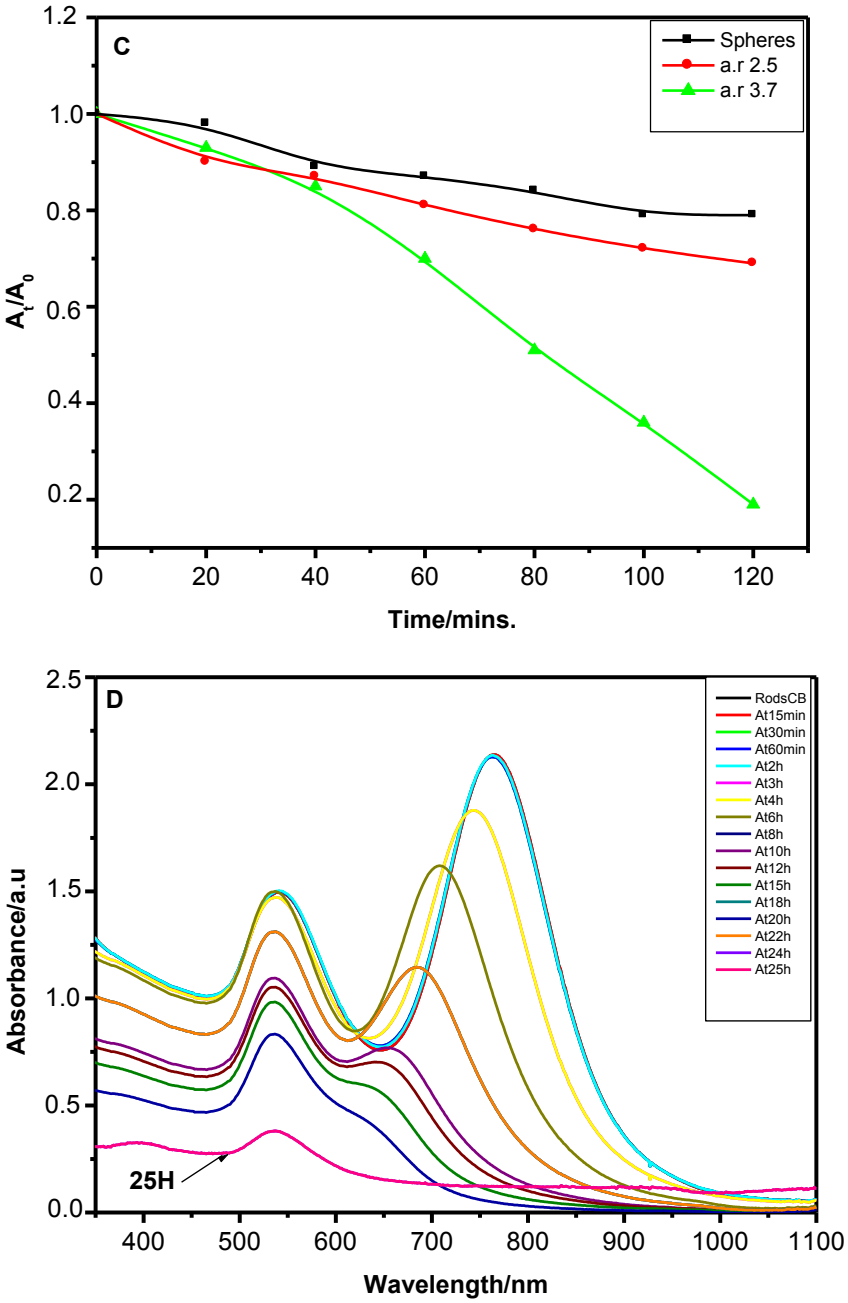

Figure 5-22: Absorption spectra showing the changes of gold nanorods of (a.r.= 2.5 and 3.7) after irradiation by UV-light (A & B, respectively); (C) normalized absorption spectra of gold nanoparticles with different shapes at different irradiation times and (D) absorption spectra showing that exposure to UV light for ~ 25 h leads to almost the complete decomposition of the rods.

The temperature of gold nanorod´s solution, under the experimental irradiation conditions, was found to be 65^0C. Therefore, one could think that reshaping and decomposition of rods could be due to the thermal effect that studied in the previous section. Therefore, we decided to repeat the experiments at lower temperatures. Figure (5-23) shows the results obtained controlling the temperature of the solution.

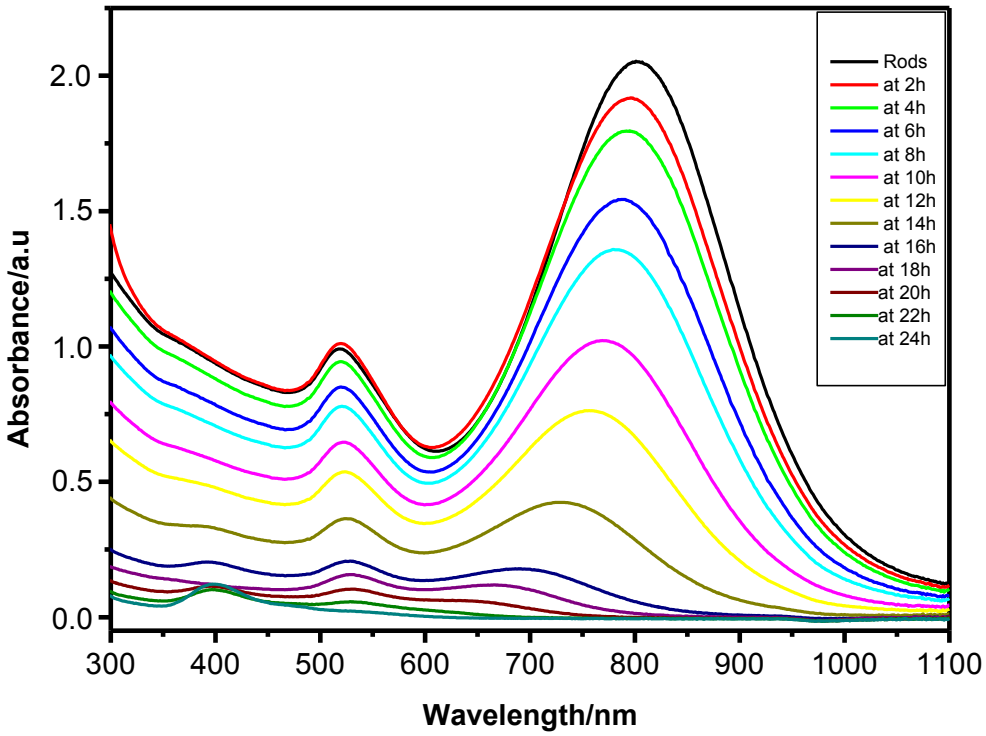

Figure 5-23: Absorption spectra showing the changes of gold nanorods (a.r. ≈ 3.9 at pH = 3.9) after irradiation under UV-light, at T= 28^0C, showing again the complete decomposition of the rods.

It is observed that the exposure of nanorods to UV-irradiation controlling the temperature of the solution (T=28^0C), leads again to the complete decomposition of the rods. Rods are now firstly transformed into nanospheres and, then, a new band at 398 nm with a small shoulder at 478 nm starts to grow from 23 hours to 30 hours. This band is totally similar to the band displayed by Au (III)-CTAB complex , which implies that rods

are not only reshaped, but they are oxidated. Figure (5-25) shows a TEM picture of the dissolved NRs after irradiation for different times. It can be seen that NRs completely dissapear and only some nanospheres remain (which are detected in the UV-vis spectra by a small band located at 520nm). It can be also seen that the number of spherical particles decreases with time showing that sperical particles also dissolve with time.

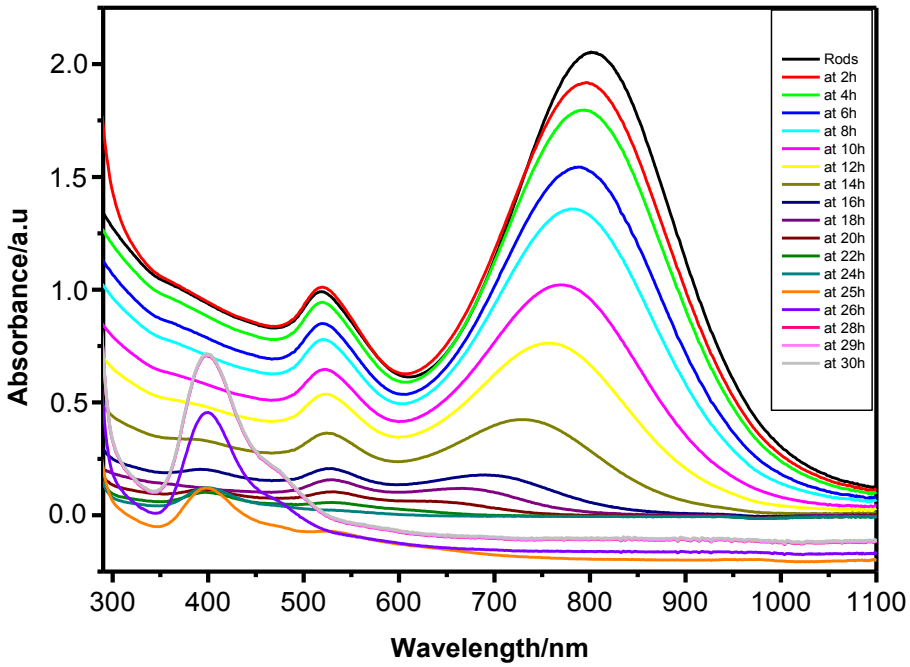

Figure 5-24: Absorption spectra showing the changes of gold nanorods of (a.r. ≈ 3.9, at pH 3.9) after irradiation under UV-light for ~ 30 h leading to the complete decomposition of the rods and the formation of Au(III)-CTAB complex, as it can be seen by the appearance of the band at 398 nm.

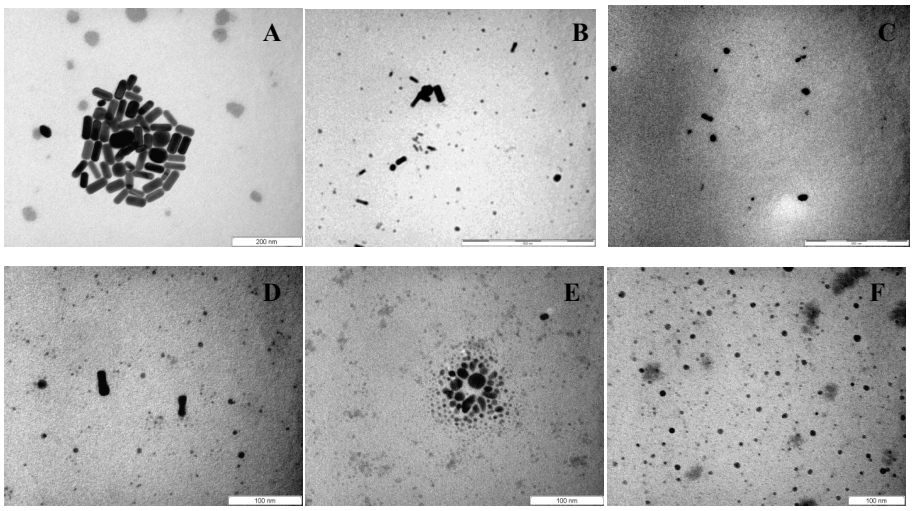

Figure 5-25: TEM images showing the effect of the UV-irradiation on gold nanorodsat different times of irradiation: (A) 0, (B) 8h, (C) 12h, (D) 18h, (E) 22h and (F) 28h.

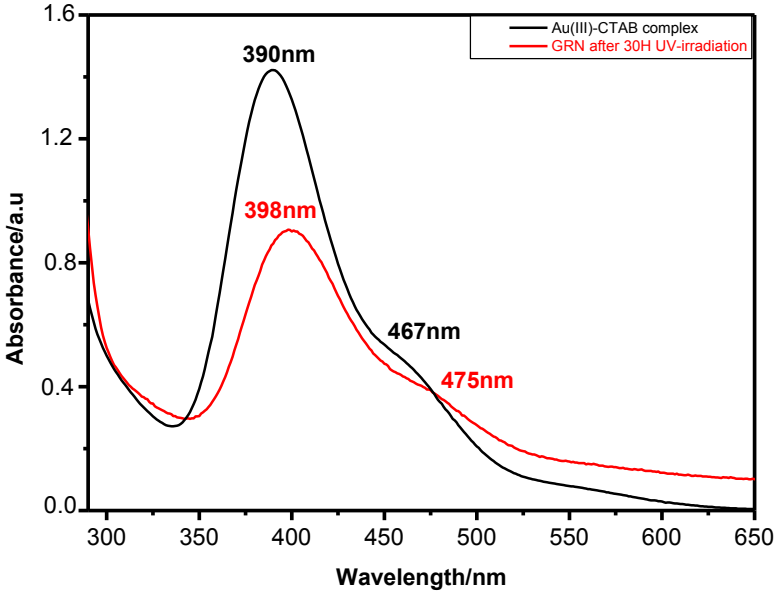

Figure 5-26: Absorption spectra showing the similarity between the absorption spectra of 0.5mM Au(III)-CTAB complex (growth solution of NRs without addition of AA) and GNRs after 30h of UV-irradiation.

Figure (5-26) shows a comparison of the UV-Vis spectra of 0.5mM of the solution of Au (III)-CTAB used for the synthesis of Au NRs (which contains Au(III), $AgNO_3$ and CTAB) and the final solution containing the

Au NRs after irradiation for 30 h. It can be seen that, besides the larger absorption at high wavelengths (probably due to the incomplete dissolution of the Au(0) nanoparticles), both spectra are very similar showing that, after irradiation, Au NRsare totally oxidized.

This is a totally surprising and unexpected result, because it is well-known that Au is a noble metal, which cannot be oxidized by UV-light. However, the results indicate that the gold NRs show a similar behaviour than that displayed by semiconductors in which photocorrosion can takes place. Because we have seen in previous chapters that Ag clusters play an important role in the formation of Au NRs, the simplest explanation of the results could be that clusters, which have semiconductor properties with absorption bands in the UV range, remain as such after the reaction carried out to synthesise the NRs. These clusters, probably protected by the surfactant CTAB, would be attached to the plane at which they show a preferential adsorption (as it was explained in chapter III, this plane is probably the {111} or {110} plane). Therefore, when they are illuminated with UV light, an exciton can be formed. Because the Fermi level of the Au NR and the attached Ag clusters are very similar, electrons and holes can easily be separated at the surface of the Au NRs and they can act as reduction/oxidation agents instead of been recombined to produce fluorescence.

The easy separation of electron and holes at the surface of the metal Au nanorod may be due to the very small (or zero) binding energy of the exciton because of the good electric shielding properties of the metal. Therefore, these sub-nano cluster/metal sub-nanojunctions should be ideal for an effective electron-hole separation. The generated electrons, with a much higher energy than the Au Fermi level, can easily lose their energy by interactions with the phonons of the lattice. However, holes generated at the gold surface can be very active as reduction agents. According to the

scheme represented in scheme (5-1), which shows an approximate representation of the cluster HOMO-LUMO levels (valence and conduction bands in semiconductors), Au atoms (located at the surface of the Au NRs at which clusters are adsorbed) will be oxidised and easily dissolved. This explains the electrochemical dissolution of the Au NRs. But, to understand the dissolution phenomena one has to think that the adsorption of clusters to the surface is a dynamic process, being the clusters-stabilized by CTAB-attached/de-attached from the Au surface. This idea was also introduced in Chapter III for explaining the reverse reaction, namely the catalytic behaviour of Ag clusters observed for the directed growth of the formation of Au NRs, without being the clusters incorporated ("swallowed") into the Au lattice. Similarly, it would explain that clusters can be continuously adsorbed/desorbed to the preferential planes of the continuously reshaping/dissolving NRs.

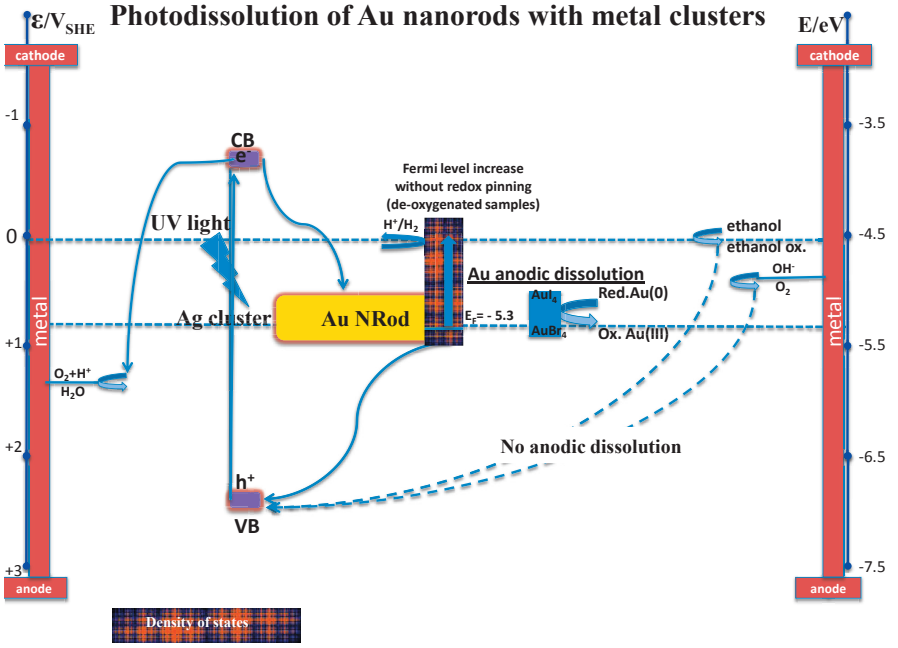

Scheme 5-1: Scheme showing the energetic involved in illustrating the photodissolution of gold nanorods with metal clusters.

In order to check that this explanation of cluster-mediated metal photocorrosion can takes place, we carried out several experiments to confirm such hypothesis.

a) Influence of ethanol.

It is well-known that ethanol is very easy to oxidize and, therefore, is normally used as a hole scavenger. If the proposed mechanism is correct dissolution of Au NRs should be avoided (or largely inhibited) by introduction of ethanol into the system. Therefore, we carried out an irradiation experiment with a mixture NRs to ethanol ratio = 2:1 by volume. Figure (5-27) shows that, in fact, the dissolution of Au NRs is greatly inhibited, and only some dissolution of the Au NR tips occurred giving rise to a decrease of the a.r. of the Au NRs, as it can be deduced by the red shift of the SP_L band.

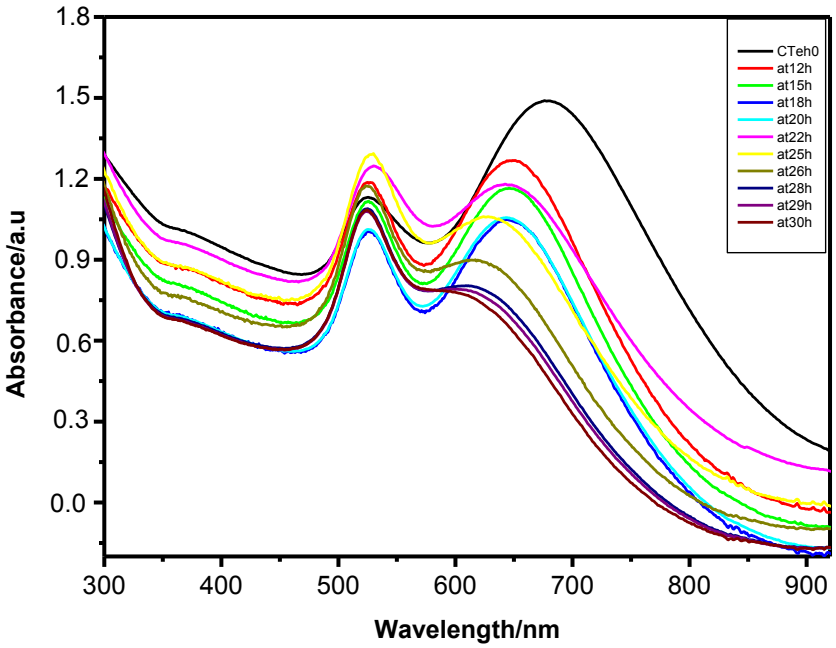

Figure 5-27: Absorption spectra showing the changes of gold nanorods with addition of a small amount of ethanol and irradiating the sample with UV-light during ~ 30 h.

b) Influence of NR´s preheating.

It is known that small metal clusters fuse at low temperatures. In particular, Ag clusters employed for the synthesis of Au NRs (see chapter III) fuse at around 120^0C-150^0C, when they are unprotected in solution (unpublished results). Therefore, a second experiment for the proof of the mechanism here proposed for the dissolution of Au NRs was to heat the solution of Au NRs to 130ºC before irradiation with UV-light. It can be assumed that at such temperatures the Ag clusters fuse and are incorporated into the NR's lattice. Therefore, in such a case the mechanism of cluster-mediated UV-dissolution of Au NRs would be avoided. Figure (5-28) shows that when NRs were preheated at 130^0C for short time (10min), although the dissolution was not completely inhibited, it was slowed down. In fact, the preheated NRs solutions after of 30h irradiation are only reshaped to spheres, in contrast to the untreated NRs, which were totally dissolved. The non-complete inhibition of the NR solution implies that the short preheating time was not enough to fuse all the clusters (maybe because clusters are more stable when they are supported over a substrate and protected with a ligand like CTAB). However, when NRs were preheated for long time (≈ 2h) all the Ag clusters fuse and the gold nanorods are very stable even under long time of UV irradiation (≈40h), which confirms the role of the clusters in the dissolution mechanisms (see figure 5-30). To further confirm this hypothesis a new experiment was carried out adding a small amount (3nM) of Ag-clusters (from Nanogap - see Chapter III-) to a preheated sample of NRs sample and irradiated this sample with UV-light. It can be seen in figure (5-31) that the dissolution of NRs occurs after a short time (4h only) compare with the results shown in figure (5-24). These results further confirm the hypothesis putted forward in Chapter III for the growth mechanism assuming that clusters would be preferentially located at the tips of the rods. Figure (5-29) shows a

comparison of colours of the final samples after 30h irradiation showing the influences of preheating the samples and adding ethanol to the solutions.

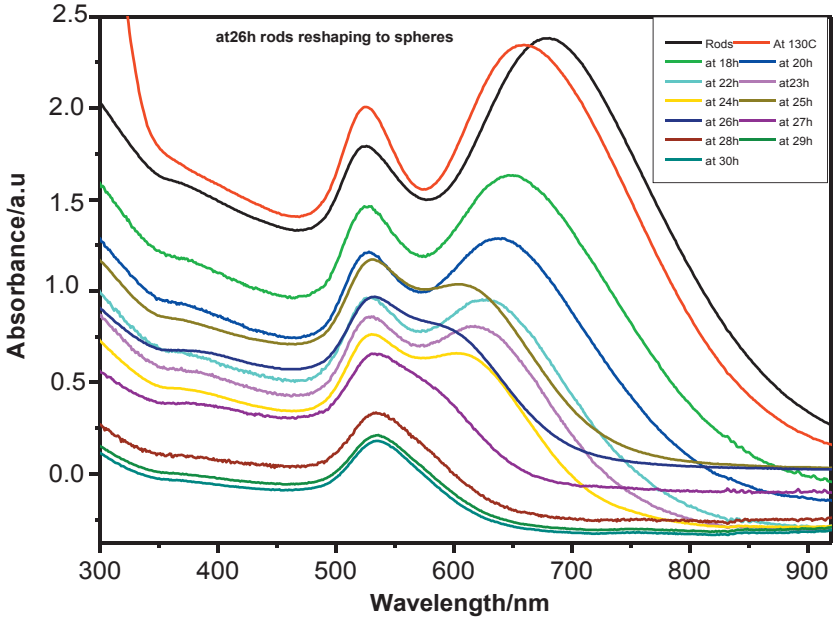

Figure 5-28: Absorption spectra showing the changes of gold nanorods pre-heated to 130^0C for 10min and irradiated with UV-light during ~ 30 h.

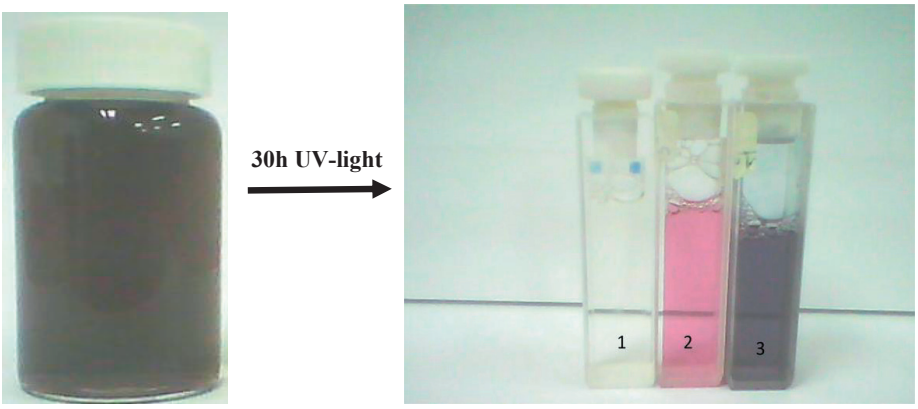

Figure 5-29: Picture showing the difference between the initial GNRs sample and irradiated gold nanorods during 30 hours (1) with pale yellow color characteristic of the formation of Au (III)-CTAB complexes, (2) for gold nanorods pre-heated to 130^0C and then irradiated during 30 hours with a pink color characteristic of the formation of gold nanospheres and (3) for gold nanorods with ethanol showing almost no change in the color of the initial GNRs solution.

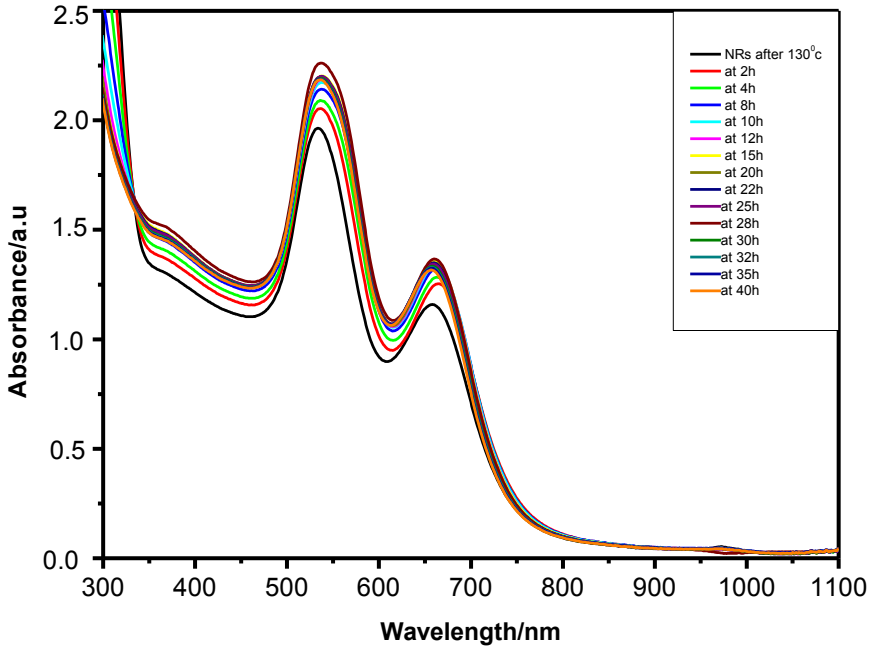

Figure 5-30: Absorption spectra showing the small changes of gold nanorods pre-heated to 130^0C for 2h and then irradiated with UV-light during ~ 40 h.

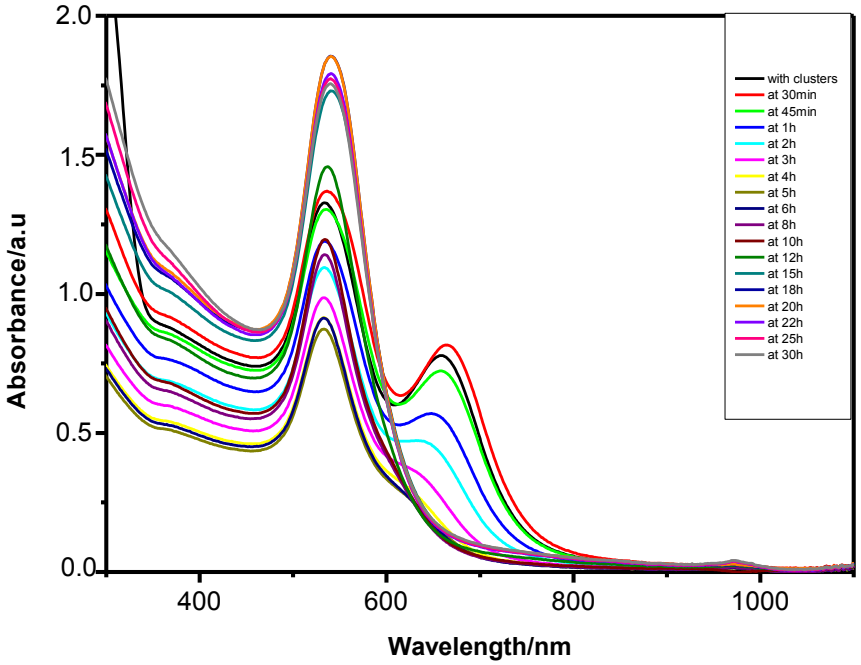

Figure 5-31: Absorption spectra showing the changes of gold nanorods pre-heated to 130^0C for 2h in the presence of external synthesized Ag clusters and then irradiated with UV-light during 30h.

c) Influence of pH.

The previous experiments were conducted at acid pHs (3.9). At basic pHs, the oxidation of water to give oxygen is favoured (ε^0 = 0.68V) in comparison with the oxidation of Au (ε^0=0.85V, for the bromide salt), so that at these pH values the oxidation of Au NRs should be largely suppressed. Figure (5-32) shows that even after 30h irradiation NRs do not decompose and only their length is decreased. Figure (5-33) shows how the normalized absorption intensities of the SP_L and SP_T bands change with the irradiation time at acid and basic pHs. It can be clearly seen that at basic pHs the dissolution is inhibited and that the diameter of the rods does not change with the irradiation time, as it can be deduced from the constant value of the SP_T band.

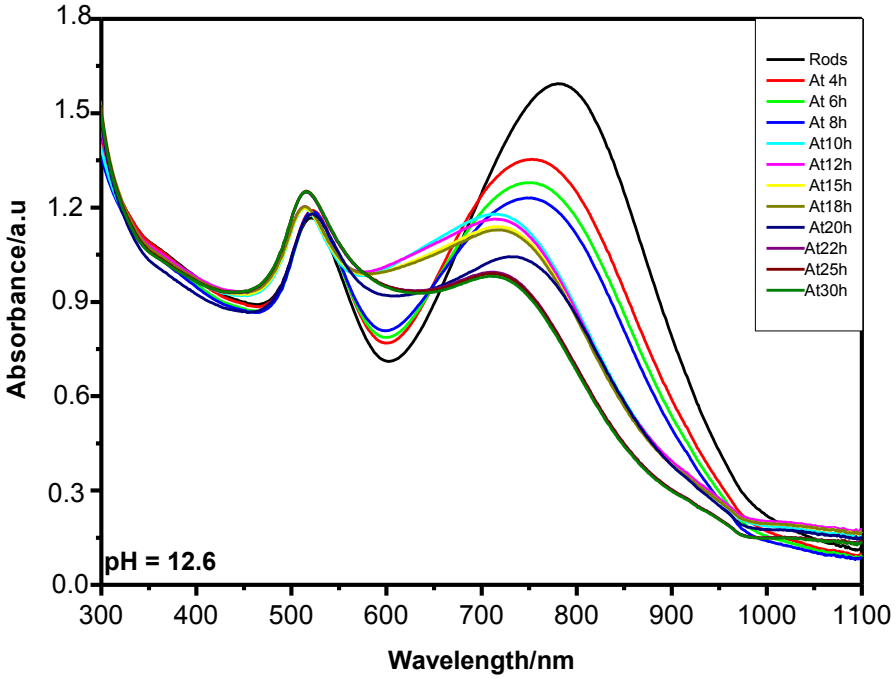

Figure 5-32: Absorption spectra showing the changes of gold nanorods (a.r ≈ 3.7, at pH 12.6) after irradiation under UV-light during ~ 30 h.

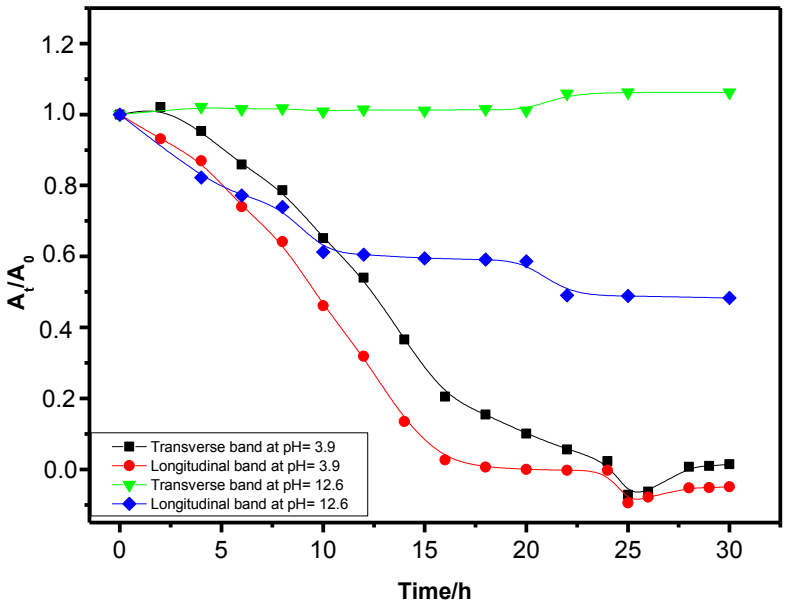

Figure 5-33: Normalized absorption intensities of the SP_L and SP_T bands of gold nanorods at both pHs (3.9 and 12.6) under UV light irradiation during 30 h.

d) Influence of NR's washing.

We carried out similar irradiation experiments with NR's samples after centrifuging 2 times at 6000rpm for 20min and washing the samples with distilled water. Also two similar experiments were carried out washing the samples and then either pre-heated to130^{0}C or in the presence of a small amount of ethanol. By this procedure (in the first experiment) some CTAB -and also the clusters linked to this ligand- would be removed, which would also inhibit in some extension the dissolution of Au NRs. In the second and third experiments more clusters would be removed/fused, which would further prevent the dissolution effect. As it can be observed in Figures (5-34, 35, and 36) after 30h, only a decrease of the length is observed, which indicates that an appreciable amount of the photocatalytic clusters, responsible for the dissolution of NRs, were effectively removed by washing.

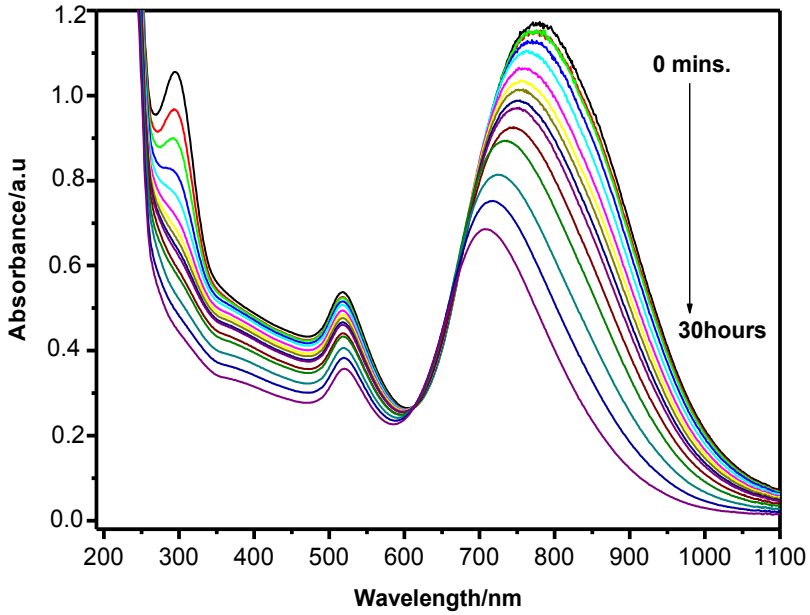

Figure 5-34: Absorption spectra showing the changes of gold nanorods after being washed 2 times and irradiated with UV-light during ~ 30 h.

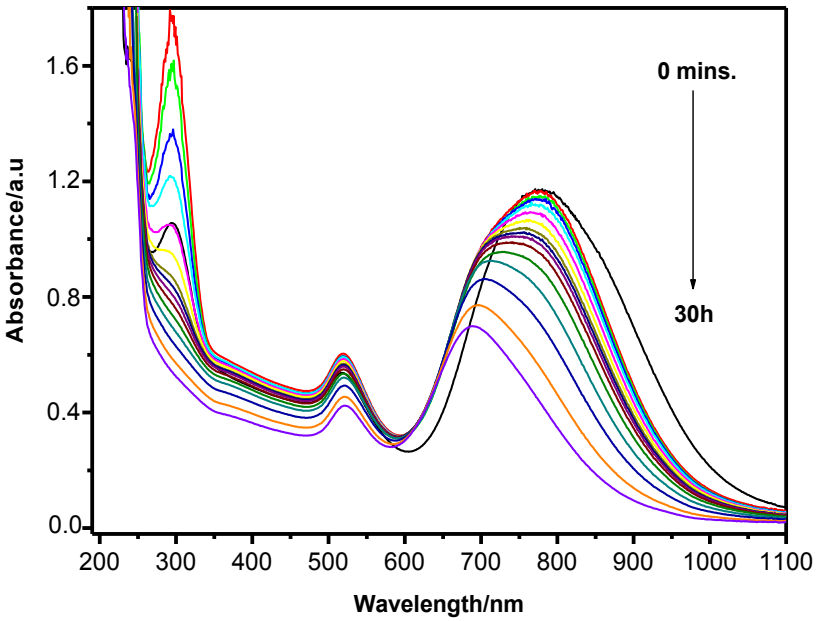

Figure 5-35: Absorption spectra showing the changes of gold nanorods after being washed 2 times and preheated to 130^0C. The sample was then irradiated with UV-light during ~ 30 h.

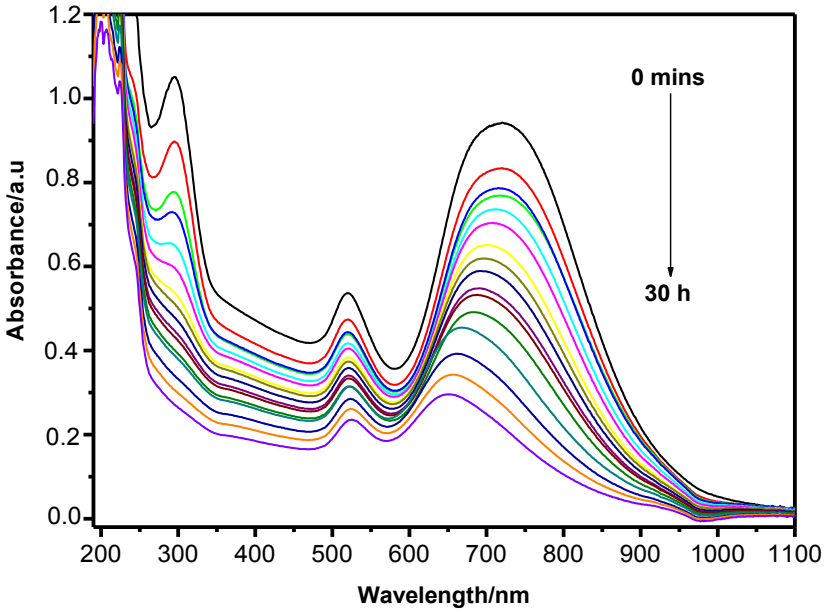

Figure 5-36: Absorption spectra showing the changes of gold nanorods after being washed 2 times. A small amount of ethanol was added to the sample and then irradiated with UV-light during ~ 30 h.

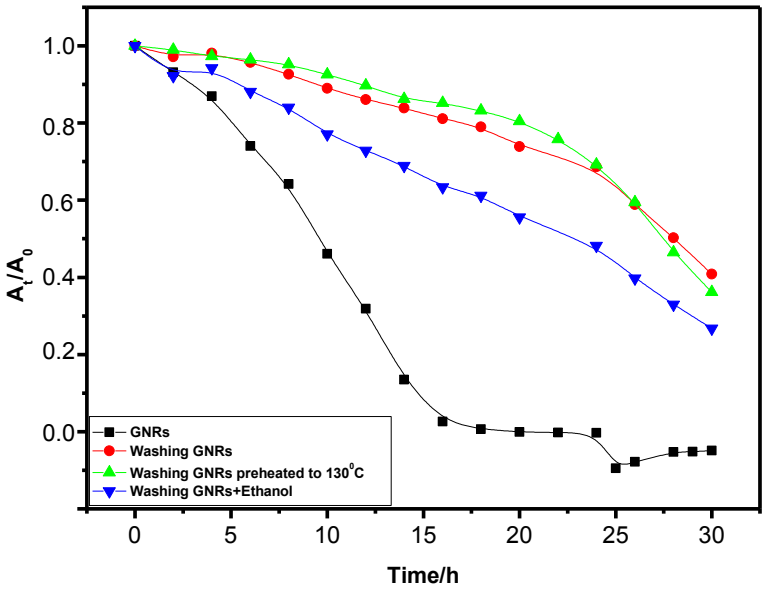

Figure 5-37: Normalized absorption intensities of the SP_L bands of gold nanorods, washed NRs, washed NRs and preheated to 130^0C, and washed NRs with a small amount of ethanol, under UV light irradiation during ~ 30 h.

e) Influence of stirring.

The dissolution of NRs (at pH=3.9) increases when the irradiation of NRs is made with stirring the sample. The band of the gold (III)-CTAB complex appears at shorter times (≈12h) compared with the unstirred samples (see Figure 5-38). It was noticed that the final pH of the solution after complete dissolution of the NRs is more acid than at the begining: pH = 2.7. In order to show that the Ag clusters remain after the dissolution of the NRs a new experiment was performed using the final solution after irradiation for the formation of Au NRs adding AA and seeds solution. As it can be seen in Figure (5-38) NRs are formed again, confirming that Ag clusters play an important role on both, the formation and dissolution of gold nanorods.

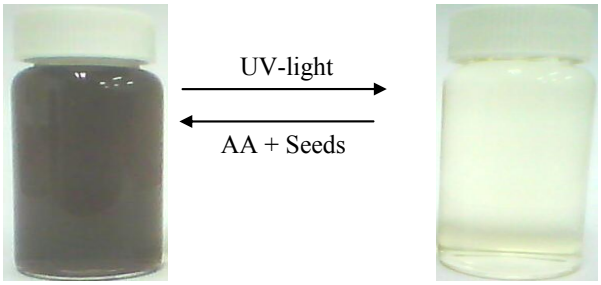

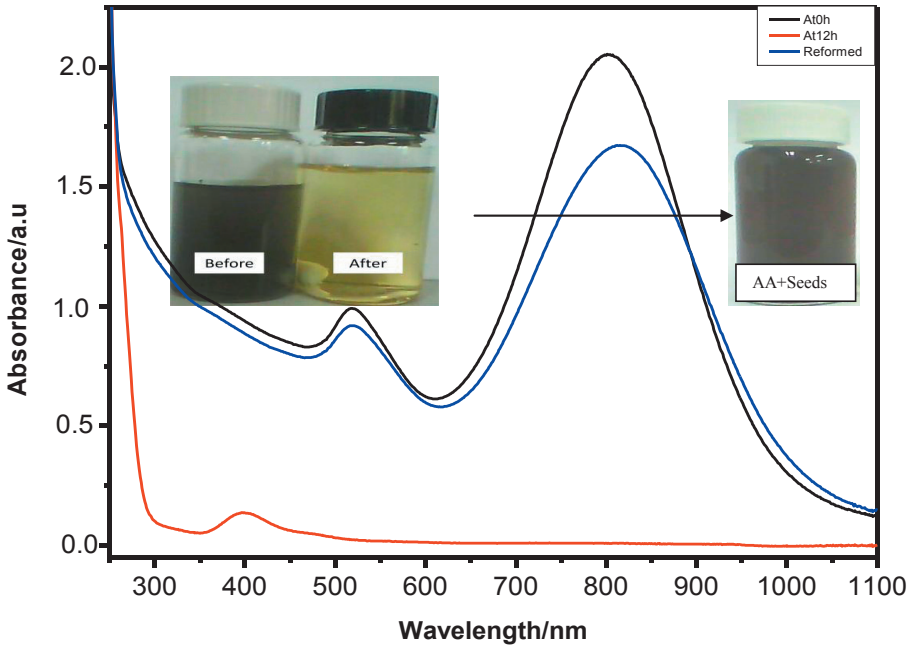

Figure 5-38: Absorption spectra showing the dissolution of gold nanorods (pH=3.9) with stirring, irradiated with UV-light during ~ 12 h; and the reformed NRs after addition of AA & seeds solution. The including picture shows the difference in color between before UV irradiation, after irradiation and after addition AA & seeds solution.

f) Influence of PVP.

Adding 15 % by weight of PVP to the nanorods solution leads to an increase of the photostability of the gold nanorods (see Figure 5-39). Upon addition of PVP, a slight shift to the red (~4nm) is observed due to the change of the dielectric constant of the surrounding medium and the absorbance slightly decreases due to the decrease of the rods concentration by adding PVP. Afterwards, there is not any absorption shift upon exposure the NRs to UV light during 4 hrs. NRs are not decomposed even after 72h of irradiation (compare this with the complete dissolution of NRs without PVP after 24h). The protection of PVP can be due to the oxidation of PVP by the generated holes avoiding in this way the oxidation of the Au

nanorods and also that PVP works as a second protecting layer besides CTAB, as it was shown in the section (5-2-3-1).

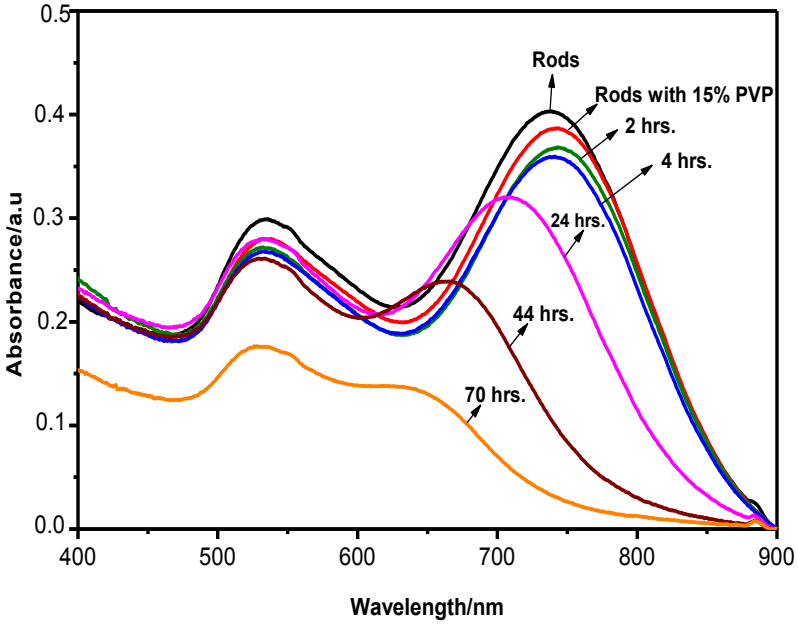

Figure 5-39: Absorption spectra showing the effect of UV-light on gold nanorods after addition of 15% PVP at different irradiation times.

g) Influence of N_2.

As it is well known oxygen is an electron scavenger. Therefore, we decide to study the dissolution of rods in de-oxygenated solutions of NRs bubbling the solutions with N_2 during 5 minutes each hour. As it can be observed in Figure (5-40), the absence O_2 inhibits the dissolution of nanorods (compare this figure with figure (5-24) in the presence of O_2). This is due to the fact that, because there is no hole scavenger in the solution, the carrier recombination is enhanced. However, when the sample is de-oxygenated and the irradiation is made in the presence of a hole scavenger, ethanol (ratio of NRs to ethanol = 2:1 by volume), the dissolution is greatly inhibited (compare with figure (5-27) in the presence of oxygen). In this case, the gold Fermi-level can increase until it is pinned by the redox pair H^+/H_2. At this moment, H_2 is produced as can be seen by the formation of

bubbles on the sides of the cuvette, which occurs after 1h of UV-irradiation. The production of H_2 was electrochemical confirmed as it will be described below.

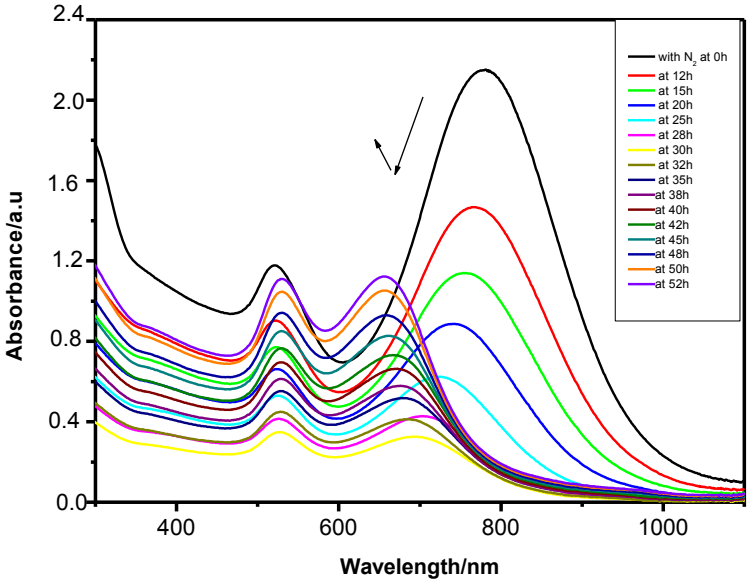

Figure 5-40: Absorption spectra showing the changes of gold nanorods in the presence of N_2 gas and irradiating the sample with UV-light during ~ 52 h.

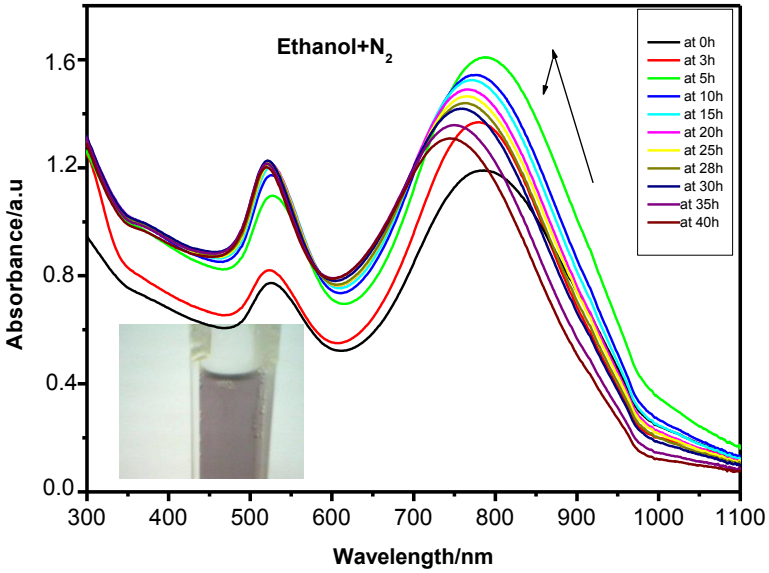

Figure 5-41: Absorption spectra showing the changes of gold nanorods adding ethanol (2:1 volume ratio) and irradiating the sample with UV-light in the presence of N_2 during ~ 40 hrs. A picture of the H_2 bubbles formed after 1h of irradiation is included.

h) Photo-production of H_2.

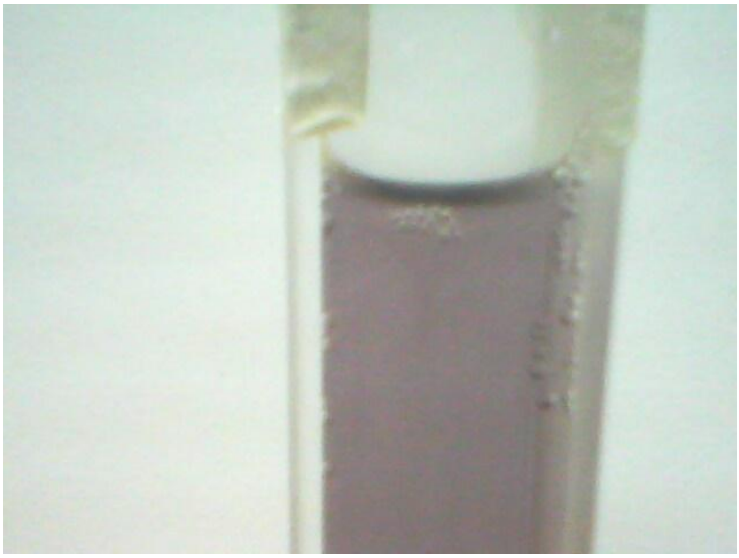

Figure 5-42: Picture of the H_2 bubbles formed after 1h of irradiation of a sample under the experimental conditions given in Figure (5-41).

The electrochemical confirmation of the production of H_2 was carried out using a typical electrochemical cell with three electrodes. Pt wires were used as working and counter electrodes, and a gold wire was used as a pseudo-reference electrode. Firstly a blank was made with a solution of $HClO_4$ (0.1M) in a saturated atmosphere of hydrogen and in the absence of gold nanorods. A cyclic voltammogram of this blank solution is displayed in figure (5-43A) showing that the oxidation peak of H_2 occurs at ≈ 0.2V (Au quasi-reference). Figure (5-43B) shows a cyclic voltammogram of a NRs solution under N_2 atmosphere adding ethanol. It can be observed that the oxidation peak of H_2 is clearly seen after 1 h of irradiation, increasing with the time of irradiation. Therefore, these results confirm that the bubbles observed in the experiment described in figure (5-41) correspond to the photo-production of H_2 gas.

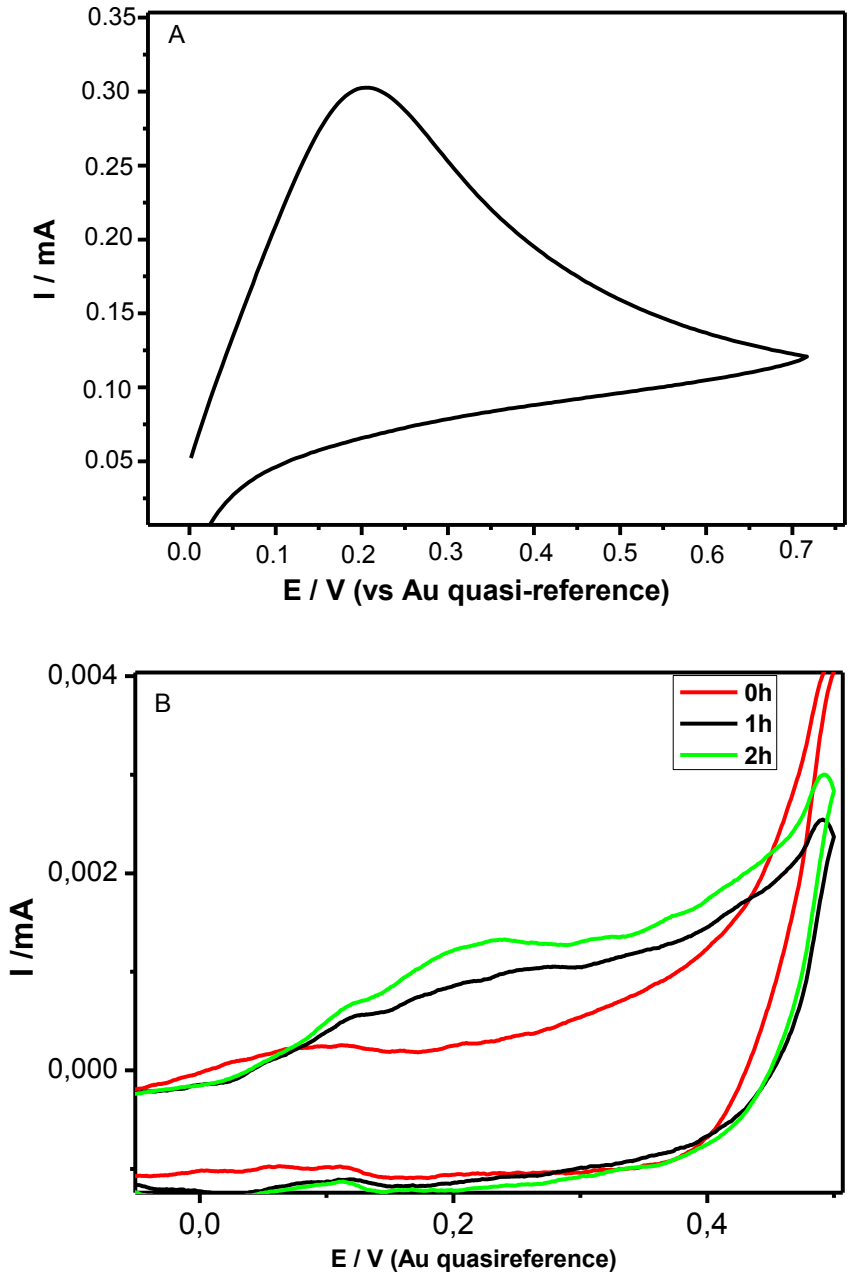

Figure 5-43: A) Cyclic voltammogram of a blank of a solution of $HClO_4$ 0.1M in a saturated atmosphere of hydrogen showing the peak of the hydrogen oxidation at around 0.2V (Au quasi-reference). B) Cyclic voltammogram of a solution of Au NRs (a.r. ≈ 3.7 at pH 3.9) with ethanol (1:1 in volume) under N_2 atmosphere without irradiation (red curve) and after been irradiated during 1h (black curve) and 2h (green curve), showing that the oxidation peak at around 0.2V (Au quasi-reference) appears only after irradiation of the sample.

In the next figure, we summarize all the results about the dissolution of gold nanorods by irradiation with UV-light in different experimental conditions:

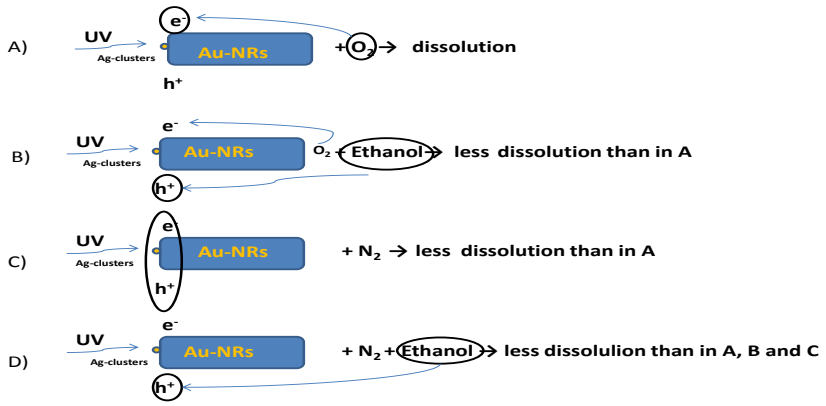

Figure 5-44: Sketch diagram showing the dissolution possibilities in the presence of O_2 (A), ethanol (B), N_2 (C) and ethanol with N_2 (D).

As it was mentioned, we postulate the presence of clusters, mainly attached to the tips of the rods, as responsible for the photodissolution of Au NRs. It should be interesting to see the presence of such clusters by HRTEM: As it can be seen in figures (5-45 and 5-46), the HRTEM of the formed rods showed the presence of very small particles (of cluster sizes) with approximate {111} faces at the tips of the formed rods. The presence of such {111} planes can be due to the fusion of some Ag clusters under the high electron beam irradiation (the rods have the faces {100} and {110} along the rods and {111} at the tips of the rods).

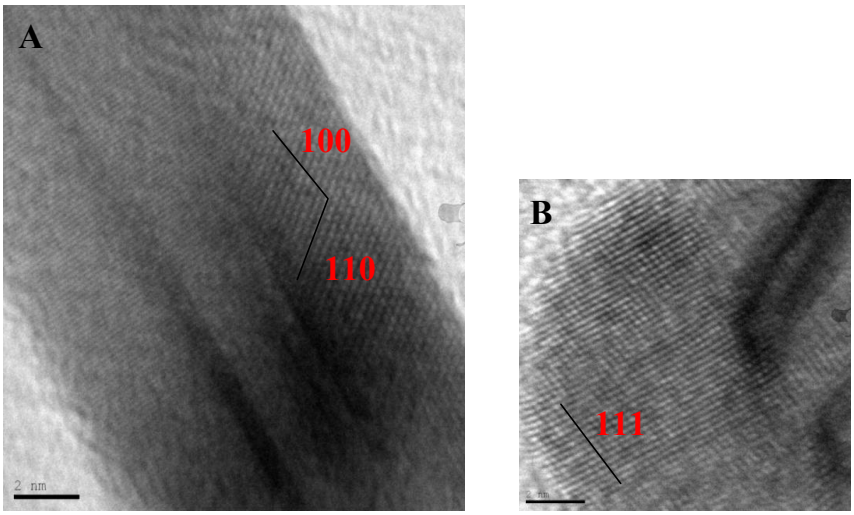

Figure 5-45: HRTEM showing the formed rods with the faces {110} and {100} along the rods and {111} at the tips (scale bar 2 nm).

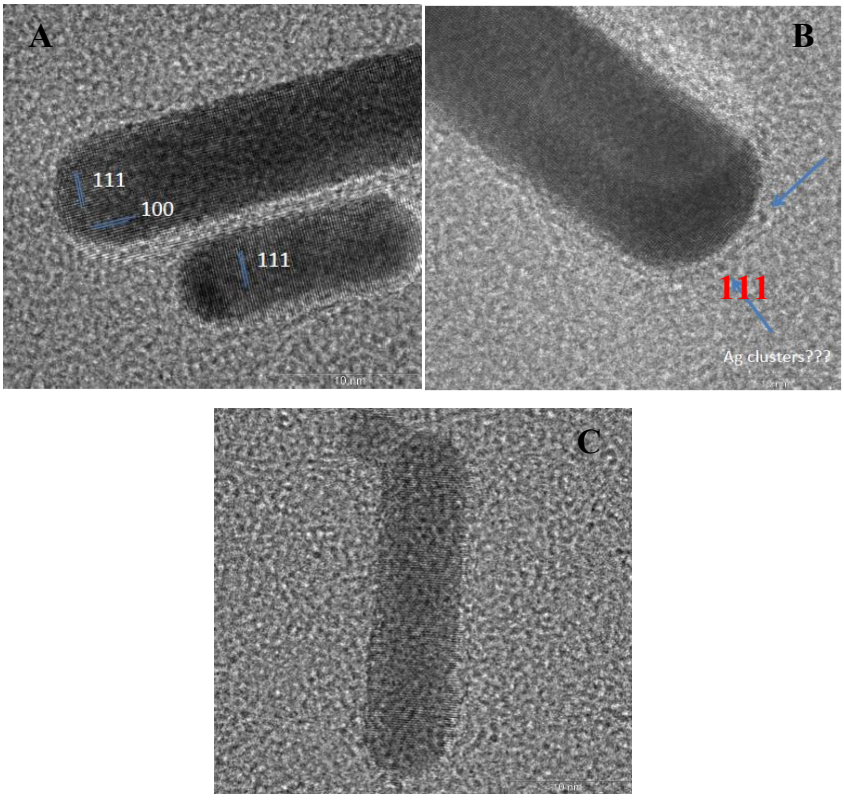

Figure 5-46: HRTEM showing the formed rods with the faces {110} and {100} along the rods and {111} at the tips. The presence of very small clusters with an approximate {111} near the tips can be observed (scale bar 10 nm).

5-3-4: Electrochemical analysis of the Au ions produced by the photo-corrosion of Au NRs.

Because in the spectrophotometric experiments described above to follow the dissolution of the Au NRs, the bands which show the presence of Au ions in the solution were observed only at the end of the experiments, we decided to carry out an electrochemical analysis of the Au ions produced during the photocorrosion experiment. For this purpose we designed a cell, which can be illuminated with UV light. The design of the cell is schematically shown in Figure (5-47). The cell is made up of Teflon and consisted of one quartz window on the top (W). One platinum wire is used as the working electrode or the source (S); one 3.5 cm ring of stainless steel wire centering on the source is used as counter electrode (C), while a gold wire is used as quasi-reference electrode. The cell is approximately 6 cm in diameter and 3 cm dip. There is a small hillock at the center to control the volume of the cell. When the lid is clasped the volume of the cell is roughly 60 ml. The working electrode sits on the top of the hillock. There is one inlet on the lid to introduce the electrolyte into the cell and another passage on the side wall to take out the electrolyte. One hole of 3 cm diameter on the lid, which is covered by a 2 mm thick quartz plate, serves as window to radiate light inside the cell.

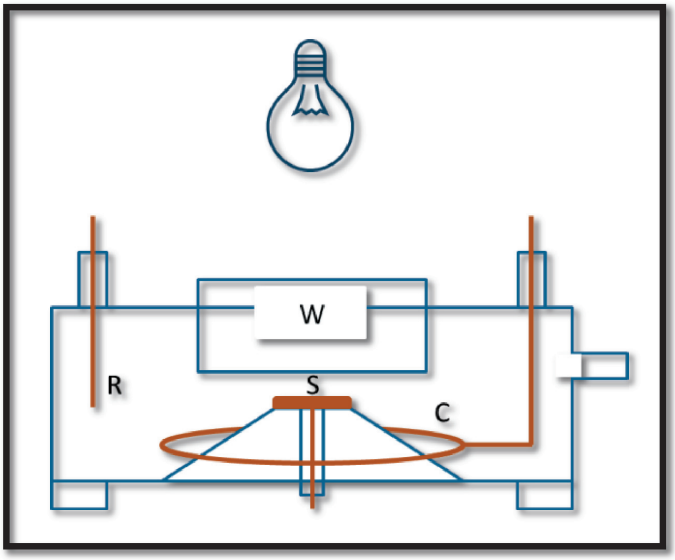

Figure 5-47: Design of the electrochemical cell used for the analysis of the Au ions released during the photocorrosion experiments.

A commercially available UV lamp with a power of 4 mwatt/cm^2 (λ_{max} = 254nm) was kept at a distance of almost 10 cm away from the window of the cell. All this set up was covered by a box which was completely wrapped with aluminum foil. All the measurements were made with Metrohm Autolab potentiostat using GPES software.

The Au quasi-reference electrode was chosen (99.95% pure, Good fellow Cambridge Limited, England) to minimize the effect of ion exchange of the gold ions formed upon irradiation by UV light with the supporting electrolyte. But, even with this disposition we saw that the open circuit voltage was not constant. A gradually increase in negative potentials was observed whenever the experiment was started. This may be attributed to formation of a double layer on the electrodes. With time the layer thickness increases hindering the ions in solution to exchange electrons with electrode. Platinum (99.95% pure, Good fellow Cambridge Limited, England) was chosen as working electrode due its purity and inertness.

With this set up we carried out a standard salt (Fe^{2+}/Fe^{3+}) characterization. For this we used a 2 mM aqueous solution of potassium ferricyanide ($K_3Fe(CN)_6,3H_20$) which has a standard reduction potential ($Fe^{3+}\rightarrow Fe^{2+}$) at 0.77 V(RHE). In our non-standard set up the hump of the reduction potential is located at +0.27 V, which shows that the non-standard reference potential of this cell is +0.5 V.

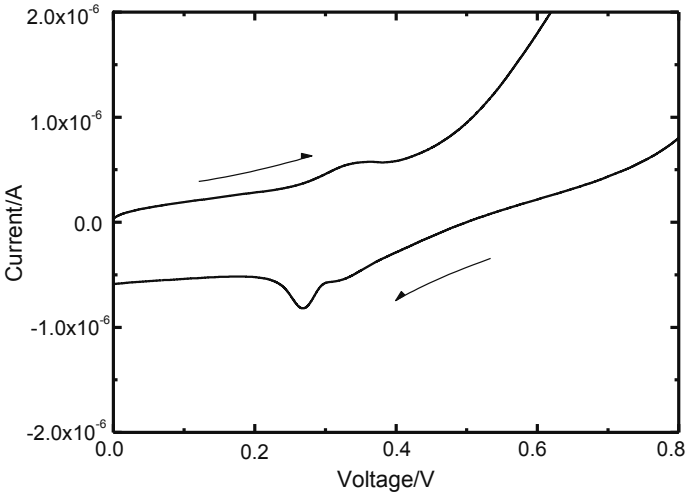

Figure 5-48: Cyclic voltammogram of 2 mM $K_3Fe(CN)_6$ taken at a scan rate of 0.05 V/s.

From the datasheet supplied by the manufacturer the intensity of the radiation at a distance of 10 cm is approximately ~ 40 μwatt/cm^2. Taken the area of the cell, it can be assumed that a power of 40x7=280 μwatt of light was illuminating the solution. This means $E=hc/\lambda = 8x10^{-19}$J/photon, and

$2.8x10^{-4}W=2.8x10^{-4}J/s$

$\therefore 2.8x10^{-4}/8x10^{-19} = 3.5x10^{14}$ photons/s, which means,

$3.5x10^{14}/6x10^{23} = 5.8x10^{-10}$ mole of photons/s ≈ 0.6 nanomoles of photons/s.

Firstly, we performed the experiment with a similar sample than the used one in figure (5-24), corresponding to Au NRs with a.r ≈ 3.9. After the UV

lamp was turned on the potential was recorded at a constant current of 1μA for 30 hours. The results are shown in the next figure.

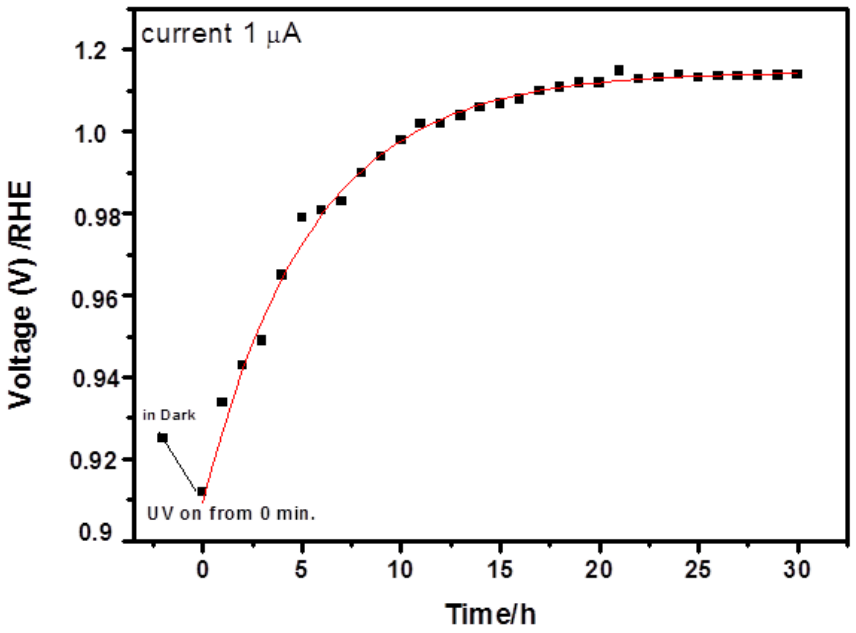

Figure 5-49: Potential recorded for gold nanorods under UV irradiation during 30hours at a constant current of 1 μA.

We can observe from the figure that the voltage firstly decreased very slightly from 0 to 4 hours and then increased approaching a limit at around 30 hours. The difference in the potential is approximately 0.1V.The first part of the curve is an artifact due to the precision of the electrochemistry measurements, usually in the range of nanomolar. This means that the time needed for the production of such an amount of Au ions needed to be detected by this technique is circa 4 hours. We also see that there is an increase of the potential during the illumination, which agrees with the idea that there is an oxidation process in the system, confirming the oxidation of the gold nanorods. From these data one can make some calculations.

As it was proposed in the scheme (5-1), when the clusters attached to the tips of the NRs are excited oxidizing holes that generated in the clusters

and transferred to the Au rods, eventually oxidizing Au atoms, which dissolved and go to the solution, giving rise to the corrosion of the rods. This process can be summarized as follows:

$$Ag(clusters) \rightarrow Ag^*(c) \rightarrow h^+ + e^-$$

$$Au_n(r) + h^+ \rightarrow Au_{n-1}(r) + Au^{3+}$$

In general: $Au^0 + 3h^+ \rightarrow Au^{3+}$

The electrochemical potential at time t and time zero are related by the expressions; $\mathcal{E}_t = \mathcal{E}_0 + (0.059/n).\log([Au^{3+}]_t / [Au^{3+}]_0)$, where n = 3. Then $\Delta\mathcal{E} = \mathcal{E}_t - \mathcal{E}_0 = 0.02 \times \log([Au^{3+}]_t / [Au^{3+}]_0)$. Taking into account that $\Delta\mathcal{E}_{t\rightarrow\infty} = 0.1V$(from fig.5-49) $= 0.02 \times \log([Au^{3+}]_{t\rightarrow\infty} / ([Au^{3+}]_{t\rightarrow 0})$, then $\log([Au^{3+}]_{t\rightarrow\infty} / [Au^{3+}]_0) = 5$. Then,

$\log[Au^{3+}]_{t\rightarrow\infty} = 5 + \log[Au^{3+}]_{t\rightarrow 0}$

From the spectrophotometric experiments (see figure 5-26) we know that the final amount of Au(III) at $t_{\rightarrow\infty}$ is, $[Au^{3+}]_{t\rightarrow\infty} = 3x10^{-4}M$.

Then, we can deduce that $[Au^{3+}]_{t\rightarrow 0} \approx 3x10^{-9}M$, which agrees with the previous comment that this concentration is in the limit to be detected by this electrochemistry technique, and explains the first part of the curve voltage-time represented in figure (5-50).

In order to make a rough estimation of the photon conversion efficiency, we can compare the amount of photons used in the experiments (0.6 nanomols/s) with the amount of ions generated, which are $3x10^{-4}M/(30x3600) \approx 5nM/s$, which means, in the total volume of the 60ml cell, 5x(60/1000) = 0.3 nanomols of Au(III)/s. Because the production of one Au-III ion needs 3 photons, the photons needed for the production of the Au III ions produced should be: 0.9 nanomols/s, which is approx. the same as the photons calculated from the illumination source. Therefore, one can say that the photon conversion in electron and holes is a very efficient process.

The second experiment that we carried out was to measure the voltage at a constant current of 1μA turning the light ON/OFF after 4 hours of illumination. The results are shown in figure (5-50).

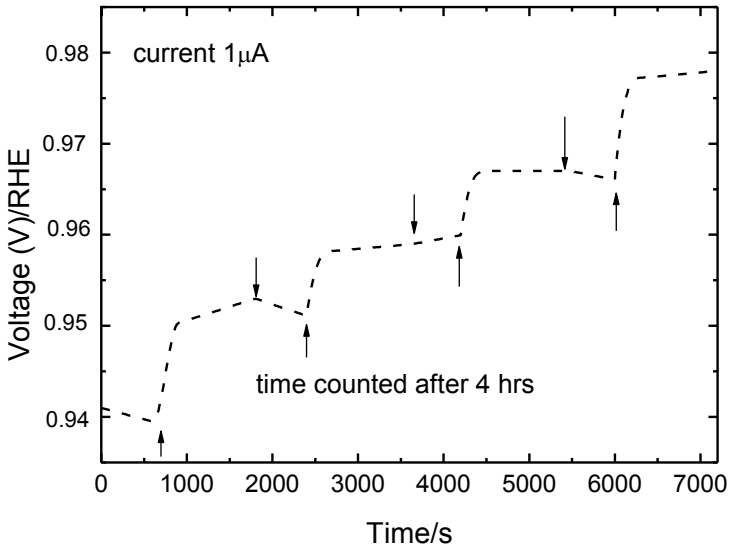

Figure 5-50: Potential recorded for gold nanorods under UV irradiation after 4hours at a constant current of 1 μA and turning on the light for 20 min and off for 10 min during 2 h.

It is clear from the figure that the voltage increases when the UV lamp is turned on and only a very little decrease is observed when the light is turned off. This confirms that light causes the production of ions, and that the photocorrosion is inhibited when the light is off.

After these experiments we tried to see if we could perform some experiments during the first minutes of irradiation. For this purpose we recorded the voltage values as a function of ON/OFF light cycles, as we did before (figure 5-50), but at lower constant currents a) 0 A and b) 10 nA.

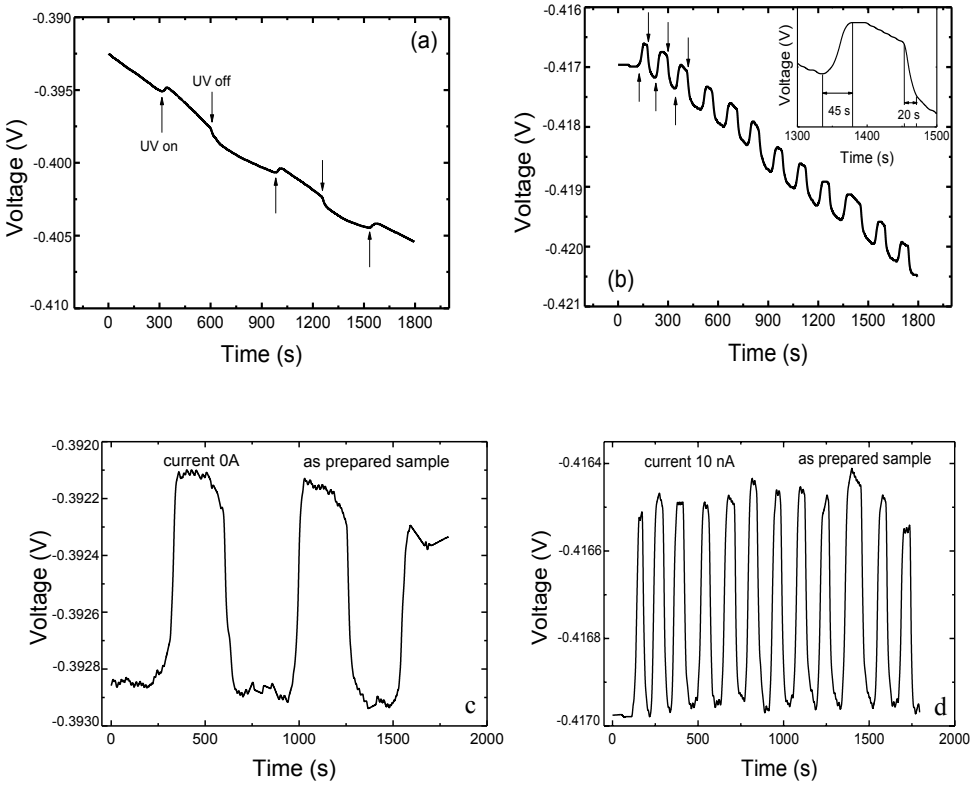

Figure 5-51: Constant current characteristics of as prepared Au nanorods solution, (a) at 0 A and (b) at 10 nA. The interval in time scale is 5 sec. Up and down arrows show UV on and off respectively. (c and d) after background corrections of (a and b).

The results shown in figure (5-51) indicate that, contrary to what happens at longer times, now the voltage after illuminating goes down to the value before illuminating. This indicates that the concentration of ions generated during the illumination is very low (near the limit of the detection of the electrochemical set-up) and that they are not well homogeneously distributed inside the solution, because not all the solution is homogeneously irradiated. Therefore, during this initial time (less than approx. ~ 4 h) the change in the voltage when the light is ON is due to the local increase (near the electrodes) of the concentration of Au ions. The voltage will turn to approx. the original value when the light in OFF

because of the diffusion of ions from the proximities of the electrodes to the bulk decreases again the concentration of ions to the sensitivity detection limit (see scheme 5-2).

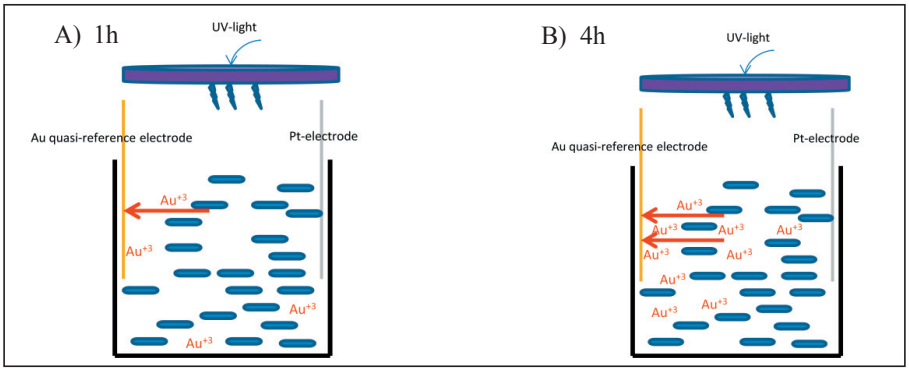

Scheme 5-2: Difference between the electrochemical measurements carried out before 1h of irradiation with UV light (A) and after 4h of irradiation (B).

To confirm the effects of the different species present in the solution we repeated the experiments, but for pure nanorods after centrifuged at 6000 rpm for 30 min and then washed and redispersed in water to separate nanorods from the other components. This washing procedure was repeated three times. Figures (5-52a) and b)) show the results for constant current at 0 A and 10 nA, respectively. As expected, clusters were washed away and there is almost no change in the recorded potential. The slope is almost the same, but the starting point of the potential is little less/more than previous one. This is because we took out CTAB from the electrolyte solution which can provide some boost in ion concentrations and also the concentration of nanorods was changed during the process by centrifugation and redispersion. The small hump like ripples seen in the characteristics regularly with turning on or off the UV light may be due to presence of very small quantity of clusters which were attached to the surface of the rods and could not been removed during the washing process.

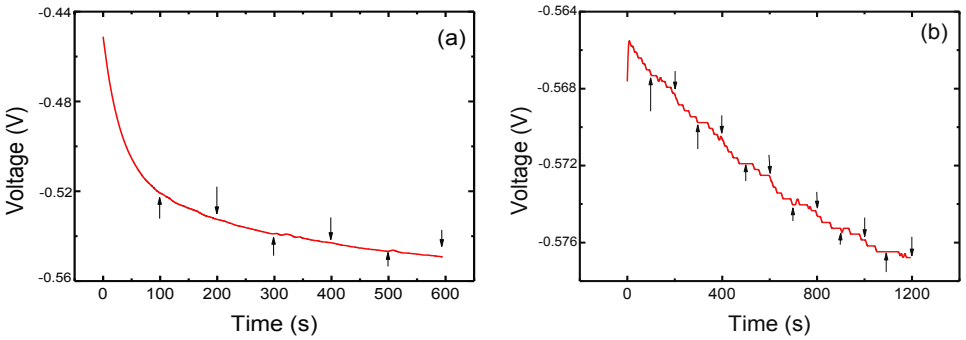

Figure 5-52: Constant current characteristics, (a) at 0 A and (b) 10nA for a washed nanorods sample.

In order to show that the presence of clusters is the key parameter for these experiments, we added Ag clusters from Nanogap (o.5 ml of 0.01mg/l) to the washed NRs solution, and repeated the previous experiment. The results can be seen in Figure (5-53).

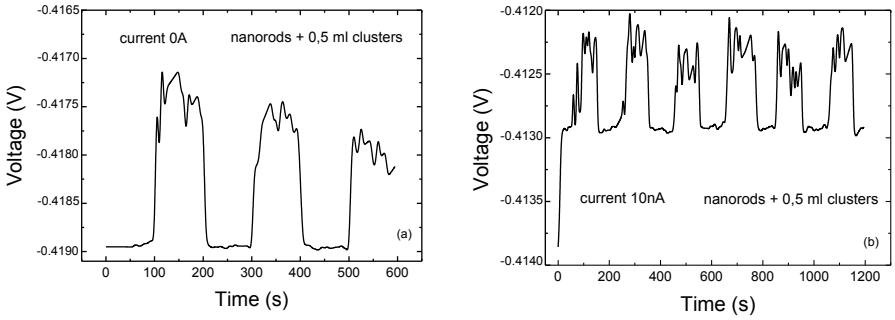

Figure 5-53: Constant current characteristics, (a) at 0 A and (b) 10nA for a mixture of 58 ml of washed nanorods and 0.5 ml cluster solution from Nanogap.

Both figures (5-52 and 5-53) clearly show that there is a significant increase in the observed signals. While in the absence of clusters there is almost no response to UV light by increasing the concentration of clusters the change between ON and OFF values of the potential are clearly seen. To increase the conductivity of the solution we added a little amount of

CTAB (1 ml of 1 mM). While CTAB itself does not have any response to UV light (Figure 5-54b) it stabilizes the current at ON state. The instability at ON state potential is clearly visible.

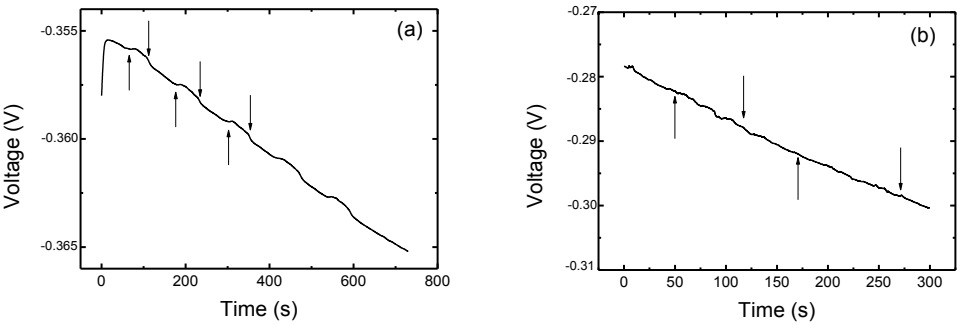

Figure 5-54: (a) Potential vs time curve for 10 nA constant current of a solution of washed nanorods + cluster + CTAB. (b) Potential vs time curve for 10 nA of only a 0.1M CTAB solution. Up and down arrows indicate on and off of UV light.

5-4: Effect of Laser irradiation on gold nanorods.

Many scientific groups[15-18] studied the interaction between metal nanoparticles and laser light. Koda et al.[19,20] reported the irradiation effect of nanosecond laser pulses (532 nm) on gold nanospheres, which leads to fragmentation of the nanodots. The slow heat transfer of the deposited laser energy into the surrounding solvent was used to explain the results. This slow heat transfer then leads to the melting and vaporization of the nanoparticles as estimated from the deposited laser energy. More information about the structural dynamics of metal nanoparticles after laser excitation can be obtained when nanoparticles having different shapes than spheres are used. Link et al.[17] studied the effect of high power (femtosecond and nanosecond) lasers on the structure of gold nanorods as a comparison study. They found that nanorods are easily converted to nanospheres by laser irradiation. For femtosecond pulses, typically pulse energies on the order of 10 mJ are sufficient to completely convert the rods into spheres. However, the exact value of the nanosecond pulse energy

needed for melting depends on the experimental conditions, primarily on the laser spot size at the sample.

Most of these studies are concentrated on the effect of femtosecond laser on gold nanoparticles. Therefore, we concentrate our study on the behavior of gold nanorods with different aspect ratios (1.8, 2.5 and 4.2) when they are irradiated by different nanosecond lasers (working at different wavelengths 1064, 532 and 355nm) in order to study the photostability of these particles and to better understand the effect of the nanosecond laser by comparing the results between the two laser modes (pulsed and continuum (CW)). Figure (5-55) shows the absorption spectra of these particles used for these studies.

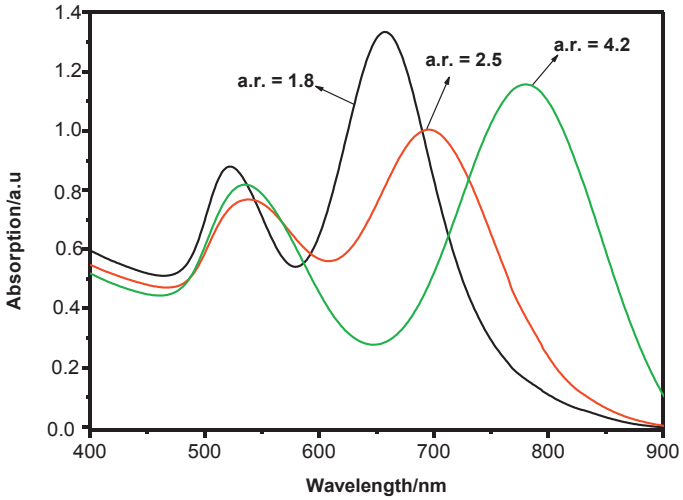

Figure 5-55: Absorption spectra showing the gold nanorods prepared using (40, 80 and 120µM of $AgNO_3$) used for the study of laser treatments.

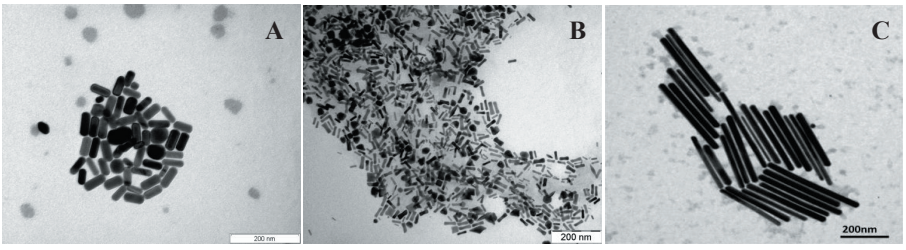

Figure 5-56: TEM images showing the gold nanorods prepared with aspect ratios 1.8, 2.5 and 4.2 (A-C), respectively, used for the study of laser treatments.

I) Laser in CW (continuous wave) mode.

In this case we used the laser output at a continuous energy level as a function of time. In this case, the laser works much like a lamp or an IR heater (since it emits in the near IR region of the EM Spectrum). These types of photons interact basically with low energy electrons which, in turn, undergo nonradiative transitions and transfer energy to lattice vibrations, thus increasing the temperature of the material. This process takes place very fast, since irradiation is an instant energy transfer process and the electron-phonon coupling (or interaction) takes place below the nanosecond time regime.

II) Pulsed Laser mode.

IIa) near IR emission:

Here we should distinguish between two regimes, one above 20 *n*s, and other below 10 *n*s. The first laser had pulse widths well above 10 *n*s, thus heating of the material is a relatively efficient process because of the electron-phonon interaction, combined with the extremely high irradiance values (W/cm^2) employed.

The second laser used emitted pulses lower than 10 *n*s, which make a significant difference for two reasons. Firstly, they involve extremely high irradiance values, well above those that correspond to plasma formation ($>>10^8$ W/cm^2) so that nonlinear optical phenomena enter into the scene, causing multiphoton absorption and a considerable increase in absorption due to the fact that the refractive index changes as a function of laser intensity at that regime. Secondly, the pulses are short enough to reduce the transfer of heat to the material, so that less thermal transfer and damage is generally observed.

IIb) Visible (532 nm, green) or UV (355 nm) emission:

Irradiation at these wavelengths causes photochemical effects to enter into the processing scene. Apart from the fact that Au absorption at the visible

is maximum because of the surface plasmon resonance, both Green & UV-irradiation exaggerate the nonlinear effects discussed earlier for the near IR, and both are associated with much less reflection from the metal particles. These are also emissions at short pulse widths, below 9 ns, so that all the nonlinear effects are observed amplified several fold. In addition, photons emitted at these corresponding energies interact with electrons which are much more energetic, at the valence bonding level (green) or at the absorption edge (UV), breaking chemical bonds and initiating reactions by destabilizing chemical species with which they interact.

In view of the above, one may expect that when the situation is under condition (I) the nanoparticles change because they absorb heat from the laser and the solution, and behave as if they were heated with a conventional source (IR lamp or furnace, heating mantle, etc), but the heating rate is higher and geometrically localized. That is, the external containment vessel is heated indirectly from the liquid in contact with the nanoparticles. The nanoparticles are heated directly by the interaction with the laser beam. Obviously, this is a largely thermal interaction mechanism.

Under condition (IIa), however, heating takes place through a photothermal mechanism which is limited in time exposure (short pulse width, limited interaction time) but suffers from much higher irradiance values than in condition (I). As the pulse width is decreased, the interaction time diminishes, the electron-phonon interaction time is reduced, but the irradiance values increase significantly, and so do the nonlinear phenomena. At such high levels of irradiance, photophysical phenomena start to take place with plasma and associated shock-wave appearance. Particles may break up because of several mechanisms, which include in part the photothermal (heat transfer), photophysical (shock waves) and the photochemical (slightly, nonlinear effects giving rise to multiphoton absorption and frequency doubling, etc.)

Under condition (IIb) absorption phenomena are dramatically increased, as the photons interact with valence and absorption edge electrons, yielding nonlinear phenomena readily, and causing chemical reactions to take place via destabilization or labialization of certain bonds (through excitation of the corresponding electrons). In the case of Au, the green emission is coincident with a plasmon resonance frequency, and it couples readily, so that the interaction with the Au nanoparticles is quite efficient, specially compared to the nIR case.

5-4-1: Effect of Nd: YAG laser and Nd:YVO_4 (continues wave mode(CW)).

It has been reported by Link et al.[17] that irradiation of gold nanorods to laser light cause melting of the rod shape particles into spheres. These rods were stabilized by a mixture of two surfactants (Cetyltrimethylammonium bromide (CTAB) and Tetraoctylammonium bromide (TOAB)); however, in our case the particles were prepared using CTAB alone. The Laser that used in the irradiation were generated from the second harmonic of Nd-YAG laser – Q-switching (continuum SLI-10) at $\lambda = 1064/2 = 532$ nm and from Nd:YVO_4 at 1064nm . These laser pulses were then focused onto a quartz cell containing the sample solution of gold nanoparticles. The energy of Nd-YAG laser was with irradiance values in the range 2.04×10^4 W/cm^2. Nd:YVO_4 with average power 12 W yields irradiance values of ca. 1.70×10^6 W /cm^2. The absorption spectra of the colored solutions were measured with a spectrophotometer after irradiation with the laser beam. As it can be seen in figure (5-57), our results indicate that gold nanorods prepared by the seed mediated method and stabilized by CTAB are very stable towards Laser light. Only a slight decrease in its absorbance occurred upon exposure for 30 minutes with Nd:YAG (CW) ; moreover, when PVP is added to the solution, the gold rods are completely stable with no noticeable absorption change .

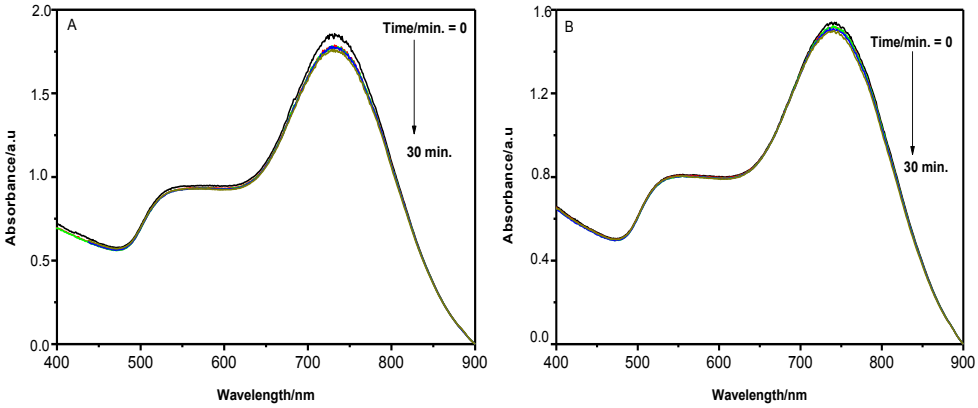

Figure 5-57: Absorption spectra showing the effect of CW-mode laser on gold nanorods (A) and on gold nanorods with 15 % PVP (B).

The laser output is at a continuous energy level as a function of time, and it works much like a lamp or an IR heater (since it emits in the near IR region of the EM Spectrum). This type of photons interacts basically with low energy electrons which, in turn, undergo nonradiative transitions and transfer energy to lattice vibrations, thus increasing the temperature of the material. In continues mode irradiation with 1064 nm emission from the Nd:YVO_4 laser used average irradiance values of ca. 1.70 x 10^6 W/cm^2. As it can be seen in figure (5-58), almost no changes are observed although the solution has been observed to heat considerably (above 60ºC). The irradiance level is below that considered as the threshold for plasma formation at the focal point. At this emission wavelength, the interaction between the laser and the species in suspension, as well as with the liquid, is expected to be essentially of a photothermal nature. In addition, the focal spot is approximately 30 μm in diameter, so that the interaction time with the gold nanorods is quite limited, due to their reduced size. Interaction of the beam is mainly taking place with the liquid, and thus it is expected to raise its temperature significantly above room temperature, since the liquid absorbs a percentage of the laser energy.

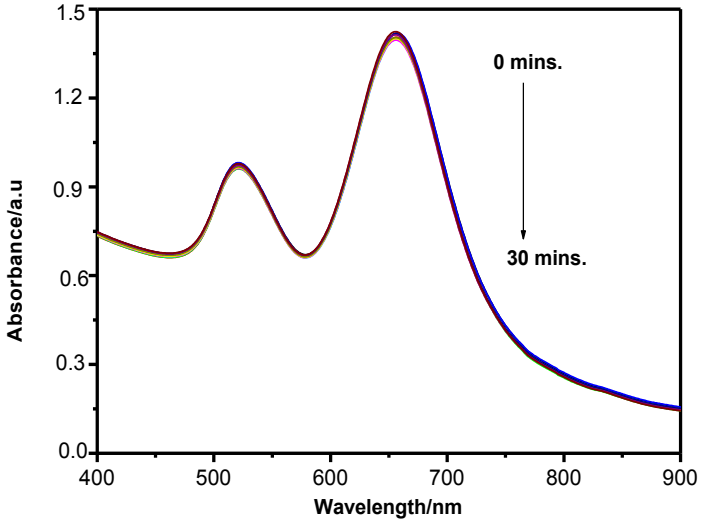

Figure 5-58: Absorption spectra showing the effect of Nd:YVO_4 in CW-mode laser on gold nanorods, which do not show any effect for 30 minutes exposure.

5-4-2: Nanosecond pulsed-mode laser.

I- Effect of Pulsed Nd: YVO_4 laser, working in Q-switch regime.

For this study all the parameters of this laser, like repetition frequency, velocity, intensity, superposition, the orientation,…etc were changed to see their influence on gold nanorods. As shown in Figure (5-59), a slight blue shift and absorbance decrease occurred when we used a beam with υ = 100 mm/s, f = 50 KHz, the pulses superposition 90 %, orientation with 90^0 angle (changed to 0^0 angle in the second line), and the intensity I was changed from 25 to 32 A (from ≈ 4 to 10.5W). Also the same effect occurred when the beam parameters changed to υ = 50 mm/s, f = 5 KHz, the pulses superposition 20 %, orientation with 0^0 angle and changed I from 20 to 32 A (from ≈ 1.5 to 10.5W). The irradiance of pulsed Q-switched mode, Nd:YVO_4 is about 1.13 x 10^8 W/cm^2.pulse (5-10 kHz). In this case, slight modifications of the nanogold structures are observed as a function of irradiance (W/cm^2) as it can be seen in Figures (5-59 and 5-60). The difference between the effects of pulsed and CW mode may be assigned to the levels of irradiance, which lie around 10^6 vs. 10^8. In the latter case,

some effect on the SP_T fundamental (transverse) band of Au nanorods, within the visible region of the spectrum, is observed. This is in contrast to the null influence that CW irradiation has over this visible transverse mode resonance band.

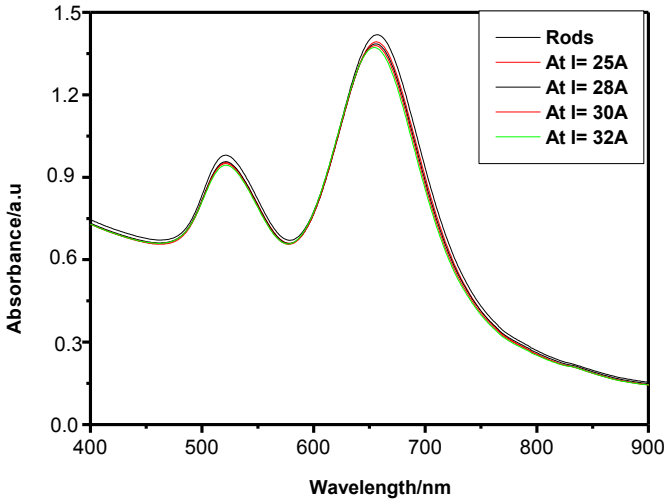

Figure 5-59: Absorption spectra showing the effect of pulsed Nd: YVO_4 laser on gold nanorods after changing the intensity from 25 to 32 A (from ≈ 4 to 10.5 W), υ = 100 mm/s, f = 50 KHz, the superposition 90 %, and orientation with 0^0.

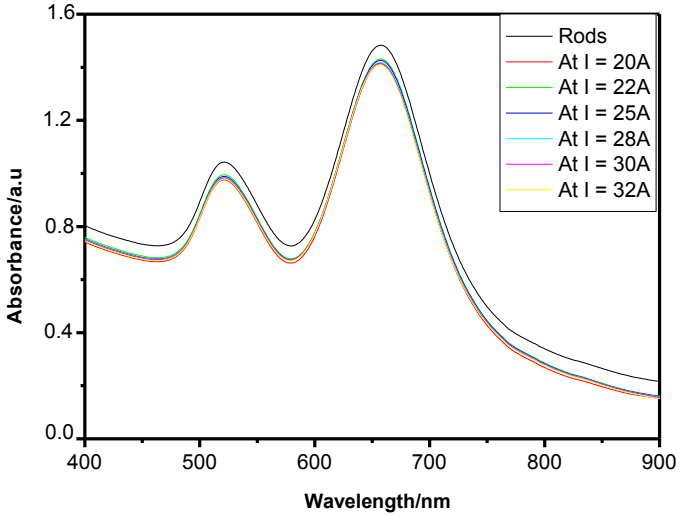

Figure 5-60: Absorption spectra showing the effect of pulsed Nd: YVO_4 laser on gold nanorods after changing the intensity from 20 to 32 A (from ≈ 1.5 to 10.5 W), υ = 50 mm/s, f = 5 KHz, the superposition 20 %, and orientation with 0^0.

II- Effect of pulsed Nd:YAG laser, working in Q-switch regime.

Experiments carried out with a pulsed Nd:YAG nanosecond regime emission laser yielded significantly different results for Au nanorods of different aspect ratios (1.8, 2.5, and 4.2), as follows from the discussion below.

1- Fundamental line at 1064 nm / 9 ns / 12.5 W / Irr ≈ 3.54 x 10^7 Wcm^{-2}/pulse.

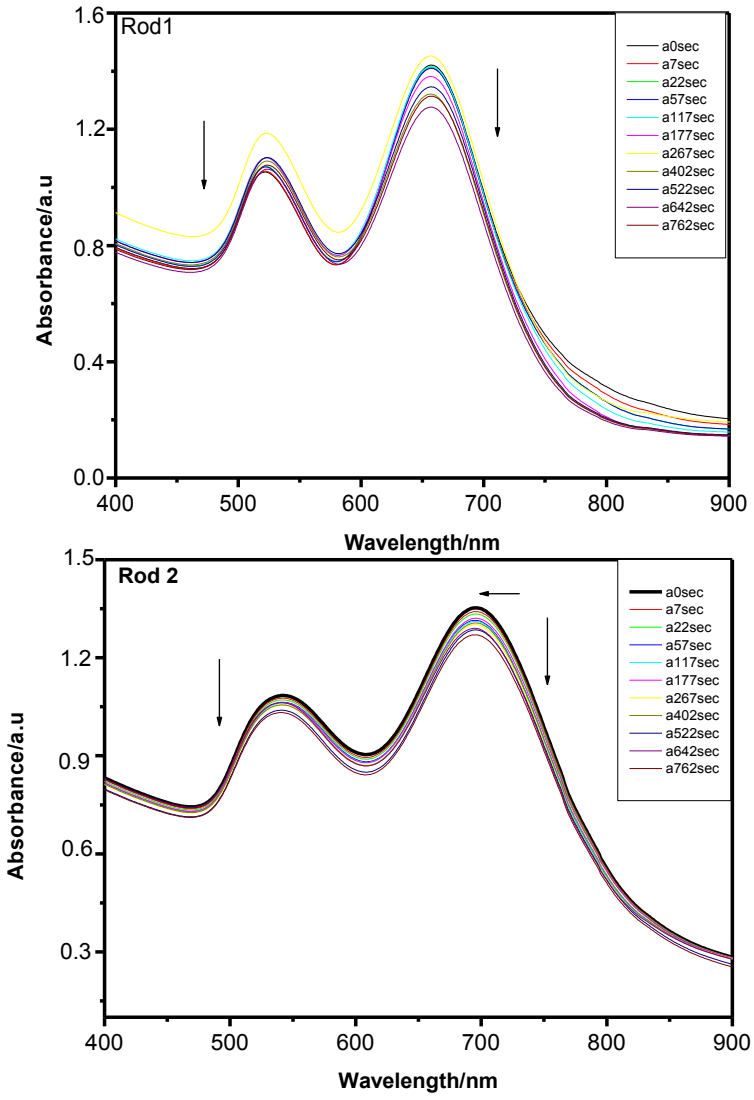

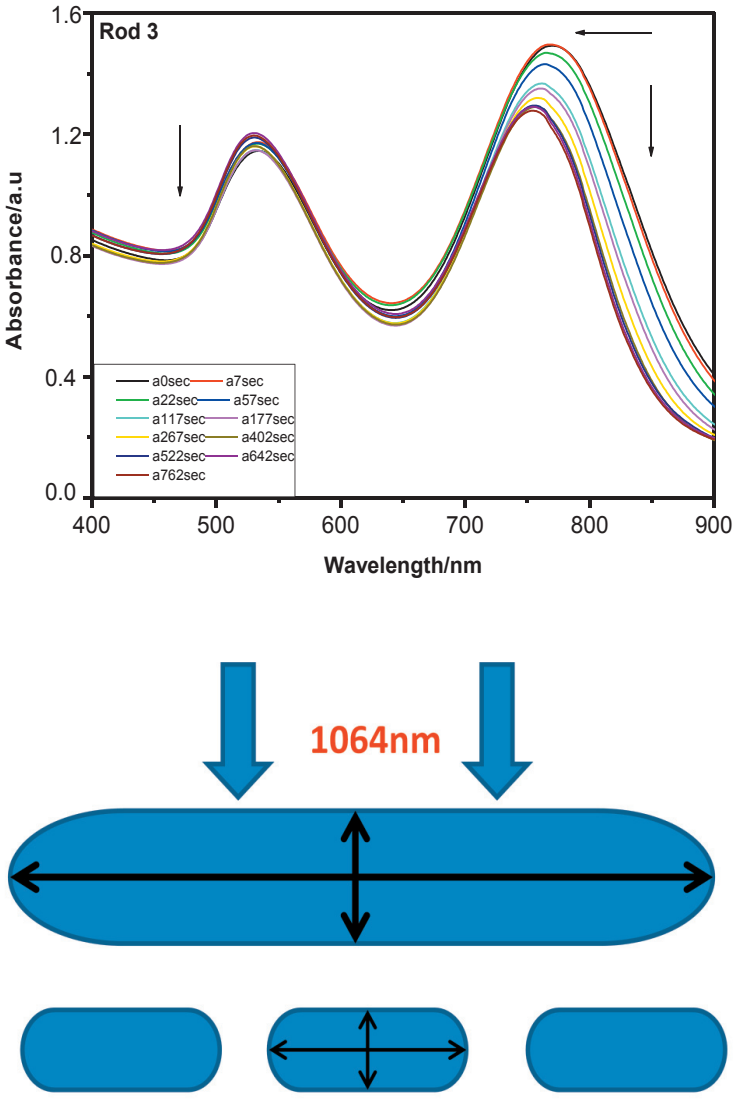

Figure 5-61: Absorption spectra showing the effect of pulsed Nd: YAG laser (at 1064 nm / 9 ns / 12.5 W / Irr ≈ 3.54 x 10^7 Wcm^{-2}/pulse) on gold nanorods with different aspect ratios (Rod1= 1.8, Rod2= 2.5 and Rod3= 4.2) from 0 to 760sec. with illustration of the possible fragmentations which can occur under illumination.

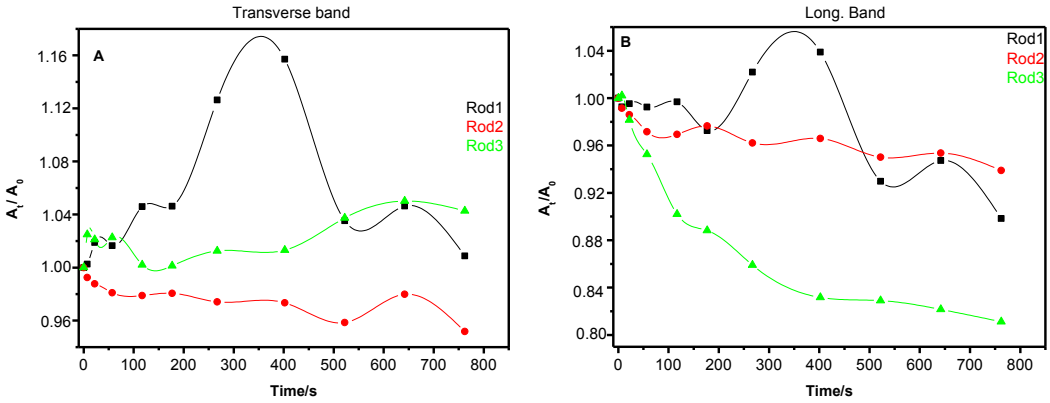

Figure 5-62: Normalized absorption spectra of rods with different aspect ratios (Rod1= 1.8, Rod2 = 2.5 and Rod3 = 4.2) for the transverse band (A) and longitudinal (B) under the effect of pulsed Nd: YAG laser (1064 nm / 9 ns / 12.5 W / Irr ≈ 3.54 x 10^7 Wcm^{-2}/pulse).

This pulsed laser Nd: YAG (1064 nm / 9 ns / 12.5 W / Irr ≈ 3.54 x 10^7 Wcm^{-2}/pulse) is used in a direct output configuration (without movement of the laser beam), so that the Au NR suspension is irradiated under cylinder type geometry with a 1 cm diameter (see illustration in figure 5-63). Fragmentation is observed under these irradiation conditions (figures 5-61 & 5-62), as reported by Link et al.[17], where laser pulses are claimed to cause excitation of the hot lattice (stage1) in the experiments with nanosecond pulses. One thus expects that absorption of more photons by the hot lattice occurring in the nanosecond experiment is what leads to an increase in the lattice internal energy and fragmentation of the gold NRs (stage 2). The longitudinal absorption band of GNR changes its maximum to shorter wavelength but retains its width, suggesting that the laser exposure changes the distribution into smaller rods.

$$[(Au)_{NP}]^{vib} \xrightarrow[\text{fragmentation}]{m h\upsilon (ns)} [(Au)_{NP}]^{vib**} \qquad (1)$$

$$[(Au)_{NP}]^{vib**} \longrightarrow [(Au)_{NP}]^{SNS} \qquad (2)$$

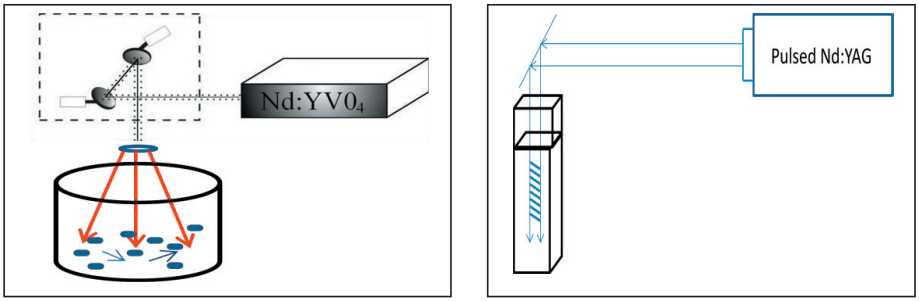

Figure 5-63: Illustration diagram showing the difference between CW and pulsed nanosecond laser effect. As one can see the pulsed laser is more concentrated to the NRs than the CW laser.

2- SH laser with 532 nm / 7 ns / 2.9 W / Irr ≈ 1.65 x 10^7 Wcm^{-2}/pulse.

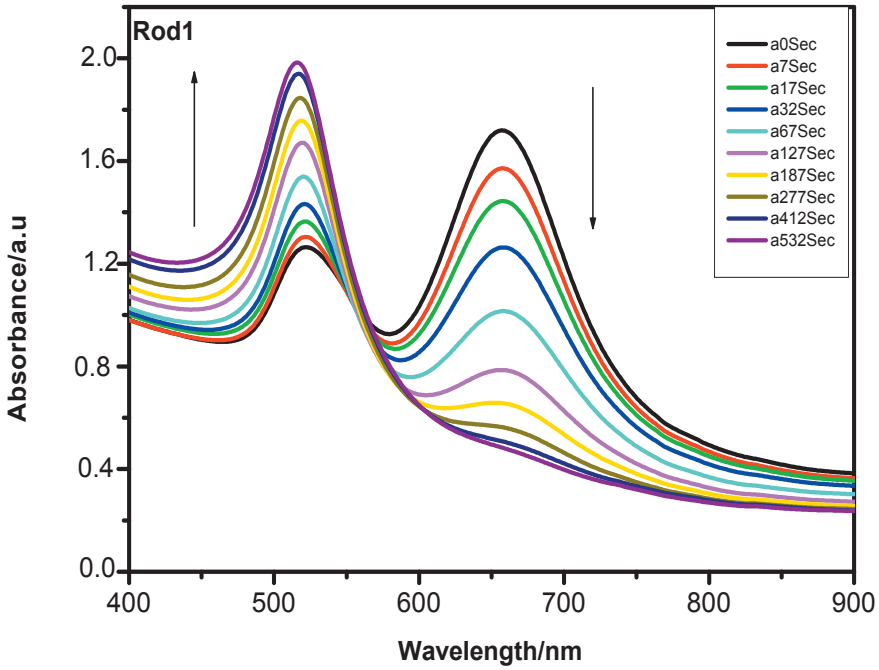

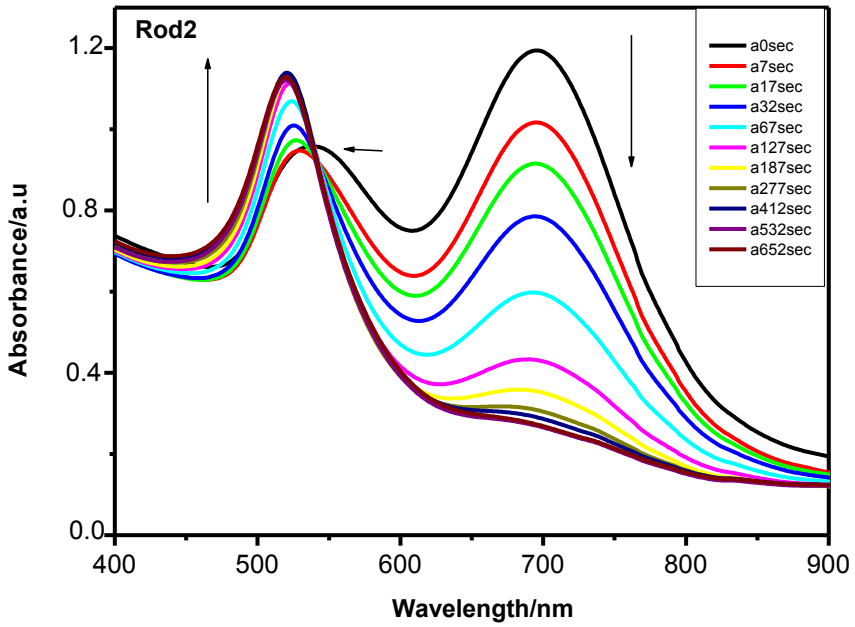
Rod2
Absorbance/a.u
Wavelength/nm
a0sec
a7sec
a17sec
a32sec
a67sec
a127sec
a187sec
a277sec
a412sec
a532sec
a652sec

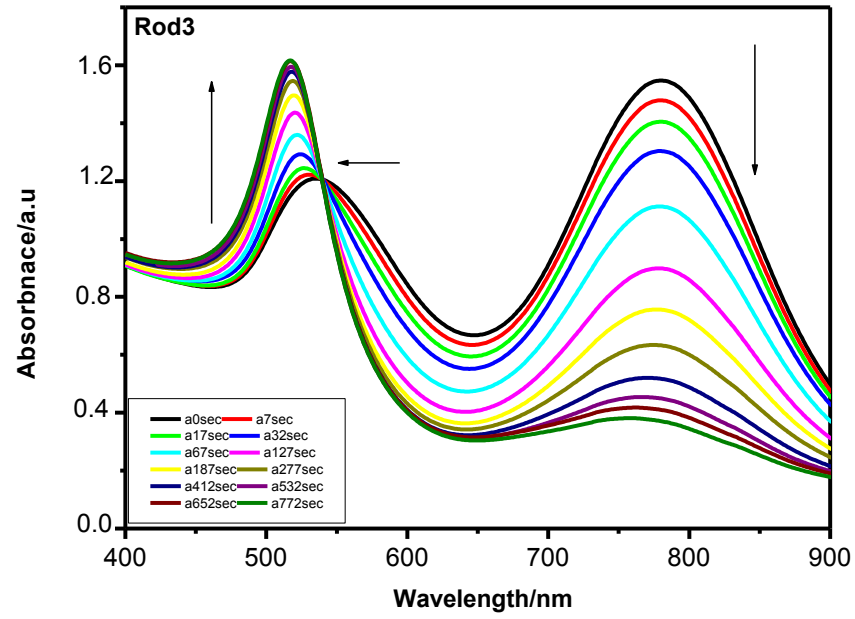
Rod3
Absorbnace/a.u
Wavelength/nm
a0sec
a7sec
a17sec
a32sec
a67sec
a127sec
a187sec
a277sec
a412sec
a532sec
a652sec
a772sec

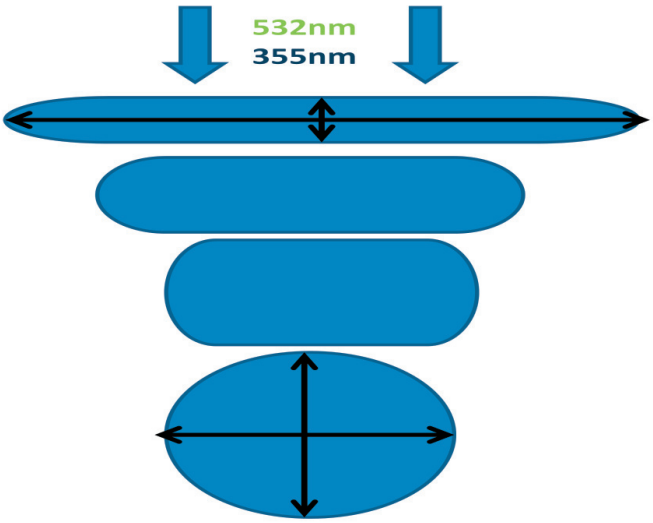

Figure 5-64: Absorption spectra showing the effect of pulsed Nd: YAG laser (SH with 532 nm / 7 ns / 2.9 W / Irr ≈ 1.65 x 10^7 Wcm^{-2}/pulse) on gold nanorods with different aspect ratios and illustration showing the possible melting mechanism.

A drastically different behavior is observed under green (532nm) laser irradiation, as compared to similar conditions in the nIR (1064 nm). Although the pulse width was slightly shorter (7 vs. 9 ns) it should not cause a significant effect on the irradiation results in terms of nanorods modification. The irradiance values are of the same magnitude, thus other type of mechanism (melting) must be responsible for such a change in the laser-nanorods interaction. In fact, the changes observed are very similar to those reported for irradiation with fs lasers (Link et al.[17]). In addition, this laser output wavelength coincides with the transverse resonance plasmon band of Au, so that it is not surprising to observe considerable effects on the corresponding Vis band in the UV-Vis spectrum recorded just upon 532 nm irradiation.

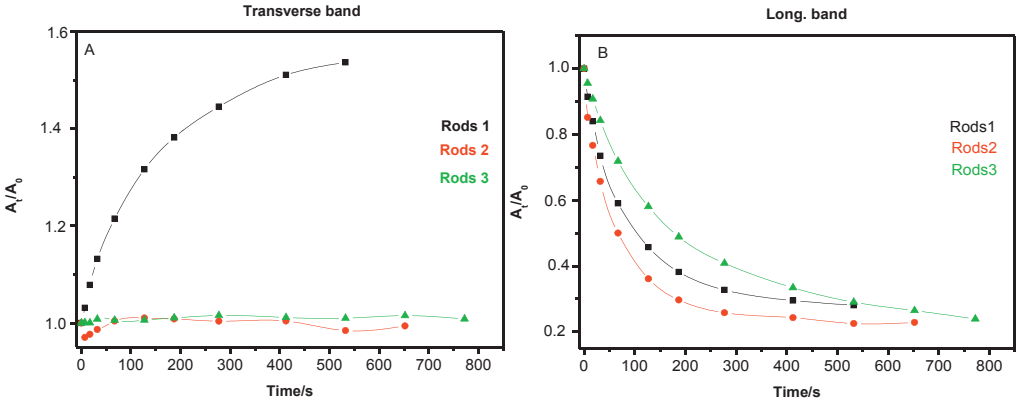

Figure 5-65: Normalized absorption spectra of rods with different aspect ratios (Rod1= 1.8, Rod2= 2.5 and Rod3= 4.2) for the transverse band (A) and longitudinal (B) under the effect of pulsed Nd: YAG laser (SH with 532 nm / 7 ns / 2.9 W / Irr ≈ 1.65 x 10^7 Wcm^{-2}/pulse).

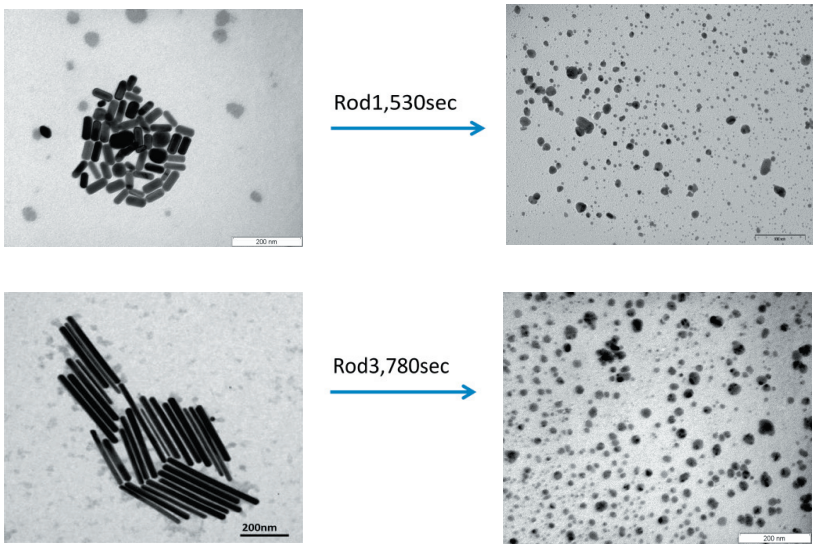

Figure 5-66: TEM images showing the effect of pulsed Nd: YAG laser (SH with 532 nm / 7 ns / 2.9 W / Irr ≈ 1.65 x 10^7 Wcm^{-2}/pulse) on gold nanorods and transformation to nanospheres through the melting mechanism (scale bar 200nm).

3- 3rd Harmonic with 355 nm / 6 ns / 0.55 W / Irr ≈ 3.67 x 10^6 Wcm^-2/pulse.

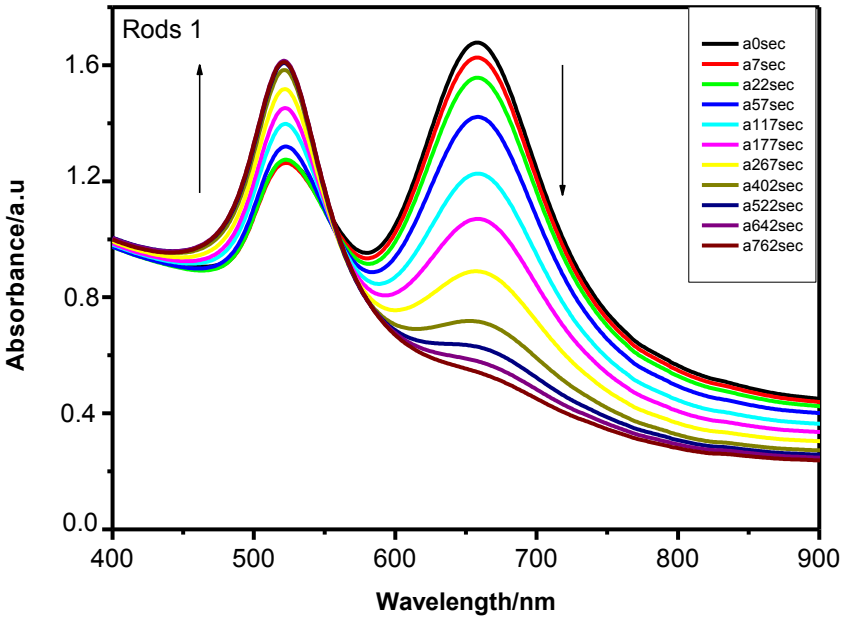

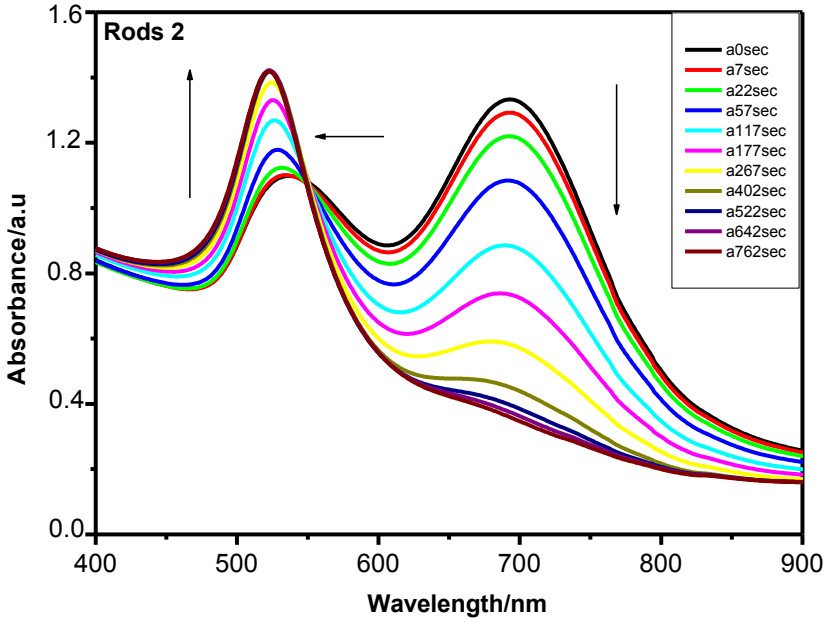

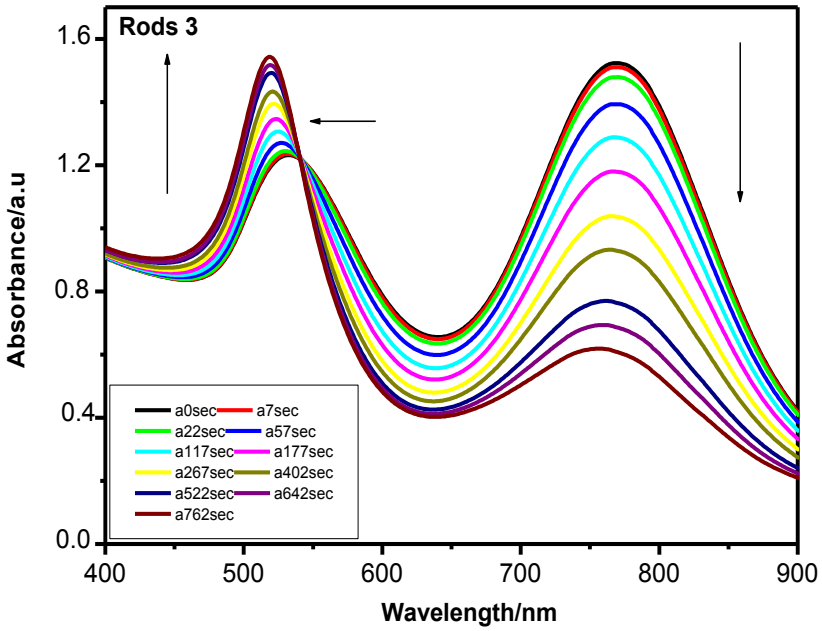

Figure 5-67: Absorption spectra showing the effect of pulsed Nd: YAG laser (3rd harmonic with 355 nm / 6 ns / 0.55 W / Irr ≈ 3.67 x 10^6 Wcm^{-2}/pulse) on gold nanorods with different aspect ratios (Rod1= 1.8, Rod2= 2.5 and Rod3= 4.2).

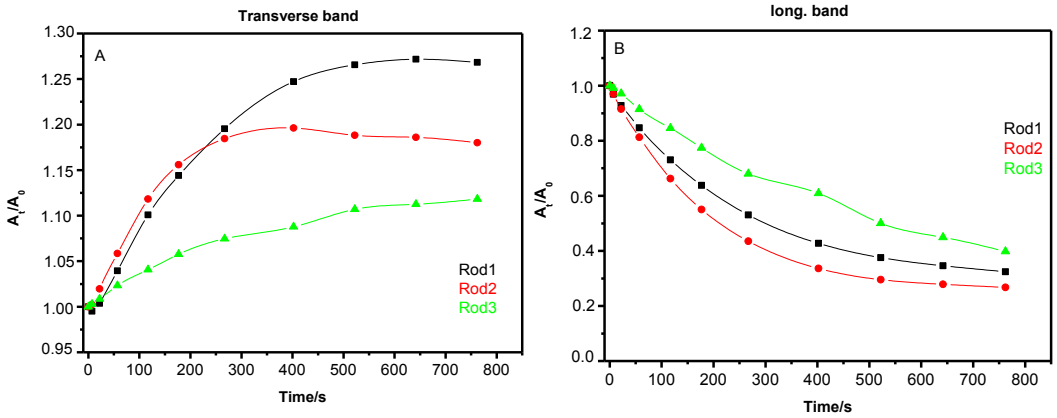

Figure 5-68: Normalized absorption spectra of rods with different aspect ratios (Rod1= 1.8, Rod2= 2.5 and Rod3= 4.2) for the transverse band (A) and longitudinal (B) under the effect of pulsed Nd: YAG laser (3rd harmonic with 355 nm / 6 ns / 0.55 W / Irr ≈ 3.67 x 10^6 Wcm^{-2}/pulse).

UV irradiation causes a similar melting behavior to that observed for the (532 nm) visible laser irradiation. The mechanism that causes changes to be observed in the nanorods must, however, be different in view of the changes in the spectra observed as a function of irradiation time. One type of rods (shorter ones) follows similar behavior at 532 nm and 355 nm. The other types, however, exhibit a contrast in behavior under both types of laser irradiation (see figures 5-65 & 5-68). Under 532 nm, they show no change after a threshold time of ca. 50 s, while under 355 nm they exhibit a gradual change up until aprox. 400 second. This different behavior must be related to the difference in interaction at these wavelengths, between the laser and the nanorods. It may be related to the plasmon resonance absorption in the visible, not at all present at the UV (355 nm). At this shorter wavelength, two possible mechanisms can be of relevance. A first possible explanation is that a mechanism similar to that proposed for UV-light irradiation described in the previous section, takes place with a photocorrosion of the gold tips. Another possible and plausible explanation is to propose some type of photon-electron interaction, which takes into account higher energy electrons for two reasons. On the one hand, because of the higher energy photons at 355 nm; on the other, because nonlinear effects become much more important at this UV emission[21]. According to the literature (reference 21 and work cited therein) nonlinear effects which cause multiphoton absorption on irradiated surfaces, are gradually more important as the wavelength is changed in the sequence nIR-Vis-UV (refer to graph (Figure 80) in reference 21, p 129). Thus these effects, which cause drastic changes in absorption and interaction with different type of electrons, although present significantly at 532 nm, are most important at 355 nm, where core shell electrons may be conveniently affected and different interaction mechanisms may thus be induced (refer to discussion by reference 21).

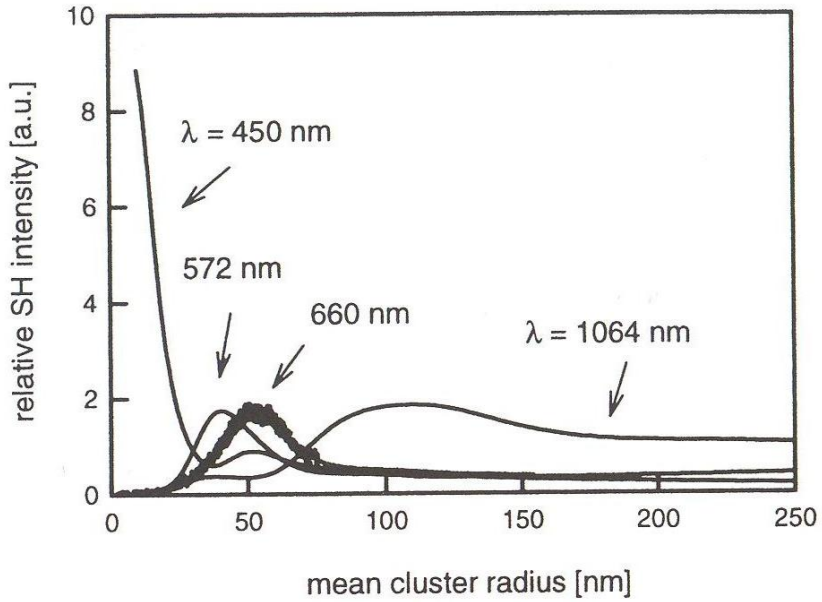

Figure 5-69: (Figure 80) in reference 21 which refer to the calculated relative SH intensities as a function of fundamental wavelength λ and mean cluster radius for sodium clusters adsorbed on dielectrics. Typical experimental values are indicated by dots.

5-5: Conclusion.

In this chapter, the effect of the gold nanoparticles shape on the stability (thermal heating and photo stability by UV-light and laser) was studied. The mechanism of particles dissociation in case of nanoprisms is different than that of nanorods under thermal heating. Great enhancement of the thermal stability has been achieved by adding specific amount of polyvinyl pyrrolidone (PVP) to the gold nanoparticles of different shapes capped with cetyltrimethylammonium bromide (CTAB). It is worth to mention that the gold nanorods stabilized by PVP are totally stable up to 220 ^{0}C. Optically, these gold particles stabilized by PVP are remarkably much stable towards thermal heating and UV light. Under long irradiation time up to 30 h with UV light it was unexpectedly found that gold nanorods totally decomposed and another band started to appear at 398nm, which is almost the same

band of the Au-CTAB complex indicating that the gold (0) is oxidized and transformed to gold (III)-ions. The results were interpreted assuming that the photocorrosion is due to the presence of Ag-clusters attached at the tips of the rods, in accordance with the results shown in previous chapter, that Ag clusters are present and play an important role in the anisotropic growth of the gold nanoparticles. It seems that those clusters, protected by the CTAB capping, are stable and remain attached to the rods after their formation.

This mechanism was further confirmed by adding ethanol to the irradiated rods and by heating the irradiated rods to 130^0C or washing the rods. In such cases the photocorrosion is highly inhibited. The photocorrosion effect was further extended with the introduction of hole and electron scavengers yielding, depending on the conditions, the production of hydrogen and oxygen. The results are of importance in photocatalysis and photovoltaic applications. Electrochemical experiments were carried out, which confirm the oxidation of these particles and the formation of gold ions.

Finally, the effect of different types of nanosecond lasers (CW and pulsed) on different aspect ratio gold nanorods was studied and different mechanisms (fragmentation and melting) were proposed for these different nanosecond pulsed laser effect.

5-6: References.

1. Murphy C.J.; Sau T.K.; Gole A.M.; Orendorf f C.J.; Gao J.; Gou L.; Hun yadi S.E; Li T., J. Phys. Chem. B,2005, 109, 13857.
2. Shi W.; Zeng H.; Sahoo Y.; Ohulchansk yy T.Y.; Ding Y.; Wang Z.L.; Swihart M.; Prasad P.N., Nano Lett. , 2006, 6, 875.
3. Sonnichsen C.; Ali visatos A.P., Nano Lett., 2005, 5, 301.
4. Orendorf f C.J.; Gole A.M.; Sau T.K.; Gao J.; Murphy C.J., J. Anal. Chem., 2005, 77, 3261.
5. Huang W.; Qian W.; El-Sayed M.A., J. Phys. Chem. B, 2005, 109, 18881.
6. Tkachenk o A.G.; Xie H.; Coleman D.; Glomm W.; Ryan J.; Anderson M.F .; Franzen S.; Feldheim D.L., J. Am. Chem. Soc., 2003, 125, 4700.

7. Mohamed B.M.; Ismail K. Z.; Link S.; El-Sayed M. A. J. Phys. Chem. B, 1998, 102, 9370.

8. Al-Sherbini M. E., Materials Chem. Phys., 2010, 121,349.

9. Petrova H.; Perez Juste J.; Pastoriza-Santos I.; Hartland G. V.; Liz-Marza´ n L. M. ; Mulvaney P., Phys. Chem. Chem. Phys., 2006, 8, 814.

10. Al-Sherbini M. E., Colloids and Surfaces A: Physicochem. Eng. Aspects, 2004, 246, 61.

11. Kang S. K.; Kim Y.; Hahn M. S.; Choi I.; Lee J.; Yi J., Current Applied Physics, 2006, 6S1, 114.

12. Becker R.; Liedberg B.; Käll P., Journal of Colloid and Interface Science, 2010, 343, 25.

13. Wang Z.; Gao R.P.; Nikoobakht B.; El-Sayed M.A., J. Phys. Chem. B, 2000, 104, 5417.

14. Nikoobakht B.; ElSayed M.A., Langmuir, 2001, 17, 6368.

15. Link S.; Burda C.; Mohamed M. B.; Nikoobakht B.; El-Sayed M. A., J. Phys. Chem. A, 1999, 103, 1165.

16. Link S.; Burda C.; Nikoobakht B.; El-Sayed M. A., J. Phys. Chem. B, 2000, 104, 6152.

17. Link S.; Wang Z. L.; El-Sayed M. A., J. Phys. Chem. B, 2000,104, 7867.

18. Petrova H.; Perez Juste J.; Pastoriza-Santos I.; Hartland G. V.; Liz-Marzan L. M.; MulvaneyP., Phys. Chem. Chem. Phys., 2006, 8, 814.

19. Kurita H.; Takami A.; Koda S. *Appl. Phys. Lett.,* 1998, *72*, 789.

20. Takami A.; Kurita H.; Koda S. *J. Phys. Chem. B,* 1999, *103*, 1226.

21. Rubahn G., Laser Applications in Surface Science and Technology book, copyright in 1999.